The Importance of Secreted Siderophores in Diagnosis and Virulence of Invasive Fungal Infections

by

Cassandra Carroll

B.Sc. (Hons.), Simon Fraser University, 2009

Thesis Submitted in Partial Fulfillment of the
Requirements for the Degree of
Doctor of Philosophy

in the
Department of Biological Sciences
Faculty of Science

SIMON FRASER UNIVERSITY
Spring 2018

Approval

Name:	**Cassandra Carroll**
Degree:	**Doctor of Philosophy**
Title:	**The Importance of Secreted Siderophores in Diagnosis and Virulence of Invasive Fungal Infections**
Examining Committee:	**Chair: Julian Christians** Associate Professor **Margo Moore** Senior Supervisor Professor **Andrew Bennet** Supervisor Professor Department of Chemistry **James Kronstad** Supervisor Professor Department of Microbiology & Immunology & Faculty of Agricultural Sciences Management The University of British Columbia **Lisa Craig** Internal Examiner Professor Department of Molecular Biology and Biochemistry **David Heinrichs** External Examiner Professor Department of Microbiology and Immunology University of Western Ontario
Date Defended/Approved:	April 25, 2018

Abstract

Iron acquisition is essential for growth. In pathogenic Mucorales fungi, reductive iron assimilation contributes to virulence whereas in *Aspergillus fumigatus*, siderophore biosynthesis is essential for pathogenesis. The overall aim of my research was to investigate the synthesis and diagnostic importance of siderophores of these two groups of pathogenic fungi.

Biosynthesis of select siderophores has been shown to occur using non-ribosomal peptide synthetase (NRPS)-independent siderophore (NIS) synthetases. I used crystal structures to compare NIS enzymes involved in the biosynthesis of 8 siderophores. I proposed a new class of Type C' synthetases, responsible for dimerization/macrocyclization of more complex and substituted intermediates. I also demonstrated that NIS enzymes are predicted to be present in all Domains of life.

I identified an NIS homolog in the fungal pathogen, *Rhizopus delemar*, and confirmed that the enzyme (Rfs) was responsible for synthesis of the polycarboxylate siderophore, rhizoferrin. Rfs kinetic parameters were comparable to bacterial NIS enzymes. Rfs used diaminobutane, ornithine, diaminopentane and diaminopropane as nucleophiles. Site-directed mutagenesis showed that H484 is essential, and that L544 may govern nucleophile specificity. These data provide the first characterization of a fungal NIS enzyme.

We identified an uncharacterized siderophore, termed Band 4, in *Aspergillus terreus*. Band 4 did not restore growth of a *sidA* mutant of *A. fumigatus* suggesting that Band 4 is structurally unrelated to *A. fumigatus* hydroxamate siderophores. Studies of an *A. terreus sidA* mutant indicated that biosynthesis of Band 4 is not co-regulated with hydroxamate siderophores. An iron-regulated NIS homologue (AtNIS) was identified and recombinant AtNIS was generated. rAtNIS can be used to confirm its involvement in Band 4 biosynthesis.

Finally, I investigated whether siderophores could be detected in serum of patients at risk for invasive aspergillosis (IA) caused by *A. fumigatus*. We used UPLC-MS/MS to quantify the major *A. fumigatus* siderophore, *N,N',N"*-triacetylfusarinine C (TAFC) in serum. In >90 serum samples from at-risk patients, TAFC was diagnostic in 29 samples, and identified in an additional 28 serum samples. TAFC was not detected in healthy serum. Thus, serum siderophore detection may be a useful tool in the diagnosis of IA caused by *A. fumigatus*.

Keywords: Siderophore biosynthesis; NRPS-independent siderophore (NIS) synthetase; invasive aspergillosis; TAFC; rhizoferrin synthetase; *Aspergillus*; Mucorales

Dedication

To my parents, for your love and support. This work would not have been possible without you.

Acknowledgements

Firstly, I would thank my senior supervisor, Dr. Margo Moore for your guidance, support and endless optimism. This project was full of challenges and frustration, but your enthusiasm and encouragement (and endless supply of tea!) always renewed my hope and made this project what it is today. You are truly an inspiration and the example you set as a scientist, and as a person, are something I strive to achieve. Thank you.

I would like to thank my committee members, Drs. Andrew Bennet and James Kronstad. Your patient guidance and support throughout my PhD have been invaluable.

To all the Moore lab members, Juliana Yeung, Jason Nesbitt, Elizabeth Steves, Sebastian Ibarra Jimenez, Nazanin Ghavam and Janey Lam, thank you for making lab life fun. I'm so grateful to have you as lab-mates and friends. Alison Hadwin and Linda Pinto your guidance and counsel, both in science and my personal life, have played a fundamental role in me completing grad school. Thank you for your unwavering support when I needed you most. I would especially like to thank Dr. Isabelle Raymond-Bouchard for introducing me to the Moore lab and for first sparking my interest in research. Your mentorship and guidance helped me become the scientist I am today. Your enthusiasm is contagious and your passion for research and science is something I always admire. You are, and always have been, an inspiration to me. Thank you.

There have been a number of undergraduate students and research assistants who have worked on this project. Your hard work and dedication were beyond what I expected. Thank you to Clark Grieve, Jamie Baker, Lindsay Woof, Elizabeth Steves, Megan Young, Indu Murugathasan, Kirsten Mossington and Ashton Wickramaratne.

As part of my PhD, I was lucky enough to have the opportunity to go the University of St. Andrews in Scotland, UK. I would like to thank Dr. James Naismith and Huanting Liu for your support and guidance. I have carried the skills I learned in your lab throughout my PhD and they have made me a better biochemist. Thank you. While living in St. Andrews, I was welcomed by a great group of people. I would especially like to thank Aleksandria Ola Dziewulska, Miriam Weckener and Clarissa Melo Czekster for answering all my questions and making me feel at home in St. Andrews.

To the people at SFU who have helped me get to this point, Heather Coatsworth, Kaveh Rayan and Alison Li, thank you for welcoming me into your labs and for your invaluable assistance. Your contribution to my project has not gone unnoticed.

To my parents, I would not be where I am today without your love, guidance and support. There have been lots of ups and downs throughout my PhD and you have been there by my side throughout it all. You have been the inspiration for how far I've come in life. You taught me to never settle for mediocre and that is a lesson I truly appreciate. Thank you.

To my sister, Stephanie, and my friends, Cheryl, Dana and Logan, I cherish the laughs, dinners and wine nights that we have shared. You have patiently listened to my frustrations and to my successes and kept me sane and grounded throughout. You ladies are my rocks and I'm beyond lucky to have you as my friends and pseudo-therapists.

Matthew, you keep my life balanced (especially on the edge of two motorcycle tires!). Thank you for your unwavering support, and for being you and reminding me to be me.

Fresca, thank you for being the best listener (and snuggler) I could ever ask for. Your unconditional happiness and love are something I cherish.

Last, but not least, I would like to thank NSERC, the department of Biological Sciences and Graduate Studies at Simon Fraser University for financial support with research grants, scholarships and travel awards.

Table of Contents

List of Tables

List of Figures

List of Acronyms

ABC	ATP-binding cassette
ABPA	Allergic bronchopulmonary aspergillosis
AC	Accessory conidia
ADP	Adenosine diphosphate
AEPDA	1-aminoethyl-1,3-propanediamine
ahLys	N^6-acetyl-N^6-hydroxy-L-lysine
AMP	Adenosine monophosphate
AMT	*Agrobacterium*-mediated transformation
ATP	Adenosine triphosphate
BAL	Bronchoalveolar lavage
BG	1→3 β-D glucan
Bmc	Baulamycin
BSA	Bovine serum albumin
CAS	Chrome azurol S
CDART	Conserved domain architecture retrieval tool
CFU	Colony forming unit
CT	Computed tomography
DAP	Diaminopropionic acid
DCM	Dichloromethane
DHB	Dihydroxybenzoic acid
DHBS	Dihydroxybenzoyl spermidine
DHB-SC	Dihydroxybenzoyl spermidyl citrate
DKA	Diabetic ketoacidosis
ELISA	Enzyme-linked immunosorbent assay
EORTC	European Organization for Research and Treatment of Cancer/Invasive Fungal Infections Cooperative Group
FTMS	Fourier transform mass spectrometry
GA	Grimm Allen medium
GC	Gas chromatography
GFP	Green fluorescent protein
GM	Galactomannan
GVHD	Graft-versus-host disease
Hph	Hygromycin phosphotransferase

HPLC	High performance liquid chromatography
HR-MS	High resolution mass spectrometry
HRP	Horseradish peroxidase
HSCT	Hematopoietic stem cell transplant
IA	Invasive aspergillosis
ITS	Inter-transcribed
KLH	Keyhole limpet hemocyanin
LB	Luria-Bertani
LC	Liquid chromatography
LC-ESI-MS	Liquid chromatography electrospray ionization mass spectrometry
LFD	Lateral flow device
LLOQ	Lower limit of quantitation
LOD	Limit of detection
LOQ	Limit of quantitation
LVS	Live vaccine strain
MESG	7‑methyl-6-thio-guanosine
MFS	Major facilitator superfamily
MS	Mass spectrometry
NADH	Nicotinamide adenine dinucleotide
NIS	NRPS-independent siderophore
NMR	Nuclear magnetic resonance
NPV	Negative predictive value
NRPS	Non-ribosomal peptide synthetase
OMT	Outer member transporter
PBS	Phosphate buffered saline
PBST	Phosphate buffered saline + tween
PC	Phialidic conidia
PDA	Potato dextrose agar
PLP	Pyridoxal phosphate
PPV	Positive predictive value
QC	Quality control
RIA	Reductive iron assimilation
RMSD	Root mean square deviation
RNAi	Ribonucleic acid interference

RSD	Relative standard deviation
SAXS	Small angle X-ray scattering
SIT	Siderophore iron transporter
SLE	Systemic lupus erythematosus
SPBP	Siderophore periplasmic binding protein
TAFC	*N,N',N''*- triacetylfusarinine C
TLC	Thin layer chromatography
UPLC	Ultra high-performance liquid chromatography
YAG	Yeast extract agar glucose medium

Preface

Aims of thesis research

The overall goal of this work was to examine the biosynthesis and diagnostic importance of siderophores in pathogenic Mucorales fungi and members of the *Aspergillus* genus. I aimed to characterize biosynthesis of the polycarboxylate siderophore, rhizoferrin, in *Rhizopus delemar;* to identify the structure of a unique siderophore, and elucidate its biosynthesis, in *Aspergillus terreus*; and to determine if siderophores can be diagnostic of invasive aspergillosis in the serum of patients with suspected or probable disease.

Chapter 1 provides a general introduction to invasive fungal infections cause by members of the Mucorales order and fungi within the *Aspergillus* genus. The spectrum of infections caused by these fungi is outlined and the populations at risk are identified. Virulence factors are also introduced for these fungi, with a particular focus on iron acquisition mechanisms, including the presence of iron permeases and siderophore biosynthesis and secretion.

Chapter 2 describes non-ribosomal-peptide-synthetase (NRPS)-independent siderophore (NIS) synthetases and their role in siderophore biosynthesis. Four NIS enzymes, AlcC, AsbB, AcsD and IucA, have been crystallized recently and the biochemistry for AscD, AsbB and IucA has been elucidated. In this chapter, I review the enzymology of these and other known and predicted NIS enzymes, with a focus on amino acids important for their functioning, substrate specificities and desymmetrization reactions. I performed a phylogenetic analysis which groups NIS enzymes into four types, with support for a fifth type, based on their substrate specificity. The majority of known NIS enzymes have been characterized in Bacteria, however, I show that NIS homologs are present in all Domains, including Fungi and Archaea.

Chapter 3 describes the characterization of the NIS enzyme, Rfs, in *Rhizopus delemar*, which was predicted to be involved in biosynthesis of the polycarboxylate siderophore, rhizoferrin. Rhizoferrin secretion was confirmed in seven species of pathogenic Mucorales fungi, and *rfs* expression was confirmed to be iron-regulated in *R. delemar*. Rfs was cloned from *Rhizopus delemar* and was shown to be active with the predicted substrates, citric acid and diaminobutane, as well as with various substrate derivatives

including oxaloacetic acid, diaminopropane, diaminopentane, tricarballylic acid, hydroxylamine and ornithine. Attempts to crystallize Rfs were unsuccessful, however structural modelling predicted three amino acids to be involved in Rfs-mediated catalysis. These three mutants, R354A, H484A, L544R, were made using site-directed mutagenesis, plus an additional mutant, E209, which is conserved across all bacterial NIS enzymes. The activity of the individual Rfs mutants was analyzed with the native substrates and with specific substrate derivatives. These results provided insights into the mechanism of action of Rfs.

Chapter 4 discusses the identification of a putative siderophore, termed Band 4, produced by *A. terreus*. Band 4 was purified from iron-limited cultures of *A. terreus* and mass spectrometry (MS) analyses showed that it is not related to other siderophores secreted by the *Aspergilli*. Purified Band 4 supported the growth of a *Neurospora crassa* mutant strain deficient in *sidA*, the gene responsible for the first committed step in hydroxamate siderophore biosynthesis. MS of base hydrolyzed Band 4 showed that it consisted of dimerum acid, a component of the hydroxamate siderophore coprogen; however, an *A. terreus ΔsidA* mutant still produced Band 4, indicating an alternative biosynthetic pathway for Band 4. We identified an NIS homolog in *A. terreus* (AtNIS) and cloned and expressed the protein. Our aims were to investigate the substrate specificity of the recombinant AtNIS, and to compare the localization of the putative AtNIS in *A. terreus* with that of the validated NIS enzyme, Rfs in the Mucorales fungus, *Rhizopus delemar.*

Chapter 5 shows that the siderophore, *N,N',N''*-triacetylfusarinine C (TAFC) can be detected in serum from patients with a diagnosis of probable aspergillosis. TAFC was purified from *Aspergillus fumigatus* cultures and spiked into human serum at known concentrations. Extraction of TAFC from serum and LC-MS/MS analysis was optimized. This method showed lower and upper limits of quantitation (LOQ) of 5 ng/ml and 750 ng/ml, respectively, and complete TAFC recovery from spiked serum. As proof of concept, we evaluated 76 serum samples from 58 patients with suspected IA that were investigated for the presence of the cell wall carbohydrate, galactomannan (GM). Fourteen serum samples obtained from 11 patients diagnosed with probable or proven IA were also analyzed for the presence of TAFC. Control sera were analyzed and a TAFC cut-off value of ≥6 ng/ml was established. Of the 36 GM-positive samples from suspected IA patients, TAFC was considered positive in 25 (69%). TAFC was also found

in 28 additional GM-negative samples. TAFC was detected in 4 of the 14 samples (28%) from patients with proven/probable aspergillosis. Overall, we show that TAFC detection in serum can be diagnostic of IA, however prospective studies are needed to validate this detection method.

Chapter 6 provides a general discussion of the results, highlights advances which have been made using this research and provides suggestions for future research.

Chapter 1.

An Overview of Invasive Fungal Infections

Invasive fungal infections caused by members of the Mucorales order or fungi within the *Aspergillus* genus cause significant morbidity and mortality in humans. In this chapter, I present an overview of invasive infections caused by these fungi, their risk factors and treatment options.

1.1 Mucormycosis

Fungi within the Mucorales order are soil-dwelling saprotrophic filamentous fungi. Reproduction occurs asexually via production of specialized hyphae called sporangiophores that terminate in sporangia containing sporangiospores (spores) that are 3 – 8 µm in size. Spore germination produces haploid coenocytic hyphae. Sexual reproduction occurs through production of zygospores[1,2]. Fungi within the Mucorales order are used in the production of food products, organic acids, ethanol, and hydrolytic enzymes[3–7]. However, they are also zoonotic pathogens and may cause both cutaneous and invasive infections in animals, called mucormycosis. The most commonly isolated clinical specimen is *Rhizopus oryzae* (syn *Rhizopus delemar)*[8,9].

Populations at risk for mucormycosis include those with hematological malignancies, particularly acute myeloid leukemia[10], as well as hematopoietic stem cell transplant recipients (HSCT)[11], patients with uncontrolled diabetes[8] or those with elevated serum iron levels[12,13]. The primary site of infection is typically the lungs where sporangiospore germination occurs. Fungal hyphae can then penetrate the epithelial and endothelial barriers of the lung parenchyma and disseminate hematogenously[14]. Most mucormycosis infections are characterized by extensive angioinvasion resulting in vessel thrombosis and tissue necrosis[15]. Angioinvasion is likely a crucial step in disseminated infections. Disseminated mucormycosis, by far the most serious form of the disease, occurs when infection in one organ spreads to other organs, via the blood stream. Individuals with iron overload or profound immune-suppression are particularly susceptible to this form of infection[8]. Mortality rates for disseminated mucormycosis approach 100%, even with antifungal treatment[8,16].

Clinical manifestations of mucormycosis depend on the immune status of the host and the site of infection. Pulmonary mucormycosis typically occurs in neutropenic patients or other hematological malignancies and is associated with a non-productive cough and an unresponsive fever. Rhinocerebral forms occur in patients with diabetic ketoacidosis and result in frequent headaches and vision changes[13,17]**.** Recently, there has been an increase in the number of reported mucormycosis cases most likely due to the rising prevalence of risk factors such as diabetes, cancer and organ transplantation in developed countries[18,19].

Diagnosis of mucormycosis is not a trivial task. Conventional diagnosis relies on microscopic or histopathologic identification of fungal biomass in tissue specimens (Figure 1.1A) which is often hindered by harsh sample preparation; the resulting fragmented hyphae are difficult to identify[20]. Culturing the organism from the infected area can be diagnostic but as Mucorales fungi are ubiquitous, they can easily contaminate a culture especially when sampling non-sterile sites[21]. Amplification of Mucorales-specific DNA can be used to diagnose mucormycosis. However, DNA extraction for use in PCR is often done from formalin-fixed tissue samples and formalin fixation often damages DNA, ultimately hindering PCR[22] and the ubiquity of these fungi also complicate interpretation of PCR results from non-sterile sites. Computed tomography (CT) scans can also be used to diagnose invasive mucormycosis (Figure 1.1B); however, diagnosis of mucormycosis specifically is not possible without additional information, such as culture or PCR results[23,24]. Neither the galactomannan nor beta-glucan commercial test kits used for detection of *Aspergillus* species are applicable to Mucorales diagnosis because these compounds are not prominent in the cell walls of these fungi[25,26].

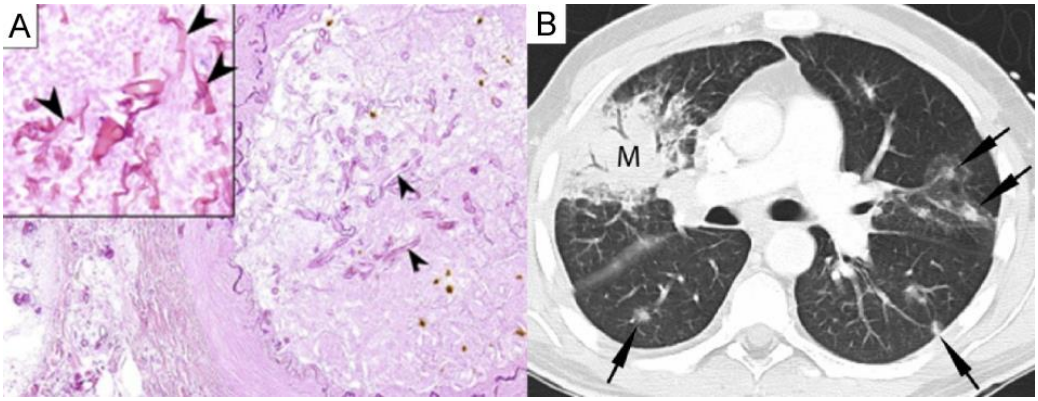

Figure 1.1[1,2]. Clinical features of mucormycosis used in diagnosis.
(**A**) Histopathology of infected lung section, stained with hematoxylin-and-eosin, shows wide, aseptate hyphae present within a pulmonary blood vessel (indicated by black arrows)[15]. (**B**) CT scan of patient with acute myeloid leukemia, showing multiple fungal lesions (black arrows) and a large fungal mass (M)[23].

Treatment of mucormycosis relies on surgical debridement and antifungal therapy with various antifungal agents including, amphotericin Band posaconazole[16,27,28]. However, resistance to azole drugs has already been reported[27,29,30] and the efficacy of these drugs is questionable at recommended doses[31].

1.2 Aspergillosis

Aspergillus fumigatus is a soil-dwelling saprophytic filamentous fungus that plays an important role in the aerobic degradation of organic matter and the recycling of environmental carbon and nitrogen[32]. *A. fumigatus* belongs to the phylum Ascomycota, *Aspergillus* subgenus, Fumigati section[33]. Asexual reproduction occurs via the production of specialized hyphae called conidiophores which produce chains of conidiospores (conidia) from phialides. These conidia are grey-green in colour, only 2 – 3 µm in size and, once they contact suitable media, give rise to haploid mycelia.

Airborne conidia from pathogenic members of the *Aspergillus* genus can be inhaled and travel through the respiratory tract to the alveoli of the lung. In immuno-competent

---

[1] Reprinted from Journal of Infection, 59 (2), Ben-Ami, R., Luna, M., Lewis, RE., Walsh, TJ., Kontoyiannis, DP., A clinicopathological study of pulmonary mucormycosis in cancer patients: Extensive angioinvasion but limited inflammatory response, 134-138, 2009, with permission from Elsevier.

[2] Reprinted from Clinical Infectious Diseases with permission from Oxford University Press

individuals, conidia are commonly cleared via the cilia lining the upper respiratory tract and in the lower respiratory tract, by the innate immune system (Figure 1.2). However, in immuno-compromised individuals, mycelial growth can occur resulting in one of several outcomes including, non-invasive allergic bronchopulmonary aspergillosis (ABPA), aspergilloma or invasive aspergillosis (IA)[33].

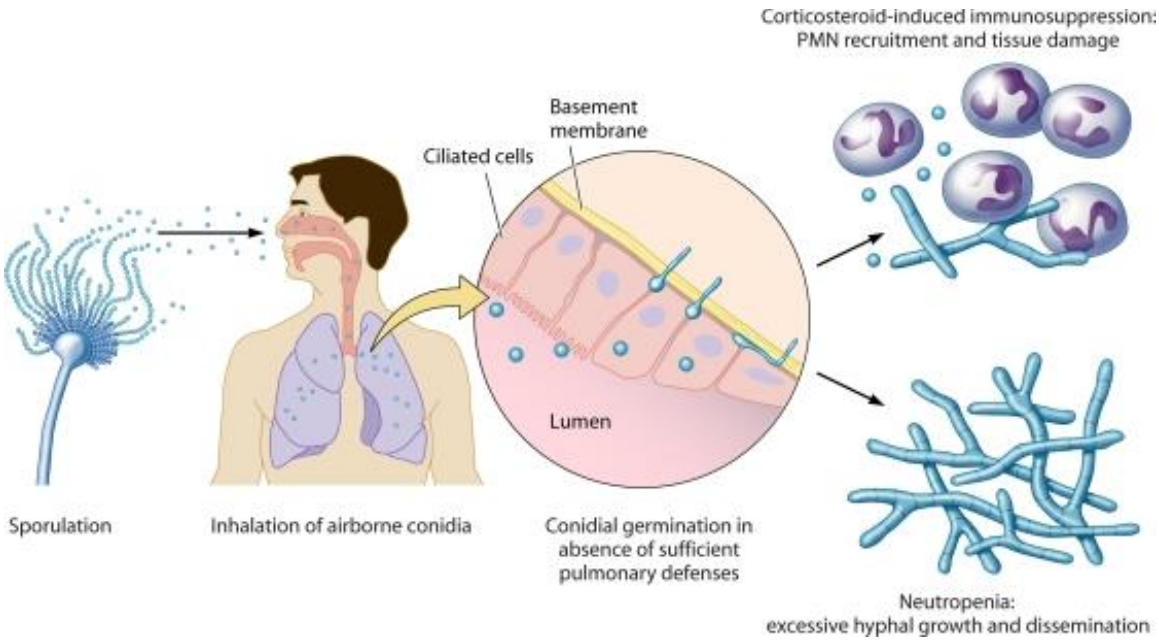

Figure 1.2[1]. Infective lifecycle of *Aspergillus fumigatus* in immuno-competent and immuno-suppressed individuals.

A. fumigatus spores are inhaled, travel to the alveoli and can cross the basement membrane of the lung. In immuno-competent hosts, polymorphonuclear (PMN) cells clear the invading hyphae, while in immuno-suppressed individuals these cells are not present and hyphae can proliferate. Figure reproduced with permission from Dagenais and Keller, 2009[34].

1.2.1 Allergic bronchopulmonary aspergillosis (ABPA)

ABPA commonly occurs in individuals with impaired mucociliary clearance, such as those with severe uncontrolled asthma or cystic fibrosis patients[35–37]. The prevalence of ABPA ranges from 1 to 15% in cystic fibrosis patients and 1 to 2% in chronic asthmatics[35]. In affected individuals, mucus accumulates in the bronchi, facilitating entrapment of the conidia thereby providing a suitable environment for establishment and growth of the fungus[37]. Symptoms of ABPA include coughing, wheezing,

[1] Reprinted from Clinical microbiology reviews, 22 (3), Dagenais, T and Keller, N. Pathogenesis of *Aspergillus fumigatus* in Invasive Aspergillosis, 447-465, 2009, with permission from the American Society of Microbiology.

inflammation and obstruction of the airway, which can lead to localized bronchiectasis (irreversible dilation of the bronchial tree) and fibrosis. Treatment for ABPA is possible through the use of oral corticosteroids or antifungal drugs[38]. Recent studies have shown that omalizumab, a monoclonal humanized IgE antibody, may be effective in treating ABPA, however, clinical trials are needed to confirm the efficacy of omalizumab[39].

1.2.2 Aspergilloma

Aspergilloma is a spherical fungal mass that develops in pre-existing lung cavities, typical in tuberculosis patients[40]. This 'fungal ball' consists of intertwined hyphae embedded in a protein matrix[41]. Typical symptoms of aspergilloma include hemoptysis, chronic cough and dyspnea. Treatment for aspergilloma is bleak as typical antifungal drugs are ineffective and surgical options, such as lobectomy, can result in severe morbidity and mortality[40,42].

1.2.3 Invasive aspergillosis

Invasive aspergillosis (IA) occurs when fungal spores germinate in the lungs and penetrate the epithelial and endothelial barriers of the lung parenchyma. Once in the blood stream, fungi will disseminate to other organs within the body.

The most common etiological agent of invasive aspergillosis is *Aspergillus fumigatus*, followed by *Aspergillus flavus*, *Aspergillus niger* and *A. terreus*[43]. *A. terreus* is primarily associated with IA[44], although aspergillomas and ABPA due to *A. terreus* have been reported[45,46].

Populations at risk for IA include patients with hematological malignancies, neutropenia, steroid use, or patients who have undergone transplantation, particularly allogenic transplantation, or developed graft-versus-host disease (GVHD)[43,44]. Patients with leukemia, prolonged neutropenia, or previous prophylactic antifungal exposure seem to be at an increased risk of developing IA from *A. terreus* compared to other aspergilli[44,47]. While there are cases of patients being asymptomatic for IA[48], typically, patients present with a fever and couch that are unresponsive to antibiotic therapy, dyspnea, hemoptysis and possible chest pain[49].

Diagnosis of IA is done by culturing the specimen from sites of infection. Histopathology of tissue biopsies and detection of fungal cell wall compounds, such as galactomannan and β-1,3-D-glucan in patient serum, can also be diagnostic of an infection[50]. CT scans are also recommended to diagnose IA and differentiate IA from aspergilloma. Fungal lesions typically have a 'halo' or ground glass appearance on CT scans due to hemorrhage and localized necrosis in invasive forms of disease (Figure 1.3)[50,51]. Other methods of diagnosis for IA are covered in depth in Chapter 5.

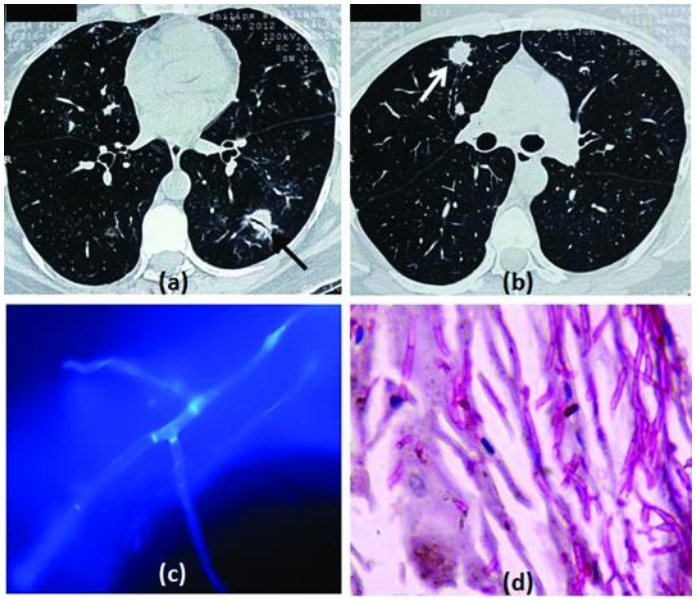

Figure 1.3[1] Contrast enhanced computed tomography thorax scan of an asthmatic patient on long-term steroid therapy.
A) Nodule present in the lower left and **B**) upper right lobe of the lung as indicated by arrows. A bronchoalveolar lavage (BAL) sample was taken and **C**) calcafluor white staining shows septate mycelia. **D**) Periodic acid–Schiff staining of lung tissue shows fungal hyphae with 45° branch angles, indicative of *Aspergilli*[51].

Treatment of IA relies on the antifungal azole drugs, voriconazole, itraconazole or posaconazole. The polyene, amphotericin B, can be used as an alternative treatment or as a prophylactic agent[50], however, *A. terreus* is particularly resistant to amphotericin B compared to other *Aspergillus* spp.[52]. Even with appropriate antifungal therapy, mortality rates for IA approach 100%[53].

[1] Figure reproduced, with permission, from Journal of clinical and diagnostic research: JCDR, 10 (4), Prasad, A., Agarwal, K., Deepak, D., Atwal, S., Pulmonary Aspergillosis: What CT can Offer Before it is too Late!, 1-5, 2016.

1.3 Virulence factors related to iron homeostasis

1.3.1 Mucormycosis

Numerous virulence factors have been suggested for mucormycosis including expression of the endothelial cell receptor GRP78[14], previous exposure to voriconazole[54], biofilm formation[55], sporangiospores size[56], rhizoxin production[57] as well as iron availability and uptake[58,59].

1.3.1.1 The iron permease, FTR1

The iron permease, FTR1, has been identified in *R. oryzae* as being responsible for iron uptake in iron-limited environments[60]. Expression of the *R. oryzae ftr1* gene in an *ftr1*-null *Saccharomyces cerevisiae* strain was shown to complement the null phenotype and restore the ability of the null mutant to grow in iron-limited media[60]. To confirm expression of FTR1 during mucormycosis infections, Ibrahim et al.[58] infected diabetic ketoacidotic (DKA) mice with a strain of *R. oryzae* expressing GFP under control of the FTR1 promoter. Histopathology of infected mouse brain tissue confirmed the presence of GFP. Interestingly, a homokaryotic *ftr1* null mutant could not be obtained in *R. oryzae* due to multi-nucleated spores, even after multiple rounds of single colony isolation and hyphal tipping. However, the authors were able to knock down expression of FTR1, using RNA interference (FTR1-RNAi). The FTR1-RNAi strain showed a reduction in ^{59}Fe uptake as well as reduced virulence and brain fungal burden in infected DKA mice. Thus, expression of FTR1 was shown to be a virulence factor for *R. oryzae* pathogenesis.

1.3.1.2 Deferoxamine treatment

Patients being treated with deferoxamine, a metal chelator used to treat iron or aluminum overload, are at an increased risk of developing mucormycosis[17]. For example, out of 25 dialysis patients who developed mucormycosis, 22 of them were receiving deferoxamine therapy. Furthermore, post mortem analysis showed that all 22 patients were infected by *Rhizopus* species[61]. *In vivo* experiments later revealed that deferoxamine acts as a siderophore to *Rhizopus*, supplying it with previously unavailable iron and thereby abolishing the fungistatic properties of serum[59]. Treatment with other iron chelators, such as deferiprone, starves *Rhizopus* species of iron and therefore does

not promote growth of the fungus *in vivo*[62]. Interestingly, treating diabetic patients with mucormycosis with the iron chelator, deferasirox, showed promising results *in vitro* and in mouse models; however these results were not reflected in a clinical trial for treatment[63].

1.3.2 Invasive aspergillosis

In *Aspergillus fumigatus*, compounds such as gliotoxins[64–67], various proteases[68] and conidia surface components such as hydrophobic proteins[69] and sialic acid residues[70,71] have been shown to contribute to, but are not essential for, virulence. However, iron uptake via siderophores, low molecular weight iron (III) chelators, has been shown to be essential for virulence in *A. fumigatus*[72,73].

1.3.2.1 Iron uptake

Schrettl et al. (2004)[73] identified three genes related to iron uptake in *A. fumigatus*. The *ftrA* gene was identified as a high affinity iron permease, *sidA* was identified as an L-ornithine-N^5-monooxygenase involved in siderophore biosynthesis and *fetC* is a ferroxidase. Individual deletion mutants were made for *ftrA (ΔftrA)* and *sidA (ΔsidA)* and a double deletion mutant was made for both *ftrA* and *sidA (ΔftrA ΔsidA*) in *A. fumigatus*. When grown in iron-limited media, the *ΔftrA* strain produced significantly higher amounts of the siderophore*, N,N',N''*-triacetylfusarinine C, while the *ΔsidA* strain displayed reduced growth and did not produce siderophores. The double mutant displayed no growth on most media, unless supplemented with siderophores. In a mouse model for IA, the *ΔftrA* strain remained virulent and caused similar mortality as the *A. fumigatus* wildtype strain. These data indicate that reductive iron assimilation is not required for virulence of *A. fumigatus*. In contrast, the *ΔsidA* strain was avirulent in an IA mouse model, demonstrating that siderophore-mediated iron acquisition is an essential virulence factor for *A. fumigatus*.

Hissen et al. (2005)[72] created a *sidA* deletion mutant in *A. fumigatus* and, in contrast to Schrettl et al. (2004)[73], showed that growth of the mutant strain was completely inhibited in iron-limited or serum-containing media without siderophore supplementation. A mouse model for IA also confirmed that the *A. fumigatus* Δ*sidA* strain was avirulent.

Siderophore biosynthesis and iron uptake play important roles in the virulence of the invasive mycoses described above. This thesis aims to further elucidate the biosynthesis and diagnostic importance of siderophores in these pathogenic fungi.

1.4 References

1. Sharma, O. P. *Textbook Of Fungi*. (Tata McGraw-Hill Education, 1989).

2. Gryganskyi, A. P. *et al.* Structure, function, and phylogeny of the mating locus in the *Rhizopus oryzae* complex. *PLoS One* **5,** e15273 (2010).

3. Huang, L. P., Jin, B., Lant, P. & Zhou, J. Biotechnological production of lactic acid integrated with potato wastewater treatment by *Rhizopus arrhizus*. *J. Chem. Technol. Biotechnol.* **78,** 899–906 (2003).

4. Celestino, K. R. S., Cunha, R. B. & Felix, C. R. Characterization of a beta-glucanase produced by *Rhizopus microsporus var. microsporus*, and its potential for application in the brewing industry. *BMC Biochem.* **7,** 23 (2006).

5. Abdel-Razek, A. S., Abdel-Ghany, T. M., Mahmoud, S. A., El-Sheikh, H. H. & Mahmoud, M. S. The use of free and immobilized *Cunninghamella elegans* for removing cobalt ions from aqueous waste solutions. *World J. Microbiol. Biotechnol.* **25,** 2137–2145 (2009).

6. Ylitervo, P. Production of ethanol and biomass from orange peel waste by *Mucor indicus*. University College of Borås, School of Engineering (2008).

7. Chang, C.-T. *et al.* Effect of fermentation time on the antioxidant activities of tempeh prepared from fermented soybean using *Rhizopus oligosporus*. *Int. J. Food Sci. Technol.* **44,** 799–806 (2009).

8. Roden, M. M. *et al.* Epidemiology and outcome of zygomycosis: a review of 929 reported cases. *Clin. Infect. Dis.* **41,** 634–53 (2005).

9. Alvarez, E. *et al.* Spectrum of zygomycete species identified in clinically significant specimens in the United States. *Society* **47,** 1650–1656 (2009).

10. Pagano, L. *et al.* Mucormycosis in patients with haematological malignancies: a retrospective clinical study of 37 cases. *Br. J. Haematol.* **99,** 331–336 (1997).

11. Sun, H. Y. & Singh, N. Emerging importance of infections due to zygomycetes in organ transplant recipients. *Int. J. Antimicrob. Agents* **32,** 115–118 (2008).

12. Boelaert, J. R., Van Cutsem, J., de Locht, M., Schneider, Y. J. & Crichton, R. R. Deferoxamine augments growth and pathogenicity of *Rhizopus*, while hydroxypyridinone chelators have no effect. *Kidney Int.* **45,** 667–71 (1994).

13. Spellberg, B., Jr, J. E., Ibrahim, A. & Edwards, J. Novel perspectives on mucormycosis : Pathophysiology, presentation, and management. *Clin. Microbiol.*

Rev. **18,** 556–569 (2005).

14. Liu, M. *et al.* The endothelial cell receptor GRP78 is required for mucormycosis pathogenesis in diabetic mice. *J. Clin. Invest.* **120,** 1914–1924 (2010).

15. Ben-Ami, R., Luna, M., Lewis, R. E., Walsh, T. J. & Kontoyiannis, D. P. A clinicopathological study of pulmonary mucormycosis in cancer patients: extensive angioinvasion but limited inflammatory response. *J. Infect.* **59,** 134–8 (2009).

16. Skiada, a *et al.* Zygomycosis in Europe: analysis of 230 cases accrued by the registry of the European Confederation of Medical Mycology (ECMM) working group on zygomycosis between 2005 and 2007. *Clin. Microbiol. Infect.* **17,** 1859–67 (2011).

17. Petrikkos, G. *et al.* Epidemiology and clinical manifestations of mucormycosis. *Clin. Infect. Dis.* **54 Suppl 1,** S23-34 (2012).

18. Marr, K. A, Carter, R. A, Crippa, F., Wald, A. & Corey, L. Epidemiology and outcome of mould infections in hematopoietic stem cell transplant recipients. *Clin. Infect. Dis.* **34,** 909–17 (2002).

19. Bitar, D. *et al.* Increasing incidence of zygomycosis (mucormycosis), France, 1997-2006. *Emerg. Infect. Dis.* **15,** 1395–401 (2009).

20. Lass-Flörl, C. Zygomycosis: conventional laboratory diagnosis. *Clin. Microbiol. Infect.* **15 Suppl 5,** 60–5 (2009).

21. Hachem, R. Y. *et al.* Utility of galactomannan enzyme immunoassay and (1,3) beta-D-glucan in diagnosis of invasive fungal infections: low sensitivity for *Aspergillus fumigatus* infection in hematologic malignancy patients. *J. Clin. Microbiol.* **47,** 129–33 (2009).

22. Dannaoui, E. *et al.* Molecular detection and identification of zygomycetes species from paraffin-embedded tissues in a murine model of disseminated zygomycosis: a collaborative European Society of Clinical Microbiology and Infectious Diseases (ESCMID) Fungal Infection Study G. *J. Clin. Microbiol.* **48,** 2043–6 (2010).

23. Lanternier, F. *et al.* Mucormycosis in organ and stem cell transplant recipients. *Clin. Infect. Dis.* **54,** 1629–36 (2012).

24. Lass-Flörl, C. *et al.* The value of computed tomography-guided percutaneous lung biopsy for diagnosis of invasive fungal infection in immunocompromised patients. *Clin. Infect. Dis.* **45,** e101-4 (2007).

25. Ibrahim, A. S. *et al.* Genomic analysis of the basal lineage fungus *Rhizopus oryzae* reveals a whole-genome duplication. *Genome* **5,** (2009).

26. Kontoyiannis, D. P. & Lewis, R. E. How I treat mucormycosis. *Blood* **118,** 1216–24 (2011).

27. Almyroudis, N. G., Sutton, D. A, Fothergill, A. W., Rinaldi, M. G. & Kusne, S. In vitro susceptibilities of 217 clinical isolates of zygomycetes to conventional and new antifungal agents. *Antimicrob. Agents Chemother.* **51,** 2587–90 (2007).

28. Perkhofer, S. *et al.* Posaconazole enhances the activity of amphotericin B against hyphae of zygomycetes in vitro. *Antimicrob. Agents Chemother.* **52,** 2636–8 (2008).

29. Gómez-López, A., Cuenca-Estrella, M., Monzón, A. & Rodriguez-Tudela, J. L. In vitro susceptibility of clinical isolates of Zygomycota to amphotericin B, flucytosine, itraconazole and voriconazole. *J. Antimicrob. Chemother.* **48,** 919–21 (2001).

30. Salas, V. *et al.* In vitro and in vivo activities of posaconazole and amphotericin B in a murine invasive infection by *Mucor circinelloides*: poor efficacy of posaconazole. *Antimicrob. Agents Chemother.* **56,** 2246–50 (2012).

31. Ibrahim, A. S. *et al.* Caspofungin inhibits *Rhizopus oryzae* 1,3-beta-D-Glucan synthase, lowers burden in brain measured by quantitative PCR, and improves survival at a low but not a high dose during murine disseminated zygomycosis. *Antimicrob. Agents Chemother.* **49,** 721–727 (2005).

32. Latgé, J. P. *Aspergillus fumigatus* and Aspergillosis. *Clin. micro* **12,** 310–350 (1999).

33. Sugui, J. A., Kwon-Chung, K. J., Juvvadi, P. R., Latgé, J.P. & Steinbach, W. J. *Aspergillus fumigatus* and Related Species. *Cold Spring Harb Perspect Med* **5,** a019786 (2015).

34. Dagenais, T. R. T. & Keller, N. P. Pathogenesis of *Aspergillus fumigatus* in Invasive Aspergillosis. *Clin. Microbiol. Rev.* **22,** 447–65 (2009).

35. Stevens, D. a *et al.* Allergic bronchopulmonary aspergillosis in cystic fibrosis--state of the art: Cystic Fibrosis Foundation Consensus Conference. *Clin. Infect. Dis.* **37 Suppl 3,** S225-64 (2003).

36. Mortensen, K. L. *et al.* A prospective survey of *Aspergillus* spp. in respiratory tract samples: prevalence, clinical impact and antifungal susceptibility. *Eur. J. Clin. Microbiol. Infect. Dis.* **30,** 1355–63 (2011).

37. Pihet, M. *et al.* Occurrence and relevance of filamentous fungi in respiratory secretions of patients with cystic fibrosis--a review. *Med. Mycol.* **47,** 387–97 (2009).

38. Knutsen, A. Allergic bronchopulmonary aspergillosis in asthma. *Expert Rev. Clin. Immunol.* **13,** 11–14 (2017).

39. Nové-Josserand, R. *et al.* Case series of omalizumab for allergic bronchopulmonary aspergillosis in cystic fibrosis patients. *Pediatr. Pulmonol.* **52,** 190–197 (2017).

40. Muniappan, A. *et al.* Surgical therapy of pulmonary aspergillomas: A 30-year

North American experience. *Ann. Thorac. Surg.* **97,** 432–438 (2014).

41. Moodley, L., Pillay, J. & Dheda, K. Aspergilloma and the surgeon. *J. Thorac. Dis.* **6,** 202–9 (2014).

42. Kim, Y. T., Kang, C., Sung, S. W. & Kim, J. H. Good long-term outcomes after surgical treatment of simple and complex pulmonary aspergilloma. *Ann Thorac Surg* **79,** 294–8 (2005).

43. Steinbach, W. J. *et al.* Clinical epidemiology of 960 patients with invasive aspergillosis from the PATH Alliance registry. *J. Infect.* **65,** 453–464 (2012).

44. Hachem, R. *et al.* Invasive aspergillosis caused by *Aspergillus terreus*: an emerging opportunistic infection with poor outcome independent of azole therapy. *J. Antimicrob. Chemother.* **69,** 3148–3155 (2014).

45. Laham, M. N. & Carpenter, J. L. *Aspergillus terreus,* a pathogen capable of causing infective endocarditis, pulmonary mycetoma, and allergic bronchopulmonary aspergillosis. *Am. Rev. Respir. Dis.* **125,** 769–72 (1982).

46. Khan, Z. U. *et al.* Bilateral pulmonary aspergilloma caused by an atypical isolate of *Aspergillus terreus*. *J. Clin. Microbiol.* **38,** 2010–4 (2000).

47. José Castó, J. *et al.* Risk factors for pulmonary *Aspergillus terreus* infection in patients with positive culture for filamentous fungi. *Chest* **131,** 230–236 (2007).

48. Qin, J. *et al.* Radiological and clinical findings of 25 patients with invasive pulmonary aspergillosis: retrospective analysis of 2150 liver transplantation cases. *Br. J. Radiol.* **85,** e429-35 (2012).

49. Yasuoka, A., Tachikawa, N., Shimada, K., Kimura, S. & Oka, S. (1->3) beta-D-glucan as a quantitative serological marker for *Pneumocystis carinii* pneumonia. *Clin. Vaccine Immunol.* **3,** 3–6 (1996).

50. Patterson, T. F. *et al.* Practice guidelines for the diagnosis and management of aspergillosis: 2016 update by the Infectious Diseases Society of America. *Clin. Infect. Dis.* **63,** e1–e60 (2016).

51. Prasad, A., Agarwal, K., Deepak, D. & Atwal, S. S. Pulmonary aspergillosis: What CT can offer before it is too late! *J. Clin. Diagn. Res.* **10,** TE01-5 (2016).

52. Mortensen, K. L. *et al.* A prospective survey of *Aspergillus spp*. in respiratory tract samples: prevalence, clinical impact and antifungal susceptibility. *Eur. J. Clin. Microbiol. Infect. Dis.* **30,** 1355–1363 (2011).

53. Steinbach, W. J. *et al.* Infections due to *Aspergillus terreus*: A multicenter retrospective analysis of 83 cases. *Clin Infect Dis* **39,** 192–198 (2004).

54. Lamaris, G. a *et al.* Increased virulence of Zygomycetes organisms following exposure to voriconazole: a study involving fly and murine models of zygomycosis. *J. Infect. Dis.* **199,** 1399–406 (2009).

55. Singh, R., Shivaprakash, M. R. & Chakrabarti, A. Biofilm formation by zygomycetes: quantification, structure and matrix composition. *Microbiology* **157,** 2611–8 (2011).

56. Li, C. H. *et al.* Sporangiospore size dimorphism is linked to virulence of *Mucor circinelloides*. *PLoS Pathog.* **7,** e1002086 (2011).

57. Partida-Martinez, L. P. & Hertweck, C. Pathogenic fungus harbours endosymbiotic bacteria for toxin production. *Nature* **437,** 884–8 (2005).

58. Ibrahim, A. S. *et al.* The high affinity iron permease is a key virulence factor required for *Rhizopus oryzae* pathogenesis. *Mol. Microbiol.* **77,** 587–604 (2010).

59. Boelaert, J. R. *et al.* Mucormycosis during deferoxamine therapy is a siderophore-mediated infection. *In vitro* and *in vivo* animal studies. *J. Clin. Invest.* **91,** 1979–86 (1993).

60. Fu, Y. *et al.* Cloning and functional characterization of the *Rhizopus oryzae* high affinity iron permease (rFTR1) gene. *FEMS Microbiol. Lett.* **235,** 169–176 (2004).

61. Boelaert, J., Fenves, A. & Coburn, J. Registry on mucormycosis in dialysis patients. *J. Infect. Dis.* **160,** 914 (1989).

62. Ibrahim, A. S., Edwards, J. E., Fu, Y. & Spellberg, B. Deferiprone iron chelation as a novel therapy for experimental mucormycosis. *J. Antimicrob. Chemother.* **58,** 1070–3 (2006).

63. Spellberg, B. *et al.* The Deferasirox-AmBisome Therapy for mucormycosis (DEFEAT Mucor) study: a randomized, double-blinded, placebo-controlled trial. *J. Antimicrob. Chemother.* **67,** 715–22 (2012).

64. Sutton, P., Waring, P. & Müllbacher, A. Exacerbation of invasive aspergillosis by the immunosuppressive fungal metabolite, gliotoxin. *Immunol. Cell Biol.* **74,** 318–22 (1996).

65. Bok, J. W. *et al.* GliZ, a transcriptional regulator of gliotoxin biosynthesis, contributes to *Aspergillus fumigatus* virulence. *Infect. Immun.* **74,** 6761–8 (2006).

66. Sugui, J. a *et al.* Gliotoxin is a virulence factor of *Aspergillus fumigatus: gliP* deletion attenuates virulence in mice immunosuppressed with hydrocortisone. *Eukaryot. Cell* **6,** 1562–9 (2007).

67. Spikes, S. *et al.* Gliotoxin production in *Aspergillus fumigatus* contributes to host-specific differences in virulence. *J. Infect. Dis.* **197,** 479–86 (2008).

68. Monod, M., Jaton-Ogay, K., Fatih, A., Paris, S. & Latgé, J.-P. The secreted proteases of pathogenic species of *Aspergillus* and their possible role in virulence. *Botany* **73,** 1081–1086 (1995).

69. Thau, N. *et al.* rodletless mutants of *Aspergillus fumigatus*. *Infect. Immun.* **62,** 4380–8 (1994).

70. Wasylnka, J. A., Simmer, M. I. & Moore, M. M. Differences in sialic acid density in pathogenic and non-pathogenic *Aspergillus* species. *Microbiology* **147,** 869–77 (2001).

71. Nesbitt, J. R. *et al.* The *Aspergillus fumigatus* sialidase (Kdnase) contributes to cell wall integrity and virulence in amphotericin B-treated mice. *Front. Microbiol.* **8,** 1–17 (2018).

72. Hissen, A. H. T., Wan, A. N. C., Warwas, M. L., Pinto, L. J. & Moore, M. M. The *Aspergillus fumigatus* siderophore biosynthetic gene *sidA*, encoding L-Ornithine-N^5-Oxygenase, is required for virulence. *Infect. Immun.* **73,** 5493–5503 (2005).

73. Schrettl, M. *et al.* Siderophore biosynthesis but not reductive iron assimilation is essential for *Aspergillus fumigatus* virulence. *J. Exp. Med.* **200,** 1213–9 (2004).

Chapter 2.

Ironing Out Siderophore Biosynthesis: A Review of Non-Ribosomal Peptide Synthetase (NRPS) Independent Siderophore Synthetases

This chapter describes characterized NIS enzymes, their biosynthetic pathways, and mechanisms of action. It also compares known NIS enzymes to predicted NIS enzymes. This chapter has been submitted as a manuscript to Critical Reviews in Biochemistry and Molecular Biology under the authorship of Cassandra Carroll and Margo Moore. Unless otherwise noted, all structural modelling figures and biosynthetic pathway figures were made by Cassandra Carroll.

2.1 Abstract

Iron is required for microbial growth and proliferation. To survive in low-iron environments, some microorganisms secrete ferric iron chelators called siderophores. Siderophore biosynthesis occurs via two pathways: the non-ribosomal peptide synthetase (NRPS) pathway and the NRPS-independent siderophore (NIS) synthetase pathway. NIS enzymes function by adenylating a carboxylic acid substrate, typically citrate or a derivative, followed by nucleophilic capture of an amine or alcohol substrate. In this review, we summarize recent advances in NIS biochemistry with a particular focus on structural biology and confirm the classification of NIS enzymes into Types A, A', B and C based on substrate specificity. Based on a phylogenetic analysis, we also propose a new subclass of NIS enzymes, Type C', responsible for dimerization and macrocyclization of complex and substituted amine or amide intermediates. Finally, we describe the role of NIS enzymes in virulence of pathogenic microbes and discuss NIS inhibitors as potential anti-microbial agents.

2.2 Microbial iron acquisition

With few exceptions, iron is an essential element for the growth of microorganisms. Because iron can exist in both ferrous (Fe^{2+}) and ferric (Fe^{3+}) forms, it is an efficient redox catalyst for numerous cellular functions including electron transport, amino acid

biosynthesis, DNA synthesis and glycolysis. The concentration of bioavailable ferric iron in the environment at neutral pH ranges from 10^{-8} to 10^{-9} M; however, microorganisms typically require ferric iron concentrations of 10^{-6} M for growth[1]. For pathogenic microbes, obtaining iron from vertebrate hosts is even more challenging: iron-binding proteins in the host maintain very low levels of free ferric iron in serum and body fluids. Thus, microbes have evolved various strategies to obtain adequate iron to support growth including, acidification of the medium, ferric oxidoreductase/permeases[2–4], secretion of hemolysins[5,6], transferrin and heme uptake[7,8] and siderophore secretion. In this review, we focus on the biosynthesis of siderophores using the NIS pathway.

Siderophores are low molecular weight organic molecules secreted into the environment under iron-limiting conditions that chelate ferric iron. They are produced by numerous species of bacteria and fungi. The affinity constants for siderophore-iron complexes are measured as pM values and calculated based on standard concentrations of free iron (1 µM) and siderophore (10 µM) at a pH of 7.4 (Table 2.1). The high affinity for ferric iron allows siderophores to scavenge iron from minerals in soil, marine and fresh water, and from plants or other organisms[9].

Table 2.1 pM values for various Fe(III)-siderophore complexes.

Siderophore complex	pM value[1]
Enterobactin[10]	35.5
N,N′,N″-triacetylfusarinine C[3]	31.8
Desferrioxamine B[11]	26.6
Ferricrocin[12]	26.5
Transferrin[13]	23.6
Aerobactin[13]	23.3
Rhizoferrin[10]	19.7

[1] The pM value is calculated as the negative log of the concentration of free iron in a solution at pH 7.4 in which the concentration of iron is 1 µM and the chelator is 10µM.

In general, siderophores are synthesized within the cell and secreted into the environment as iron-free (desferri-) compounds. Once bound by ferric iron (ferrated), they are taken up into the cytosol of the cell using a variety of uptake systems. In Gram negative bacteria, the ferrated siderophore is recognized by high affinity outer membrane transport (OMT) proteins and transported into the periplasm. A siderophore periplasmic binding protein (SPBP) recognizes the ferrated siderophore and TonB shuttles the complex to an ATP-binding cassette (ABC) protein on the inner membrane. The complex is then transported into the cytoplasm in an ATP-dependent manner. A

similar mechanism is employed by Gram positive bacteria but without the OMT and periplasmic TonB proteins[14]. Once in the cytosol, ferric iron is reduced by an iron reductase enzyme and, as siderophores have a lower affinity for ferrous iron, Fe^{2+} is released from the siderophore. In Fungi, siderophore iron transporters (SITs) actively transport siderophores across the plasma membrane[15]. In some fungi, there is evidence that the ferri-siderophore complex is taken up into the cell where it is degraded, releasing free iron into the cell[16,17]. Uptake of free ferrous iron after reduction at the cell surface is also possible in several fungal species[2–4,18].

2.3 Siderophore classes

There are four classes of siderophores based on the chemical moieties that donate ligands to coordinate Fe(III). These include hydroxamate, catecholate, carboxylate siderophores as well as mixed siderophores that use a combination of donor group configurations to chelate ferric iron. Representative siderophores from each class are shown in Figure 2.1.

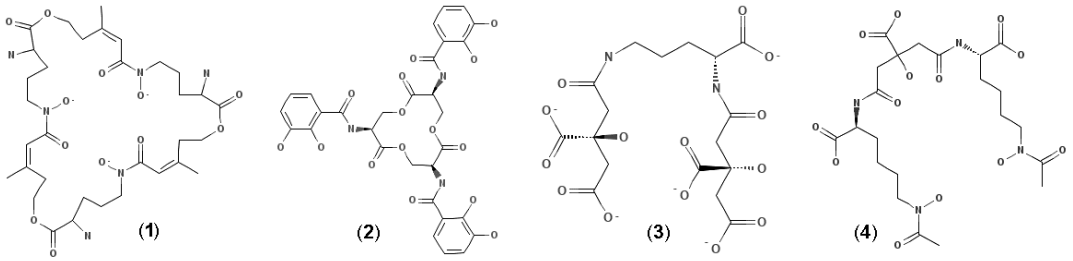

Figure 2.1 Representative siderophores for each of the four classes.
N,N′,N″-triacetylfusarinine C (1) is a hydroxamate siderophore[19], enterobactin (2) is a catecholate siderophore[20], staphyloferrin A (3) is a polycarboxylate siderophore[21,22] and aerobactin (4) is a mixed hydroxamate-polycarboxylate siderophore[23] using both carboxylate and hydroxamate groups to coordinate iron.

Typically, charged oxygen groups are used as donor atoms, and most siderophores coordinate iron in the thermodynamically-favourable hexadentate conformation[9].

2.4 Siderophore biosynthesis

Siderophore biosynthesis occurs via two main pathways; the first pathway uses non-ribosomal peptide synthetase (NRPS) enzymes. NRPS are modular, multi-domain enzymes in which the alkylation, thiolation and condensation domains function in a

coordinated and sequential fashion to link amino acids via thiol-based intermediates. Siderophores biosynthesized via NPRS enzymes include, yersiniabactin (*Yersinia pestis)*[24], vibriobactin (*Vibrio cholerae)*[25], mycobactin (*Mycobacterium tuberculosis)*[26] and enterobactin (*Escherichia coli)*[27].

The focus of this review is siderophore biosynthesis by NRPS-independent siderophore (NIS) synthetases. NIS synthetases are responsible for a single enzymatic reaction and typically function to condense citric acid, or a derivative, with an amine or alcohol group. NIS enzymes all possess a conserved N-terminal IucA/IucC domain and have a C-terminal domain related to iron transport or metabolism.

Here, we present recent advances in NIS synthetase enzymology, with a focus on structural biology. This review will also re-examine the classification of NIS enzymes and provide an update on characterized NIS synthetases, their mechanism of action and the role of NIS enzymes in the virulence of microbial pathogens.

2.5 The distribution of putative NIS enzymes

We used the sequence of the conserved IucA (Iron uptake chelate) domain involved in the biosynthesis of aerobactin from *Escherichia coli* (accession: ABA54740.1) to search for proteins using the Conserved Domain Architecture Retrieval Tool (CDART)[28]. This search returned 21 different domain architectures, each containing an IucA domain with various other domains, such as ferric iron reductase (FhuF) or acetyltransferase domains. The most common domains reported were IucA alone (16, 818 sequences predicted/known to have this domain), and IucA with an FhuF domain, common to many NIS enzymes (791 sequences). Interestingly, while NIS enzymes have only been characterized in Bacteria and one species of Fungi, there are many predicted NIS sequences in Fungi, and a few in slime molds, a paraphyletic group within Eukarya and Archaea. More details on Archaeal NIS enzymes are provided in Section 2.9. Figure 2.2 depicts the origin for the 791 sequences predicted to have both IucA and FhuF domains.

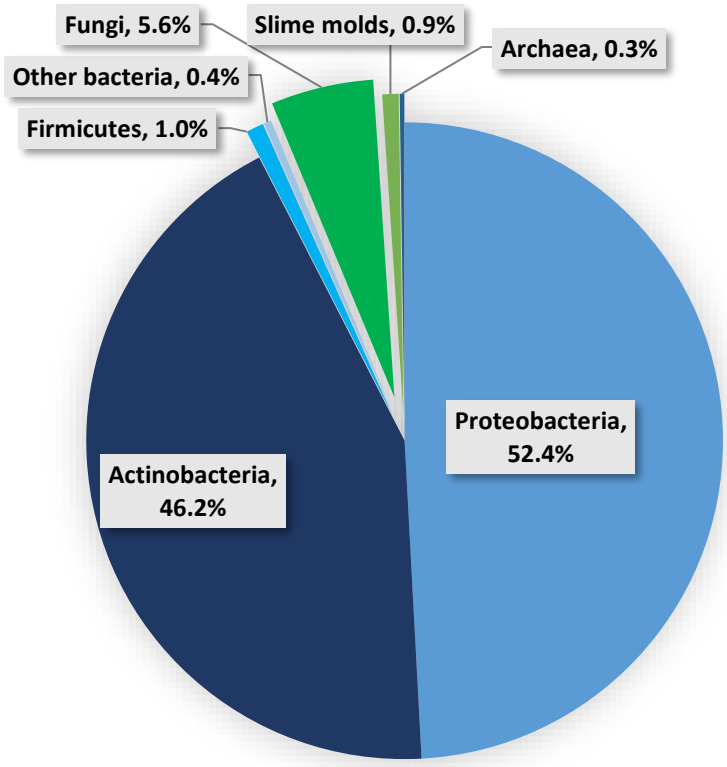

Figure 2.2 CDART[28] analysis of proteins containing IucA and FhuF domains. Most of the sequences are from Bacteria; however, Fungi and two species of Archaea are predicted to have NIS enzymes. Fungi predicted to have NIS enzymes include Basidiomycetes, Mucorales, Ascomycetes, and Kickxellales. Archaea predicted to have NIS enzymes are from the genera *Haloterrigena* and *Halovivax*.

It should be noted that the distribution of NIS enzymes presented here is influenced by the proportion of organisms which have been sequenced. As the number of sequenced organisms increases across all Domains, so too should the number of predicted NIS enzymes.

2.6 Phylogenetic analysis of characterized NIS enzymes

Phylogenetic analysis of NIS synthetases by Oves-Costales (2009)[29] grouped them into four Types: A, A', B and C based on their substrate specificity. Type A enzymes have specificity for citric acid and mono-amine or amide substrates. A subclass of Type A enzymes, classified as Type A', are grouped based on the enantioselective nature of the substrates and the chirality of the final siderophore. Type B enzymes are specific for α-ketoglutarate and citryl-amine intermediates whereas Type C enzymes are specific for monoamine or amide substrates with citryl- or succinyl- based intermediates. This

classification system was based on the function of known NIS synthetases as well as NIS enzymes with a predicted function[29,30]. Since 2009, the number of characterized NIS enzymes has increased from 10 to 17, and our understanding of their mechanism of action has increased significantly. We therefore performed a phylogenetic analysis using 17 validated and six proposed NIS synthetases. The results show that with current data, NIS enzymes separate into five rather than four Types, with Type C enzymes forming a phylogenetically-distinct group, though the enzymes in each group remain the same (Figure 2.3).

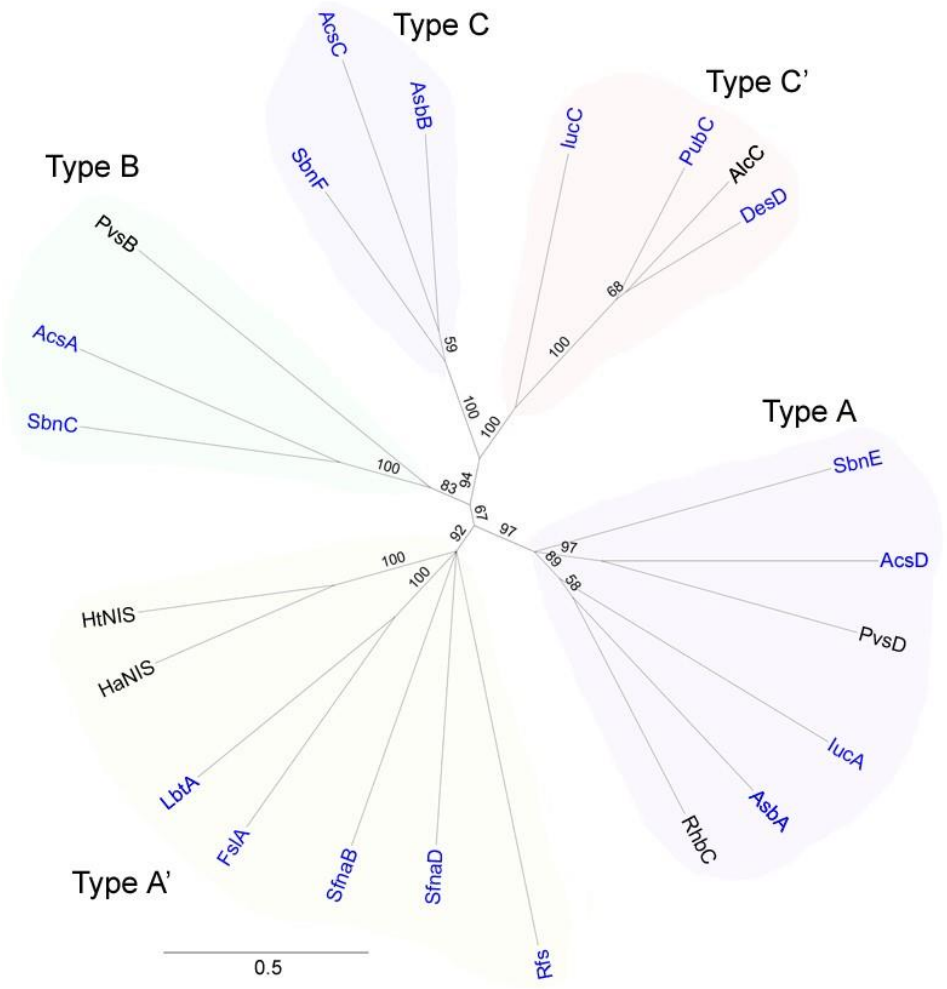

Figure 2.3 Phylogenetic analysis of 17 validated and six proposed bacterial NIS protein sequences using a MUSCLE alignment.

Phylogenetic analysis of 17 validated and six proposed bacterial NIS protein sequences using a MUSCLE alignment. The neighbour-joining phylogenetic tree was constructed using Geneious 11.0[31] and bootstrap values are indicated at branch nodes. Enzymes in blue have been biochemically characterized or gene knockout studies have confirmed their involvement in siderophore biosynthesis. HtNIS and HaNIS are predicted NIS enzymes from Archaea, discussed below. NIS enzyme sequences used in the tree and the siderophore they biosynthesize are as

follows: AsbB and AsbA – anthrax siderophore biosynthesis (petrobactin); DesD – desferrioxamine biosynthesis[32]; AlcC – alcaligin biosynthesis; FslA – rhizoferrin biosynthesis; SfnaB and SfnaD – staphyloferrin A biosynthesis; SbnF and SbnE – staphyloferrin B biosynthesis; LbtA – rhizoferrin biosynthesis; RhbC – rhizobactin biosynthesis[33]; IucA and IucC – aerobactin biosynthesis; AcsD and AcsC – achromobactin biosynthesis; PvsD – vibrioferrin biosynthesis[34]; PubC – putrebactin biosynthesis[35]. References for NIS enzymes not provided in the caption are provided in the text below.

Type C NIS enzymes have two separate branches; therefore, the previous classification of Type C NIS enzymes may be split into Type C enzymes, that condense a mono-amide or amine with a citryl or succinyl intermediate, and Type C', a possible category of NIS enzymes that dimerize citryl- or succinyl- intermediates followed in some cases by macrocyclization.

The proposed Type C' enzymes include IucC which has been shown to dimerize N^6-acetyl-N^6-hydroxy-L-lysine with citryl-N^6-acetyl-N^6-hydroxy-L-lysine[36]; AlcC that dimerizes two molecules *N*-hydroxy-*N*-succinyl-1,4-diamino-2-butanol and also catalyzes the macrocyclization of the two intermediates to form full alcaligin[37]. DesD, also classified as Type C', that dimerizes three molecules of *N*-hydroxy-*N*-succinylcadaverine and cyclizes the intermediate to form desferrioxamine E, or two molecules of *N*-hydroxy-*N*-succinylcadaverine with *N*-hydroxy-*N*-acetylcadaverine followed by cyclization to form desferrioxamine B[32]. PubC condenses and cyclizes three molecules of *N*-hydroxy-*N*-succinylputrescine to form putrebactin in *Shewanella putrefaciens*[35]. These enzymes are unique in their ability to dimerize complex, highly-substituted amine or amide intermediates, and can also catalyze macrocyclization to form a fully cyclized siderophore.

In contrast, Type C enzymes condense simple mono-amines or amides with a citryl or succinyl intermediate. For example, AsbB condenses spermidine with either a citryl-spermidine intermediate or a dihydroxybenzoyl-spermidinyl citryl intermediate[38–40]; SbnF condenses diaminopropionic acid with a citryl-diamino-ethane intermediate[41]; and AcsC condenses 2,4-diaminobutyrate with O-citryl-ethanolamine[42,43]. The difference in substrate complexity of the previously grouped Type C NIS enzymes suggests that these may form a distinct class of Type C NIS enzymes.

While these enzymes form a phylogenetically distinct group, sequences from more validated NIS proteins are needed to make the analysis more robust and confirm the presence of Type C' NIS enzymes.

2.7 Mechanism of action of NIS enzymes

As a general mechanism of action, NIS synthetases are responsible for a single enzymatic reaction and typically function to activate citric acid, via adenylation from ATP, followed by nucleophilic capture of an amine or alcohol group. This releases a citryl intermediate and AMP from the enzyme active site (Figure 2.4).

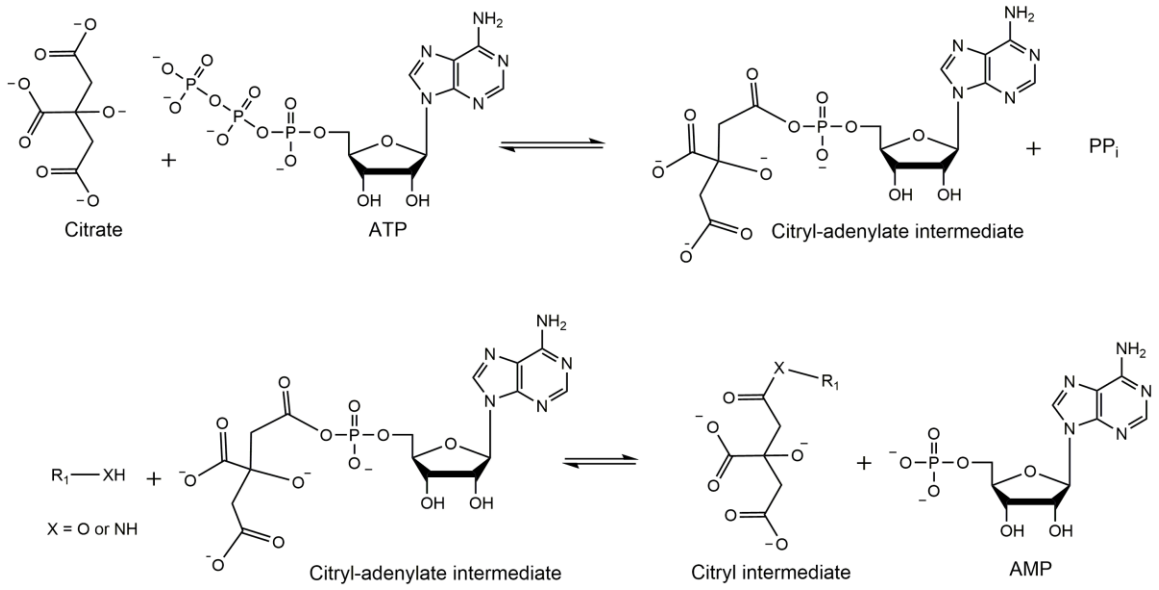

Figure 2.4. Mechanism for the formation of a citryl-adenylate intermediate within the active site of NIS enzymes.

In the first step, citrate, or a derivative, is adenylated using ATP to form a citryl-adenylate intermediate. This intermediate is acted upon in the second step by an incoming nucleophile to release AMP and a full citryl intermediate from the active site of the enzyme.

Kinetic parameters for citrate usage of various NIS enzymes are outlined in Table 2. This mechanism of action makes NIS enzymes unique members of the adenylating family of enzymes[44].

This review is organized by siderophore rather than by NIS Type because many siderophores require more than one NIS enzyme for their biosynthesis.

Table 2.2 Kinetic parameters for the NIS enzymes discussed in this paper.

Siderophore	Organism	Assay used	Substrates	Km (mM)	Vmax (μM/min)	kcat (sec^{-1})	Vmax/ Km	Reference
AcsD	*Pseudomonas syringae*	Hydroxyl-amine	Citric acid + hydroxylamine	1.9 ± 0.3	-	2.25 X 10^{-3}	-	Berti and Thomas, 2009[42]
AcsD	*Pectobacterium chrysanthemi*	AMP assay	Citric acid + serine	5.96 ± 0.86	71.44 ± 4.06	2.14 x 10^{3}	-	Schmelz et al., 2009[43]
IucA	*Klebsiella pneumonia*	AMP assay	Citric acid + hydroxylamine	0.180 ± 0.030	42 ± 1	21 ± 1 (min)	-	Bailey et al., 2016[45]
AsbA	*Bacillus anthracis*	MESG[1] assay	Citric acid + spermidine	5.65 ± 1.60	-	8.90 x10^{-1} ± 0.074		Nusca et al., 2012[38]
AsbB	*Bacillus anthracis*	MESG assay	Citryl intermediate + spermidine	-	-	-	2.4 x 10^{2} M^{-1} s^{-1}	Nusca et al., 2012[38]
SbnE	*Staphylococcus aureus*	Hydroxyl-amine	Citric acid + diaminopropionic acid	0.99 ± 0.12	40.0 ± 2.0	1.03 x 10^{-3}	-	Cheung et al., 2009[41]
Rfs	*Rhizopus delemar*	AMP assay	Citric acid + diaminobutane	4.97 ± 3.73	24.46 ± 8.04	-	-	Carroll et al., 2017[46]

[1]MESG: 7‑methyl-6-thio-guanosine.

2.7.1 Achromobactin: AcsA, AcsC, AcsD

AcsD catalyzes the biosynthesis of the polycarboxylate siderophore achromobactin produced by three bacteria in the Class, Gammaproteobacteria: *Dickeya dadantii* (formerly *Pectobacterium (*syn. *Erwinia) chrysanthemi)*[47], *Pseudomonas syringae*[42] and the tsetse fly commensal symbiont, *Sodalis glossinidius*[48]*.* Elucidating the biosynthetic pathway for achromobactin has not been trivial; two pathways, using different substrates, have been proposed by Schmelz et al. (2009)[43] and Berti and Thomas (2009)[42].

Berti and Thomas (2009)[42] identified an achromobactin biosynthetic operon in *P. syringae*, with structural similarity to the operon first identified in *D. dadantii*[49]. This operon consisted of AcsA-F, with AcsA, AcsC and AcsD predicted to be IucA/IucC homologs[49]. AcsA, AcsC and AcsD were cloned and individually expressed and purified in order to reconstitute the proposed achromobactin biosynthetic pathway (Figure 2.5). Using a hydroxylamine assay[50], they showed that AcsD is a Type A NIS enzyme that recognizes citrate and ethanolamine, AcsC is a Type C NIS enzyme, condensing the citryl intermediate with 2,4-diaminobutyrate, and that AcsA is a Type B NIS enzyme that condenses two molecules of α-ketoglutarate with the intermediate to form full achromobactin.

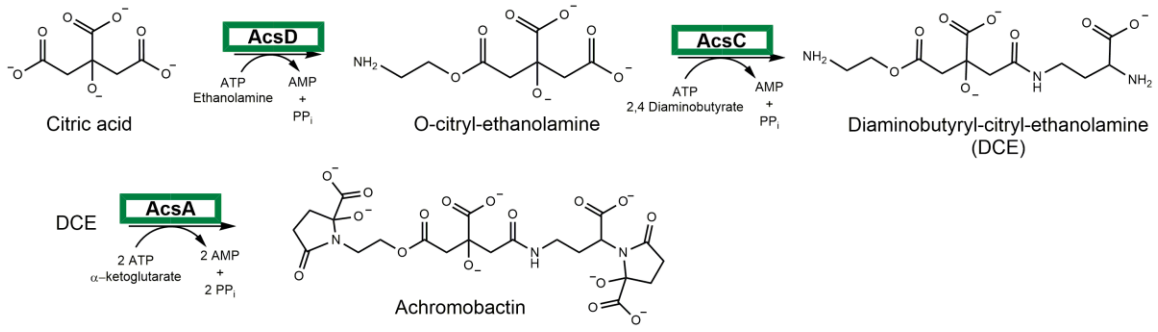

Figure 2.5 Proposed biosynthetic pathway for achromobactin biosynthesis based on data from Berti and Thomas (2009)[42].

The enzymes shown in bold were purified and used to biosynthesize achromobactin *in vitro*, as confirmed by LC-MS. NIS enzymes are boxed in green.

LC-MS data showed that a combination of AcsD, AcsC and AcsA, in the presence of the substrates outlined in Figure 2.5, produced achromobactin. Achromobactin produced under these conditions was also biologically active, and able to restore growth to a *P. syringae* mutant which lacked the genes for siderophore biosynthesis. The substrate

specificity of AcsD was examined using ethanolamine derivatives including, serine, 1,3 diaminopropane, ethylene diamine, ethylene glycol, β-mercaptoethanol and 3-amino-1-propanol. Only 1,3-diaminopropane and ethylene diamine were able to produce full achromobactin analogs and restore growth of the *P. syringae* siderophore mutant in a bioassay. This is the first report of full achromobactin siderophore biosynthesis using recombinant enzymes[42].

Schmelz et al. (2009)[43] worked on achromobactin synthesis in another bacterium, *Dickeya dadantii*. They cloned the AcsD gene from *D. dadantii*, crystallized the enzyme and investigated its kinetics, substrate specificity and stereochemistry. Using a hydroxylamine assay[50], Schmelz et al. confirmed that AcsD had the highest activity with citrate; near background levels of activity were seen with α-ketoglutarate and oxaloacetic acid. Nucleophile specificity was investigated using an NADH consumption assay coupled to AMP production[51]. Schmelz et al. (2009) found that AcsD had the highest activity with L-serine, followed by hydroxylamine and then D-serine and ethanolamine (Table 2). This is in contrast to Berti and Thomas (2009)[42] who found that when serine was used as a substrate, a mono-α-ketoglutaryl-diaminobutyryl-citryl serine intermediate accumulated, indicating that AcsA could only condense one molecule of α-ketoglutarate forming an achromobactin intermediate; fully formed achromobactin was not found. These data indicate that serine must be decarboxylated prior to addition of a second molecule of α-ketoglutarate. Schmelz et al (2009)[43] suggested that AcsE, a gene within the achromobactin biosynthetic operon and predicted to be a pyridoxal phosphate (PLP)-dependent decarboxylase, would decarboxylate serine after AcsD catalyzed the incorporation of citric acid. As proposed by Schmelz et al (2009)[43], the full biosynthetic pathway, including the predicted activity of AcsE, is outlined in Figure 2.6.

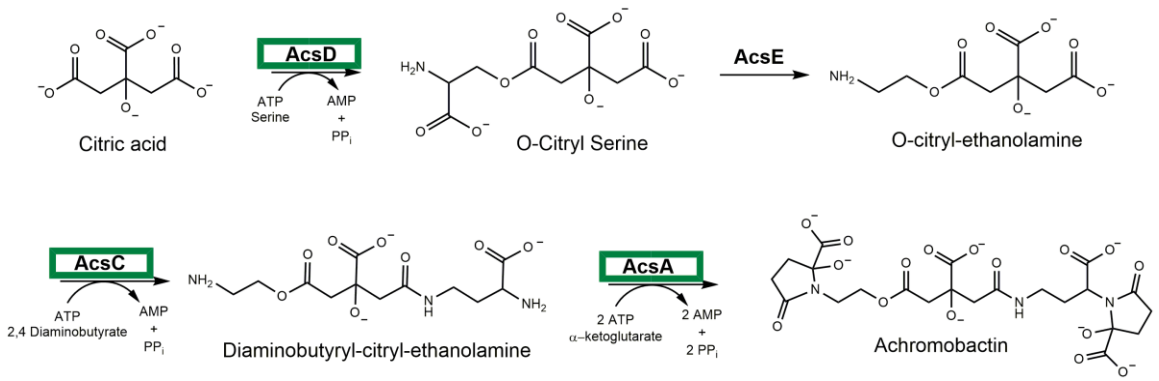

Figure 2.6 Biosynthetic pathway for achromobactin proposed by Schmelz et al. (2009)[43] incorporating the predicted PLP-dependent decarboxylase AcsE.

Kinetic analysis showed the preferred substrate of AcsD to be L-serine, not ethanolamine as previously reported[42]. NIS enzymes are boxed in green.

Crystallization of AcsD showed that the enzyme formed a dimer and had a unique 'cupped hand' topology not found in other adenylating enzymes[43]. The 'cupped hand' was made up of 3 domains (Figure 2.7): Domain 1 (residues 7-147) was the thumb, consisting of a three-helix bundle with a four stranded anti-parallel β-sheet. Co-crystallization of AcsD with citric acid and ATP showed that Domain 1 did not interact with the substrates; instead, it was proposed that it acts as an oligomerization interface domain.

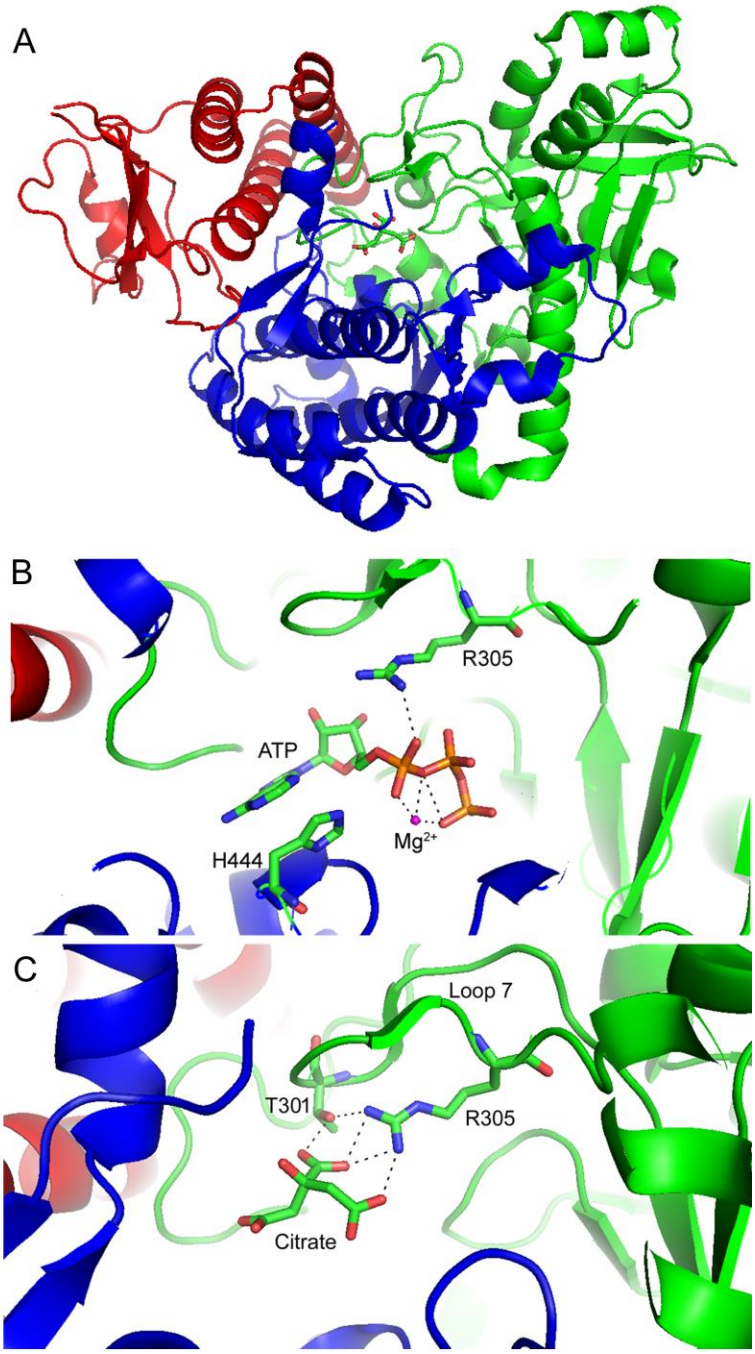

Figure 2.7 'Cupped hand' topology of AcsD from *D. dadantii* highlighting the three domains and specific interactions within the enzyme active site.

A. AcsD consists of three Domains: Domain 1 (red; residues 7-147) is the thumb Domain, Domain 2 (blue; residues 381 – 587) is the palm Domain and Domain 3 (green; residues 198-380) is the finger Domain. **B**. Residues within Domain 2 and 3 interact with ATP. Arg305 forms hydrogen bonds with the α phosphate of ATP, while Mg^{2+} (magenta) forms hydrogen bonds with the β and γ phosphates. This positions ATP in a unique horseshoe shape not seen in other adenylating enzymes[43,44]. **C**. Residues T301 and R305 on Loop 7 in Domain 3 form hydrogen bonds with the central carboxylate and terminal hydroxyl groups of citrate (PDB: 2W02).

Domain 2 represents the 'palm' domain. Co-crystallization of AcsD with citric acid showed that this domain had two upward facing loops, L9 and 10, which appear to have conserved residues involved in the active site. In particular, L9 contains a histidine at position 444 (H444) that forms hydrogen bonds with the terminal carboxylate group of citric acid. Site-directed mutagenesis found that H444 is essential for AcsD functioning as no ATP turnover was seen in this mutant. Domain 3 is the 'fingers' domain. Loop 7 and Loop 4 from Domain 3 sit on top of Domain 2 and interact with substrates in the active site. L7 was found to be conserved within Type A NIS enzymes and had the conserved residues Arg305 and Thr301 which form hydrogen bonds with the central carboxylate group of citric acid (Figure 2.7C). This positioning of citrate, in combination with H444 anchoring the terminal carboxylate group, makes adenylation of the *pro-R* carboxylate group of citrate the favourable enantiomeric reaction. This was confirmed by NMR experiments using ^{13}C-labelled citric acid. ATP bound with the triphosphate groups sitting in a positively charged pocket such that R305 hydrogen bonds with the α-phosphate group on ATP while Mg^{2+} bonds with the α and γ phosphates of ATP. Consequently, ATP is bound in a unique horseshoe shape (Figure 2.7B) that allows for nucleophilic attack by citrate, releasing PPi into an adjacent water-filled channel. The PPi appears to be retained within that channel until the citryl-intermediate is released from the enzyme active site by acylation with L-serine.

Interestingly, using citrate and L-serine as substrates, it was expected that *O*-citryl-L-serine would be the intermediate for AcsD. However, using NMR, MS/MS and MS/MS/MS, Schmelz et al. (2009)[43] showed that the more stable *N*-citryl-L-serine was formed through spontaneous intramolecular acyl migration. Because O-citryl-L-serine is the desired substrate for achromobactin, it implies that downstream biosynthetic steps, such as decarboxylation, must occur faster to avoid conversion to the undesired *N*-citryl-L-serine intermediate.

Schmelz et al (2011)[52] further investigated the substrate specificity of the second acylation step in AcsD using L-serine derivatives and site-directed mutagenesis of select amino acids. As substrates for nucleophilic attack, they found that AcsD uses (from highest activity to lowest): L-2,3-diamino propionic acid, L-serine, ethylenediamine, 1,2-diaminopropane, D-serine and L-isoserine. These data indicate that AcsD prefers substrates that have a carboxyl group two carbons away from an amino group, and that

amino group is two carbons away from an attacking nucleophile, typically an amine or alcohol, forming amide and esters bonds, respectively (Figure 2.8A). Co-crystallization of AcsD with a serine analog showed that E442 and R305 may govern the 2-carbon backbone preference; two oxygen atoms from E442 interact with two nitrogen atoms on the substrate, while nitrogen groups from R305 interact with the substrate carboxyl group (Figure 2.8B). Mutagenesis of R305 to R305A rendered the enzyme inactive, while R305K had only 1.5% of wild type activity. These data highlight the importance of these residues in maintaining enzyme activity.

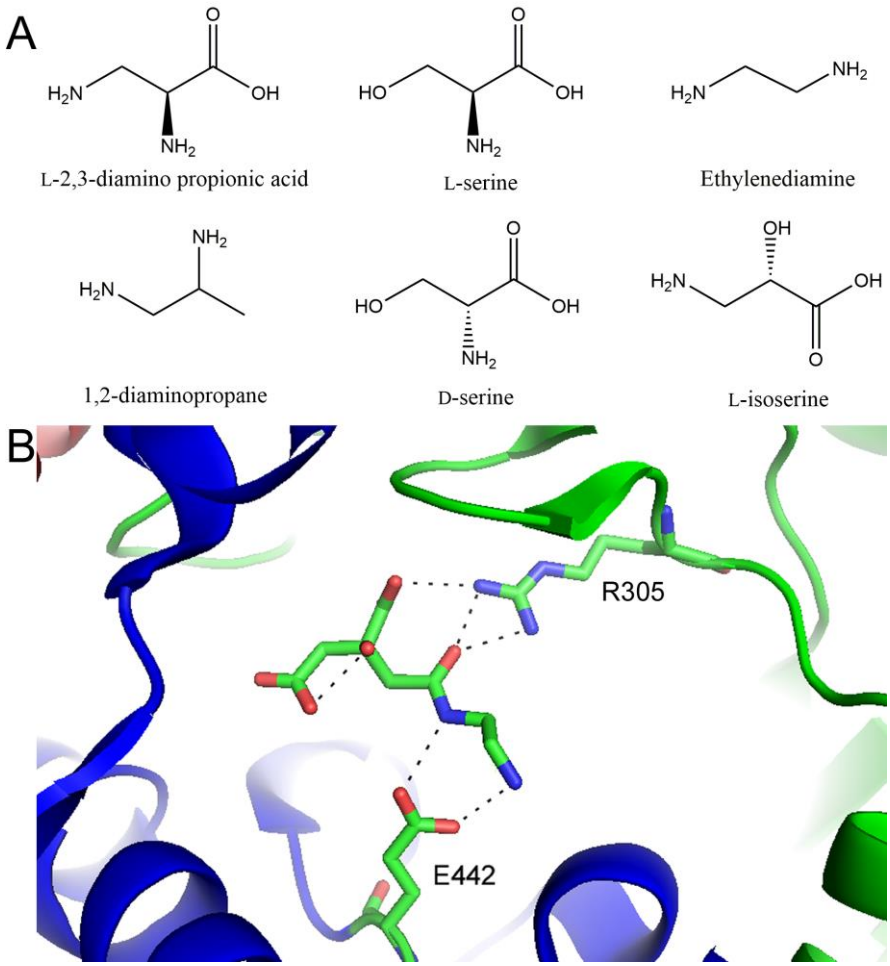

Figure 2.8 Preferred substrates for the second acylation step in AcsD from *D. dadantii.*

A. There is a general trend in having an attacking amine or alcohol group two carbons away from an amino group of the substrate. **B**. Structural alignment of AcsD with a serine derivative show this trend is most likely governed by the two oxygen atoms of E442 interacting with the substrate amine groups and R305 interacting with the substrate carboxyl group[52] (PDB: 2X3J).

2.7.2 Aerobactin: IucA and IucC

IucA and IucC are part of the iron uptake chelate (iuc) operon involved in the biosynthesis of aerobactin. These enzymes were first identified and described by Bindereif et al. (1983)[53] in *Escherichia coli* K-12 and are considered the prototypical enzymes for the NIS family. The aerobactin biosynthetic pathway was described by De Lorenzo et al. in 1986[36] and is summarized in Figure 2.9.

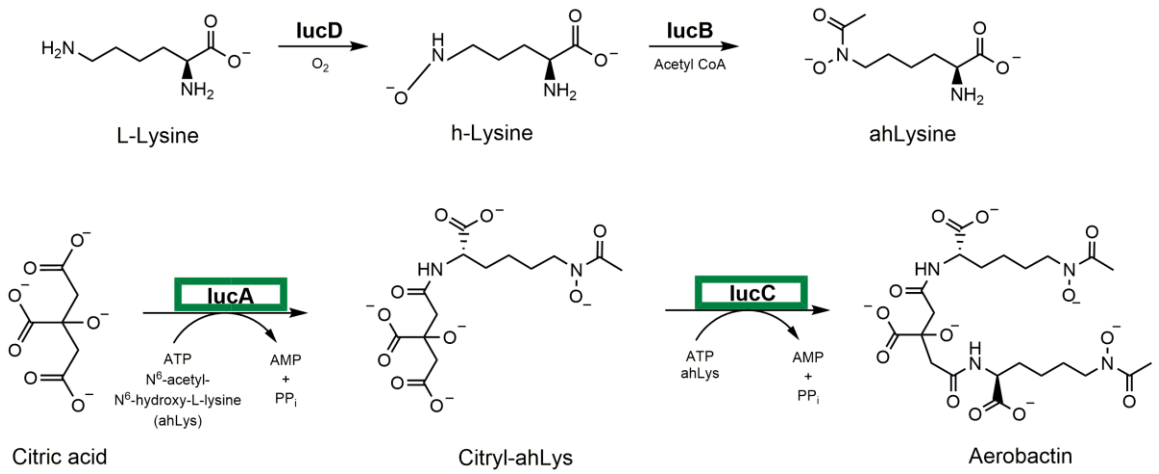

Figure 2.9 Aerobactin biosynthetic pathway.
Reactions performed by the NIS enzymes, IucA and IucC are outlined on the bottom panel in green. h-Lysine – hydroxy-lysine; ahLys – N^6-acetyl-N^6-hydroxy-L-lysine.

Aerobactin biosynthesis has been identified in a number of other bacteria from the Class Gammaproteobacteria including *Vibrio* species[54,55], *Yersinia* species[56], members of the *Pseudomonas* genus[57], and *Shigella flexneri*[58]. Elucidation of the structure and mechanism of IucA was completed by Bailey et al. (2016)[45]. In this study, the authors cloned *iucA* from hypervirulent *Klebsiella pneumoniae,* in which aerobactin is the predominant siderophore[59]*,* expressed and crystallized the enzyme. Although the sequence similarity between AcsD, AlcC and AsbB (an NIS enzyme discussed below) is low (approximately 20%), the crystal structures are remarkably similar with RMSD values ≤ 4.0 Å. IucA has the cupped hand topology, as described by Schmelz et al. (2009)[43] with a 'thumb', 'palm' and 'finger' domain (Figure 2.7). The thumb domain (residues 9-122) consists of a three-helix bundle with five anti-parallel β-sheets. Similar to AcsD, residues with this region do not appear to be involved in the active site. The finger domain (residues 175-357) appears to have the most interaction with ATP. His147

appears to interact with the adenosine ring, while the phosphates sit in a positively charged pocket created by residues Arg264, 288, 347, Ser262, 288 and Lys276 (Figure 2.10).

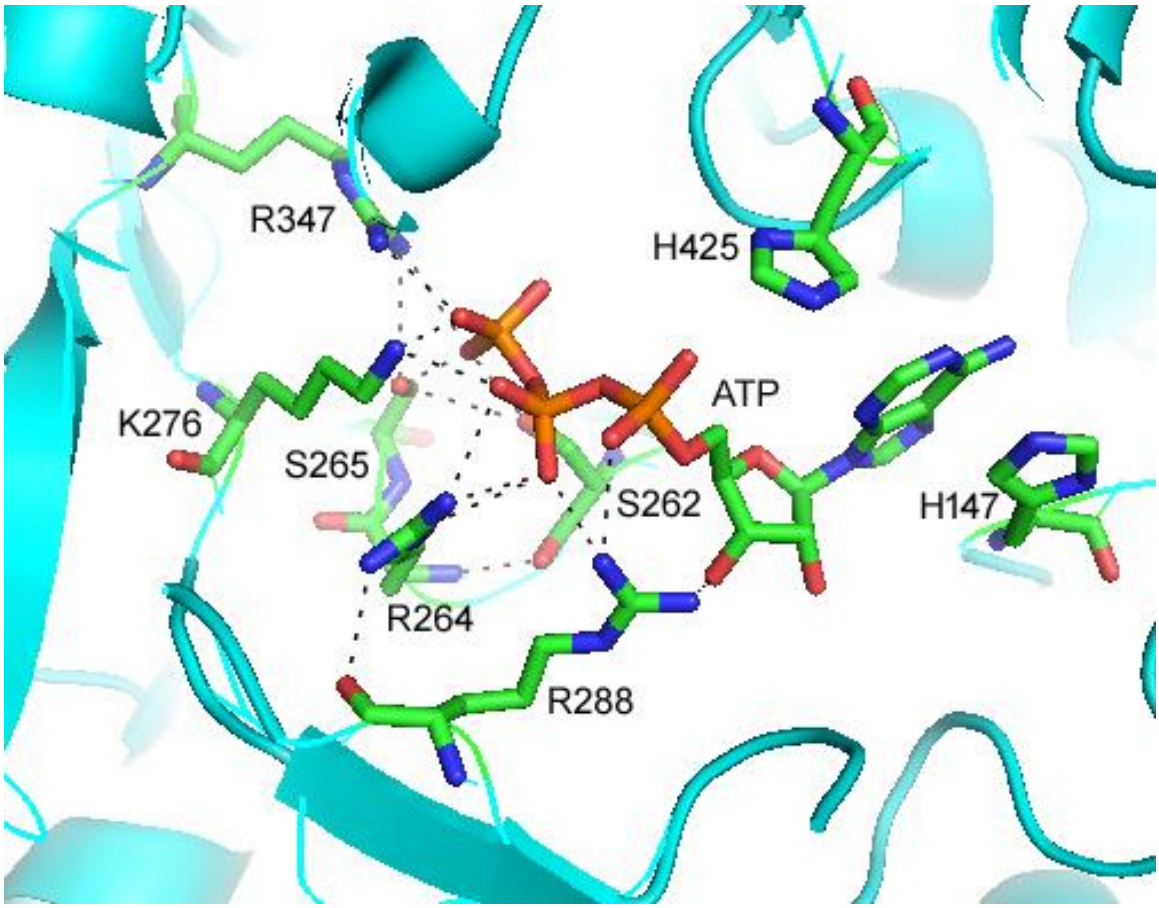

Figure 2.10 Structure of IucA showing amino acids in the active site involved in coordinating ATP.

His147 interacts with the adenosine ring of ATP, while residues Arg264, 288, 347, Ser262, 265 and Lys276 create a positively charged pocket to stabilize the phosphate groups (PDB: 5JM8).

The palm region (residues 358-557) has two main loops that interact with Mg^{2+} and ATP; specifically, His425 interacts with the phosphates on ATP, and Gln427, Asn428 and Asp445 interact with Mg^{2+}. Crystal structures could not be obtained for IucA with either of its substrates, citrate or ahLys; however, Bailey et al. (2016), used computational analysis, with AcsD as a template, to model substrate binding for IucA. Citrate was predicted to interact with Thr284, Arg288, His425 and Tyr482. Similar to AscD, interaction with these amino acids would position the pro-*R* carboxyl group of citrate to attack the α-phosphate on ATP[45]. It appears that there is a solvent accessible channel

extending from the β and γ phosphates of ATP which Schmelz et al. (2009)[43] proposed to be involved in harbouring PP_i after the initial adenylation of citrate[43]. Because the resolution of the solvent channel for IucA was not high enough, this hypothesis could not be confirmed; however, computational modelling showed PP_i to be a good fit for the region. In contrast to other characterized NIS enzymes, IucA appears to form a tetramer in solution. This was confirmed by native gel electrophoresis analysis and small-angle X-ray scattering (SAXS) analysis of the unliganded protein. When ATP is bound there were minor conformation changes seen in the crystal structure, possibly due to an unorganized loop in the finger domain forming a more organized structure or 'lid' over the bound ATP; however, this did not change the oligomerization state of the enzyme[45].

The substrate specificity of IucA was investigated using the hydroxylamine assay[50] and, similar to AcsD, IucA has a very narrow range for carboxylate derivatives. It binds citrate well but binding of α-ketoglutarate, glutarate and malonate were near background levels. IucA displayed greater flexibility in the nucleophile substrate specificity as assessed by the ATP turnover assay[51]. The highest activity was seen with hydroxylamine, followed by N^6-acetyl-lysine and very minimal levels of activity with arginine and glutamic acid. No activity was seen with lysine, glutamine or aspartic acid[45]. Structurally, IucA is very similar to AscD having a 'cupped-hand' topology. Furthermore, similar residues appear to play a role in substrate specificity though this may be because AcsD was used a template to model IucA substrate binding. Co-crystallization of IucA and its substrates would be useful in determining the exact residues involved in substrate binding and specificity for IucA.

2.7.3 Petrobactin: AsbA and AsbB

The anthrax siderophore biosynthetic (asb) operon was first identified in *Bacillus anthracis* (Phylum Firmicutes; Class Bacilli) and is involved in the biosynthesis of the mixed carboxylate/catechol siderophore, petrobactin[60,61] The operon consists of asbABCDEF; AsbA and AsbB are predicted to be IucA/IucC homologs[60,61].

Lee et al. (2007)[40] first proposed the petrobactin biosynthetic pathway outlined in Figure 2.11. In this proposed pathway, spermidine is converted to 3,4-dihydoxybenzoyl spermidine (DHBS) using AsbC, AsbD, AsbE and AsbF[62]. AsbA then adds citrate to this

intermediate followed by AsbB which adds another 3,4-DHBS to create the full petrobactin siderophore.

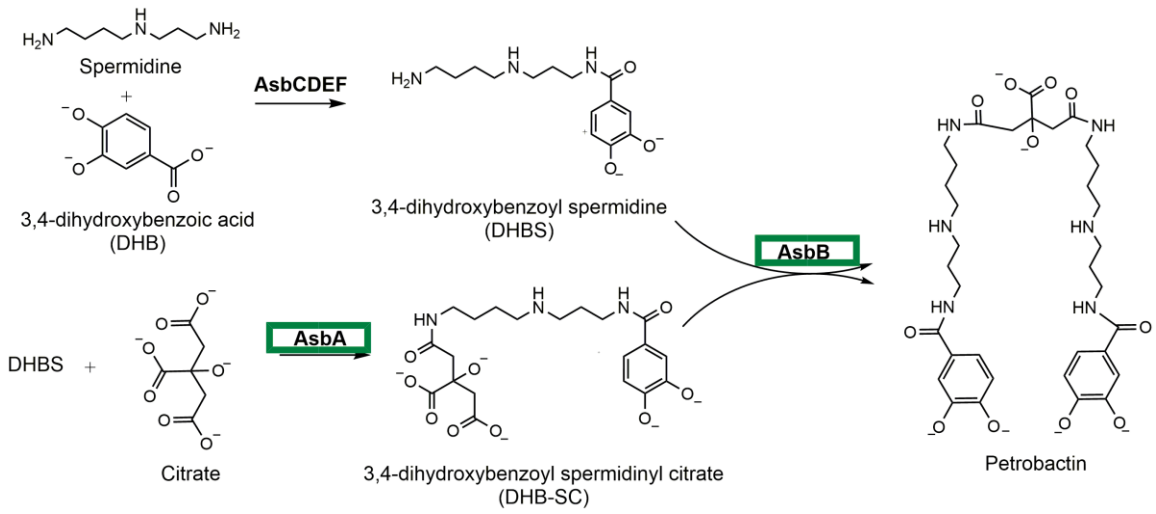

Figure 2.11 The petrobactin biosynthetic pathway as proposed by Lee et al. (2007)[40].

In this pathway, AsbCDEF are responsible for biosynthesis of 3,4-dihydroxybenzoyl spermidine (DHBS). A citryl intermediate is then made using AsbA and the final step in formation of the petrobactin siderophore is performed by AsbB with that addition of a second 3,4-dihydroxybenzoyl spermidine molecule. NIS enzymes are boxed in green.

To confirm the steps of this pathway, Lee et al. (2007) made in-frame deletion mutants of all six *asb* genes and analyzed the culture supernatants using HPLC, LC-MS and MS/MS, to detect intermediates that accumulated in the individual mutants. In *ΔasbA*, *ΔasbB* and *ΔasbAB* deletion mutants, 3,4-dihydroxybenzoyl spermidyl citrate (DHB-SC) was found to accumulate confirming that AsbCDEF catalyzes the synthesis of 3,4-DHB-SC. When AsbB alone was deleted, both 3,4-DHBS and 3,4-DHB-SC accumulated providing additional proof that AsbB is not necessary for the biosynthesis of 3,4-DHBS or for the addition of citrate to 3,4-DHBS. Interestingly, the *ΔasbA* mutant produced small amounts of the full petrobactin siderophore. The authors proposed that AsbB could accommodate citrate and DHBS to compensate for loss of AsbA. It is also interesting to note that Lee et al. (2007)[40] used MS/MS and detected 3,4-DHBS isomers where 3,4-DHB was added on to either the three or four carbon end of spermidine with no apparent preference; similar results were found for the condensation of citrate with 3,4-DHBS. The authors found no evidence for isomeric forms of petrobactin and they speculated that isomers not incorporated into petrobactin were most likely degraded or recycled[40].

Shortly after the report by Lee et al. (2007)[40], Oves-Costales et al. (2007)[63] published their investigation of AsbA and AsbB. They expressed and purified AsbA and used the hydroxylamine assay[50] and the ATP turnover assay[51] to confirm that AsbA adenylates citrate producing AMP. When AsbA was combined with citrate, Mg^{2+}, ATP and spermidine, LC-MS and HR-MS detected the intermediate compound, N^8-citryl-spermidine. Interestingly, no peaks were detected when 3,4-DHBS was added to the reaction mix instead of spermidine confirming that AsbA was responsible for condensing citrate with spermidine, not with 3,4-DHBS. Further experiments confirmed that AsbA is enantioselective and will only add spermidine to the *pro-R* configuration of citrate[64]. AsbB was also investigated by Oves-Costales et al. (2008)[39]. Using recombinant AsbB and LC-ESI-MS, they detected products formed in reactions containing the substrate pairs, spermidine and citryl-spermidine, 3,4-DHBS and citryl-spermidine, 3,4-DHB-SC and spermidine and 3,4-DHB-SC and 3,4-DHBS, although this last pair produced an intermediate that could only be detected in trace amounts. To confirm the preferred substrates, relative reaction rates were compared for the substrate pairs tested using an ATP turnover assay[51]; spermidine plus citryl spermidine, and spermidine with 3,4-DHB-SC yielded the first and second highest reaction rates, respectively. These data led them to propose an alternative petrobactin biosynthetic pathway shown in Figure 2.12.

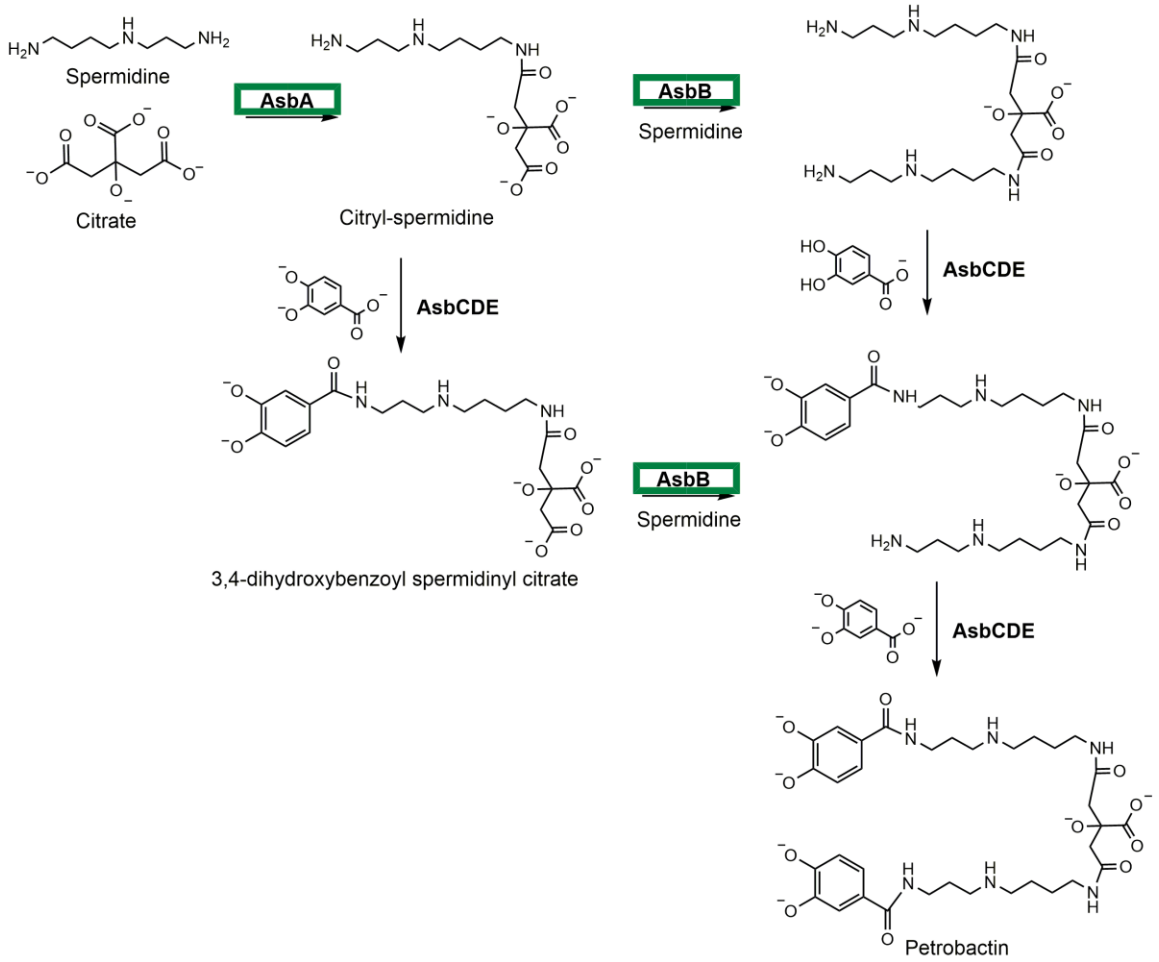

Figure 2.12 Petrobactin biosynthetic pathway in *B. anthracis* as proposed by Oves-Costales et al.[39,63,64].

In this pathway, the Type A NIS enzyme, AsbA condenses spermidine and citrate to form a citryl intermediate which is then the substrate for the Type B NIS enzyme, AsbB. AsbB can also condense spermidine onto a dihydroxybenzoyl spermidinyl intermediate. NIS enzymes are boxed in green.

Recently, Nusca et al. (2012)[38] investigated the biochemistry and enzymology of AsbA and AsbB but with the addition of purified AsbC-E. In a 'one-pot' reaction, they confirmed via LC-MS that petrobactin is biosynthesized from spermidine, citrate, 3,4-DHB, ATP and $MgCl_2$. Similar to the study by Lee et al. (2007)[40], they found that omission of AsbA but not AsbB, from the reaction mixture still produced petrobactin, confirming that AsbB can condense citrate with spermidine if AsbA is not present.

Oke et al. (2010) solved the crystal structure of AsbB and found that it closely resembles AlcC, a protein predicted to be involved in alcaligin biosynthesis in *Bordetella*

bronchiseptica, although biochemical studies have yet to confirm the activity of AlcC[65]. Size exclusion chromatography and bioinformatic analyses confirmed that AsbB forms a dimer. Like AcsD, AsbB has three domains in a 'cupped hand' topology. The numerous sequence variations are likely due to the difference in substrates between AsbB and AcsD. The thumb domain of AsbB (residues 1-136) is very similar to AcsD; however, a connecting loop (residues 137-183) between the thumb and finger domains has five small helices that form part of the substrate-binding pocket. The finger domain (residues 184-384) is similar to AcsD and it is thought that dimer formation in AsbB occurs via helix 1, 2 and 3 in the thumb domain of one monomer interacting with helix 3 and 4 on the finger domain of the second monomer. The palm domain (residues 380-601) is larger than that of AcsD and was predicted to comprise a major part of the substrate-binding pocket. The substrate-binding pocket for AsbB was 18.3 Å at its widest part and had a cleft volume of 8500 $Å^3$. In comparison, the substrate-binding pocket in AscD is only 3500 $Å^3$. The authors speculated that the catalytic mechanism of action for AsbB is similar to AcsD and that the larger number of loops in the binding pocket of AsbB may explain why it can use both spermidine and 3,4-DHB-SC as substrates. Unfortunately, co-crystallization attempts of AsbB with citrate, spermidine, ATP and ADP were unsuccessful, so this hypothesis could not be confirmed.

Kinetic parameters were investigated for both AsbA and AsbB using a 7‑methyl-6-thio-guanosine (MESG) assay, in which enzymatically produced PP_i is degraded to P_i, causing the breakdown of MESG to a coloured product. Kinetic parameters using natural substrates are listed in Table 2.

Previous work has shown that AsbA can use norspermidine, diaminooctane, diaminoheptane and diaminopentane in place of spermidine, and tricarballylic acid in place of citrate to form full petrobactin derivatives as detected by LC-MS[64]. Using the MESG assay, Nusca et al. (2012)[38] confirmed that AsbA uses norspermidine as a spermidine derivative and that AsbA does so with a higher activity than its natural substrate, spermidine. This was unexpected as norspermidine is a symmetrical molecule with three carbons separating each amine. AsbA has been shown to condense citrate onto the four-carbon side of spermidine but not the three-carbon side, indicating a strong regioselectivity. They also demonstrated that AsbB uses (in order of highest activity to lowest): spermidine, norspermidine, spermine, putrescine and 1-aminoethyl-1,3-propanediamine (AEPDA). To explain the regioselectivity in AsbA and AsbB, the authors

aligned the known AsbB structure with AsbA and found good alignment between the residues Lys311 and Glu459 in AsbB and Lys315 and Gln468 in AsbA predicted to be within the active site. Site-directed mutagenesis was used to evaluate the importance of Gly459 and Lys311 in the recognition of spermidine substrate derivatives. Overall, they found that Lys311 and Glu459 govern amine specificity and may play a role in the regioselectivity of the amino substrate. Additional analysis of crystal structures of various mutants bound to substrate derivatives should provide conclusive data regarding the amino acids governing the specificity of the amino substrate.

2.7.4 Alcaligin: AlcA, AlcB and AlcC

Alcaligin is a hydroxamate siderophore whose biosynthesis involves NIS enzymes. Alcaligin was first isolated from the bacterium, *Alcaligenes denitrificans*[66] and subsequently from *Bordetella pertussis* and *B. bronchiseptica*[67,68], all members of the Class Betaproteobacteria, family Burkholderiales. Interestingly, AlcA from *B. brontiseptica* was shown to have significant homology with IucD. Genetic complementation studies with an *alcA* gene knockout mutant confirmed that AlcA is involved in alcaligin biosynthesis[69]. Based on the homology to IucD, the authors predicted that putrescine, or an ornithine derivative, was a substrate for AlcA although experiments were not carried out to confirm this[69]. Further genetic complementation studies[70] and DNA sequence analyses[37] revealed an *alc* operon which consisted of *alcA, alcB,* and *alcC,* whose predicted proteins were homologous with IucD, IucB and IucC, respectively. The *alc* operon was also confirmed to be iron regulated[37]. Based on their shared homology, a biosynthetic pathway for alcaligin was proposed (Figure 2.13)[70].

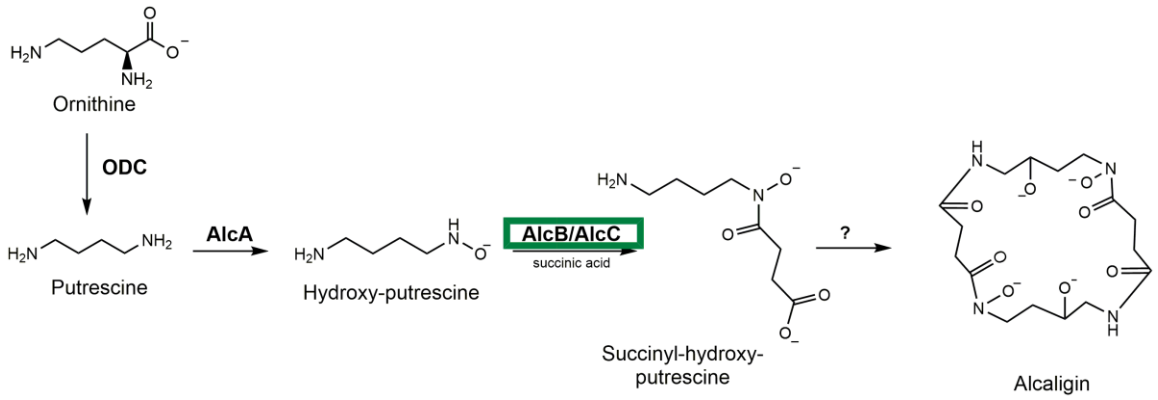

Figure 2.13 First proposed pathway for alcaligin biosynthesis[70].
The pathway is based on shared homology with genes in the Iuc operon. ODC – ornithine decarboxylase. Predicted NIS enzymes are boxed in green.

Further computational research into the *alc* operon by Pradel et al., (1998) revealed the presence of two additional genes, *alcD* and *alcE*[71]. Blastp and CDART analyses indicated that AlcD is a member of the siderophore iron reductase superfamily, enzymes that remove iron from hydroxamate siderophores. AlcE was predicted to be a dioxygenase[71,72] Based on these analyses, they proposed a revised biosynthetic pathway for alcaligin that included AlcD and AlcE (Figure 2.14). We performed a recent Blastp analysis using AlcE and it was predicted to be a ring hydroxylating dioxygenase and part of the HcaE superfamily. This suggests that hydroxylation of C3 in *N*-hydroxy-succinyl-putrescine may occur after AlcC-mediated dimerization and cyclization of the siderophore; however, the activity of the AlcABCE enzymes have yet to be confirmed.

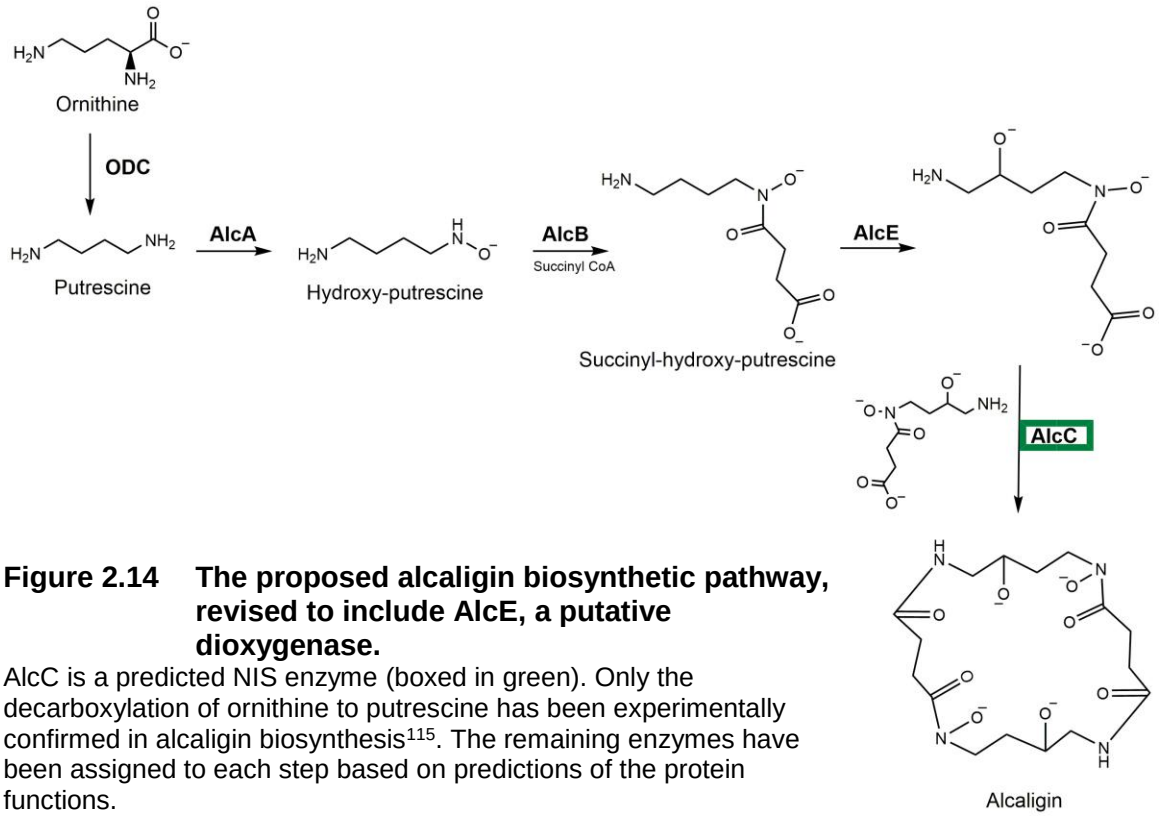

Figure 2.14 The proposed alcaligin biosynthetic pathway, revised to include AlcE, a putative dioxygenase.

AlcC is a predicted NIS enzyme (boxed in green). Only the decarboxylation of ornithine to putrescine has been experimentally confirmed in alcaligin biosynthesis[115]. The remaining enzymes have been assigned to each step based on predictions of the protein functions.

Recently, the crystal structure of AlcC was published as part of a proof-of-principle high-throughput screening assay[65] but unfortunately, no biochemical data was reported for AlcC. Alignment of AlcC with AscD showed that the position of H444 and R305 in AscD were conserved in AlcC as residues H449 and R312[44]. Bioinformatic analysis classified AlcC as a Type C NIS synthetase and based on the proposed reaction pathway shown in Figure 2.14, AlcC aids in dimerization and macrocyclization to form alcaligin. This mechanism of action is very similar to AsbB and structural modelling of residues within the active sites of the AlcC and AsbB showed good overall alignment; however, individual amino acids within the active site are variable, possibly due to a difference in substrate recognition[38] (Figure 2.15).

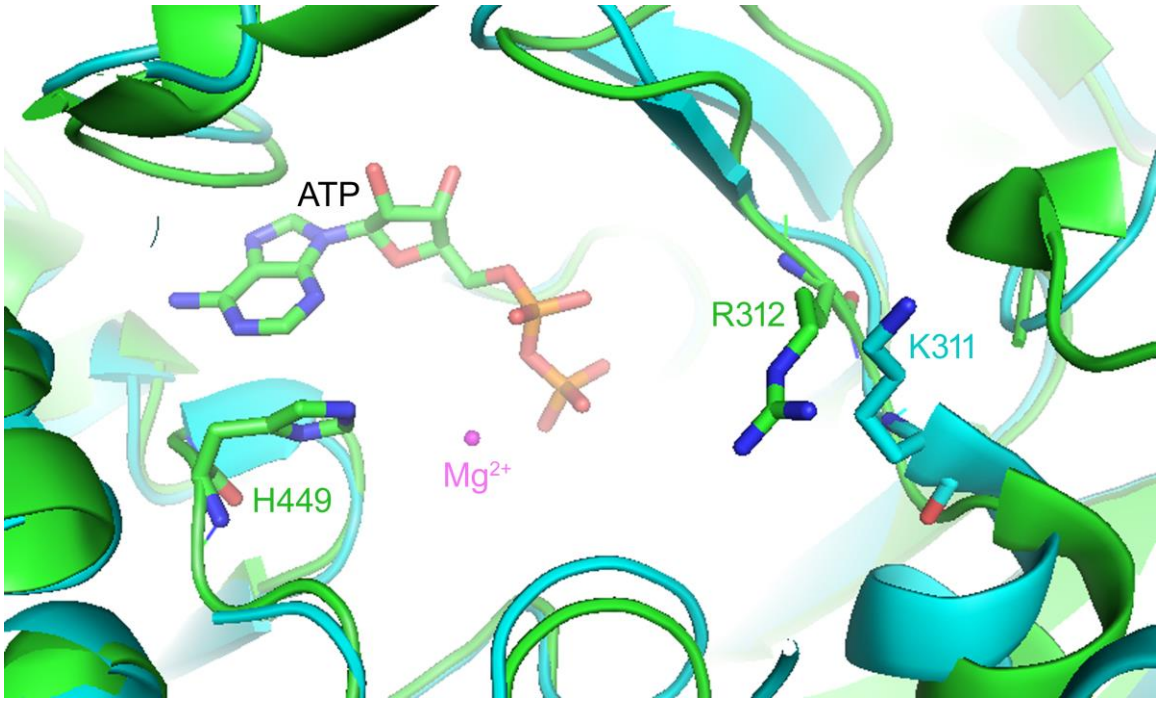

Figure 2.15 Structural alignment of the active site of the two NIS synthetases, AsbB (cyan) and AlcC (green).
H449 and R312 in AlcC were shown to align with H444 and R305 in AcsD[44]. K311 was shown to play a role in governing amino substrate specificity in AsbB[38] (PDB: AlcC 2X0Q, AsbB 3TO3).

2.7.5 Staphyloferrin A and B: SbnE, SbnC and SbnF

The bacterium, *Staphylococcus aureus* (Phylum Firmicutes, Class Bacillales) produces two polycarboxylate siderophores, staphyloferrin A and staphyloferrin B[21,22,73,74]. Biosynthesis of staphyloferrin A uses the *sfa* operon and involves condensation of D-ornithine with two molecules of citric acid via the NIS enzymes, SfnaB and SfnaD[75,76] The mechanism of action for these enzymes is predicted to be similar to other NIS enzymes and has been reviewed elsewhere[29].

Staphyloferrin B is composed of citrate, L-2,3-diaminopropionic acid, ethylene diamine and a succinic semialdehyde, determined using acid hydrolysis followed by gas chromatography (GC) and GC-MS. Furthermore, NMR confirmed the presence of these moieties in the overall structure of the molecule[73].

The *sbn* operon was first identified in *Staphylococcus aureus* and was shown to contain nine genes, *sbnA-I*[77]. By inserting *lacZ* reporter genes into various open reading frames, it was shown that expression of all nine genes was iron-regulated. To determine if the

operon contributed to iron acquisition, the *sbnE* gene was arbitrarily chosen for deletion. Growth assays showed that ***ΔsbnE*** strains had severely attenuated growth in low iron media compared to wildtype and *sbnE*-complemented strains. This result confirmed that the *sbn* operon was involved in iron acquisition[77]. A homologous gene cluster in *Ralstonia solanacearum* was linked with staphyloferrin B biosynthesis[78], therefore, it was predicted that the *sbn* operon was responsible for staphyloferrin B biosynthesis in *S. aureus*.

Cheung et al. (2009)[41] made the link between the *sbn* operon and staphyloferrin B biosynthesis. The authors used LC-ESI-MS to compare low-iron culture supernatants from *S. aureus* strains lacking the *sfa* operon (***Δsfa***) and strains lacking both *sfa* and *sbn* operons (***Δsfa Δsbn***). Staphyloferrin B was detected in ***Δsfa*** culture supernatants but not in ***Δsfa Δsbn*** confirming that *sbn* genes are required for staphyloferrin B biosynthesis.

SbnCEF were predicted to be NIS enzymes; however, Cheung et al. (2009)[41] found that a 'one pot' reaction containing all three recombinant enzymes and their predicted substrates, diaminopropionic acid, citrate, diaminoethane, α-ketoglutarate, ATP and $MgCl_2$, did not produce staphyloferrin B. Only after addition of SbnH, a predicted PLP-decarboxylase was the full staphyloferrin B siderophore detected by LC-ESI-MS. Furthermore, the staphyloferrin B produced *in vitro* was biologically active as it restored growth of an *S. aureus* strain deficient in ferric hydroxamate uptake[41,79]

To construct the biosynthetic pathway for staphyloferrin B, the activity of each recombinant Sbn enzyme was analyzed. SbnE formed a monomer and dimer in solution, as indicated by gel filtration. Cheung et al. (2009) used the hydroxylamine assay[50] to confirm that SbnE used citrate as a substrate. The presence of a citryl-diaminopropionic acid intermediate was determined using LC-ESI-MS when SbnE was combined with citrate and diaminopropionic acid (DAP). Thus, DAP acts as a nucleophile to release the adenylated citryl compound from the enzyme active site. Interestingly, SbnE can also use diaminoethane as a nucleophilic substrate, as LC-ESI-MS detected a citryl-diaminoethane intermediate. However, when DAP and diaminoethane are present in equimolar concentrations, the citryl-diaminoethane intermediate was not found, indicating that DAP is the preferred substrate[38]. Kinetic parameters for SbnE recognition of citrate are shown in Table 2.

Surprisingly, the hydroxylamine assay showed that SbnF reacted with citryl-diaminoethane but not citryl-DAP. The authors hypothesized that the citryl-DAP intermediate formed by SbnE must be decarboxylated by another enzyme before being acted upon by SbnF[38]. Using LC-ESI-MS, they confirmed that SbnH, a predicted PLP-dependent decarboxylase within the *sbn* operon decarboxylated citryl-DAP to form citryl-diaminoethane. SbnF then binds citryl-diaminoethane and condenses it with another molecule of DAP. The final step in staphyloferrin B biosynthesis is the SbnC-mediated addition of α-ketoglutarate. Based on their data, the authors have confirmed all of the steps of the staphyloferrin B biosynthetic pathway as shown in Figure 2.16.

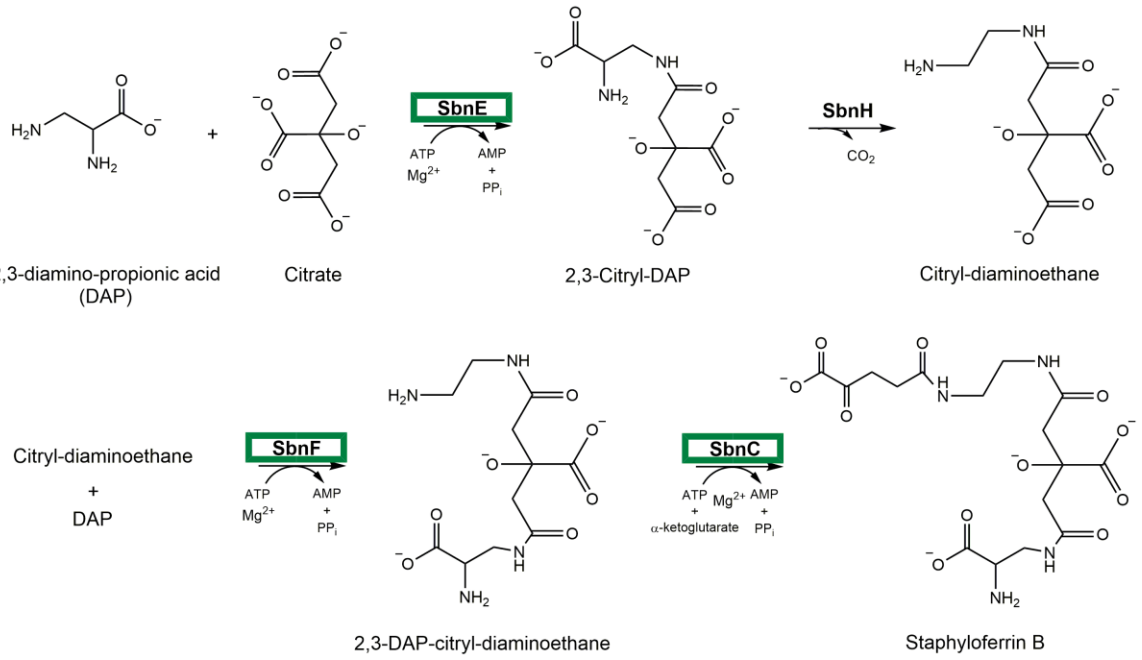

Figure 2.16 Biosynthetic pathway for staphyloferrin B as proposed by Cheung et al. (2009)[41].

NIS enzymes are boxed in green and their activity has been confirmed.

Because SbnE is able to use diaminoethane as a secondary substrate to form a citryl intermediate, it would be interesting to investigate the substrate specificity of the other enzymes in the biosynthetic pathway. Furthermore, as SbnE and SbnF catalyze similar reactions to the staphyloferrin A biosynthetic enzymes, SfnaD and SfnaB, respectively, it would be interesting to determine which amino acids govern substrate specificity for biosynthesis of the closely related siderophores.

2.7.6 *(R,R)*-Rhizoferrin: Rfs

Fungi within the Mucorales order are known to produce the polycarboxylate siderophore rhizoferrin[80,81], with a chemical structure of diaminobutane linked to two citric acid moieties with an (*R,R)*-configuration around the chiral center[82].

Carroll et al. (2017)[46] characterized Rfs, the first fungal NIS enzyme identified. The *rfs* gene was successfully cloned and expressed. Native gel analysis indicated that Rfs formed oligomers but monomers formed in the presence of the substrates, diaminobutane, citrate, $MgCl_2$ and ATP. Rhizoferrin biosynthesis from citrate and diaminobutane was confirmed using high resolution LC-MS, and both the full rhizoferrin compound and its mono-citryl intermediate were detected. Thus, Rfs forms an adenylated-citryl intermediate that is displaced from the active site upon nucleophilic capture of diaminobutane. Based on this data, the rhizoferrin biosynthetic pathway is outlined in Figure 2.17. As biosynthesis of rhizoferrin involves the sequential reaction of only one enzyme, it is the simplest NIS-catalyzed siderophore biosynthetic pathway characterized to date.

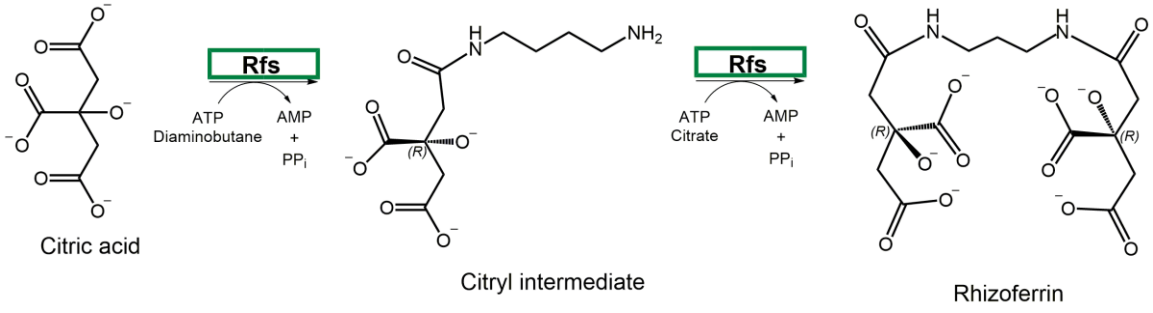

Figure 2.17 Rhizoferrin biosynthetic pathway.
Rfs is an NIS enzyme (boxed in green) which preforms two enantioselective reactions forming (*R,R*)- rhizoferrin.

Kinetic analysis of Rfs was performed using the ATP turnover assay[51] and initial rates of citrate utilization fit a two-site binding model with V_{max} and K_d values for two isozymes. This model suggests that Rfs has two binding sites for citrate adenylation. However, computational predictions using Phyre[83] and structural alignments to other NIS enzymes, including AscD, do not predict two binding sites; hence, Rfs may function as both a monomer and dimer in vitro. This is similar to Sbn enzymes which have also been found to form monomers and dimers in vitro[41]. Further research is required to confirm the

monomer to dimer transition in Rfs. Kinetic parameters for Rfs are comparable to the bacterial NIS enzymes (Table 2).

The nucleophile substrate preference was determined for Rfs and activity of the recombinant enzyme was (from highest to lowest activity): diaminobutane, diaminopropane, diaminopentane, hydroxylamine and ornithine. Unlike AcsD and IucA, Rfs showed activity with citrate derivatives including oxaloacetic acid and tricarballylic acid. Interestingly, LC-MS/MS detected only partial rhizoferrin derivatives with oxaloacetic acid and diaminopentane; whereas a mono-citryl intermediate and full rhizoferrin derivative were detected with diaminopropane, and ornithine derivatives. Tricarballylic acid formed a full rhizoferrin derivative with no mono-substituted intermediate being detected in this reaction. These data indicate that Rfs has a broader substrate specificity compared to AcsD and IucA suggesting that amino acids necessary for Rfs catalysis may be quite different from other NIS enzymes.

Attempts to crystallize Rfs under various conditions and in the presence and absence of substrates were unsuccessful. However, based on a multiple sequence alignment of validated NIS enzymes, R354 and H484 were both predicted to be involved in citrate and ATP recognition, similar to R305 and H444 in AcsD. L544 aligned with R501 in the active site of AcsD which plays an indirect role in governing specificity for L-serine[52], and E209 was conserved across all NIS enzymes. Consequently, four amino acid mutations were made in Rfs using site directed mutagenesis: R354A, H484A, E209A and L544R (Figure 2.18). The E209A mutant expressed poorly and was not evaluated.

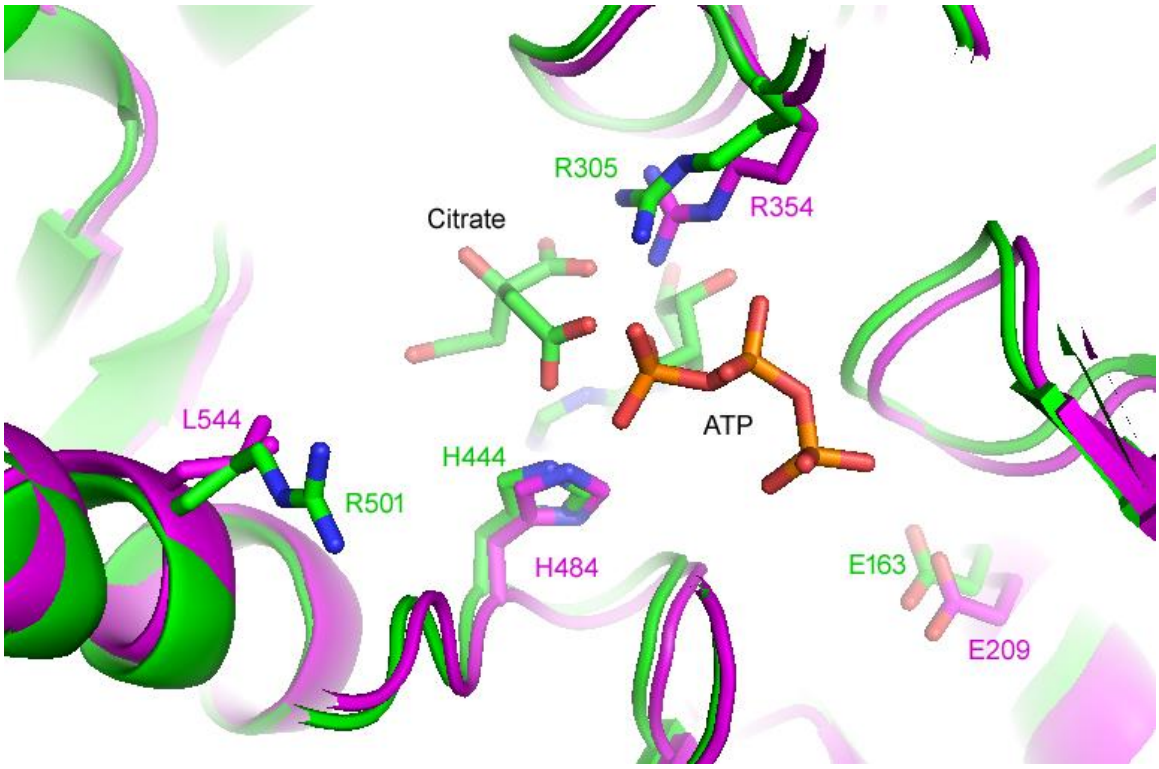

Figure 2.18 Modelling the predicted active site of Rfs (magenta) with the active site of AscD (green).

Phyre[83] was used to generate the predicted structure for Rfs and gave AcsD as a top hit with 100% confidence. The following mutations were made and the catalytic enzyme activity was compared to the wild type enzyme: R354A, H484A and L544R (PDB AcsD: 2W02).

Interestingly, H484A was inactive as predicted, while the R354A mutant enzyme had wild type Rfs activity. This was unexpected because the equivalent residues in AcsD (R305 and H444, respectively) are both crucial for its function[43]. Interestingly, L544R did not alter Rfs activity with diaminobutane; however, L544R activity was considerably enhanced with serine, a substrate not used by wildtype Rfs. R501 in AcsD is predicted to aid in proper placement of E442 which most likely makes a bidentate interaction with serine (see Figure 2.8)[52]. In wildtype Rfs, the equivalent amino acid, E482 is probably in a sub-optimal position to form the bidentate interaction necessary for serine utilization. However, in the L544R mutant, the alignment of E442 would be similar to what is seen in AcsD, facilitating the incorporation of serine into the active site. These data were based on an ATP turnover assay, so it is unclear if a full rhizoferrin derivative would be formed with serine.

2.7.7 *(S,S)*-Rhizoferrin: FslA

Francisella tularensis (Class Gammaproteobacteria, Order Thiotrichales) secretes *(S,S)*-rhizoferrin in low iron conditions[84,85]. The *fsl*A-E operon (also termed the *fig*A-F operon) has been shown to be responsible for biosynthesis, secretion and uptake of rhizoferrin[84–88].

Sullivan et al. (2006)[84] were the first to characterize rhizoferrin secretion and biosynthesis in *F. tularensis*. They identified rhizoferrin in low-iron cultures of *F. tularensis* and showed that partially purified rhizoferrin could enhance growth when supplemented back into low-iron cultures. A search of the *F. tularensis* genome showed an IucA homolog within an unidentified operon; they termed the operon *fsl* and the IucA homolog, *fslA* and confirmed that expression of the operon was iron-regulated. A deletion mutant for *fslA* was made and siderophore secretion was compared using a CAS assay, where a colourimetric change of the CAS dye indicated the presence of an iron binding compound. Wildtype *F. tularensis* secreted a siderophore and had significant CAS activity, while the Δ*fslA* mutant had background levels of CAS activity. Significant CAS activity could be restored to the mutant upon complementation with a plasmid carrying the *fslA* gene.

Shortly thereafter, Deng et al. (2006)[89] confirmed the production of a siderophore and iron-regulated expression of its biosynthetic genes in *F. novicida*; however the chemical identify of the siderophore was not determined. The *figA* gene was identified as being necessary for biosynthesis of the siderophore, as determined by growth of wildtype and a *figA* deletion mutant on CAS media.

Kiss et al (2008)[85] further characterized the *figB, figC, figD* and *figE* genes in *F. novicida* by creating multiple gene deletion mutants. They found that *ΔfigA*, *ΔfigB,* and *ΔfigC* were deficient in production and/or secretion of rhizoferrin as determined by the CAS assay, while *ΔfigD and ΔfigE* strains retained CAS activity equivalent to wildtype strains of *F. novicida.* These data, and computational analysis of the *figE* gene, led to the prediction of it being in the outer membrane and acting as a ferric-rhizoferrin transport protein. This was later confirmed by Ramakrishnan et al. (2008)[86]. *figD and figB* encode for transport proteins and are involved in import and export of rhizoferrin, respectively[85,90]. Interestingly, very little work has been done with FigC, however, it is predicted to be a

PLP-dependent decarboxylase[90]. We speculate that FigC is necessary for decarboxylation of ornithine to diaminobutane, a substrate in the biosynthesis of rhizoferrin (Figure 2.19).

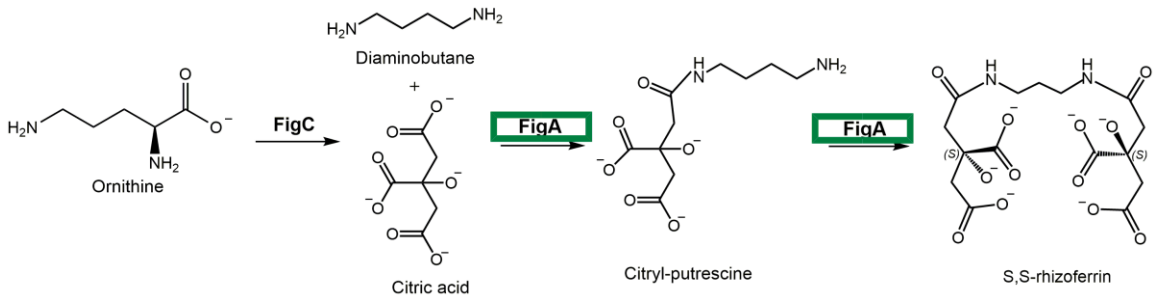

Figure 2.19 Proposed biosynthetic pathway of *S,S*-rhizoferrin in *F. tularensis* and *F. novicida*.
Reactions catalyzed by FigA have been inferred based on gene deletion studies[84,89]; however biochemical characterization of FigA has not been carried out. The role of FigC is predicted based on Ramakrishnan, G. (2017)[90] and we speculate that the reaction for FigC is decarboxylation of ornithine.

While it seems likely that FigA carries out two acylation reactions on diaminobutane, a symmetrical molecule (Figure 2.19), this has not been confirmed biochemically to date.

2.7.8 Legiobactin: LbtA

Legiobactin was first identified in low-iron culture supernatants of *Legionella pneumophila* (Class Gammaproteobacteria, Order Legionellales), using the Chrome Azurol S (CAS) assay[91], which relies on the colourimetric change in ferrated versus desferri- forms of the CAS dye. Secretion of the siderophore was found to be dependent on the growth stage of the starting inoculum, the amount of inoculum used and the growth temperature[91,92]. Furthermore, CAS reactive fractions were not present in iron replete media.

The *lbt* operon encoding LbtA and LbtB was first thought to be involved in legiobactin biosynthesis based on sequence homology to both IucA and IucC, and the presence of a Fur box located upstream of the operon[92]. To investigate its role in biosynthesis, an LbtA deletion mutant was made in *L. pneumophila*. CAS reactivity dropped by 40-70% compared to the wildtype strain and while this is promising, residual CAS activity indicates the presence of another possible iron binding compound still active in the

mutant. A bioassay using the culture supernatant from *ΔlbtA* could not restore growth of a *feoB* mutant (deficient in high affinity iron transport)[93] whereas the supernatant from an LbtA complemented strain restored growth. Similar results were seen for LbtB and based on these data, it appears that both LbtA and LbtB are required for biosynthesis of legiobactin. However, a Blast analysis of LbtB predicts that it is a member of the Major Facilitator Superfamily (MFS) of transport proteins. Thus, the exact role of LbtB in biosynthesis of the siderophore remains unknown.

Using MS and NMR analyses, legiobactin was determined to be identical in structure to the polycarboxylate siderophore, rhizoferrin[94]. The configuration of the chiral center was not determined; however, as noted above, the bacterium *Francisella tularensis* produces (*S,S)*-rhizoferrin[84] and the authors hypothesized that rhizoferrin produce by *L. pneumophila* would adopt the same enantiomeric configuration[94]. With structural data established for legiobactin, a biosynthetic pathway was proposed using LbtA[94] (Figure 2.20) . LbtC and LbtU, members of the same operon, were later identified as inner membrane and outer membrane transport proteins, respectively, for rhizoferrin[95,96].

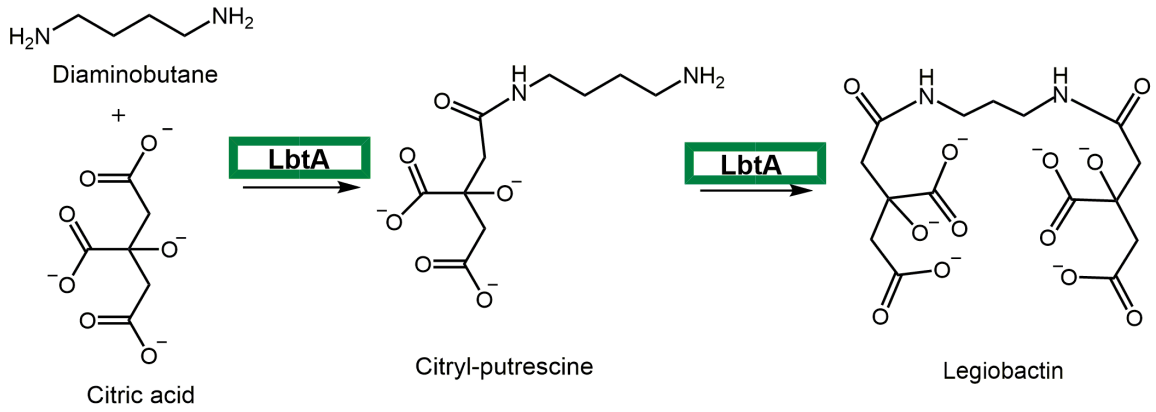

Figure 2.20 Proposed biosynthetic pathway for legiobactin, a polycarboxylate siderophore with the same chemical composition as rhizoferrin[94].

Further research is necessary to confirm the legiobactin biosynthetic pathway and the mechanism of action of LbtA.

2.8 The role of NIS enzymes in virulence

An enhanced understanding of NIS synthetase biochemistry is important for the development of enzyme inhibitors. In the following section, we highlight the importance of NIS enzymes in the virulence of some of the pathogenic microorganisms covered in the previous sections.

Free iron is highly damaging to cells. In the presence of free ferrous iron and H_2O_2, the Haber-Weiss reaction[97], based on Fenton chemistry[98], generates free hydroxyl radicals which have the potential to damage DNA, proteins and lipids. For this reason, the concentration of iron in human serum is highly regulated by iron binding proteins such as transferrin and lactoferrin, and estimated to be 10^{-24}M[99]. In order for microbial pathogens to survive in this environment, many secrete siderophores to scavenge and steal iron from host-iron binding proteins. Siderophore biosynthesis has been shown to be a virulence factor in numerous bacterial species including *Dickeya dadanti*[49]*, Escherichia coli*[100], *Neisseria gonorrhoeae*[101] and enteropathogenic *Yersinia* species[102]. In the following section, we present recent developments regarding the involvement of NIS enzymes in pathogenesis.

The host immune system has evolved to recognize siderophores as foreign and produces the peptide, siderocalin, which binds siderophores with dissociation constants (K_d) in the nanomolar range[103]. Siderocalin mainly binds catechol siderophores such as enterobactin[103], however, there are mixed catechol siderophores that can evade siderocalin binding. These siderophores are known as ‘stealth siderophores’; and one such example is petrobactin secreted by *Bacillus anthracis*[104].

B. anthracis secretes two siderophores, bacillibactin and petrobactin[60,105]. Bacillibactin is tightly bound by siderocalin and does not appear to contribute to virulence[61]. Petrobactin is not bound by siderocalin and its ability to evade siderocalin binding is thought to be due to the incorporation of 3,4-dihydroxybenzoic acid, instead of the more common 1,2-dihydroxybenzoic acid[104]. This unusual moiety is incorporated into petrobactin using the NRPS enzymes, AsbCDE, part of the *asb* operon. AsbA is also in the *asb* operon and involved in petrobactin biosynthesis; it is a Type A NIS enzyme responsible for condensation of citrate with spermidine. To determine if AsbA contributes to virulence of *B. anthracis*, Cendrowski et al. (2003)[61] knocked out *asbA* and infected mice using a

mouse model of systemic anthrax. They found that mice subcutaneously infected with the wildtype *B. anthracis* strain succumbed at much lower inoculum concentrations compared to mice infected with the *ΔasbA* strain of *B. anthracis*, indicating a reduction in virulence in the mutant. The authors also infected cultured mouse macrophages because these play a role in the early transport of *B. anthracis* spores from the lung to the lymph nodes[60]. There was no difference in uptake by macrophages between wildtype and *ΔasbA* strains; however, after 24 hours of incubation, the wildtype strain grew significantly within macrophages and showed at least 50% cytotoxicity. In comparison, the *ΔasbA* strain did not show any appreciable growth within macrophages after 24 hours and was less than 25% cytotoxic to macrophages[61]. These data indicate that AsbA, and therefore petrobactin biosynthesis, is required for full virulence in anthrax infections.

In *Staphylococcus aureus,* a similar study showed that knocking out the gene encoding SbnE, the Type A NIS enzyme responsible for condensation of citrate and diaminopropionic acid, eliminated staphyloferrin B production and significantly reduced growth of the bacteria in a non-lethal kidney abscess mouse model[77]. Mice were infected via the tail vein with either wildtype *S. aureus* or *ΔsbnE* strains and after five days, the number of colony forming units (CFU) in the kidney was reduced by 2-log fold in the *ΔsbnE* strain compared to the wildtype strain. After six days of infection, no bacteria were recovered from mice infected with the *ΔsbnE* strain, indicating clearance by the host immune system. Furthermore, visual assessment of the kidneys showed large abscesses in mice infected with wildtype *S. aureus*, while no abscesses were observed in mice infected with the *ΔsbnE* strain[77]. This confirms that at least in a mouse model, the NIS enzyme SbnE, and therefore staphyloferrin B biosynthesis, contributes to the virulence of *S. aureus*.

To our knowledge, there are no studies directly linking NIS enzymes from the *alc* operon, responsible for alcaligin biosynthesis, to virulence. Previous research has shown that AlcA, the enzyme responsible for *N*-hydroxylation of putrescine, is required for full virulence in a swine model of pneumonia caused by *Bordetella bronchiseptica*[106]. Pigs infected with a *ΔalcA* mutant showed reduced colonization in the snout, lungs and trachea compared to pigs infected with wildtype *B*. *bronchiseptica*[106]*.* In contrast, deletion of AlcR, a transcriptional regulator for the *alc* operon, showed no change in virulence in mice infected intranasally with *Bordetella pertussis*[71]. These data indicate

that virulence in *Bordetella* species is complex and multi-factorial and that siderophore biosynthesis contributes to virulence but is not solely governed by it.

Francisella species secrete the polycarboxylate siderophore, (*S,S)*-rhizoferrin. The *fslA* gene (alternatively named the *figA* gene) has been implicated in (*S,S)*-rhizoferrin biosynthesis in *Francisella tularensis* and *F. novicida* and functions similarly to Rfs and LbtA (Figure 2.17 and Figure 2.20)[84,89]. A *ΔfslA* mutant was made in the *F. tularensis* live vaccine strain (LVS) and production of rhizoferrin was not detected by either the CAS assay or MS peaks corresponding to rhizoferrin[84]. Virulence was assessed by infecting a murine macrophage cell line. After 24 hours, growth of the bacteria within the macrophage was comparable between the *ΔfslA* and wildtype strains[107]. In contrast, when a double mutant was made for *fslA* and *feoB*, the high affinity ferrous iron transport protein, growth of the double mutant in macrophages was significantly inhibited for up to 48 hours post-infection compared to wild type. The *ΔfslAΔfeoB* strain also resulted in no mortality over 14 days in a murine model of tularemia, and the individual gene mutants showed reduced mortality compared to mice infected with the wildtype strain. Thus, siderophore-mediated iron acquisition is an important virulence factor in *F. tularensis,* however, there are compensatory mechanisms to ensure adequate iron uptake for survival of the microbe[107].

The antimicrobial compounds baulamycin A (BmcA) and baulamycin B (BmcB) were isolated from *Streptomyces tempisquensis* and using purified NIS enzymes, Tripathi et al., (2014) showed that BmcA and BmcB competitively inhibit AsbA and SbnE, although BmcA was more effective at inhibiting the enzymes[108]. BmcA was highly specific at inhibiting the Type A NIS enzymes, AsbA and SbnE, while the Type C NIS enzyme, AsbB, was unaffected by the compound. BmcA inhibited growth of *S. aureus*, *B. anthracis*, *Escherichia coli* and *Shigella flexneri,* all of which harbour NIS enzymes. *Salmonella typhimurium* also possess IucA and IucC, however its growth was not inhibited significantly compared to untreated controls[108]. While this data is promising, additional research is needed to determine the efficacy and toxicity of these compounds to treat bacterial infections *in vivo*.

2.9 Putative NIS synthetases in Archaea

Research is limited on iron uptake by organisms in the domain, Archaea. As free iron is more easily available to Archaea living in acidic or reducing environments, it appears that iron uptake is predominantly dependent on reduction at the cell surface[109]. To our knowledge there is only one report of siderophore isolation from Archaea, these include species within the genera, *Halococcus*, *Haloterrigena*, *Halorubrum* and *Halogeometricum*[110]. Chemical tests and bioassays showed that the siderophores were carboxylates although exact structures were not determined[110]. A previous report showed that IucA and IucC homologs existed in four of the ten sequenced haloarchaeal genomes[111].

We performed bioinformatic analyses using CDART[28] and the IucA protein sequence from *E. coli* (accession: ABA54740.1) and identified two species within Archaea with predicted IucA/FhuF domains: *Halovivax asiaticus* (WP_007698633.1) and *Haloterrigena turkmenica* (WP_012942097.1) Phyre alignment[83] of the protein sequences showed that the predicted NIS from *Halovivax asiaticus* (HaNIS) aligned with IucA from *K. pneumoniae* with 100% confidence and 21% identity with 78% coverage. Structural alignment between the two enzymes had an RMSD of 0.5 Å and showed very good alignment between catalytic residues involved in ATP binding (Figure 2.21).

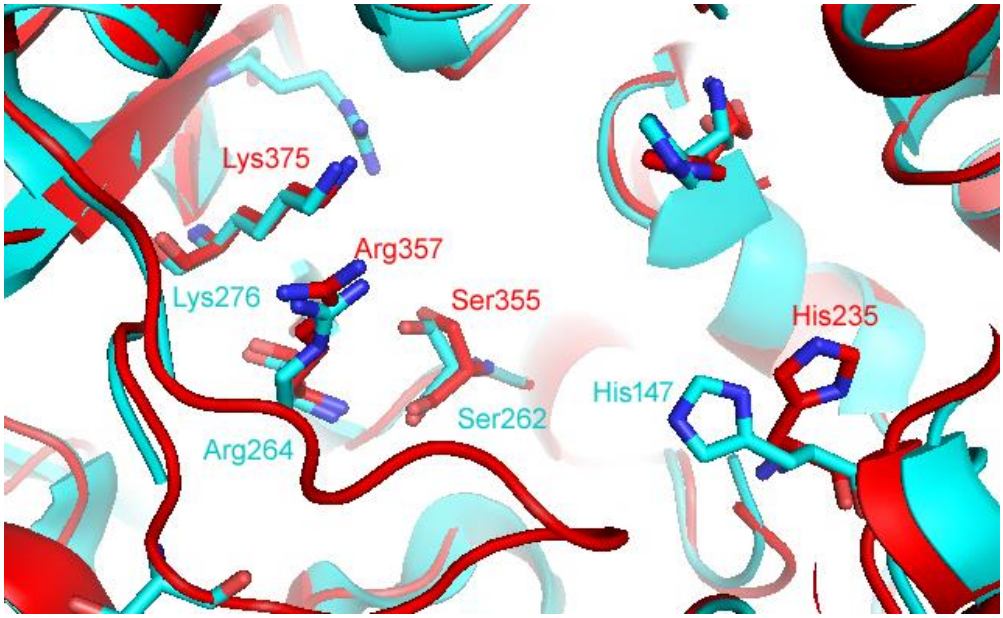

Figure 2.21 Structural alignment of IucA from *Klebsiella pneumoniae* (cyan) and the Phyre model for HaNIS from *Halovivax asiaticus* (red).
Residues shown to be involved in ATP binding in IucA, and their equivalent residues in HaNIS, are highlighted (PDB: 5JM7).

The NIS Phyre model from *Haloterrigena turkmenica* (HtNIS) aligns with AlcC from *B. bronchiseptica* with 100% confidence and 21% identity over 78% of the enzyme. Structural alignment of the two enzymes gave an RMSD value of 0.01 Å indicating very good conservation between the residues of the two proteins. Arg312 and His449 in AlcC align with Arg415 and His564 such that they are indistinguishable in the modeled alignment. This suggests that the mechanism of action for HtNIS is likely very similar to that of AlcC in *B. bronchiseptica*. i.e., dimerization and macrocyclization of succinyl-dihydroxy-putrescine intermediates.

Phylogenetic analyses of the HtNIS and HaNIS proteins using MUSCLE[112] places them in the Type A' NIS group, i.e., they catalyze enantioselective reactions forming siderophores with chiral centers (Figure 2.3).

Haloterrigena turkmenica is a chemoorganotrophic archeon that was isolated from hypersaline sulphate soils[113] and *Halovivax asiaticus* is an extremely halophilic archeon isolated from lake sediments[114]. Both are aerobes. Although there is some evidence that few Archaea are periodontal pathogens[113], *Halovivax* and *Haloterrigena* genera have not been implicated in human disease; therefore siderophore secretion by these species is likely a competitive advantage in their environmental niche.

2.10 Conclusions and future work

The NIS pathway functions primarily in the biosynthesis of polycarboxylate or mixed-type siderophores. In general, NIS synthetases catalyze the ATP-dependent activation of citric acid, or a citrate derivative, followed by nucleophilic capture by an amine or alcohol group and release of the mono-citryl intermediate and AMP from the enzyme active site. This mechanism of action makes NIS enzymes members of the adenylating superfamily of enzymes.

Recent research has focussed on NIS enzymes in Bacteria, however putative NIS enzymes are present in all Domains, including Fungi and Archaea. The NIS enzymes predicted to be in the Archaea are of particular interest, as siderophore secretion has not been well characterized in these organisms. Furthermore, only one fungal NIS enzyme has been characterized, Rfs[46], and its mechanism of action is identical to bacterial NIS enzymes.

Previously, the mechanism of action and substrate usage profile for NIS enzymes has split them into four classes[29,30]. Here, we performed a phylogenetic analysis of known NIS enzymes and propose five types of NIS enzymes. Classification of Type A, A' and B NIS enzymes remains the same; however, there is some evidence that Type C NIS enzymes may be further subdivided into Type C and Type C' classes: Type C enzymes condense simple mono-amides or amines with a citryl or succinyl intermediate, whereas Type C' enzymes dimerize a citryl- or succinyl- intermediate, occasionally followed by macro-cyclization to fully form a siderophore.

The involvement of NIS enzymes in the virulence of many microbial pathogens has been confirmed experimentally, and there are exciting developments in the identification of small molecule inhibitors of specific NIS enzymes. Exploration of novel NIS synthetases and their mechanisms will not only deepen our understanding of their catalytic capabilities and their role in virulence, but also assist in the identification of inhibitors to control microbial growth.

2.11 References

1. Miethke, M. Molecular strategies of microbial iron assimilation: from high-affinity complexes to cofactor assembly systems. *Metallomics* **5,** 15–28 (2013).

2. Kwok, E. Y., Severance, S. & Kosman, D. J. Evidence for iron channeling in the Fet3p-Ftr1p high-affinity iron uptake complex in the yeast plasma membrane. *Biochemistry* **45,** 6317–6327 (2006).

3. Adjimani, J. P. & Emery, T. Iron uptake in *Mycelia sterilia* EP-76. *J. Bacteriol.* **169,** 3664–8 (1987).

4. Fu, Y. *et al.* Cloning and functional characterization of the *Rhizopus oryzae* high affinity iron permease (rFTR1) gene. *FEMS Microbiol. Lett.* **235,** 169–176 (2004).

5. Vandenesch, F. *et al. Staphylococcus aureus* hemolysins, bi-component leukocidins, and cytolytic peptides: a redundant arsenal of membrane-damaging virulence factors? *Front. Cell. Infect. Microbiol* **2,** 1–15 (2012).

6. Bielaszewska, M., Aldick, T., Bauwens, A. & Karch, H. Hemolysin of enterohemorrhagic *Escherichia coli*: Structure, transport, biological activity and putative role in virulence. *Int. J. Med. Microbiol.* **304,** 521–529 (2014).

7. Mahendra Boradia, V. *et al. Mycobacterium tuberculosis* acquires iron by cell-surface sequestration and internalization of human holo-transferrin. *Nat. Commun.* **5,** 4730 (2014).

8. Contreras, H., Chim, N., Credali, A. & Goulding, C. W. Heme uptake in bacterial pathogens. *Curr Opin Chem Biol* **19,** 34–41 (2014).

9. Hider, R. C. & Kong, X. Chemistry and biology of siderophores. *Nat. Prod. Rep.* **27,** 637 (2010).

10. Carrano, C. J. *et al.* Coordination chemistry of the carboxylate type siderophore rhizoferrin: The iron(III) complex and its metal analogs. *Inorg Chem* **35,** 6429–6436 (1996).

11. Harris, W. R. & Raymond, K. N. Ferric ion sequestering agents. The spectrophotometric and potentiometric evaluation of two new enterobactin analogues: 1,5,9-*N,N',N'*-Tris(2,3-dihydroxybenzoyl)-cyclotriazatridecane and 1,3,5-*N,N',N'*-Tris(2,3-dihydroxybenzoyotriaminomethylbenzene. *J. Am. Chem. Soc.* **101,** 6534–6541 (1979).

12. Wong, G. B., Kappel, M. J., Raymond, K. N., Matzanke, B. & Winkelmann, G. Coordination chemistry of microbial iron transport compounds. 24. Characterization of coprogen and ferricrocin, two ferric hydroxamate siderophores. *J. Am. Chem. Soc.* **105,** 810–815 (1983).

13. Harris, W. R. *et al.* Coordination chemistry of microbial iron transport compounds. 19. Stability constants and electrochemical behavior of ferric enterobactin and model complexes. *J. Am. Chem. Soc.* **101,** 6097–6104 (1979).

14. Winkelmann, G. Microbial siderophore-mediated transport. *Biochem. Soc. Trans.* **30,** 691–696 (2002).

15. Haas, H. Fungal siderophore metabolism with a focus on *Aspergillus fumigatus*.

Nat. Prod. Rep. **31,** 1266–76 (2014).

16. Kragl, C. *et al.* EstB-mediated hydrolysis of the siderophore triacetylfusarinine C optimizes iron uptake of *Aspergillus fumigatus*. *Eukaryot. Cell* **6,** 1278–85 (2007).

17. Gründlinger, M., Gsaller, F., Schrettl, M., Lindner, H. & Haas, H. *Aspergillus fumigatus* SidJ mediates intracellular siderophore hydrolysis. *Appl. Environ. Microbiol.* **79,** 7534–6 (2013).

18. Ibrahim, A. S. *et al.* The high affinity iron permease is a key virulence factor required for *Rhizopus oryzae* pathogenesis. *Mol. Microbiol.* **55,** 328–333 (2013).

19. Moore, R. E. & Emery, T. Nα-acetylfusarinines: Isolation, characterization and properties. *Biochemistry* **15,** 2719–2723 (1976).

20. Pollack, J. R. & Neilands, J. B. Enterobactin, an iron transport compound from *Salmonella typhimurium*. *Biochem. Biophys. Res. Commun.* **38,** 989–992 (1970).

21. Meiwes, J. *et al.* Isolation and characterization of staphyloferrin A, a compound with siderophore activity from *Staphylococcus hyicus* DSM 20459. *FEMS Microbiol. Lett.* **67,** 201–205 (1990).

22. Konetschny-Rapp, S., Jung, G., Meiwes, J. & Zaehner, H. Staphyloferrin A: a structurally new siderophore from staphylococci. *Eur. J. Biochem.* **191,** 65–74 (1990).

23. Gibson, F. & Magrath, D. The isolation and characterization of a hydroxamic acid (aerobactin) formed by *Aerobacter aerogenes* 62-1. *Biochim. Biophys. Acta - Gen. Subj.* **192,** 175–184 (1969).

24. Gehring, A. M., Mori, I., Perry, R. D. & Walsh, C. T. The nonribosomal peptide synthetase HMWP2 forms a thiazoline ring during biogenesis of yersiniabactin, an iron-chelating virulence factor of *Yersinia pestis*. *Biochemistry* **37,** 11637–11650 (1998).

25. Keating, T. A., Marshall, C. G. & Walsh, C. T. Reconstitution and characterization of the *Vibrio cholerae* vibriobactin synthetase from VibB, VibE, VibF, and VibH. *Biochemistry* **39,** 15522–30 (2000).

26. Quadri, L. E., Sello, J., Keating, T. A., Weinreb, P. H. & Walsh, C. T. Identification of a *Mycobacterium tuberculosis* gene cluster encoding the biosynthetic enzymes for assembly of the virulence-conferring siderophore mycobactin. *Chem. Biol.* **5,** 631–45 (1998).

27. Gehring, A. M., Mori, I. & Walsh, C. T. Reconstitution and characterization of the *Escherichia coli* enterobactin eynthetase from EntB, EntE, and EntF. *Biochemistry* **37,** 2648–2659 (1998).

28. Geer, L. Y., Domrachev, M., Lipman, D. J. & Bryant, S. H. CDART: Protein Homology by Domain Architecture. *Genome Res.* **12,** 1619–1623 (2002).

29. Oves-Costales, D., Kadi, N. & Challis, G. L. The long-overlooked enzymology of a nonribosomal peptide synthetase-independent pathway for virulence-conferring siderophore biosynthesis. *Chem. Commun. (Camb).* 6530–41 (2009). doi:10.1039/b913092f

30. Challis, G. L. A widely distributed bacterial pathway for siderophore biosynthesis independent of nonribosomal peptide synthetases. *ChemBioChem* **6,** 601–611 (2005).

31. Kearse, M. *et al.* Geneious Basic: an integrated and extendable desktop software platform for the organization and analysis of sequence data. *Bioinformatics* **28,** 1647–9 (2012).

32. Kadi, N., Oves-Costales, D., Barona-Gomez, F. & Challis, G. L. A new family of ATP-dependent oligomerization- macrocyclization biocatalysts. *Nat. ch* **3,** 652–656 (2007).

33. Lynch, D. *et al.* Genetic organization of the region encoding regulation, biosynthesis, and transport of rhizobactin 1021, a siderophore produced by *Sinorhizobium meliloti*. *J. Bacteriol.* **183,** 2576–2585 (2001).

34. Tanabe, T. *et al.* Identification and characterization of genes required for biosynthesis and transport of the siderophore vibrioferrin in *Vibrio parahaemolyticus*. *J. Bacteriol.* **185,** 6938–49 (2003).

35. Kadi, N., Arbache, S., Song, L., Oves-Costales, D. & Challis, G. L. Identification of a gene cluster that directs putrebactin biosynthesis in *Shewanella* species: PubC catalyzes cyclodimerization of N-hydroxy-N-succinylputrescine. *J. Am. Chem. Soc.* **130,** 10458–9 (2008).

36. De Lorenzo, V., Bindereif, A., Paw, B. H. & Neilands, J. B. Aerobactin biosynthesis and transport genes of plasmid colV-K30 in *Escherichia coli* K-12. *J. Bacteriol.* **165,** 570–578 (1986).

37. Giardina, P. C., Foster, L.-A., Toth, S. I., Roe, B. A. & Dyer, D. W. Analysis of the *alcABC* operon encoding alcaligin biosynthesis enzymes in *Bordetella bronchiseptica*. *Gene* **194,** 19–24 (1997).

38. Nusca, T. D. *et al.* Functional and structural analysis of the siderophore synthetase AsbB through reconstitution of the petrobactin biosynthetic pathway from *Bacillus anthracis*. *J. Biol. Chem.* **287,** 16058–16072 (2012).

39. Oves-Costales, D. *et al.* Petrobactin biosynthesis: AsbB catalyzes condensation of spermidine with N8-citryl-spermidine and its N1-(3,4-dihydroxybenzoyl) derivative. *Chem Commun* **0,** 4034–4036 (2008).

40. Lee, J. Y. *et al.* Biosynthetic analysis of the petrobactin siderophore pathway from *Bacillus anthracis*. *J. Bacteriol.* **189,** 1698–1710 (2007).

41. Cheung, J., Beasley, F. C., Liu, S., Lajoie, G. A. & Heinrichs, D. E. Molecular characterization of staphyloferrin B biosynthesis in *Staphylococcus aureus*. *Mol.*

Microbiol. **74,** 594–608 (2009).

42. Berti, A. D. & Thomas, M. G. Analysis of achromobactin biosynthesis by *Pseudomonas syringae pv. syringae* B728a. *J. Bacteriol.* **191,** 4594–4604 (2009).

43. Schmelz, S. *et al.* AcsD catalyzes enantioselective citrate desymmetrization in siderophore biosynthesis. *Nat. Chem. Biol.* **5,** 174–82 (2009).

44. Schmelz, S. & Naismith, J. H. Adenylate-forming enzymes. *Curr Opin Struct Biol* **19,** 666–671 (2009).

45. Bailey, D. C., Drake, E. J., Grant, T. D. & Gulick, A. M. Structural and functional characterization of aerobactin synthetase IucA from a hypervirulent pathotype of *Klebsiella pneumoniae*. *Biochemistry* **55,** 3559–3570 (2016).

46. Carroll, C. S. *et al.* The rhizoferrin biosynthetic gene in the fungal pathogen *Rhizopus delemar* is a novel member of the NIS gene family. *Int. J. Biochem. Cell Biol.* **89,** (2017).

47. Münzinger, M., Budzikiewicz, H., Expert, D., Enard, C. & Meyer, J. M. Achromobactin, a new citrate siderophore of *Erwinia chrysanthemi*. *J. Biosci.* **55,** 328–32 (2000).

48. Smith, C. L., Weiss, B. L., Aksoy, S. & Runyen-Janecky, L. J. Characterization of the achromobactin iron acquisition operon in *Sodalis glossinidius*. *Appl. Environ. Microbiol.* **79,** 2872–81 (2013).

49. Franza, T., Mahé, B. & Expert, D. *Erwinia chrysanthemi* requires a second iron transport route dependent of the siderophore achromobactin for extracellular growth and plant infection. *Mol. Microbiol.* **55,** 261–275 (2005).

50. Kadi, N. & Challis, G. L. *Chapter 17. Siderophore biosynthesis a substrate specificity assay for nonribosomal peptide synthetase-independent siderophore synthetases involving trapping of acyl-adenylate intermediates with hydroxylamine. Methods in enzymology* **458,** 431-457, (Elsevier Inc., 2009).

51. Wu, M. X. & Hill, K. A. W. A continuous spectrophotometric assay for the aminoacylation of transfer RNA by alanyl-transfer RNA synthetase. *Anal. Biochem.* **211,** 320–323 (1993).

52. Schmelz, S. *et al.* Structural basis for acyl acceptor specificity in the achromobactin biosynthetic enzyme AcsD. *J. Mol. Biol.* **412,** 495–504 (2011).

53. Bindereif, A. & Neilands, J. B. Cloning of the aerobactin-mediated iron assimilation system of plasmid Co1V. *J. Bacteriol.* **153,** 1111–1113 (1983).

54. Suzuki, K. *et al.* Identification and transcriptional organization of aerobactin transport and biosynthesis cluster genes of *Vibrio hollisae*. *Res. Microbiol.* **157,** 730–740 (2006).

55. Moon, Y. H. *et al.* Identification and characterization of two contiguous operons

required for aerobactin transport and biosynthesis in *Vibrio mimicus*. *Microbiol. Immunol.* **48,** 389–398 (2004).

56. Stuart, S. J., Prpic, J. K. & Robins-Browne, R. M. Production of aerobactin by some species of the genus *Yersinia*. *J. Bacteriol.* **166,** 1131–3 (1986).

57. Buyer, J. S., de Lorenzo, V. & Neilands, J. B. Production of the siderophore aerobactin by a halophilic Pseudomonad. *Appl. Environ. Microbiol.* **57,** 2246–50 (1991).

58. Vokes, S. A., Reeves, S. A., Torres, A. G. & Payne, S. M. The aerobactin iron transport system genes in *Shigella flexneri* are present within a pathogenicity island. *Mol. Microbiol.* **33,** 63–73 (1999).

59. Russo, T. A. *et al.* Aerobactin mediates virulence and accounts for increased siderophore production under iron-limiting conditions by hypervirulent (hypermucoviscous) *Klebsiella pneumoniae*. *Infect. Immun.* **82,** 2356–2367 (2014).

60. Wilson, M. K., Abergel, R. J., Raymond, K. N., Arceneaux, J. E. L. & Byers, B. R. Siderophores of *Bacillus anthracis, Bacillus cereus*, and *Bacillus thuringiensis*. *Biochem. Biophys. Res. Commun.* **348,** 320–325 (2006).

61. Cendrowski, S., MacArthur, W. & Hanna, P. *Bacillus anthracis* requires siderophore biosynthesis for growth in macrophages and mouse virulence. *Mol. Microbiol.* **51,** 407–417 (2004).

62. Pfleger, B. F. *et al.* Characterization and analysis of early enzymes for petrobactin biosynthesis in *Bacillus anthracis*. *Biochemistry* **46,** 4147–4157 (2007).

63. Oves-Costales, D. *et al.* Enzymatic logic of anthrax stealth siderophore biosynthesis: AsbA catalyzes ATP-dependent condensation of citric acid and spermidine. *J. Am. Chem. Soc.* **129,** 8416–8417 (2007).

64. Oves-Costales, D., Song, L. & Challis, G. L. Enantioselective desymmetrisation of citric acid catalysed by the substrate-tolerant petrobactin biosynthetic enzyme AsbA. *Chem Commun* **11,** 1389–1391 (2009).

65. Oke, M. *et al.* The Scottish structural proteomics facility: Targets, methods and outputs. *J. Struct. Funct. Genomics* **11,** 167–180 (2010).

66. Nishio, T. *et al.* Isolation and structure of the novel dihydroxamate siderophore alcaligin. *J. Am. Chem. Soc.* **110,** 8733–8734 (1988).

67. Moore, C. H., Foster, L. a., Gerbig, D. G., Dyer, D. W. & Gibson, B. W. Identification of alcaligin as the siderophore produced by *Bordetella pertussis* and *B. bronchiseptica*. *J. Bacteriol.* **177,** 1116–1118 (1995).

68. Brickman, T. J., Hansel, J. G., Miller, M. J. & Armstrong, S. K. Purification, spectroscopic analysis and biological activity of the macrocyclic dihydroxamate siderophore alcaligin produced by *Bordetella pertussis* and *Bordetella*

bronchiseptica. *Biometals* **9,** 191–203 (1996).

69. Giardina, P. C., Foster, L.-A., Toth, S. I., Roe, B. A. & Dyer, D. W. Identification of *alcA*, a *Bordetella bronchiseptica* gene necessary for alcaligin production. *Gene* **167,** 133–136 (1995).

70. Young Kang, H., Brickman, T. J., Beaumont, F. C. & Armstrong, S. K. Identification and characterization of iron-regulated *Bordetella pertussis* alcaligin siderophore biosynthesis genes. *J. Bacteriol.* **178,** 4877–4884 (1996).

71. Pradel, E., Guiso, N. & Locht, C. Identification of AlcR, an AraC-type regulator of alcaligin siderophore synthesis in *Bordetella bronchiseptica* and *Bordetella pertussis*. *J. Bacteriol.* **180,** 871–880 (1998).

72. Brickman, T. J. *et al. Bordetella* iron transport and virulence. *Biometals* **20,** 303–322 (2007).

73. Drechsel, H. *et al.* Purification and chemical characterization of staphyloferrin B, a hydrophilic siderophore from staphylococci. *Biometals* **6,** 185–192 (1993).

74. Haag, H. *et al.* Isolation and biological characterization of staphyloferrin B, a compound with siderophore activity from staphylococci. *FEMS Microbiol. Lett.* **115,** 125–30 (1994).

75. Beasley, F. C. *et al.* Characterization of staphyloferrin A biosynthetic and transport mutants in *Staphylococcus aureus*. *Mol. Microbiol.* **72,** 947–963 (2009).

76. Cotton, J. L., Tao, J. & Balibar, C. J. Identification and characterization of the *Staphylococcus aureus* gene cluster coding for staphyloferrin A. *Biochemistry* **48,** 1025–35 (2009).

77. Dale, S. E., Doherty-kirby, A., Lajoie, G. & Heinrichs, D. E. Role of siderophore biosynthesis in virulence of *Staphylococcus aureus*: Identification and characterization of genes involved in production of a siderophore. *Infect. Immun.* **72,** 29–37 (2004).

78. Bhatt, G. & Denny, T. P. *Ralstonia solanacearum* iron scavenging by the siderophore staphyloferrin B is controlled by PhcA, the global virulence regulator. *J. Bacteriol.* **186,** 7896–7904 (2004).

79. Sebulsky, M. T., Hohnstein, D., Hunter, M. D. & Heinrichs, D. E. Identification and characterization of a membrane permease involved in iron-hydroxamate transport in *Staphylococcus aureus*. *J. Bacteriol.* **182,** 4394–400 (2000).

80. Drechsel, H. *et al.* Rhizoferrin—a novel siderophore from the fungus *Rhizopus microsporus var. rhizopodiformis*. *BioMetals* **4,** 238–243 (1991).

81. Thieken, A. & Winkelmann, G. Rhizoferrin: A complexone type siderophore of the mocorales and entomophthorales (Zygomycetes). *FEMS Microbiol. Lett.* **94,** 37–41 (1992).

82. Drechsel, H., Jung, G. & Winkelmann, G. Stereochemical characterization of rhizoferrin and identification of its dehydration products. *BioMetals* **5,** 141–148 (1992).

83. Kelley, L. A., Mezulis, S., Yates, C. M., Wass, M. N. & Sternberg, M. J. E. The Phyre2 web portal for protein modeling, prediction and analysis. *Nat. Protoc.* **10,** 845–858 (2015).

84. Sullivan, J. T., Jeffery, E. F., Shannon, J. D. & Ramakrishnan, G. Characterization of the siderophore of *Francisella tularensis* and role of *fslA* in siderophore production. *J. Bacteriol.* **188,** 3785–95 (2006).

85. Kiss, K., Liu, W., Huntley, J. F., Norgard, M. V. & Hansen, E. J. Characterization of *fig* operon mutants of *Francisella novicida* U112. *FEMS Microbiol. Lett.* **285,** 270–277 (2008).

86. Ramakrishnan, G., Meeker, A. & Dragulev, B. *fslE* Is necessary for siderophore-mediated iron acquisition in *Francisella tularensis* Schu S4. *J. Bacteriol.* **190,** 5353–5361 (2008).

87. Bhaswati Sen, Meeker, A. & Ramakrishnan, G. The *fslE* Homolog, FTL_0439 (fupA/B), mediates siderophore-dependent iron uptake in *Francisella tularensis* LVS. *Infect. Immun.* **78,** 4276–4285 (2010).

88. Pérez, N., Johnson, R., Sen, B. & Ramakrishnan, G. Two parallel pathways for ferric and ferrous iron acquisition support growth and virulence of the intracellular pathogen *Francisella tularensis* Schu S4. *Microbiol. Open* **5,** 453–468 (2016).

89. Deng, K., Blick, R. J., Liu, W. & Hansen, E. J. Identification of *Francisella tularensis* genes affected by iron limitation. *Infect. Immun.* **74,** 4224–4236 (2006).

90. Ramakrishnan, G. Iron and virulence in *Francisella tularensis*. *Front. Cell. Infect. Microbiol* **7,** (2017).

91. Liles, M. R., Scheel, T. A. & Cianciotto, N. P. Discovery of a nonclassical siderophore, legiobactin, produced by strains of *Legionella pneumophila*. *J. Bacteriol.* **182,** 749–757 (2000).

92. Allard, K. A., Viswanathan, V. K. & Cianciotto, N. P. lbtA and lbtB are required for production of the *Legionella pneumophila* siderophore legiobactin. *J. Bacteriol.* **188,** 1351–1363 (2006).

93. Robey, M. & Cianciotto, N. P. *Legionella pneumophila* feoAB promotes ferrous iron uptake and intracellular infection. *Infect. Immun.* **70,** 5659–5669 (2002).

94. Burnside, D. M., Wu, Y., Shafaie, S. & Cianciotto, N. P. The *Legionella pneumophila* siderophore legiobactin is a polycarboxylate that is identical in structure to rhizoferrin. *Infect. Immun.* **83,** 3937–3945 (2015).

95. Chatfield, C. H., Mulhern, B. J., Burnside, D. M. & Cianciotto, N. P. *Legionella pneumophila* LbtU acts as a novel, TonB-independent receptor for the legiobactin

siderophore. *J. Bacteriol.* **193,** 1563–1575 (2011).

96. Chatfield, C. H., Mulhern, B. J., Viswanathan, V. K. & Cianciotto, N. P. The major facilitator superfamily-type protein LbtC promotes the utilization of the legiobactin siderophore by *Legionella pneumophila*. *Microbiology* **158,** 721–735 (2012).

97. Kehrer, J. P. The Haber-Weiss reaction and mechanisms of toxicity. *Toxicology* **149,** 43–50 (2000).

98. Fenton, H. J. Oxidation of tartaric acid in presence of iron. *J. Chem. Soc.* **65,** 899–910 (1894).

99. Chipperfield, J. R. & Ratledge, C. Salicylic acid is not a bacterial siderophore: A theoretical study. *BioMetals* **13,** 165–168 (2000).

100. Neilands, J. B. Mechanism and regulation of synthesis of aerobactin in *Escherichia coli* K12 (pColV-K30). *Can. J. Microbiol.* **38,** 728–33 (1992).

101. Finkelstein, R. A. & Yancey, R. J. Effect of siderophores on virulence of *Neisseria gonorrhoeae*. *Infect. Immun.* **32,** 609 (1981).

102. Heesemann, J. Chromosomal-encoded siderophores are required for mouse virulence of enteropathogenic *Yersinia* species. *FEMS Microbiol. Lett.* **48,** 229–233 (1987).

103. Goetz, D. H. *et al.* The neutrophil lipocalin NGAL is a bacteriostatic agent that interferes with siderophore-mediated iron acquisition. *Mol. Cell* **10,** 1033–1043 (2002).

104. Abergel, R. J. *et al.* Anthrax pathogen evades the mammalian immune system through stealth siderophore production. *Proc Natl Acad Sci* **103,** 18499–18503 (2006).

105. Koppisch, A. T. *et al.* Petrobactin is the primary siderophore synthesized by *Bacillus anthracis* Str. Sterne under conditions of iron starvation. *BioMetals* **18,** 577–585 (2005).

106. Register, K. B., Ducey, T. F., Brockmeier, S. L. & Dyer, D. W. Reduced virulence of a *Bordetella bronchiseptica* siderophore mutant in neonatal swine. *Infect. Immun.* **69,** 2137–2143 (2001).

107. Pérez, N. M. & Ramakrishnan, G. The reduced genome of the *Francisella tularensis* Live Vaccine Strain (LVS) encodes two iron acquisition systems essential for optimal growth and virulence. *PLoS One* **9,** (2014).

108. Tripathi, A. *et al.* Baulamycins A and B, broad-spectrum antibiotics identified as inhibitors of siderophore siosynthesis in *Staphylococcus aureus* and Bacillus *anthracis*. *J Am Chem Soc. January* **29,** 1579–1586 (2014).

109. Hubmacher, D., Matzanke, B. F. & Anemüller, S. Iron-uptake in the Euryarchaeon *Halobacterium salinarum*. *BioMetals* **20,** 539–547 (2007).

110. Dave, B. P., Anshuman, K. & Hajela, P. Siderophores of halophilic archaea and their chemical characterization. *Indian J. Exp. Biol.* **44,** 340–344 (2006).

111. Anderson, I. *et al.* Novel insights into the diversity of catabolic metabolism from ten Haloarchaeal genomes. *PLoS One* **6,** (2011).

112. Edgar, R. C. MUSCLE: multiple sequence alignment with high accuracy and high throughput. *Nucleic Acids Res.* **32,** 1792–7 (2004).

113. Saunders, E. *et al.* Complete genome sequence of *Haloterrigena turkmenica* type strain (4kT). *Stand. Genomic Sci.* **2,** 107–116 (2010).

114. Castillo, A. M. *et al. Halovivax asiaticus gen. nov., sp. nov.,* a novel extremely halophilic archaeon isolated from Inner Mongolia, China. *Int. J. Syst. Evol. Microbiol.* **56,** 765–770 (2006).

115. Brickman, T. J. & Armstrong, S. K. The ornithine decarboxylase gene *odc* is required for alcaligin siderophore biosynthesis in *Bordetella spp.*: Putrescine is a precursor of alcaligin. *J. Bacteriol.* **178,** 54–60 (1996).

Chapter 3.

The rhizoferrin biosynthetic gene in the fungal pathogen *Rhizopus delemar* is a novel member of the NIS gene family

This chapter has been published in the International Journal of Biochemistry and Cell Biology, by Elsevier, 2017, with permission, under the authorship of Carroll CS, Grieve CL, Murugathasan I, Bennet AJ, Czekster CM, Liu H, Naismith J, Moore MM. The rhizoferrin biosynthetic gene in the fungal pathogen *Rhizopus delemar* is a novel member of the NIS gene family. Int J Biochem Cell Biol 89:136-146. doi: 10.1016/j.biocel.2017.06.005. Minor modifications were made to the publication for inclusion in this chapter. These modifications were: addition of the supplementary data to the main text and revision of the Rfs model using AcsD as a template.

Author contributions: This project was designed by Prof. Margo Moore and Cassandra Carroll. I purified and quantified rhizoferrin for the different Mucorales species. I also performed the bioinformatics for Rfs. Indu Murugathasan and I cloned the *rfs* gene from *R. delemar*. I optimized expression and purification conditions for the enzyme with invaluable assistance from Huanting Liu and James Naismith. I optimized the Rfs activity assay and performed statistical analyses. Andrew Bennet interpreted kinetics data for Rfs. Clark Grieve purified wildtype Rfs, cloned the Rfs mutant enzymes and ran activity assays with various substrate derivatives. Clarissa Melo Czekster performed all LC-MS and high-resolution mass spectrometry.

3.1 Abstract

Iron is essential for growth and in low iron environments such as serum many bacteria and fungi secrete ferric iron-chelating molecules called siderophores. All fungi produce hydroxamate siderophores with the exception of Mucorales fungi, which secrete rhizoferrin, a polycarboxylate siderophore. Here we investigated the biosynthesis of rhizoferrin by the opportunistic human pathogen, *Rhizopus delemar* from the Mucorales order. We searched the genome of *R. delemar* 99-880 for a homologue of the bacterial NRPS-independent siderophore (NIS) protein, SfnaD that is involved in biosynthesis of

the carboxylate siderophore staphyloferrin A in *Staphylococcus aureus*. We identified a protein in *R. delemar* with 22% sequence identity and 37% similarity with SfnaD, containing a putative N-terminal IucA/IucC family domain, and a putative C-terminal conserved ferric iron reductase FhuF-like transporter domain. Expression of the putative fungal rhizoferrin synthetase (*rfs*) gene was repressed by iron. The *rfs* gene was cloned and expressed in *E. coli* and siderophore biosynthesis from citrate and diaminobutane was confirmed using high resolution LC-MS. Substrate specificity was investigated showing that Rfs produced AMP when oxaloacetic acid, tricarballylic acid, ornithine, hydroxylamine, diaminopentane and diaminopropane were employed as substrates. Based on the production of AMP and the presence of a mono-substituted rhizoferrin, we suggest that Rfs is a member of the superfamily of adenylating enzymes. We used site-directed mutagenesis to mutate selected conserved residues predicted to be in the Rfs active site. These studies revealed that H484 is essential for Rfs activity and L544 may play a role in amine recognition by the enzyme. This study on Rfs is the first characterization of a fungal NIS enzyme. Future work will determine if rhizoferrin biosynthesis is required for virulence in Mucorales fungi.

3.2 Introduction

Mucormycosis is a potentially life-threatening infection in immunocompromised individuals caused by Mucorales fungi. The most commonly-isolated clinical specimens belong to the genera *Rhizopus, Mucor, Cunninghamella* and *Lichtheimia*[1,2] though *Rhizopus* species account for up to 70% of mucormycosis infections[3]. Some species within *Rhizomucor, Saksenaea* and *Apophysomyces* are also pathogenic but are less commonly isolated[3]. As Mucorales fungi are opportunistic pathogens, they affect immunocompromised individuals such as those with hematological malignancies, particularly acute myeloid leukemia[4], as well as HSCT recipients[5], patients with uncontrolled diabetes [3] or those with elevated serum iron levels[6,7]. Patients with diabetic ketoacidosis (DKA) are particularly susceptible to mucormycosis and the ability to colonize DKA patients is unique to Mucorales fungi; *Aspergillus* and *Candida* infections are uncommon in this patient group[8]. Liposomal amphotericin B and posaconazole are the main antifungal agents used in chemotherapy[9]; however, even with treatment, mortality rates can be as high as 70%[10].

Iron is an essential nutrient for both the host and pathogen as it is required for many biological processes including DNA synthesis and cellular respiration[11]. To limit the growth of pathogens *in vivo*, serum contains iron-binding proteins such as transferrin and lactoferrin that maintain a very low concentration of free iron (~10^{-18} M). To overcome this iron limitation, microbes employ numerous strategies, including reductive iron assimilation (RIA) and uptake by a high-affinity Fe^{2+} transporter[12,13]. In *R. delemar*, reduced expression of the high affinity iron permease, FTR1, resulted in attenuated infection and reduced mortality in DKA mice[14]. An alternative mechanism of iron uptake involves the biosynthesis and secretion of siderophores, low molecular weight organic molecules that are released into the environment under iron-limiting conditions to chelate ferric iron. Hydroxamate siderophores (named for the moiety that complexes ferric iron) are the major class produced by non-Mucorales fungi. In contrast, fungi within the order Mucorales have been shown to produce the polycarboxylate siderophore rhizoferrin [15,16]. The chemical structure of rhizoferrin consists of a diaminobutane backbone linked to two citric acid moieties, with an *R,R*- configuration around the chiral center (Figure 3.1A)[17]. Rhizoferrin is also produced by *Francisella tularensis* and *Ralstonia* (*Pseudomonas*) *pickettii*[18,19]. The two siderophores have the same molecular formula; however, bacterial rhizoferrin is an enantiomer of fungal rhizoferrin with an *S,S* configuration around the chiral center[18,19]. While the structure of *R,R*-rhizoferrin has been elucidated, little is known about its biosynthesis in Mucorales.

The biosynthesis of siderophores is known to occur via two main pathways. The first involves non-ribosomal peptide synthetases (NRPS) that catalyze the condensation of multiple amino acids to form siderophores. The second relies on an NRPS-independent siderophore (NIS) pathway. NIS enzymes function by adenylating a substrate carboxyl group for subsequent condensation with a polyamine or amino alcohol[20]. At present, there are four proposed classes for NIS enzymes based on their substrate specificity for polyamines or amino alcohols and which substrate is activated for downstream condensation[21,22]. Type A NIS synthetases catalyze condensation of citric acid with various amines and alcohols. The Type A' NIS synthetase sub category catalyzes condensation of citric acid specifically with amines. Type B NIS synthetases are predicted to catalyze condensation of α-ketoglutarate with amines; however, only one such enzyme has been biochemically characterized[23]. Type C NIS synthetases are specific for monoamine or monoester derivatives of citric acid, or monohydroxamate

derivatives of succinic acid, and some type C NIS synthetases are known to catalyze formation of oligomeric/macrocyclic siderophores[22].

The Type A' NIS enzymes, SfnaD and SfnaB are responsible for biosynthesis of the polycarboxylate siderophore, staphyloferrin A (Figure 3.1B) in the bacterial pathogen, *Staphylococcus aureus*. In *S. aureus,* SfnaD condenses one molecule of citric acid to D-ornithine forming a citryl-ornithine intermediate which is then used as substrate by SfnaB to condense a second molecule of citrate, yielding the final product staphyloferrin A[21]. Unlike staphyloferrin A, rhizoferrin is a symmetric molecule; therefore, we hypothesized that the synthesis of rhizoferrin should require only a single Sfna-like enzyme to catalyze the condensation of two molecules of citrate to one molecule of diaminobutane in sequential reactions.

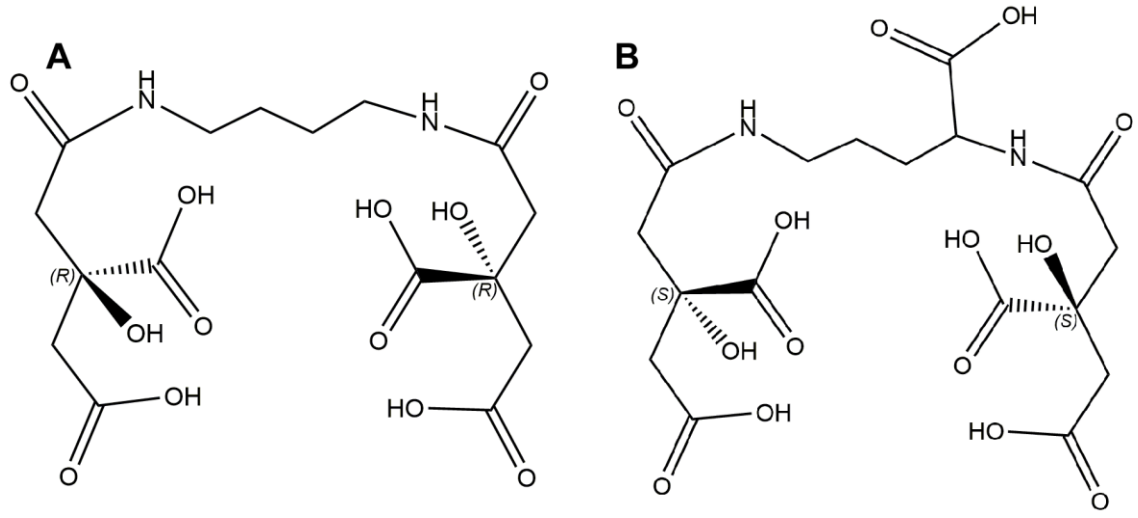

Figure 3.1 The chemical structures of (A) *R,R*-rhizoferrin and (B) *S,S*-staphyloferrin.

3.3 Materials and methods

3.3.1 Bioinformatic analyses

Bioinformatic analyses were conducted using the genomic sequence of *Rhizopus delemar* (99-880) published by Ibrahim et al., 2009[24], and acquired from Genbank (accession: PRJNA13066). Genetic information about *rfs* (accession: RO3G_06864) was obtained from NCBI. Conserved domains were identified in the Rfs protein sequence using the NCBI Conserved Domain Database[25] and Blastp was used to identify Rfs

homologs[26]. Phyre and I-TASSER[27,28] were used to predict the structure of Rfs using the crystal structure of AcsD as a template (PDB: 2W02). PyMOL was used for structural alignments and to produce all protein structure figures (The PyMOL Molecular Graphics System, Version 1.8 Schrödinger, LLC).

Phylogenetic analyses were carried out on NIS synthetases using a Clustal Omega multiple sequence alignment[29]. NIS enzymes used for the alignment are listed in the supplementary information. Analysis of the multiple sequence alignment was done using Jalview (version 2.10.1[30]). Phylogenetic analyses were completed using Geneious (version 9.1.5[31]) and a Neighbor-Joining consensus tree was made. Bootstrap values are indicated at branch nodes.

3.3.2 Strains, media and culture conditions

Rhizopus delemar 99-880 was obtained from American Type Culture Collection (ATCC). *Mucor circinelloides* (UAMH 8307), *Lichtheimia corymbifera* (UAMH 10324) and *Rhizomucor pusillus* (UAMH 10076) were obtained from the University of Alberta Microfungus Collection and Herbarium. *Syncephalastrum racemosum, Cunninghamella echinulata* and *Mucor heimalis* were obtained from the culture collection at Simon Fraser University (Burnaby, Canada). To induce siderophore expression, fungi were grown in low iron media, Media A (20 g sucrose, 3 g (NH4)2SO4, 1 g K2HPO4, 1 g KH2PO4, 25 mg MgSO4• 7H2O, 10 mg CaCl2• 2H2O, 0.2 mg ZnSO4• 7H2O, 1 L water) or Eagle's Minimum Essential Medium (MEM; Sigma) + 10% human serum (male AB positive; Sigma). *Escherichia coli* DH5α was used in standard cloning procedures. Tuner *E. coli* was used for protein expression. Both *E. coli* strains were grown on Luria-Bertani (LB) media (10 g tryptone, 10 g NaCl, 5 g yeast extract, 1 L water) supplemented with ampicillin (100 µg/ml) or kanamycin (30 µg/ml) as needed. All transformations were done using heat-shock and *E. coli* cells were made competent via incubation in 100 mM CaCl2 or in some cases *E. coli* cells were made ultra-competent [32].

3.3.3 Rhizoferrin quantification

Total siderophores were quantified using the Chrome Azurol S (CAS) assay. This assay is based on the CAS dye which is blue in its iron-bound state and yellow/orange in its iron-free form. The CAS solution was prepared as previously described[33]. In a 96-well

plate, equal volumes of CAS solution and fungal supernatant were mixed together and incubated for 30 minutes at room temperature. Absorbance measurements were taken at 630 nm.

3.3.4 Rhizoferrin purification from culture media

Rhizoferrin was purified from Media A according to Drechsel et al., 1991. Briefly, sporangiospores were inoculated into Media A (10^5 spores/ml) and incubated overnight at 37^0 C with shaking at 150 rpm. Mycelia were removed by filtration through Miracloth and the pH of the clarified culture medium was adjusted to 7.0. Rhizoferrin was purified through a Dowex 50WX8 column (formate form) followed by a Biogel P2 column (Bio-Rad Laboratories). One milliliter fractions were collected and CAS-active fractions were pooled and dried by vacuum evaporation.

3.3.5 Confirmation of rhizoferrin production in pathogenic Mucorales

High pressure liquid chromatography (HPLC) was used to verify the presence of rhizoferrin. Rhizoferrin was purified from cultures as described above and dried or freeze-dried samples were re-constituted in water. Ten microliters were injected into a Gemini C18 column (Phenomenex, 250 x 4.6 mm, 5 µm particle size) and compounds were separated using a gradient of 2% - 40% solvent A over 25 minutes using a flow rate of 1 ml/min. Solvent A consisted of acetonitrile (Fisher Scientific, HPLC grade) plus 0.2% trifluoroacetic acid (Caledon Laboratories). Solvent B was water. Absorbance was monitored at 220 nm. To confirm the presence of rhizoferrin, fractions were collected and mass spectrometry was performed using the Agilent 1200 HPLC and a Bruker maXis Ultra-High Resolution tandem TOF (UHR-Qq-TOF) mass spectrometer. Samples were introduced by flow injection via HPLC with acetonitrile/water (0.1 % formic acid) as mobile phase and spectra were collected under positive electrospray ionization (+ESI).

3.3.6 Quantification of rhizoferrin production in pathogenic Mucorales

Fungal spores (10^6 spores/ml) were inoculated into MEM containing 10% human serum (male AB positive, Sigma) and incubated at 37°C with shaking. At designated time

points, 50 µl aliquots were removed and stored at -80^0 C until the CAS assay could be run. Absorbance values were compared to a standard curve constructed using purified rhizoferrin and absolute amounts of siderophore were normalized to fungal dry weights.

3.3.7 Construction of the pEHISTEV-*rfs* vector and *rfs* mutant sequences

R. delemar spores (10^6) were inoculated into Media A and incubated overnight at 37°C with shaking. Mycelia were harvested and RNA was extracted using the NucleoSpin RNA Plant kit (Macherey-Nagel) and cDNA was synthesized using the iScript cDNA Synthesis Kit (Bio-Rad Laboratories). The putative rhizoferrin synthetase gene *(rfs)* was amplified using the primers BamHI-RfsRev and NotI-RfsFor (Table 3.1) and cloned into the multiple cloning site of the pEHISTEVa vector [34] under control of the IPTG inducible promoter and in-frame with a His_6 N-terminal tag. A Tobacco Etch Virus (TEV) cleavage site was present for C-terminal His-tag removal. The resulting vector, pEHISTEV-*rfs* was transformed into competent *E. coli* DH5α and following plasmid purification using the NucleoSpin Plasmid kit (Macherey-Nagel) the cloned *rfs* gene was sequenced (Genewiz, New Jersey, USA) to confirm its fidelity.

Site-directed mutagenesis of the *rfs* gene was done using KAPA HiFi Readymix (KAPA Biosystems). The QuikChange Primer Design program (Agilent Technologies) was used to design primers for mutagenesis (Table 3.1). PCR reactions were carried out according to the manufacturers recommended protocol and products were treated with *DpnI* to digest parental template DNA. Mutant pEHISTEV-*rfs* plasmids were transformed into ultra-competent DH5α *E. coli* cells and selected for by growth on LB containing kanamycin. Successful mutations were confirmed via sequencing (Genewiz, New Jersey, USA).

Table 3.1 Primers employed in this study.
Mutated nucleotides are underlined and recognition sites for restriction endonucleases are in bold.

Primer name	Primer Sequences (5'— 3')	Purpose
NotI-RfsFor	**GCGGCCGC**TTAGATTGCCTCAGGAACACTTTGAGG	Cloning
BamHI-RfsRev	CT**GGATCC**ATGCCTGTTGCCTCGAGTGAA	Cloning
SDM E209A	TTCTTCTACCATAAAATGGGCACAATCGGTTGTTGAAGGAC GTCCTTCAACAACCGATTGTGCCCATTTTATGGTAGAAGAA	Site directed mutagenesis
SDM_R354A	TTGGGTATCAAAATCTCTTCTGCCCTTGCGACCGTCACACCATTC GAATGGTGTGACGGTCGCAAGGGCAGAAGAGATTTTGATACCCAA	Site directed mutagenesis
SDM_H484A	TATAAACGGTGTCGCATTTGAAGCTGCCGGTCAAAACACATTAG CTAATGTGTTTTGACCGGCAGCTTCAAATGCGACACCGTTTATA	Site directed mutagenesis
SDM L544R	CAGTTTAGAAGAGGTCTTCAAACGCTTATATCACACTTTATTCCACT AGTGGAATAAAGTGTGATATAAGCGTTTGAAGACCTCTTCTAAACTG	Site directed mutagenesis
RFS-RT5'	CTGTAGCACGACCGGATATTT	qPCR
RFS-RT3'	TCCGAAATAGGTGGTGAATGG	qPCR
Act1-RT5'	TGAACAAGAAATGCAAACTGC	qPCR
Act1-RT3'	CAGTAATGACTTGACCATCAGGA	qPCR
FTR1- RT5'	GGTGGTGTCTCCTTGGGTAT	qPCR
FTR1-RT3'	AAGGAAACCGACCAAACAAC	qPCR

Wildtype and mutant pEHISTEV-rfs plasmids were purified using the NucleoSpin Plasmid kit (Macherey-Nagel) and transformed into competent Tuner *E. coli* (F– ompT hsdSB (rB– mB–) gal dcm lacY1(DE3)) cells for protein expression.

3.3.8 O-CAS bioassay for siderophore production

Siderophore secretion by *E. coli* transformants was detected on solid media with a CAS overlay (O-CAS) as described by Perez-Miranda et al., 2007. Briefly, Tuner *E. coli* transformed with the pEHISTEV-*rfs* plasmid were grown overnight at 37°C in liquid LB containing 100 µg/ml ampicillin. Five microliters of culture were spotted onto O-CAS media supplemented with 1 mM citric acid and 1 mM diaminobutane, with or without 1 mM of the inducer, IPTG. Cultures were incubated for 5 days at room temperature.

3.3.9 Expression and purification of Rfs

Rfs was expressed and purified according to Oke et al., 2010 with minor modifications. Briefly, Tuner *E. coli* cultures were incubated until an OD_{600} of 0.8-1.0 and then protein expression was induced with 1 mM IPTG overnight at 16ºC. Cells were pelleted, the

supernatant was removed and cells were lysed using either glass beads (5 µm) or the One Shot cell disruptor (Constant Systems Ltd) in PBS, 10 mM imidazole, 400 mM NaCl and 1 mg/ml lysozyme. Cellular debris was pelleted by centrifugation and Rfs was bound to Ni-NTA agarose beads (Qiagen). Beads were washed with PBS, 0.4 M NaCl, 20 mM imidazole and Rfs was eluted using PBS, 0.4 M NaCl, 250 mM imidazole. Elution fractions containing Rfs were pooled, dialyzed against 50 mM Tris (pH 7.5), 0.4 M NaCl, 1 mM DTT, 0.5 mM EDTA and treated with 1 mg/ml of TEV protease overnight at 4^0 C. TEV protease was purified as previously described [36]. TEV protease was removed via passage over a second Ni-NTA column and the column flow through and washes were pooled and concentrated using an Amicon Ultra 10K MWCO filter (EMD Millipore). Gel filtration was performed with a HiLoad 16/600 Superdex 200 prep grade column (GE Healthcare Life Sciences) using 10 mM Tris (pH 7.5) containing 0.15 M NaCl. Fractions containing Rfs were pooled and concentrated using an Amicon Ultra 50K MWCO filter (EMD Millipore). Protein concentrations were determined using the Pierce BCA protein assay kit (ThermoFisher Scientific). Samples were snap frozen in aliquots and stored at -80^0 C. To confirm protein identity and integrity, an SDS-PAGE was run and the 72 kDa band was excised, digested with trypsin and analyzed via mass spectrometry.

The oligomerization state of Rfs was determined using BlueNative gels as described by [37]. Acrylamide gels (4% – 13%) were run for 2 hours at 100 V at 4°C. Rfs (50 µg) was run alone or in the presence of 1 mM citric acid and 7 mM diaminobutane or 70 mM DTT. Molecular masses were determined using the NativeMark™ Unstained Protein Standard (Life Technologies, Carlsbad, CA, USA).

3.3.10 Rfs activity assay

We used a coupled 96-well plate enzyme assay to detect Rfs activity based on the enzymatic production of AMP coupled to lactate dehydrogenase-dependent oxidation of NADH as described by Schmelz et al., 2009. Rfs activity was monitored using the following conditions: 50 mM Tris (pH 8.0), 1 mM ATP, 15 mM $MgCl_2$, 10 mM diaminobutane, 2 mM citric acid, 1.5 mM phosphoenol pyruvate, 8.4 U pyruvate kinase, 12.6 U lactate dehydrogenase, 4 U myokinase and 0.5 µM Rfs. Samples were incubated at 37°C and NADH oxidation was monitored at 340 nm for 30-60 minutes. Control samples contained either no enzyme or enzyme that had been heat inactivated (98°C for 10 min). Controls adding AMP to the reaction mixture were used to show that the other

enzymes used in this assay (pyruvate kinase, lactate dehydrogenase and myokinase) were not limiting the rate of the reaction.

3.3.11 Monitoring the effect of iron on *rfs* expression by qPCR

R. delemar spores were inoculated into Media A and incubated at 37°C with shaking. After overnight incubation, 100µM $FeCl_3$ was added to the cultures at time 0 and the cultures returned to the incubator. At specific times after iron addition, mycelia were harvested by filtration using filter paper and stored in RNAlater (Thermo Fisher Scientific) at 4°C overnight or at -20°C for longer storage. RNA extraction was done according to Warwas et al., 2010. RNA (400 ng) was used to synthesize cDNA with the iScript reverse transcription supermix for RT-qPCR kit (Bio-Rad Laboratories). qPCR primers for *rfs* were designed using the Oligo-dT Analyzer and PrimerQuest (Integrated DNA Technologies). Primers for the housekeeping gene actin *(act1),* and the high-affinity iron permease, *ftr1*, were based on Ibrahim et al., 2010[14] (Table 1). qPCR was performed using the EvaGreen qPCR Mastermix (Applied Biological Materials Inc.) with the following cycling parameters: 95^0 C for 10 minutes followed by 30 cycles of 95^0 C for 15 seconds and 60^0 C for 1 minute. Primer efficiencies for qPCR were comparable for *act1*, *rfs* and *ftr1* gene primers sets (the range was 92 – 98%).

3.3.12 LC–MS and high resolution mass spectrometry

Lyophilized enzyme reactions were re-suspended in 100 µl dH_2O and separation of rhizoferrin or its derivatives were carried out using Phenomenex Luna reverse phase C18 column (100Å, 150mm X 4.6mm). Mobile phase A consisted of 0.1 % trifluoroacetic acid in water while mobile phase B was acetonitrile. A gradient separation using 2 % - 40 % mobile phase A was performed at a flow rate of 1 ml/min. The injection volume was 25 µL and the run was performed at room temperature. For high-resolution mass spectrometry, samples were dissolved in water and injected into an Orbitrap Velos Pro with Dionex Ultimate 3000 HPLC using an Xbridge C18 2.1x100mm column. The mass spectrometry data were acquired in FTMS (Orbitrap) mode from 150-1000m/z from 0-20mins at 30000res in positive ionisation profile mode (ESI+).

3.3.13 Statistical analyses

Growth experiments and qPCR assays were performed in biological triplicates with three technical replicates. AMP assays were performed with three technical replicates for each condition tested. Data were analyzed using GraphPad Prism software. For qPCR experiments and AMP data, a one-way ANOVA with Tukey's multiple comparison test was used to evaluate significantly different gene expression levels ($P < 0.001$) and enzyme activity. All enzyme assays were performed in technical triplicates and a two-site binding model was used to fit the initial rate data for citric acid utilization ($R^2 = 0.965$).

3.4 Results

3.4.1 Rhizoferrin production by species of pathogenic Mucorales

Seven pathogenic Mucorales species including *Rhizopus delemar, Mucor circinelloides, Lichtheimia (Absidia) corymbifera, Syncephalastrum racemosum, Mucor heimalis, Rhizomucor pusillus* and *Cunninghamella echinulata* were grown in iron-limited media (Media A) overnight and rhizoferrin secretion was confirmed in all species using HPLC and mass spectrometry (MS; data not shown); a representative chromatogram and MS spectrum for *R. delemar* is shown in Figure 3.2.

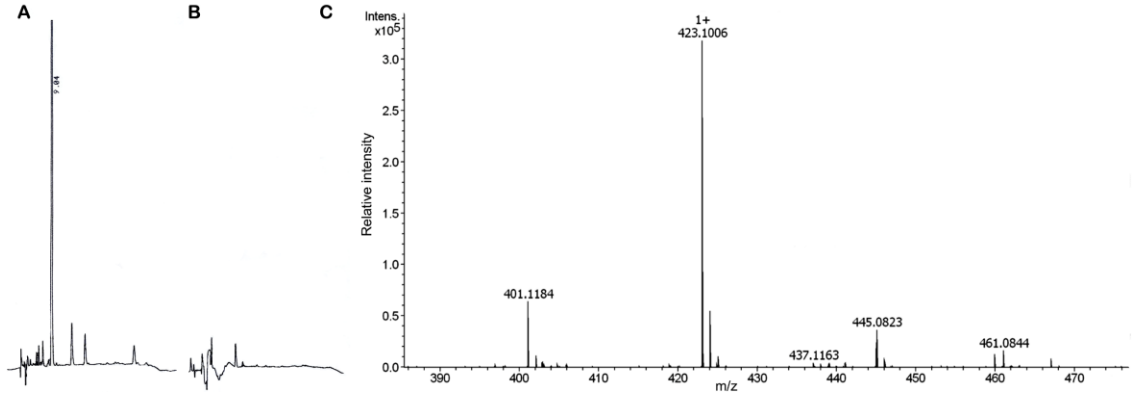

Figure 3.2 Representative HPLC chromatograms of extracted growth medium from *Rhizopus delemar*.

HPLC traces of culture extracts from *R. delemar* grown in (A) low iron medium and (B) iron replete medium. Arrow: the peak corresponding to rhizoferrin at 9.04 min. (C) Mass spectrum showing detection of rhizoferrin from the extract from A. The main peak corresponds to rhizoferrin – $2H_2O$ +Na+ (m/z = 423.10) while the next most abundant peak is rhizoferrin – $2H_2O$(m/z = 401.11).

Rhizoferrin elutes with a retention time of 9.0 minutes and the main mass peaks correspond to rhizoferrin – $2H_2O$ + Na^+ (m/z = 423.10) and rhizoferrin – $2H_2O$ (m/z = 401.11). The chrome azurol S (CAS) assay was used to quantify total rhizoferrin secretion into serum-containing medium. Siderophore concentrations ranged from approximately 7-30 µg/mg dry weight for the 7 species, comparable to levels found in other filamentous fungi [12]. Although *Rhizopus delemar* produced the highest amount of rhizoferrin during log phase (data not shown), when normalized to biomass, *Lichtheimia corymbifera* yielded the most rhizoferrin (Figure 3.3). Though *L. corymbifera* produced the greatest amount of siderophores per mass, we chose to characterize the NIS gene from *Rhizopus delemar* because *Rhizopus* spp. are the most frequent cause of mucormycosis [40,41].

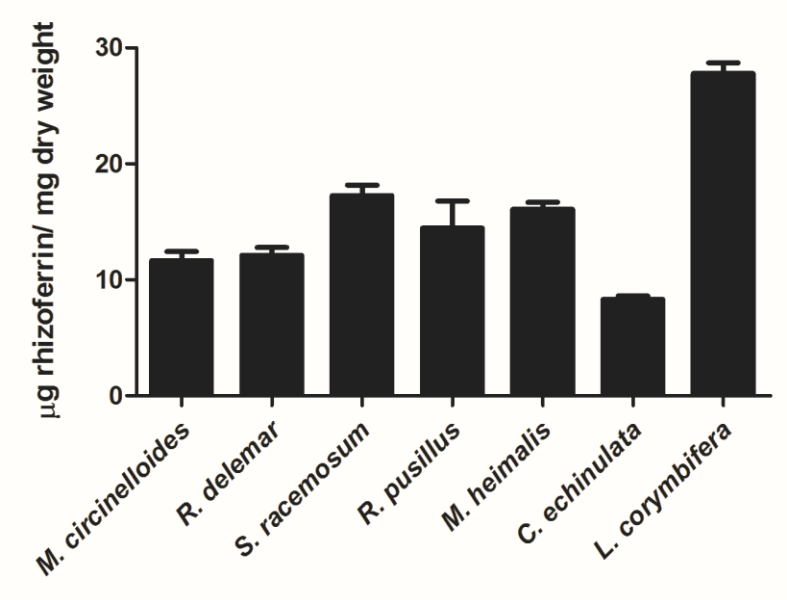

Figure 3.3 Siderophore production by 7 species of pathogenic Mucorales fungi grown in iron-limited medium.

Fungi were inoculated into MEM plus serum and grown at 37°C. Total siderophore content of the culture supernatant was determined during exponential phase (approximately 15 hours) using the CAS assay. The values are normalized to dry biomass yield and error bars represent the standard deviation of three independent measurements.

3.4.2 Bioinformatic analyses

The NIS enzymes SfnaD and SfnaB are responsible for the two-step biosynthesis of the polycarboxylate siderophore, staphyloferrin A in *Staphylococcus aureus.* A homologue of SfnaD was identified in *R. delemar* (strain 99-880) with 22% identity and 37% similarity

with 65% coverage between the putative Rfs protein and SfnaD. The 2.1 kb *rfs* gene was predicted to contain 6 exons and 5 introns. The protein was predicted to be cytosolic, have 634 amino acids and contain the conserved N-terminal IucA/IucC family domain, responsible for biosynthesis of the carboxylate siderophore, aerobactin[42]. A C-terminal conserved ferric iron reductase FhuF-like transporter domain was also predicted in the protein. I-Tasser modelling[28] generated a protein structure alignment with AcsD with 100% confidence. Based on this information, we proposed a biosynthetic pathway for rhizoferrin in which Rfs catalyzes the ATP-dependent condensation of citrate with diaminobutane in the first step followed by the addition of a second citrate to the monocitryl-diaminobutane intermediate (Figure 3.4).

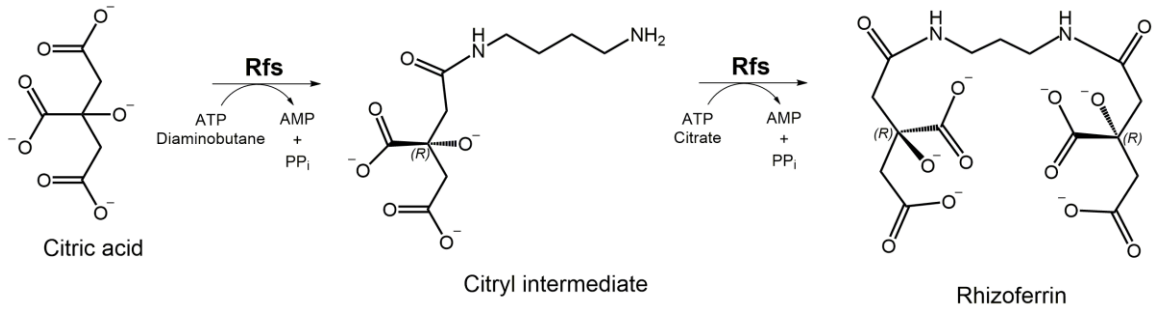

Figure 3.4 Proposed biosynthetic pathway for fungal rhizoferrin.

3.4.3 Phylogenetic analysis of the putative rhizoferrin synthetase gene of *Rhizopus delemar*

Phylogenetic analysis of the predicted Rfs protein resulted in good agreement with Type A' NIS enzymes (Figure 3.5). These enzymes, including FslA and SfnaD, use citric acid and either diaminobutane or ornithine in the formation of bacterial siderophores *(S,S-)* rhizoferrin and staphyloferrin A, respectively.

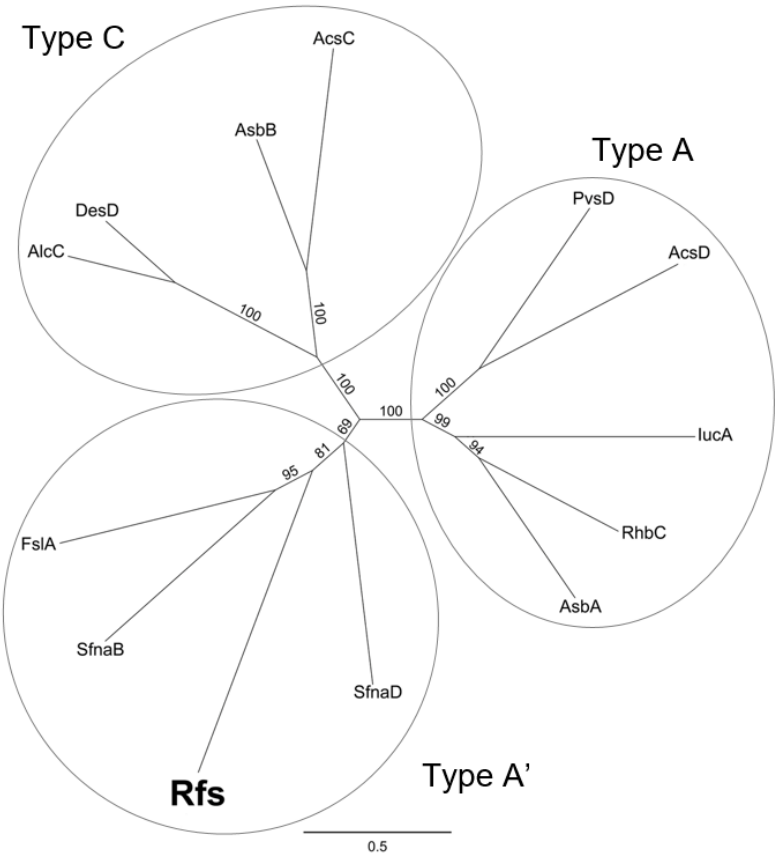

Figure 3.5 Phylogenetic analysis of *rfs* with bacterial NIS enzymes shows that Rfs (in bold) is a Type A' NIS.

The neighbour-joining phylogenetic tree was constructed using Geneious 9.1.5[31] and bootstrap values are indicated at branch nodes. NIS enzyme sequences used in the tree and the siderophore they biosynthesize are as follows: AsbB and AsbA - Anthrax siderophore biosynthesis (petrobactin); DesD - desferrioxamine biosynthesis; AlcC - alcaligin biosynthesis; FslA – S, S-rhizoferrin biosynthesis; SfnaB and SfnaD – staphyloferrin A biosynthesis; RhbC - rhizobactin biosynthesis; IucA – aerobactin biosynthesis; AcsD and AcsC – achromobactin biosynthesis; PvsD – vibrioferrin biosynthesis.

3.4.4 Regulation of *rfs* expression by iron

To determine whether expression of the putative *rfs* gene is regulated by iron, RNA was extracted from *R. delemar* mycelia over time. qPCR analysis confirmed that *rfs* expression was repressed in iron-replete media within 30 minutes and remained at low levels of expression for 3 h post transfer (Table 3.2). Previous work using Northern blots showed that expression of *ftr1*, the high affinity iron permease gene present in *R. delemar*, is iron-regulated[14]. Here, qPCR analysis confirmed that *ftr1* expression levels are repressed under iron supplementation. This trend is similar to *rfs* expression levels, confirming the iron-regulated nature of *rfs* expression.

Table 3.2. *rfs* and *ftr1* gene expression in iron limited and iron replete media.

Rhizopus delemar was grown overnight in Media A (iron limited media) and then transferred to iron replete media (low iron media supplemented with 100µM $FeCl_3$) at time 0. Mycelia were harvested at specific times and RNA was extracted. Mycelia grown in complete media (MEA) was used as an iron-replete control. [a]Data reported are the mean of independent triplicate qPCR reactions conducted for each sample of RNA from the different growth conditions, with the exception of *rfs* expression in MEA which was run in duplicate. *act1* was used as the reference gene to normalize data. [b]ΔC_T = C_T value of gene of interest - C_T value of *act1*. [c]$\Delta\Delta C_T$ = ΔC_T test condition - ΔC_T calibrator condition. The calibrator condition is the zero hour time point. [d]Fold change value is calculated as $2^{-\Delta\Delta CT}$.

	rfs expression					*ftr1* expression				
Growth condition[a]	*rfs* avg. C_T	*act1* avg. C_T	Δ C_T	ΔΔ C_T	Fold change in *rfs* expression $(2^{-\Delta\Delta CT})$[d] (range)	*ftr1* avg. C_T	*act1* avg. C_T	Δ C_T	ΔΔ C_T	Fold change in *ftr1* expression $(2^{-\Delta\Delta CT})$[d] (range)
0 hr	16.09	17.84	-1.75	0.00	1.01 (0.82 – 1.17)	17.08	17.84	-1.45	0.00	1.02 (0.88 – 1.27)
0.5 hr	20.24	17.73	2.51	4.26	0.06 (0.02 – 0.12)	20.80	17.73	1.30	2.75	0.15 (0.13 – 0.18)
1 hr	21.36	18.97	2.39	4.14	0.06 (0.03 – 0.12)	22.28	18.97	3.61	5.06	0.03 (0)
2 hr	20.98	18.58	2.40	4.15	0.06 (0.03 – 0.11)	22.43	18.58	3.38	4.83	0.04 (0.03 – 0.04)
3 hr	21.42	18.29	3.14	4.89	0.04 (0.02 – 0.05)	22.59	18.29	4.07	5.52	0.02 (0.02 – 0.03)
MEA	24.38	22.97	1.41	3.16	0.05 (0.04 – 0.08)	24.11	22.97	3.86	5.31	0.03 (0.02 – 0.03)

3.4.5 Activity of Rfs overexpressed in *E. coli*

The *rfs* gene was successfully cloned and expressed in Tuner *E. coli* and *E.coli* cells harbouring the pEHISTEVa-*rfs* plasmid were capable of producing a siderophore from diaminobutane and citric acid. O-CAS media was inoculated with Tuner cells harbouring the pEHISTEV-*rfs* vector and siderophore production was detected by the presence of halos around colonies induced for Rfs expression and in the presence of the substrates, citrate and diaminobutane (Figure 3.6).

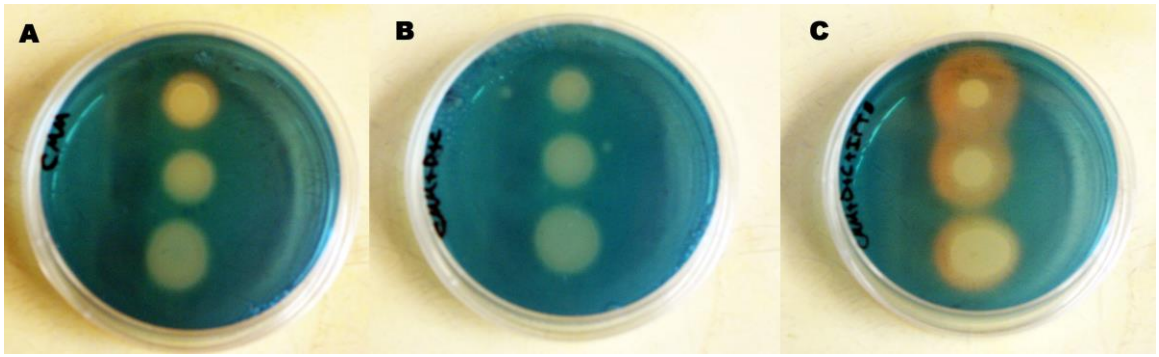

Figure 3.6 O-CAS minimal media plates confirm biosynthesis of siderophores by Tuner *E. coli* harbouring pEHISTEV-*rfs*.

O-CAS minimal media was spotted with 2, 5 or 10 µl of bacteria culture (top to bottom of plate). (**A**) O-CAS minimal media alone, (**B**) in the presence of citrate and diaminobutane and (**C**) in the presence of citrate and diaminobutane and Rfs expression was induced by adding 1mM IPTG. Siderophore production is shown by the large halos surrounding the bacterial colonies as seen in panel C.

Expression conditions for Rfs in Tuner *E. coli* were optimized, and a 72 kDa HIS-tagged protein corresponding to Rfs was purified by nickel affinity chromatography, followed by gel filtration (Figure 3.7).

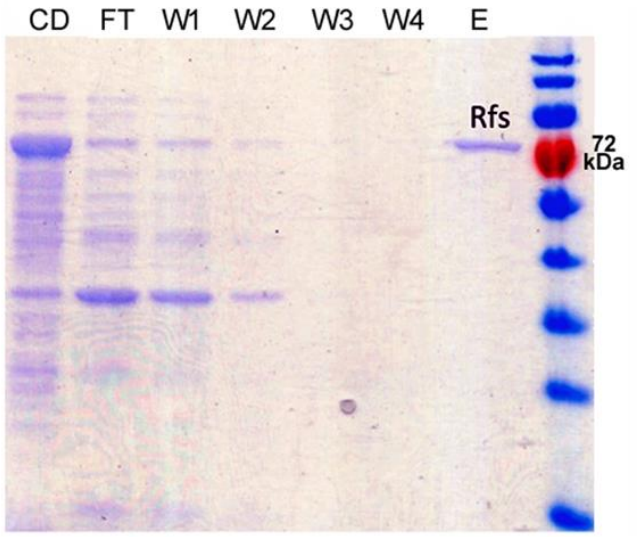

Figure 3.7 Expression and purification of recombinant Rfs from Tuner *E. coli*. Coomassie gel analysis of induced and uninduced Tuner cultures containing the pEHISTEV-*rfs* vector. Rfs expression and purification were as described in the Materials and Methods. CD – cellular debris; FT – NiNTA column flow-through; W1-4 – column washes 1-4; E – elution. The expected molecular mass of Rfs is 72kDa.

Gel filtration indicated that Rfs formed an oligomeric complex in pH 7.5 buffer; however, when in pH 8.0 buffer (used in the AMP assay) and in the presence of citric acid and diaminobutane, Rfs adopts a monomer configuration as determined by BlueNative gel electrophoresis (Figure 3.8).

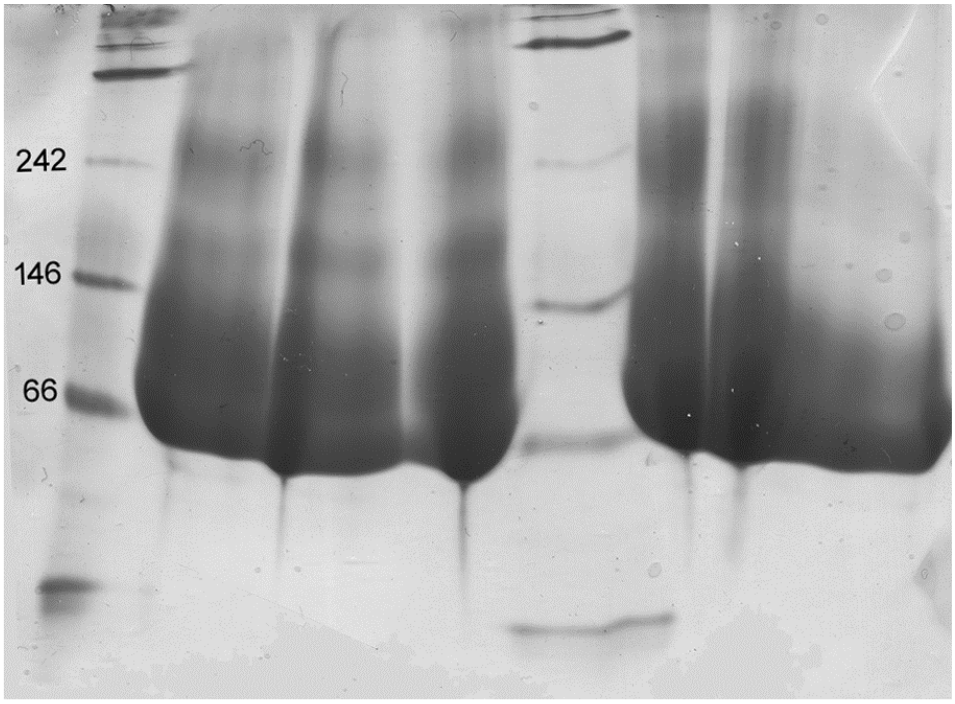

Figure 3.8 The oligomerization of Rfs determined by BlueNative gel electrophoresis using 4% – 13% acrylamide gels.

Rfs was run alone or in the presence of 1 mM citric acid and 7 mM diaminobutane or 70 mM DTT. Rfs was diluted to 50µg in either 10mM Tris (pH 7.5), 150mM NaCl or 10mM Tris (pH 8.0), 150mM NaCl. In the presence of its substrates and at pH 8.0, Rfs forms a monomer. The expected mass of Rfs is 72 kDa. Without substrates and at pH 7.5, Rfs forms an oligomeric complex as indicated by the bands at higher molecular weights. The NativeMark™ Unstained Protein Standard is labelled and all molecular masses are in kDa.

Rhizoferrin biosynthesis by purified Rfs from citrate and diaminobutane was confirmed using high resolution LC-MS (Figure 3.9). The main peak observed corresponds to rhizoferrin + H^+ (*m/z* = 437.1393) and a peak was also observed for rhizoferrin - H_2O (*m/z* = 419.1296). A peak corresponding to the mono-citryl intermediate was also observed (m/z = 263.1234). This suggests that Rfs forms an adenylated-citryl intermediate that is displaced from the active site upon nucleophilic capture of diaminobutane. These peaks were not present in control reactions prepared using boiled Rfs enzyme (data not shown).

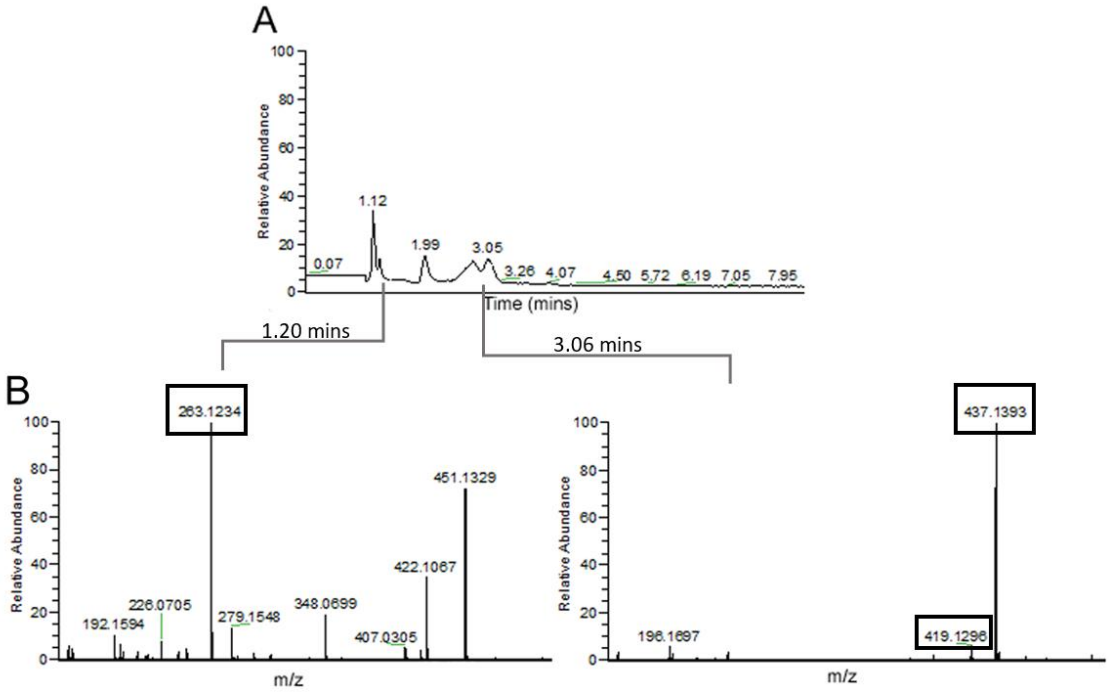

Figure 3.9 LC-MS/MS confirmation of rhizoferrin biosynthesis in vitro by recombinant Rfs from *R. delemar.*

A. Liquid chromatography trace of the Rfs reaction and (**B**) the corresponding mass spectra from peaks at 1.20 minutes and 3.06 minutes. Masses corresponding to rhizoferrin are highlighted in boxes. The mono-citryl intermediate of rhizoferrin was found (m/z = 263.1234) as well as the full compound (rhizoferrin + H^+ (*m/z* = 437.1393)). A dehydrated form of rhizoferrin was also present (rhizoferrin - H_2O (*m/z* = 419.1296)).

3.4.6 Recombinant Rfs kinetic analysis

A coupled AMP production/NADH oxidation assay[38] was used to monitor Rfs activity. A schematic of this assay is shown in Figure S3.15. First, we demonstrated that other enzymes used in this coupled enzyme assay, myokinase and lactate dehydrogenase, were not rate limiting; therefore, the rate-limiting step in all reactions was the Rfs catalysis (Figure 3.10). Kinetic analysis of the fungal NIS showed that Rfs efficiently used diaminobutane and citric acid as substrates. Rfs kinetic parameters were determined using the initial rate of citric acid utilization over a range of 0.05 - 5 mM.

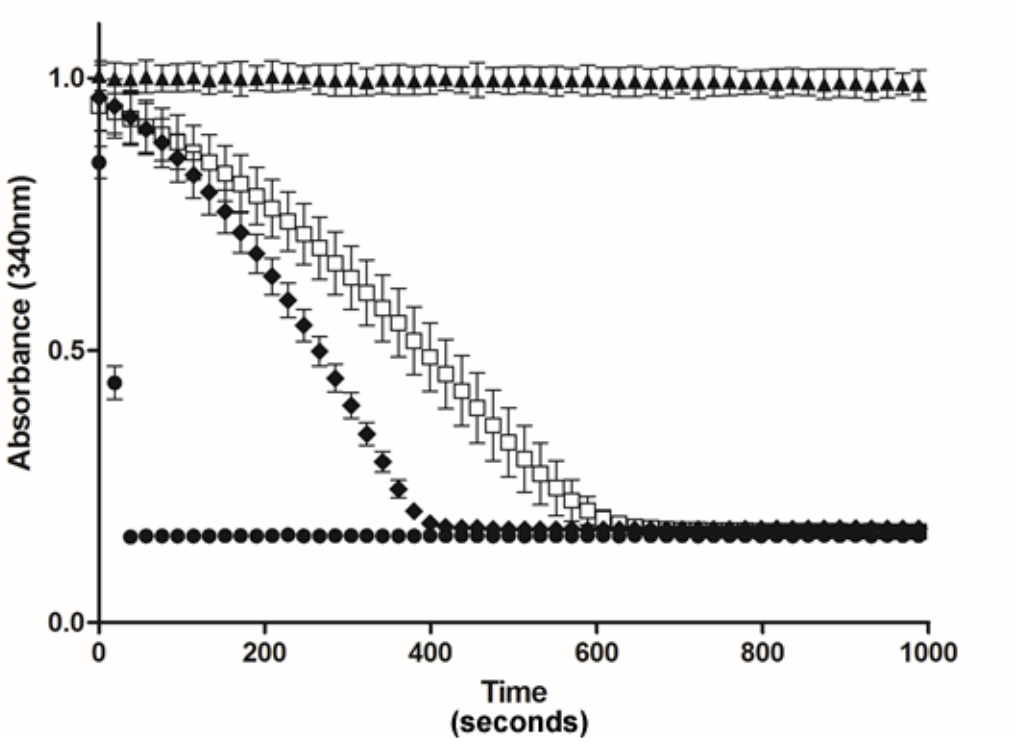

Figure 3.10 Enzymes used in the AMP turnover assay are not rate-limiting.
In the AMP turnover assay, formation of AMP is crucial for activity of downstream enzymes and the eventual oxidation of NADH to NAD^+. When AMP alone is added (without Rfs), the reaction goes to completion within 40 seconds (●). Upon addition of Rfs, the oxidation of NADH slows, indicating that Rfs is the rate limiting enzyme in the reaction (□). Furthermore, when the concentration of Rfs in the reaction is doubled (♦), the reaction rate increases, confirming that the rate – determining step is catalyzed by Rfs. Boiled Rfs was used a control that shows no abiotic oxidation of NADH (▲). Error bars represent the standard deviation of three replicates.

Concentrations of 20 mM citric acid and above were found to be inhibitory to the downstream enzymes in the AMP assay (data not shown) and were not included in data analysis. The best fit to our data was found using a two-site binding model yielding V_{max} and K_d values for two isozymes. For the first species, the V_{max} and K_d were 9.03 ± 1.47 μM/min and 0.03 ± 0.01 mM, respectively; for the second species the V_{max} and K_d were 24.46 ± 8.04 μM/min and 4.97 ± 3.73 mM, respectively. As this model gave the best fit for citric acid utilization, it suggests that Rfs has two binding sites for citric acid adenylation; however, bioinformatic analyses do not predict these two sites to be within one enzyme implying that Rfs may be functional as both a monomer and dimer under the conditions tested. While BlueNative gel analysis (Figure 3.8) shows predominantly a monomer at pH 8.0 in the presence of substrates, there may be assembly and/or disassembly of the more favourable form over time that would not be seen during gel

analysis. Furthermore, the two-site binding model implies that the dimer to monomer transition, and vice-versa, is slow relative to kinetics; however, as dimers were not observed in the gel analysis (Figure 3.8), the ratio of monomer to dimer cannot be determined. Therefore, k_{cat} and k_{cat}/K_m cannot be calculated.

3.4.7 Activity of recombinant Rfs with different substrates

When analyzing substrate derivative data, K_m and V_{max} values could not be determined because linear regression of the NADH consumption versus time data did not produce a random plot of the residuals (data not shown). Instead, we compared the substrate derivatives by measuring the time required for Rfs to consume 50% of the initial NADH present. Shorter periods of time indicated faster consumption of NADH and therefore, more rapid Rfs activity.

The activity of Rfs using the native substrates was compared with equimolar concentrations of various analogues of both citrate and diaminobutane. Oxaloacetic acid and tricarballylic acid were active as citrate analogs in the assay; succinic acid and α-keto glutaric acid showed no activity. The following compounds were active in the assay as diaminobutane derivatives (from highest to lowest activity): diaminopropane, diaminopentane, hydroxylamine and ornithine (Figure 3.11). Negligible activity was detected with butylamine, 4-amino-1-butanol and serine.

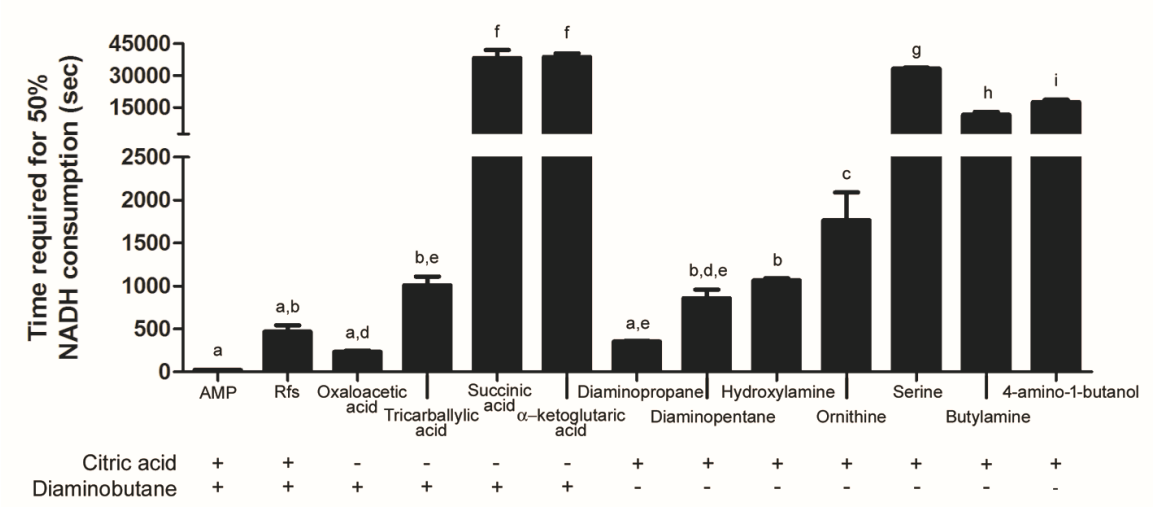

Figure 3.11 Activity of Rfs using various substrate derivatives.
Data is presented as the amount of time required to reach 50% NADH consumption; therefore smaller values indicated faster NADH consumption. The data represent the mean of three measurements and error bars indicate the standard deviation. A one-way ANOVA was used to evaluate significantly different means. Means with the same letter are not significantly different from each other ($P<0.001$).

To determine whether Rfs completes the condensation of the analogues for the various substrates, LC-MS/MS was performed on lyophilized enzyme reactions. Rfs formed only a mono-substituted intermediate with oxaloacetic acid and diaminopentane whereas both mono-citryl intermediates and full rhizoferrin derivatives were detected when diaminopropane, and ornithine were used as substrates. Tricarballylic acid only formed a rhizoferrin derivative; no mono-substituted intermediate was detected in this reaction (Table 3.3).

Table 3.3. Expected and actual masses or rhizoferrin derivatives obtained from mass spectrometry analysis of Rfs reactions.

Reactions where no product was observed show only the expected mass in brackets.

	Diaminobutane + Citric acid	Diaminopentane + Citric acid	Diaminopropane + Citric acid	Ornithine + Citric acid	Oxaloacetic acid + Diaminobutane	Tricarballylic acid + Diaminobutane
	Observed mass (expected mass)	Observed mass (expected mass)	Observed mass (expected mass)	Observed mass (expected mass)	Observed mass (expected mass)	Observed mass (expected mass)
M + H	437.1403 (437.1402)	451.1556 (451.1558)	423.1245 (423.1245)	481.1303 (481.1303)	(317.0979)	405.1504 (405.1503)
M - H_2O + H	(419.1296)	(433.1452)	405.1142 (405.1139)	(463.1197)	(299.0873)	387.1399 (387.1397)
M - citryl + H	263.128 (263.124)	277.1392 (277.1399)	249.1082 (249.1086)	307.1130 (307.1141)	143.0815 (143.082)	(231.1344)

3.4.9 Site-directed mutagenesis of Rfs

Based on multiple sequence alignments of NIS proteins from bacteria (Figure 3.12), we used site-directed mutagenesis to mutate selected conserved residues in the Rfs active site (Figure 3.13). Protein modelling showed that the amino acids chosen for mutation aligned with residues found to be critical in the NIS enzyme, AcsD[38]. Specifically, four mutations were made in Rfs: arginine at position 354 (R354), histidine at position 484 (H484) and glutamate at position 209 (E209) were all mutated to alanine residues, whereas leucine at position 544 was mutated to an arginine (L544R) (Figure 3.12). R354A and H484A were chosen because these amino acids are predicted to be involved in citrate and ATP recognition in the active site of AcsD. L544R was constructed such that the active site in Rfs mimicked AcsD which is able to use serine[43]. E209 was one of two resides conserved across all NIS enzymes and is located on the periphery of the enzyme active site (Figure 3.13). However, expression of the E209A protein was poor in multiple bacterial expression hosts under various conditions (data not shown). Structural modelling showed that E209 in Rfs forms salt bridges with several nearby residues, particularly R505, which may be involved in maintaining the overall structure of Rfs (Figure S3.16). These data suggest that E209 is a conserved residue that is required for proper folding of Rfs and possibly all NIS enzymes.

Figure 3.12 Multiple sequence alignment of NIS protein sequences.

The Rfs protein sequence is highlighted by the arrow. E209 is one of two amino acids conserved across all NIS proteins analyzed (indicated with an asterix). E209 was chosen for mutation as it is predicted to be within a helical domain and is located on the periphery of the enzyme active site as shown with 3D protein modelling. The secondary structure prediction for Rfs is denoted on the bottom of the alignment. Red bars – helix domains, green arrows – β-sheet domains. The following bacterial proteins were used for the alignment: RhbC (*Sinorhizobium meliloti;* accession: WP_010968203.1), AcsD (*Dickeya dadantii*; accession: WP_013317292.1), IucA (*Escherichia coli*; accession: AAZ29624.1), PvsD (*Vibrio*

alginolyticus; accession: ABM30202.1), AcsC (*Dickeya chrysanthemi*; accession: AAL14570.1), AlcC (*Bordetella spp*.; accession: WP_010926978.1), DesD (*Streptomyces scabiei*; accession: WP_013003384.1), AsbB (*Bacillus cereus*; accession: WP_011053144.1), SfnaD (*Staphylococcus aureus*; accession: WP_001052566.1), SfnaB (*Staphylococcus aureus*; accession: WP_072519492.1), FslA (*Francisella tularensis*; accession: WP_003022888.1) and AsbA (*Bacillus anthracis*; accession: WP_000679659.1).

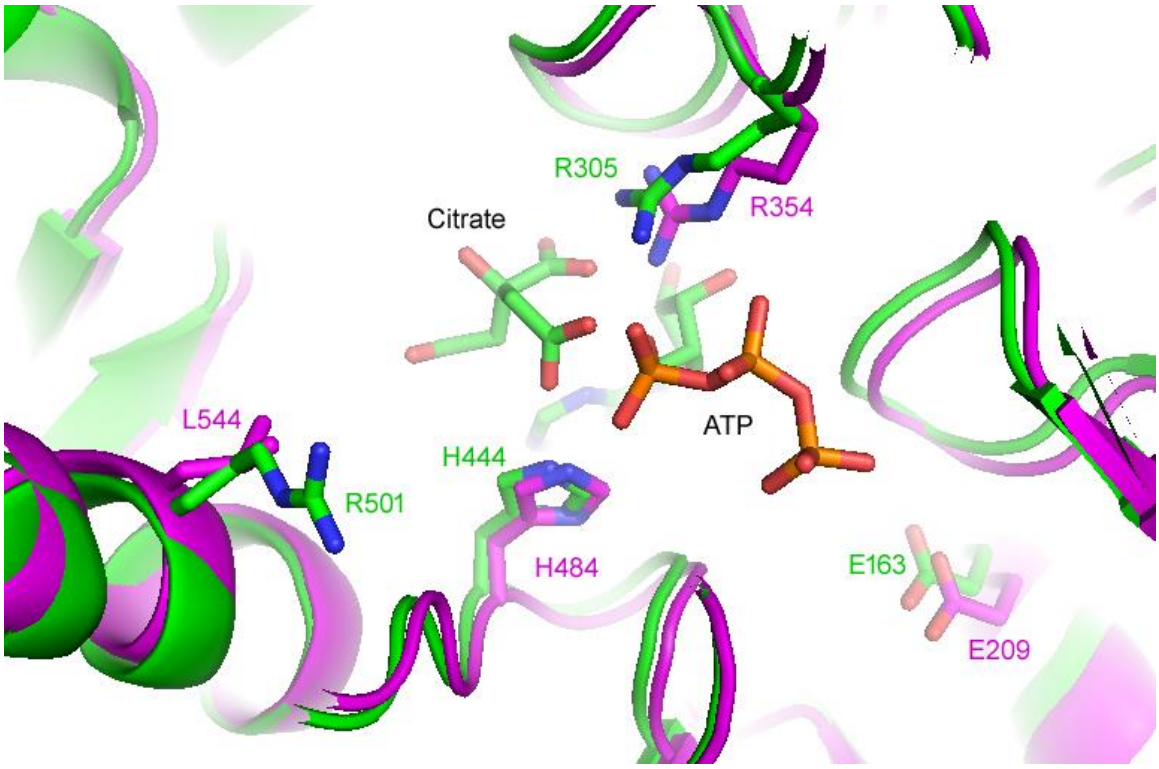

Figure 3.13 Modelling of the Rfs active site (green) using AcsD (magenta) as a template.

The following substitutions were made and the catalytic enzyme activity was compared to the wild type enzyme: R354A, H484A, L544R and E209A. E209A was not expressed efficiently in Tuner *E. coli* and was therefore excluded from analysis.

The R354A mutation did not alter NADH consumption compared to the wild type enzyme (Figure 3.14). In contrast, H484A was inactive, demonstrating a crucial role in catalysis and/or substrate binding. Using the native substrates diaminobutane and citric acid, L544R had similar activity to the wildtype enzyme. Interestingly, when serine was added in place of diaminobutane, the wild type enzyme had zero activity but L544R was able to accommodate serine in the active site and consumed NADH at a significantly higher rate (Figure 3.14). This enhanced activity shows that we were successful in expanding the substrate binding pocket of Rfs and may indicate that the residue at position 544 in Rfs plays a role in governing the amino-substrate specificity of NIS enzymes.

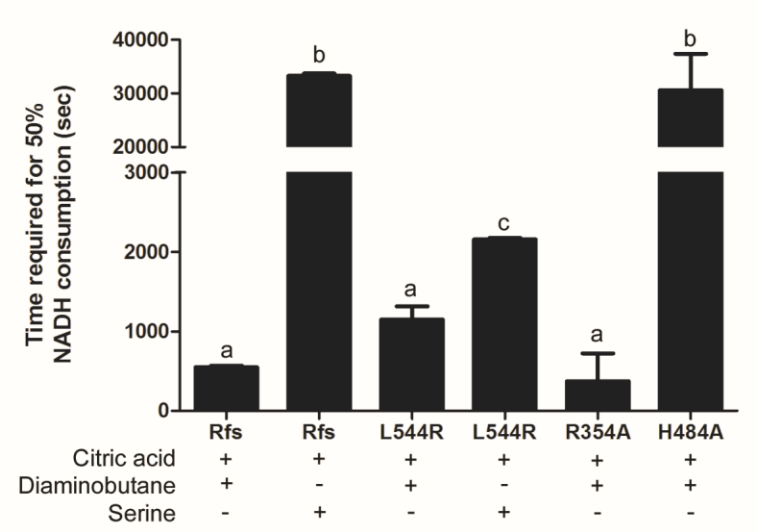

Figure 3.14 Activity of wild type and mutant Rfs enzymes.
Activity of the wild type and Rfs mutants was assessed using the AMP assay with the native substrates, diaminobutane and citric acid, or with serine. H484A displayed very little NADH consumption, while R354A used diaminobutane and citric acid as substrates and consumed NADH at the same rate as the wild type enzyme. L544R can use diaminobutane, citric acid and serine as substrates. The data represent the mean of three measurements and error bars indicate the standard deviation. A one-way ANOVA and Tukey's Multiple Comparison test were used to evaluate significantly different means. Means with the same letter are not significantly different from each other ($P<0.001$).

3.5 Discussion

This study confirmed and quantified rhizoferrin secretion in seven pathogenic species of Mucorales fungi. While rhizoferrin production has been confirmed in *Mucor mucedo*, *Rhizopus microsporus var. rhizopodiformis* and *Cunninghamella elegans*[15], this is the first confirmation of rhizoferrin production in *Rhizopus delemar, Mucor circinelloides, Lichtheimia (Absidia) corymbifera, Syncephalastrum racemosum, Mucor heimalis, Rhizomucor pusillus* and *Cunninghamella echinulata.* We have also identified and characterized the NIS synthetase responsible for rhizoferrin biosynthesis (Rfs) in the fungal pathogen *Rhizopus delemar*. Of the Mucorales genomes that have been sequenced, Rfs homologues were identified in the following species based on the presence of the conserved IucA/IucC domain[44]: *L. corymbifera*, *L. ramosa*, *Mucor ambiguus*, *M. circinelloides f. lusitanicus*, *M. circinelloides f. circinelloides*, *Rhizopus microsporus*, *Absidia glauca*, *Parasitella parasitica*, *Choanephora cucurbitarum* and *Phycomyces blakesleeanus*. Future work will aim to eliminate expression of *rfs* in one of these Mucorales species to determine the role Rfs plays in virulence.

The fungal NIS synthetase characterized in this study was shown to be part of the Type A' NIS family and, similar to other siderophore biosynthetic genes, its expression is repressed by iron. In *Aspergillus fumigatus*, the global iron regulatory protein HapX is responsible for transcriptional regulation of a suite of genes involved in iron uptake, including siderophore biosynthetic genes and transport genes[45]. HapX homologues have been identified in other filamentous fungi, including various *Aspergillus* and *Penicillium* species; however, HapX homologs have yet to be identified or characterized in Mucorales fungi.

Based on the work described here, we proposed a mechanism for rhizoferrin biosynthesis involving ATP-dependent formation of a mono-citryl rhizoferrin intermediate using 1 molecule of citric acid and 1 molecule of diaminobutane (Figure 3.4). The intermediate is then condensed with another molecule of citric acid to form rhizoferrin, using Mg^{2+} as a cofactor and 2 molecules of ATP in total. A similar mechanism has been described for the NIS enzyme, AcsD[38]. In AcsD, adenylation of the carboxylate group in citrate results in an enzyme-bound acyl adenylate intermediate that is condensed with an amine/alcohol resulting in displacement of AMP and the formation of the amide/ester product. This mechanism has also been confirmed in the NIS enzymes SbnE, SbnC and SbnF, which are involved in biosynthesis of the carboxylate siderophore, staphyloferrin B[46]. In this reaction, a citryl adenylate intermediate is formed using the Type A NIS enzyme, SbnE, followed by condensation with 2,3 diaminopropionic acid. This intermediate is decarboxylated and the now citryl-diaminoethane intermediate is adenylated by the Type C NIS enzyme, SbnF and condensed with diaminopropionic acid again. The full staphyloferrin B compound is created when α-ketoglutarate is added by the Type B NIS synthetase, SbnC[46] This mechanism of action makes AcsD, SbnE, SbnF and SbnC members of the superfamily of adenylating enzymes[38]. Based on their sequence similarity, the production of AMP in the assay and LC-MS detection of the mono-citryl rhizoferrin intermediate, we propose that Rfs is a member of the superfamily of adenylating enzymes and the first fungal member of the NIS family.

Rfs is capable of using citric acid derivatives as well as diaminobutane derivatives as substrates. Rfs used oxaloacetic acid and tricarballylic acid as citric acid derivatives and diaminopropane, diaminopentane, hydroxylamine, and ornithine as diaminobutane derivatives. Interestingly, Rfs was capable of using these derivatives to form di-substituted rhizoferrin derivatives, with the exception of oxaloacetic acid and

diaminopentane which formed mono-substituted compounds. In contrast, Tschierske et al. (1996)[47] produced rhizoferrin analogues using directed fermentation with *C. elegans,* and gas chromatography and mass spectrometry confirmed the production of a di-substituted diaminopentane derivative; a derivative using ornithine was not detected and only the mono-substituted tricarballylic acid derivative was found in very low yield. Similar to our study, Tschierske et al. (1996)[47] found that diaminobutane derivatives were more readily incorporated to make rhizoferrin analogues compared to citric acid derivatives. This suggests that citrate recognition in the enzyme active site is stricter compared to the choice of nucleophile. However, it is worth noting that only a few substrate combinations were analyzed and more experiments are required to further elucidate the recognition mechanism and catalytic kinetics with different substrate derivatives.

To investigate the amino acids crucial for Rfs functioning, several mutants were made. Of these mutants, H484A was shown to be essential, most likely involved in ATP binding, as seen in AscD[38]. Additionally, we mutated L544 to an arginine, mimicking the AcsD binding site for serine, a substrate not used by wild type Rfs. We showed that L544R was catalytically active using diaminobutane in the formation of rhizoferrin. Interestingly, L544R successfully utilized serine as a substrate suggesting that L544 does play a role in nucleophile recognition. Experiments are underway to obtain a crystal structure in complex with substrates for Rfs to confirm this hypothesis.

Rhizoferrin secretion has been identified in bacteria, including *Francisella tularensis*, *Ralstonia pickettii, Morganella morganii* and recently, in *Legionella pneumophila*[18,19,48. 49]. The molecular formula of rhizoferrin isolated from bacteria and fungi is identical but they are enantiomers (Figure 3.1)[17,18]. Biosynthesis of bacterial rhizoferrin is catalyzed by the NIS enzyme, FslA in *F. tularensis*[19] and expression of *fslA* was shown to be iron regulated and transcription occurred as part of an operon[50]. This phenomenon was also observed in the biosynthesis of other polycarboxylate siderophores including, staphyloferrin A[21], staphyloferrin B[51], achromobactin[52], vibrioferrin[53] and petrobactin[54]. Typically, genes transcribed as part of this operon encode proteins involved in secretion of the desferri-siderophore (iron free) or uptake of the ferrated compound. Bioinformatic analyses of the locus surrounding *rfs* in *R. delemar* did not reveal any genes related to metal transport (Figure S3.17). Uptake of ferrated rhizoferrin has been characterized in the bacteria *M. morganii* and *L. pneumophila*. In *L. pneumophila* the inner membrane

transporter, LbtB was shown to be involved in export of the desferri-siderophore, while the outer and inner membrane proteins, LbtU and LbtC mediate ferri-rhizoferrin uptake[49]. In *M. morganii*, uptake of ferrated rhizoferrin occurs via the RumA and RumB proteins[48]. A search of the *R. delemar* proteome did not uncover any homologues (with >16% sequence coverage) to LbtB, LbtU or LbtC. A hypothetical homolog was found for the RumB protein using DELTA-BLAST[55]; the match was weak with 23% coverage and 28% identity for rumB. As no significant homologues are present in *R. delemar*, uptake of ferrated-rhizoferrin in Mucorales fungi may occur via a novel mechanism.

This work has successfully identified and characterized the enzyme responsible for rhizoferrin biosynthesis in the pathogenic fungus *Rhizopus delemar*. NIS enzymes are not present in humans and therefore Rfs represents a potential target for development of novel antifungal agents. However, first the role of Rfs in the virulence of Mucorales fungi must be confirmed in animal models of mucormycosis. In addition, some *Rhizopus* spp. are plant pathogens and, because iron acquisition in the environment is important for pathogen growth, fungal NIS enzymes may also represent a target for control agents in agriculture.

3.6 Supplementary data

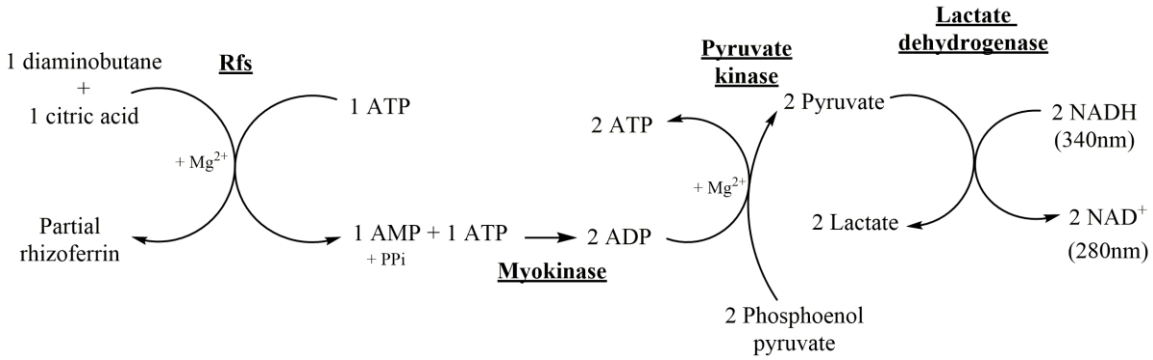

Figure S3.15. Schematic of the coupled AMP production/NADH oxidation assay used to evaluate Rfs activity[38].

Enzymes used in the assay are highlighted in bold and underlined. They are placed above or below the reactions they catalyze.

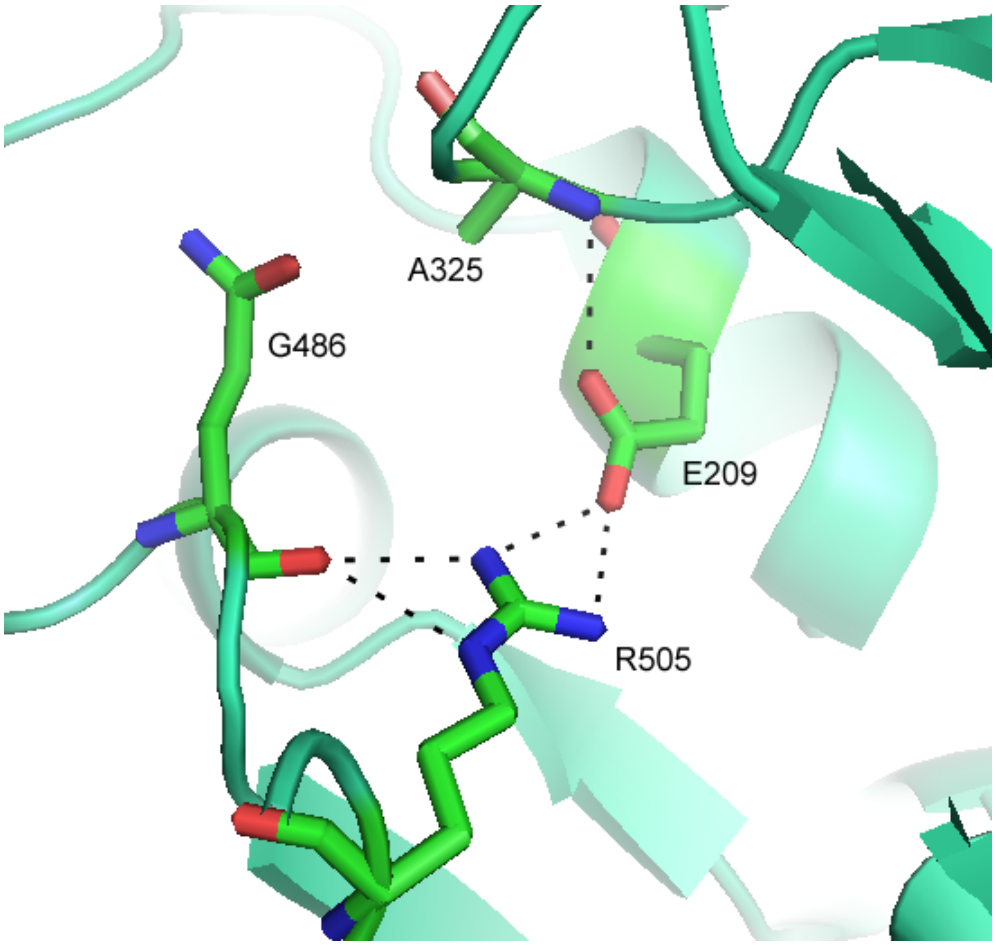

Figure S3.16. E209 interacts with numerous nearby residues and may be required for proper folding of NIS enzymes.
R505, G486 and A325 appear to interact with E209 and may play a role in maintaining the stability of folded Rfs.

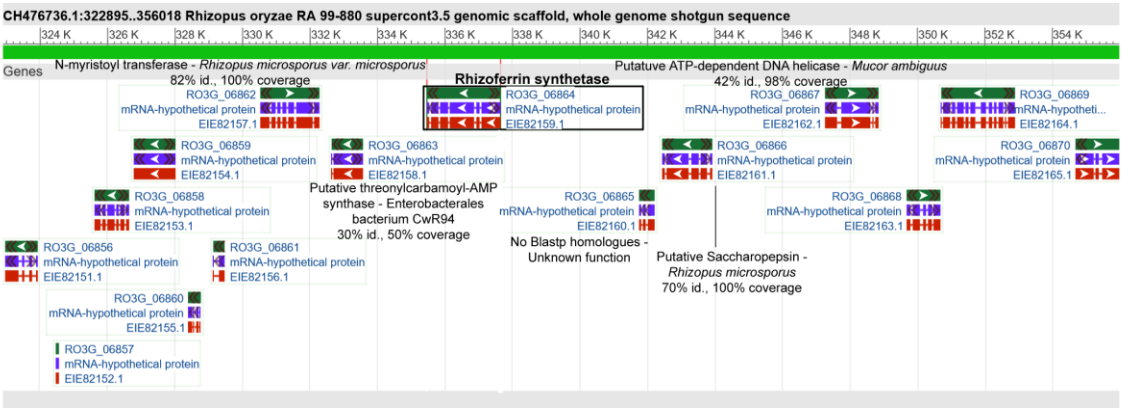

Figure S3.17. Genetic locus surrounding the *rfs* gene in *R. delemar*.
Genes surrounding the *rfs* gene (Boxed in black - R03G_06864) are not involved in iron transport or utilization. Blastp was performed to identify predicted homologues and results are shown in black text. The percent identity and percent coverage of the top putative protein are shown.

3.7 References

1. Alvarez, E. *et al.* Spectrum of zygomycete species identified in clinically significant specimens in the United States. *Society* **47,** 1650–1656 (2009).

2. Park, B. J. *et al.* Invasive non-*Aspergillus* mold infections in transplant recipients, United States, 2001-2006. *Emerg. Infect. Dis.* **17,** 1855–1864 (2011).

3. Roden, M. M. *et al.* Epidemiology and outcome of zygomycosis: a review of 929 reported cases. *Clin. Infect. Dis.* **41,** 634–53 (2005).

4. Pagano, L. *et al.* Mucormycosis in patients with haematological malignancies : a retrospective clinical study of 37 cases. *Br. J. Haematol.* **99,** 331–336 (1997).

5. Sun, H. Y. & Singh, N. Emerging importance of infections due to zygomycetes in organ transplant recipients. *Int. J. Antimicrob. Agents* **32,** 115–118 (2008).

6. Boelaert, J. R., Van Cutsem, J., de Locht, M., Schneider, Y. J. & Crichton, R. R. Deferoxamine augments growth and pathogenicity of *Rhizopus*, while hydroxypyridinone chelators have no effect. *Kidney Int.* **45,** 667–71 (1994).

7. Spellberg, B., Jr, J. E., Ibrahim, A. & Edwards, J. Novel perspectives on mucormycosis: Pathophysiology, presentation, and management. *Clin. Microbiol. Rev.* **18,** 556–569 (2005).

8. Liu, M. *et al.* The endothelial cell receptor GRP78 is required for mucormycosis pathogenesis in diabetic mice. *J. Clin. Invest.* **120,** 1914–1924 (2010).

9. Cornely, O. A. *et al.* ESCMID and ECMM joint clinical guidelines for the diagnosis and management of mucormycosis 2013. *Clin. Microbiol. Infect.* **20,** 5–26 (2014).

10. Kyvernitakis, A. *et al.* Initial use of combination treatment does not impact survival of 106 patients with haematologic malignancies and mucormycosis: a propensity score analysis. *Clin. Microbiol. Infect.* **22,** 811.e1-811.e8 (2016).

11. Haas, H. Molecular genetics of fungal siderophore biosynthesis and uptake: the role of siderophores in iron uptake and storage. *Appl. Microbiol. Biotechnol.* **62,** 316–30 (2003).

12. Hissen, A. H. T., Chow, J. M. T., Pinto, L. J. & Moore, M. M. Survival of *Aspergillus fumigatus* in serum involves removal of iron from transferrin: The role of siderophores. *Infect. Immun.* **72,** 1402–1408 (2004).

13. Li, K., Chen, W.-H. & Bruner, S. D. Microbial siderophore-based iron assimilation and therapeutic applications. *Biometals* **29,** 377–388 (2016).

14. Ibrahim, A. S. *et al.* The high affinity iron permease is a key virulence factor required for *Rhizopus oryzae* pathogenesis. *Mol. Microbiol.* **77,** 587–604 (2010).

15. Thieken, A. & Winkelmann, G. Rhizoferrin: A complexone type siderophore of the mocorales and entomophthorales (Zygomycetes). *FEMS Microbiol. Lett.* **94,** 37–41 (1992).

16. Drechsel, H. *et al.* Rhizoferrin—a novel siderophore from the fungus Rhizopus microsporus var. rhizopodiformis. *BioMetals* **4,** 238–243 (1991).

17. Drechsel, H., Jung, G. & Winkelmann, G. Stereochemical characterization of rhizoferrin and identification of its dehydration products. *BioMetals* **5,** 141–148 (1992).

18. Taraz, K. *et al. S, S*-rhizoferrin (enantio-rhizoferrin) – a siderophore of *Ralstonia* (*Pseudomonas*) *pickettii* DSM 6297 – the optical antipode of *R, R*-rhizoferrin isolated from fungi. *Biometals* **12,** 189–193 (1999).

19. Sullivan, J. T., Jeffery, E. F., Shannon, J. D. & Ramakrishnan, G. Characterization of the siderophore of *Francisella tularensis* and role of *fslA* in siderophore production. *J. Bacteriol.* **188,** 3785–95 (2006).

20. Gulick, A. M. Ironing out a new siderophore synthesis strategy. *Nat. Chem. Biol.* **5,** 143–4 (2009).

21. Cotton, J. L., Tao, J. & Balibar, C. J. Identification and characterization of the *Staphylococcus aureus* gene cluster coding for staphyloferrin A. *Biochemistry* **48,** 1025–35 (2009).

22. Oves-Costales, D., Kadi, N. & Challis, G. L. The long-overlooked enzymology of a nonribosomal peptide synthetase-independent pathway for virulence-conferring siderophore biosynthesis. *Chem. Commun. (Camb).* 6530–41 (2009). doi:10.1039/b913092f

23. Kadi, N. & Challis, G. L. *Chapter 17. Siderophore biosynthesis a substrate specificity assay for nonribosomal peptide synthetase-independent siderophore synthetases involving trapping of acyl-adenylate intermediates with hydroxylamine. Methods in enzymology* **458,** (Elsevier Inc., 2009).

24. Ibrahim, A. S. *et al.* Genomic analysis of the basal lineage fungus *Rhizopus oryzae* reveals a whole-genome duplication. *Genome* **5,** (2009).

25. Marchler-Bauer, A. *et al.* CDD: NCBI's conserved domain database. *Nucleic Acids Res.* **43,** D222–D226 (2015).

26. Altschul, S. F., Gish, W., Miller, W., Myers, E. W. & Lipman, D. J. Basic local alignment search tool. *J. Mol. Biol.* **215,** 403–10 (1990).

27. Kelley, L. A., Mezulis, S., Yates, C. M., Wass, M. N. & Sternberg, M. J. E. The Phyre2 web portal for protein modeling, prediction and analysis. *Nat. Protoc.* **10,** 845–858 (2015).

28. A. Roy, A. Kucukural, Y. Z. I-TASSER: a unified platform for automated protein structure and function prediction. *Nat. Protoc.* **5,** 725–738 (2011).

29. Sievers, F. *et al.* Fast, scalable generation of high-quality protein multiple sequence alignments using Clustal Omega. *Mol. Syst. Biol.* **7,** 539 (2011).

30. Waterhouse, A. M., Procter, J. B., Martin, D. M. A., Clamp, M. & Barton, G. J. Jalview Version 2--a multiple sequence alignment editor and analysis workbench. *Bioinformatics* **25,** 1189–1191 (2009).

31. Kearse, M. *et al.* Geneious Basic: an integrated and extendable desktop software platform for the organization and analysis of sequence data. *Bioinformatics* **28,** 1647–9 (2012).

32. Sambrook, J. & Russell, D. W. The Inoue method for preparation and transformation of competent *E. Coli*: 'Ultra-Competent' cells. *Cold Spring Harb. Protoc.* **2006,** pdb.prot3944-prot3944 (2006).

33. Alexander, D. B. & Zuberer, D. A. Use of chrome azurol S reagents to evaluate siderophore production by rhizosphere bacteria. *Biol. Fertil. Soils* **12,** 39–45 (1991).

34. Liu, H. & Naismith, J. H. A simple and efficient expression and purification system using two newly constructed vectors. *Protein Expr. Purif.* **63,** 102–111 (2009).

35. Perez-Miranda, S., Cabirol, N., George-Tellez, R., Zamudio-Rivera, L. & Fernandez, F. O-CAS, a fast and universal method for siderophore detection. *J. Microbiol. Methods* **70,** 127–131 (2007).

36. Oke, M. *et al.* The Scottish structural proteomics facility: Targets, methods and outputs. *J. Struct. Funct. Genomics* **11,** 167–180 (2010).

37. Wittig, I., Braun, H.-P. & Schägger, H. Blue native PAGE. *Nat. Protoc.* **1,** 418–428 (2006).

38. Schmelz, S. *et al.* AcsD catalyzes enantioselective citrate desymmetrization in siderophore biosynthesis. *Nat. Chem. Biol.* **5,** 174–82 (2009).

39. Warwas, M. L. *et al.* Cloning and characterization of a sialidase from the filamentous fungus, *Aspergillus fumigatus*. *Glycoconj. J.* (2010). doi:10.1007/s10719-010-9299-9

40. Lewis, R. E., Georgiadou, S. P., Sampsonas, F., Chamilos, G. & Kontoyiannis, D. P. Risk factors for early mortality in haematological malignancy patients with pulmonary mucormycosis. *Mycoses* (2013). doi:10.1111/myc.12101

41. Lanternier, F. *et al.* Mucormycosis in organ and stem cell transplant recipients. *Clin. Infect. Dis.* **54,** 1629–36 (2012).

42. Neilands, J. B. Mechanism and regulation of synthesis of aerobactin in *Escherichia coli* K12 (pColV-K30). *Can. J. Microbiol.* **38,** 728–33 (1992).

43. Schmelz, S. *et al.* Structural basis for Acyl acceptor specificity in the achromobactin biosynthetic enzyme AcsD. *J. Mol. Biol.* **412,** 495–504 (2011).

44. Geer, L. Y., Domrachev, M., Lipman, D. J. & Bryant, S. H. CDART: Protein Homology by Domain Architecture. *Genome Res.* **12,** 1619–1623 (2002).

45. Schrettl M., Beckmann N., Varga J., et al. HapX-mediated adaption to iron starvation is crucial for virulence of *Aspergillus fumigatus* . Cowen LE, ed. *PLoS Path.* **6**:e1001124 (2010).

46.Cheung, J., Beasley, F. C., Liu, S., Lajoie, G. A. & Heinrichs, D. E. Molecular characterization of staphyloferrin B biosynthesis in *Staphylococcus aureus*. *Mol. Microbiol.* **74,** 594–608 (2009).

47. Tschierske, M., Drechsel, H., Jung, G. & Zahner, H. Production of rhizoferrin and new analogues obtained by directed fermentation. *Appl. Microbiol. Biotechnol.* **45,** 664–670 (1996).

48. Braun, V., Kuhn, S. & Koster, W. Ferric rhizoferrin uptake into *Morganella morganii*: Characterization of genes involved in the uptake of a polyhydroxycarboxylate siderophore. *Microbiology* **178,** 496–504 (1996).

49. Burnside, D. M., Wu, Y., Shafaie, S. & Cianciotto, N. P. The *Legionella pneumophila* siderophore legiobactin is a polycarboxylate that is identical in structure to rhizoferrin. *Infect. Immun.* **83,** 3937–3945 (2015).

50. Kiss, K., Liu, W., Huntley, J. F., Norgard, M. V. & Hansen, E. J. Characterization of *fig* operon mutants of *Francisella novicida* U112. *FEMS Microbiol. Lett.* **285,** 270–277 (2008).

51. Hannauer, M., Sheldon, J. R. & Heinrichs, D. E. Involvement of major facilitator superfamily proteins SfaA and SbnD in staphyloferrin secretion in *Staphylococcus aureus*. *FEBS Lett.* **589,** 730–737 (2015).

52. Berti, A. D. & Thomas, M. G. Analysis of achromobactin biosynthesis by *Pseudomonas syringae pv. syringae* B728a. *J. Bacteriol.* **191,** 4594–4604 (2009).

53. Tanabe, T. *et al.* Identification and characterization of genes required for biosynthesis and transport of the siderophore vibrioferrin in *Vibrio parahaemolyticus*. *Society* **185,** 6938–6949 (2003).

54. Lee, J. Y. *et al.* Biosynthetic analysis of the petrobactin siderophore pathway from *Bacillus anthracis*. *J. Bacteriol.* **189,** 1698–1710 (2007).

55. Boratyn, G. M. *et al.* Domain enhanced lookup time accelerated BLAST. *Biol. Direct* **7,** 12 (2012).

Chapter 4.

Characterization of an NRPS-independent siderophore synthetase (NIS) in the ascomycete fungal pathogen, *Aspergillus terreus*

This chapter is a manuscript in preparation under the authorship of Alison Hadwin, Cassandra Carroll, Jamie Baker, and Margo Moore.

Author contributions: This project was designed by Prof. Margo Moore, Alison Hadwin and Cassandra Carroll. Alison Hadwin created and characterized the *Aspergillus terreus ΔsidA* strain. She also purified siderophores from *A. terreus* and *Aspergillus fumigatus* and performed the *A. fumigatus* and *Neurospora crassa* growth experiments. Cassandra Carroll cloned the NIS enzyme and was assisted by Jamie Baker with expression and purification of the AtNIS enzyme. Mass spectrometry experiments were performed by Hongwen Chen and interpreted by Cassandra Carroll and Alison Hadwin. Localization experiments were performed by Cassandra Carroll.

4.1 Abstract

In this work, we confirm that *Aspergillus terreus* secretes the hydroxamate siderophores, coprogen and ferrichrysin. We also found a third putative siderophore, termed Band 4, present in culture supernatants of *A. terreus* grown in iron-limited media. This compound was purified and mass spectrometry showed that it consisted of dimerum acid, a component common to the coprogen family of siderophores. Purified Band 4 was found to restore growth to a siderophore deficient strain of *Neurospora crassa*; however, Band 4 did not restore growth to a siderophore deficient strain of *Aspergillus fumigatus*. These data indicate that Band 4 is structurally distinct from the main *A. fumigatus* siderophore, *N,N,N*-triacetylfusarinine C (TAFC) but possibly related to coprogen. An *A. terreus ΔsidA* mutant was created and Band 4 was still produced using iron-limited conditions. Thus, we hypothesized that biosynthesis of Band 4 is not related to the NRPS pathway for biosynthesis of hydroxamate siderophores, but possibly dependent on the NRPS-independent pathway. This pathway uses NRPS-independent synthetases (NIS). An NIS homolog was found in the genome of *A. terreus* (AtNIS). Expression of AtNIS was

confirmed to be iron regulated and the gene was cloned into a protein expression vector. Optimization of protein expression is underway. Experiments are also underway to compare localization of AtNIS in *A. terreus* with the validated NIS enzyme, Rfs in the Mucorales fungus, *Rhizopus delemar.*

4.2 Introduction

Aspergillus terreus is a soil dwelling, saprotrophic filamentous fungus that is classified in the phylum Ascomycota, section *Terrei*. Asexual reproduction in *A. terreus* occurs via specialized hyphae called conidiophores which produce chains of yellow to brown conidiospores from phialides (phialidic conidia (PC), 2 – 3.5 µm in diameter) that give rise to haploid mycelia once they contact suitable media. Interestingly, *A. terreus* is the only known *Aspergillus* species to produce individual conidia directly on the cell surface, typically at branch points on the surface of hyphae. These accessory conidia (AC) and range in size from 4 – 7 µm in diameter[1]. *A. terreus* conidia are multi-nucleated: PC possess 2-3 nuclei per cell and AC have up to 7 nuclei per cell[2].

Aspergillus terreus is best known for its industrial uses, e.g., production of lovastatin, a cholesterol lowering drug, and itaconic acid, a precursor for the polymer industry[3–5]. *A. terreus* is also used in the production of plant-cell wall degrading enzymes, such as cellulases and mannanases, production of pectin and (+)-terrein, a potentially beneficial compound with uses in both agriculture and medicine[6–9].

4.2.1 Infections caused by *Aspergilli*

Members of the *Aspergillus* genus can be pathogens of both plants and animals. *A. terreus* is known to cause foliar blight disease in potatoes[10], it can inhibit plant root formation and also produce lesions on various fruit surfaces[11]. *A*. *terreus* has also been reported as a primary pathogen in dogs and birds[12,13]. In humans, the most severe illness caused by *Aspergillus* species is invasive aspergillosis (IA) in which inhaled conidia germinate and spread within the lung parenchyma, often followed by dissemination to other organs[14].

The most common etiological agent of invasive aspergillosis is *Aspergillus fumigatus*, followed by *Aspergillus flavus, Aspergillus niger* and *A. terreus*[15]. *A. terreus* is primarily

associated with IA[16], although aspergillomas and ABPA due to *A. terreus* have been reported[17,18].

Populations at risk for IA due to *A. terreus* are similar to risk groups identified for other *Aspergillus* species including patients with hematological malignancies, neutropenia, steroid use, or patients who have undergone transplantation, particularly allogenic transplantation, or developed GVHD[15,16]. Patients with leukemia, prolonged neutropenia, or previous prophylactic antifungal exposure seem to be at an increased risk of developing IA from *A. terreus* compared to other aspergilli[16,19].

Treatment of IA relies on the antifungal azole drugs, voriconazole, itraconazole or posaconazole. The polyene, amphotericin B, can be used as an alternative treatment or as a prophylactic agent[20], however, *A. terreus* is particularly resistant to amphotericin B compared to other *Aspergillus* spp.[21]. Even with appropriate antifungal therapy, mortality rates for IA due to *A. terreus* approach 100%[22].

4.2.2 Virulence factors of IA

In *Aspergillus fumigatus*, compounds such as gliotoxins[23–26], various proteases[27] and conidia surface components such as hydrophobic proteins[28] and sialic acid residues[29,30] have been shown to contribute to, but are not essential for, virulence. By comparison, very few studies have investigated virulence factors in *A. terreus*.

Deak et al (2011)[2] compared the cell wall structure and virulence of AC and PC derived conidia of *A. terreus*. The authors found AC-derived conidia contained higher β-glucan levels and elicited significantly higher levels of chemokine and cytokine production compared to PC-derived conidia during an intratracheal challenge in mice. Histological staining of mouse lungs also showed increased pulmonary infiltrates with AC-derived conidia compared to PC-derived conidia. However, survival tests were not preformed in this mouse model, so the effect of AC-derived conidia in *A. terreus* virulence remains unclear.

Using a *Galleria mellonella* model of infection, Maurer et al. (2015) showed that previous exposure to the antifungal agent amphotericin B, increased the virulence of *A. terreus*[31]; however the mechanism of action was not determined. Further studies are needed to

confirm whether the increase in mortality was due to an increase in fungal virulence or to amphotericin B-mediated toxicity to the host[32].

4.2.3 Siderophore secretion is a virulence factor in *Aspergillus fumigatus*

Siderophores are low molecular weight organic molecules that are released into the environment under iron-limiting conditions to chelate ferric iron, an essential nutrient for many biological processes including DNA synthesis and the electron transport chain[33]. In human sera, the concentration of free iron is very low due to circulating iron-binding proteins such as transferrin and lactoferrin. For many pathogenic microbes, siderophore secretion is an important mechanism of iron acquisition.

There are four main types of siderophores, hydroxamate, catecholate, carboxylate and mixed-siderophores, which differ based on the functional group used to coordinate Fe (III). In Fungi, the main siderophores which have been identified are hydroxamate siderophores, with the exception of the Mucorales fungi; these fungi secrete the polycarboxylate siderophores, rhizoferrin[34]. Biosynthesis of siderophores occurs via two pathways: the non-ribosomal peptide synthetase (NRPS) pathway in which multi-enzyme complexes function in a coordinated fashion to adenylate a substrate, then covalently bind the substrate to the enzyme via a thiol intermediate, and finally release the intermediate through formation of a peptide bond with the incoming substrate[35]. The NRPS-independent siderophore (NIS) biosynthetic pathway consists of individual enzymes which adenylate a substrate carboxyl group, typically citrate or a derivative, followed by condensation with an amino or alcohol group, releasing the citryl-intermediate, which is free for catalysis by the subsequent enzyme in the pathway[36].

In *A. fumigatus*, the hydroxamate siderophore, *N,N',N*''-triacetylfusarinine C (TAFC) effectively removes iron from transferrin[37]. In *A. fumigatus*, the biosynthesis of hydroxamate siderophores occurs via the NRPS pathway, using enzymes encoded by the *sid* genes (Figure 4.1). The first step in biosynthesis is catalyzed by SidA, an L-ornithine N^5-oxygenase. When *sidA* was disrupted in *A. fumigatus*, fungal germination did not occur and IA failed to develop in a mouse model of aspergillosis[38,39]*;* thus, hydroxamate siderophore biosynthesis is required for virulence in *A. fumigatus.*

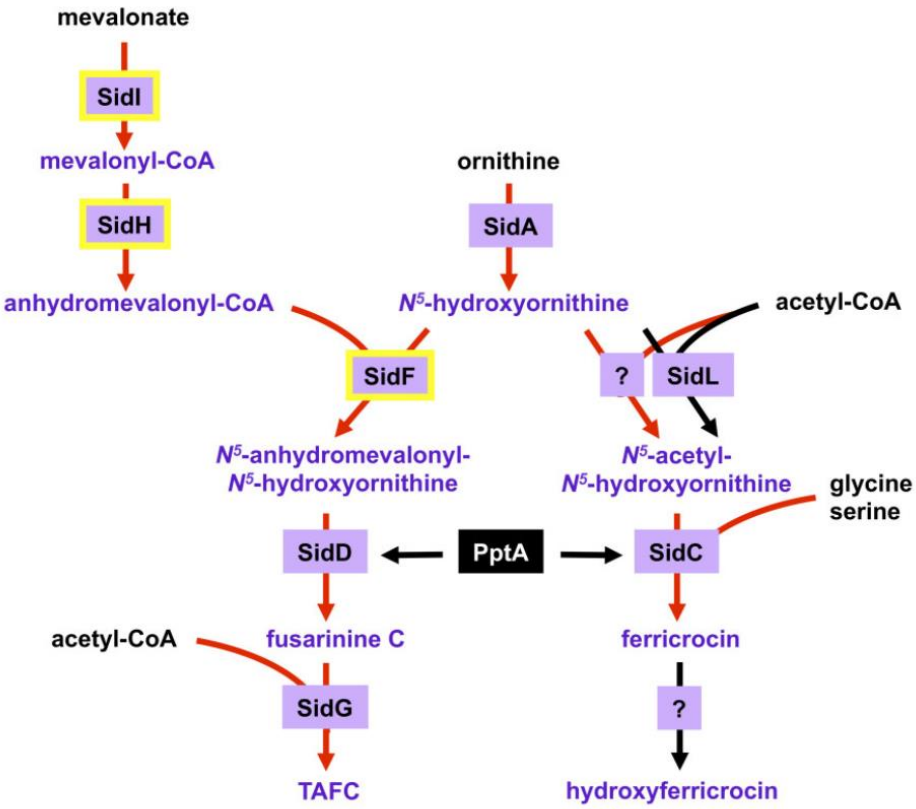

Figure 4.1. Biosynthesis of hydroxamate siderophores in *A. fumigatus* occurs via NRPS.

SidI, SidH and SidF, outlined in yellow have been localized to peroxisomes in *A. fumigatus* and SidI was localized to peroxisomes in *Neurospora crassa*. Figure replicated from Gründlinger et al. (2013)[40] with permission[1].

4.2.4 Siderophores secreted by *Aspergillus terreus*

A. terreus produces the hydroxamate siderophores coprogen and ferrichrysin, under iron limited conditions[41]. Coprogen consists of three molecules of *N*-acetyl fusarinine; two molecules are joined to form dimerum acid and the final *N*-acetyl fusarinine molecule is joined via an ester bond to form coprogen. Ferrichrysin is a member of the ferrichrome family of hydroxamate siderophores, similar to ferricrocin, and is composed of three molecules of *N*-acetyl-*N*-hydroxy-lysine joined to a cyclic backbone of two serine

[1] Reprinted from Molecular Microbiology, 88 (5), Gründlinger, M., Yasmin, S., Lechner, BE., Geley, S., Schrettl, M., Hynes, M. and Haas, H. Fungal siderophore biosynthesis is partially localized in peroxisomes.862-875, 2013, with permission from John Wiley and Sons

residues and one glycine reside (Figure S4.17). Biosynthesis of these siderophores occurs via the NRPS pathway, and, as shown in Figure 4.1, hydroxylation of L-ornithine catalyzed by *sidA* is the first step in the biosynthesis of all hydroxamate siderophores described in *Aspergillus* species to date (Table 4.1).

Table 4.1. Hydroxamate siderophores produced by various fungi, with a focus on members of the *Aspergillus* genus.

Species	Siderophores							Ref	sidA homolog (GI accession number)
	Ferricrocin	Ferri-chrome	Fusigen	TAFC	Coprogens	Ferrichrysin	Other		
A. fumigatus	+	-	-	+	-	-	-	[42]	50845194
A. oryzae	-	-	-	-	-	+	-	[43]	83775230
A. nidulans	+	-	+	+	-	-	Fusigen B	[44,45]	32709393
A. niger	-	+	-	-	+	-		[46]	134075043
A. ochraceous	-	-	+	-	-	+	Ferrirubin, asperchromes	[47]	No sequence available
A. terreus	-	-	-	-	+	+		[41,43]	115386048
Penicillium chrysogenum	+	-	-	-	+	-		[45]	KZN92759.1
Magnaporthe grisea	+	-	-	-	+	-		[48]	LOFB01000052.1
Histoplasma capsulatum	-	-	-	-	+	-	Dimerum acid, acetyl dimerum acid, fusarinine	[49]	GG692436.1
Trichoderma spp.	+	-	-	-	+	-		[50]	XP_006969374.1 (*Trichoderma reesei*)

We have confirmed that *A. terreus* produces the siderophores, coprogen and ferrichrysin, however, a third unique siderophore is present in iron-limited culture supernatants of *A. terreus*. We identified a *sidA* homolog in the genome of *A. terreus* and disrupted the *sidA* gene using a knockout construct containing a hygromycin-selectable marker with *Agrobacterium*-mediated transformation of PC-derived conidia[51]. When grown in iron-limited medium, the *A. terreus sidA* mutant produced only trace amounts of coprogen and ferrichrysin; however, the third siderophore remained in HPLC traces but disappeared when the mutant was grown in iron-replete media, indicating that the synthesis of this unidentified compound is regulated by iron.

A search of the *A. terreus* genome uncovered an NIS homolog and preliminary studies showed the gene was expressed in iron-limiting conditions. Together, these data indicated that *A. terreus* may synthesize a unique polycarboxylate or mixed-type siderophore. To date, there are no reports of non-hydroxamate siderophores produced by Ascomycetes.

4.2.5 Research aims

We hypothesized that the NIS gene in *A. terreus* (AtNIS) may be involved in the biosynthesis of the unidentified siderophore. Therefore, the aims of the research described in this Chapter were 1) to identify the unknown compound produced by *A. terreus* and determine whether it is able to act as a siderophore in *sidA*-deficient strains of fungi, 2) to heterologously express and purify the NIS enzyme from *A. terreus*, 3) to investigate the substrate specificity of the recombinant AtNIS, and 4) to compare the localization of the putative AtNIS in *A. terreus* with that of the validated NIS enzyme, rhizoferrin synthetase (Rfs) in the Mucorales fungus, *Rhizopus delemar*.

4.3 Materials and methods

4.3.1 Bioinformatic analyses

Bioinformatic analyses were conducted using the genomic sequence of *A. terreus* strain A1156. Genetic information about AtNIS (gi: 115437856) was obtained from NCBI and *Aspergillus* Genome Database (aspgd.org). Conserved domains were identified in the protein sequence using the NCBI Conserved Domain Database[52]. Phyre and I-

TASSER[53,54] were used to predict the structure of AtNIS and WoLF PSORT (https://www.genscript.com/wolf-psort.html) was used for subcellular localization predictions. PyMOL was used for structural alignments with the crystal structures of three validated NIS enzymes, AcsD (PDB: 2W02), AsbB (PDB: 3TO3) and IucA (PDB: 5JM7 and 5JM8) as templates (The PyMOL Molecular Graphics System, Version 1.8 Schrödinger, LLC).

4.3.2 Strains, media and culture conditions

Aspergillus terreus (A1156) and *Rhizopus delemar* (99–880) were obtained from the American Type Culture Collection (ATCC). The *Aspergillus fumigatus ΔsidA* strain was created by Hissen et al. (2005)[38] and the *Neuorspora crassa ΔsidA* mutant (FGSC 20170 (het)) was obtained from the Fungal Genetics Stock Center. *A. terreus* and *A. fumigatus* were maintained on Yeast Extract Agar Glucose Medium (YAG; 5 g yeast extract, 10 g dextrose, 15 g agar, 1 L water) with or without the presence of Hutners' trace elements without iron (5 g $Na_2EDTA \cdot 2H2O$, 2.2 g $ZnSO_4 \cdot 7H2O$, 1.14 g H_3BO_3, 0.5 g $MnCl_2 \cdot 4H_2O$, 161 mg $CoCl_2 \cdot 6H_2O$, 157 mg $CuSO_4 \cdot 5H_2O$, 110 mg $(NH_4)6Mo_7O_{24} \cdot 4H_2O$, 100 mL water; pH 6.5-6.8) and 1 ml of 1000X vitamins (0.01 g biotin, 0.01 g pyridoxin, 0.01 g thiamine, 0.01 g riboflavin, 0.01 g p-aminobenzoic acid, 0.01 g nicotinic acid, 100 ml water). *R. delemar* was maintained on Potato Dextrose Agar (PDA; BD Difco) and *N. crassa* was maintained on Vogel's Medium N[55]. *N. crassa* FGSC 20170 is a heterokaryon so media was always supplemented with 50 µg/ml hygromycin. For iron-limited conditions, *A. terreus, A. fumigatus* and *N. crassa*, were grown in modified Grimm Allen (GA) media[56]. For *A. terreus* GA media was supplemented with Hutners' trace elements without iron and supplemented with vitamins. *R. delemar* was grown in low-iron media (Media A) to induce expression of Rfs, the NIS enzyme responsible for rhizoferrin biosynthesis[57]. Low iron cultures were made iron replete by the addition of 100 µM $FeCl_3$. *Escherichia coli* (DH5α) was used in standard cloning procedures and Tuner *E. coli* (Novagen) was used for protein expression. *E. coli* was grown on Luria-Bertani (LB) media (10 g tryptone, 10 g NaCl, 5 g yeast extract, 1 L water) supplemented with either ampicillin (100 µg/ml) or kanamycin (30 µg/ml) as necessary. Transformations were done using $CaCl_2$ competent *E. coli* cells or ultra-competent *E. coli* cells[58] via heat-shock.

4.3.3 Construction of an *Aspergillus terreus ΔsidA* strain

The *A. fumigatus sidA* protein (AFUA_2G07680) was used in a Blastp search of the *A. terreus* (A1156) genome to identify potential orthologs. The *A. terreus sidA* gene (ATEG_06879) was identified. A gene deletion cassette was created via fusion PCR with AccuPrime DNA polymerase (ThermoFisher Scientific). The deletion construct consisted of the hygromycin resistance cassette from pID620[38], flanked by DNA sequences from 1000 bp upstream and downstream of the *sidA* gene. Primers used to amplify each portion of the deletion cassette are listed in Table 4.2.

Table 4.2. Primers used to construct the *A. terreus sidA* deletion cassette.

Primer name	Sequence (5' – 3')	Purpose
Nested forward primer	CGAATTCCAGGTACAATACACTCCGTAGG	Amplified the full deletion cassette
Nested reverse primer	CGAATTCCAGCAGCAGAAGACTTTACC	Amplified the full deletion cassette
Upstream forward	AGCCGGTGGTTGTATGGTAGT	Amplified 1000 bp upstream of the *sidA* gene
Upstream reverse	CTTCGTTGTTTGGGGAGGAGT	Amplified 1000 bp upstream of the *sidA* gene
Downstream forward	GAGCGGACATGGTGCGATAG	Amplified 1000 bp downstream of the *sidA* gene
Downstream reverse	CGAGGACAGACCGAGCCTAA	Amplified 1000 bp downstream of the *sidA* gene
Fusion forward	CGCTCTAGAACTAGTGGATCCGAGCGGAGATGGTGCGATAG	Amplified the HPH cassette
Fusion reverse	AGCTCCAGCTGCCATAGCCTTCGTTGTTTGGGGAGGAGT	Amplified the HPH cassette

The deletion cassette was digested with *EcoRI* and cloned into the similarly digested pCambia0380 vector[59] and transformed into competent *Agrobacterium tumefaciens*. This vector was used for *Agrobacterium*-mediated transformation of *A. terreus* according to Michielse et al. (2008)[51].

Putative *A. terreus* transformants were selected on Weak Complete media (1 g sucrose, 1 g peptone, 1 g yeast extract, 15 g agar, 1 L water) supplemented with 100 – 200 µg/ml

hygromycin. Multiple rounds of single spore isolations were performed to try to obtain a clonal colony. Agar overlays were added to some plates with 10 µM ferrichrysin to encourage sporulation of putative transformants.

4.3.4 Purification of siderophores from wildtype *A. terreus* using high pressure liquid chromatography (HPLC)

A. terreus was grown in modified GA media (10^6 spores/ml), mycelia were removed by filtration and $FeCl_3$ was added to the culture supernatant until no more colour change was observed. The ferrated siderophores in the culture supernatant were then incubated with Amberlite XAD16 resin (Sigma Aldrich) for 30 minutes at 30°C - 37°C or overnight at 4°C. The Amberlite was poured into a column and un-bound compounds were washed away with distilled water. Bound siderophores were eluted in a batch process using 25% methanol, 75% water, 0.05% acetic acid for 30 minutes, followed by 25% methanol, 75% water, then 50% methanol and 50% water. Any remaining compounds were eluted in a final solution of 100% methanol. Fractions were sampled after each solution and $FeCl_3$ was added to determine if siderophores were present; most siderophores eluted in washes containing 25% methanol, 75% water ± acetic acid. Extracted siderophores were lyophilized, re-suspended in water and separated by HPLC. Ten microliters were injected into a Gemini C18 column (Phenomenex, 250 × 4.6 mm, 5µm particle size) using a gradient of 10 % – 40 % solvent A over 30 min with a flow rate of 1 ml/min. Solvent A consisted of acetonitrile (Fisher Scientific, HPLC grade) plus 0.2 % trifluoroacetic acid (Caledon Laboratories). Solvent B was water. Absorbance was monitored at 220 nm.

4.3.5 Purification of Band 4 from an *A. terreus ΔsidA* mutant

A. terreus was inoculated into liquid GA media supplemented with 150 – 200 µg/ml hygromycin. Cultures were incubated at 37°C for 8 days, mycelia were harvested and extracted as outlined above. Following Amberlite extractions, Band 4 was separated on a low-pressure C18 silica gel (60A; 40-75 um, 19% carbon load, endcapped; Sorbent Technologies) and the presence of Band 4 was confirmed by the addition of $FeCl_3$ and separation via thin layer chromatography (TLC) using water: methanol: DCM (4:30:70). Multiple extractions were performed, and Band 4 isolates were pooled, lyophilized to

dryness and stored in a desiccator at room temperature. The purity of Band 4 was confirmed by mass spectrometry (MS).

4.3.6 Mass spectrometry with and without base hydrolysis and MS and MS/MS analysis

Band 4 was purified from wildtype *A. terreus* as described above and analyzed by MS using the Agilent 1200 HPLC and a Bruker maXis Ultra-High Resolution tandem TOF (UHR-Qq-TOF) mass spectrometer. Samples were introduced by flow injection via HPLC with acetonitrile/water (0.1 % formic acid) as mobile phase and spectra were collected under positive electrospray ionization (+ESI). Band 4 was also base hydrolyzed according to Howard et al. (2000)[49]. Hydrolysis products were examined as described above.

4.3.7 Effect of medium supplementation on the growth of siderophore deficient strains of *Aspergillus* and *Neurospora*.

A. fumigatus (10^6 spores/ml) and *N. crassa* (10^6 spores/ml) *ΔsidA* strains were inoculated into liquid GA media with 100 – 200 µg/ml and 50 µg/ml hygromycin, respectively. Iron chloride or 10 µM additions of various siderophores were made to select cultures. Siderophores were isolated from either *A. fumigatus* or *A. terreus* as described in Section 4.3.4. Cultures were incubated at 30 and 37°C for *N. crassa* and *A. fumigatus*, respectively. Growth of the mutant strains was determined by measuring the dry weight, on pre-dried filter papers, after 48 hours for *N*. *crassa* and 7 days for *A. fumigatus*. A one-way AVONA and Dunnett's post test (with Band 4 data used as the control column) was used to evaluate significantly different amounts of growth.

4.3.8 RT-PCR to confirm iron regulated expression of *AtNIS*

A. terreus (10^7 PC-spores/ml) was grown in GA media or GA media supplemented with iron for 24 hours at 37°C. Mycelia were filtered using Miracloth (EMD-Millipore), stored in RNAlater (ThermoFisher Scientific) for 24 hours and RNA was extracted using the NucleoSpin RNA Plant kit (Macherey-Nagel). cDNA was synthesized using the recommended protocol for the iScript cDNA Synthesis Kit (Bio-Rad Laboratories) and

PCR was preformed with Kodaq DNA polymerase (Applied Biological Materials, BC, Canada). A portion of the *AtNIS* gene was amplified with the primers AtNISFor277 (GCGGTGGAAAGGAAGACTGT) and AtNISRev701 (GACAGACAGGTCGCTATGGG). PCR products were run on a 0.8 % agarose gel and visualized using Gel-Red (VWR International) and UV exposure.

4.3.9 Construction of the pEHISTEV-AtNIS vector

A. terreus was grown and RNA was harvested as described above. cDNA was synthesized using the All-In-One RT MasterMix (Applied Biological Materials, BC, Canada). The AtNIS gene was amplified using Kodaq DNA polymerase (Applied Biological Materials, BC, Canada) and the primers AtNISFor (ATGACAACTACCACCACACG) and AtNISRev (TCAAGTCCAATGCAAAGAAG). PCR products around the expected size for AtNIS were extracted from an agarose gel (0.8 %) using the NucleoSpin Gel and PCR cleanup kit (Macherey-Nagel), blunt-end ligated into pJET (CloneJET PCR Cloning Kit, ThermoFisher Scientific), and transformed into *E. coli* DH5α. Successful transformants were confirmed by PCR and sequencing (Genewiz, New Jersey, USA) which confirmed that the correct AtNIS reading frame was present. The AtNIS gene was amplified from pJET transformants using the AtNISFor and AtNISRev primers with added *EcoRI* and *XhoI* restriction cut sites for cloning into the pEHISTEV vector with a C-terminal HIS-tag[60]. pEHISTEV-AtNIS was transformed into *E. coli* DH5α, and the plasmid was purified using the NucleoSpin Plasmid kit (Macherey-Nagel) and transformed into Tuner *E. coli* for protein induction.

NIS proteins are proposed to interact via their N-terminal ‘thumb’ domains (See Chapter 2). To reduce the potential for protein aggregation, we made N-terminal truncations of AtNIS using the forward primers NtruF91 (CTAA**GAATTC**ATGGCGGTGGAAAGGAA) to remove the first 91 amino acids or NtruF138 (CTAA**GAATTC**ATGAGGATGGCTGCAGG) to remove the first 138 amino acids. AtNISRev was used as the reverse primer in these reactions. Sequencing (Genewiz, New Jersey, USA) was used to confirm the truncations.

4.3.10 Expression and purification of AtNIS

AtNIS was purified according to Carroll et al. (2017)[57]. Briefly, Tuner *E. coli* was grown to an OD_{600} of 0.8 and expression was induced with 0.5 mM or 0.25 mM IPTG. Cultures were incubated overnight at 14°C with shaking. Cells were lysed by sonication and some purifications were done in buffers supplemented with 1 mM citrate and 10% glycerol. Attempts to purify AtNIS were done using one round of nickel-affinity chromatography.

4.3.11 Generation of polyclonal antiserum to the NIS enzyme, Rfs

Rfs was purified according to Carroll et al. (2017)[57]. The purified protein was sent to Pacific Immunology Corp. (Ramona, CA, USA) and a polyclonal antiserum was generated in two rabbits. Pre-immune bleeds were taken before immunization and the generation of a reactive antiserum was confirmed using ELISA assays. Briefly, various concentrations of Rfs were coated onto black hydrophobic coated 96-well assay plates (Sarstedt, Germany) at 4°C overnight. Excess protein was removed, wells were washed, and blocked with 5% skim milk in PBS for one hour at 37°C. Antisera was incubated at 37°C for one hour, wells were washed, and the HRP-conjugated goat anti-rabbit secondary antibody (1/1000) was added. Antibody titers were determined by incubation with Pierce™ ECL Western Blotting Substrate (ThermoFisher Scientific) and chemiluminescent readings were taken for each well. Antiserum from the third bleed of each rabbit was combined and affinity-purified by Pacific Immunology Corp. using purified Rfs. Antibody concentrations were confirmed using the Pierce BCA protein assay kit (ThermoFisher Scientific).

4.3.12 Localization of NIS enzymes by indirect immunofluorescence

A. terreus and *R. delemar* were grown on poly-L-lysine-coated slides at 30°C in GA media or Media A, respectively, without shaking for 36 hours. Mycelia were fixed with 4% formaldehyde in phosphate-buffered saline (PBS) at room temperature for one hour. Hyphae were permeabilized with PBS containing 0.01% Triton-100 for *A. terreus* or PBS containing 0.01% Tween-20 for *R. delemar* for 30 minutes at room temperature. Slides were washed, blocked with PBS + 5% BSA at room temperature for 35 minutes and then

polyclonal anti-Rfs antiserum (1:50), pre-immune serum (1:50) or anti-SKL antibody (1:100) was added. Slides were incubated at 4°C overnight, washed and incubated with the secondary AlexaFluor 594 goat anti-rabbit antibody (Jackson ImmunoResearch; 1:250) at room temperature for up to two hours. For peroxisome localization experiments, a donkey anti-guinea pig CF405S secondary antibody (Biotium; 1:250) was used. Prolong Gold anti-fade (ThermoFisher Scientific) was added and slides were sealed and stored at 4°C. Fluorescence was visualized on a spinning disk confocal microscope (WaveFX spinning disk, Quorum Technologies) with the Volocity 6.3 imaging software (PerkinElmer) with the exception of co-localization of Rfs and peroxisomes; these slides were imaged on the FV3000RS high resolution confocal laser scanning microscope (Olympus). Z-stacks were taken for all images with the exception of the *A. terreus* pre-immune and iron supplemented samples.

4.4 Results

4.4.1 *A. terreus* synthesizes an unknown iron-regulated compound along with coprogen and ferrichrysin

Culture supernatants of wildtype *A. terreus* grown in low iron media showed peaks corresponding to coprogen, ferrichrysin (confirmed by purification and mass spectrometry – see Figure S4.17) and an unknown peak which we called Band 4, that had a similar retention time to coprogen (Figure 4.2A). Culture supernatants from *A. terreus* grown in iron-replete media did not contain Band 4 although trace amounts of coprogen were present in these cultures (Figure 4.2B).

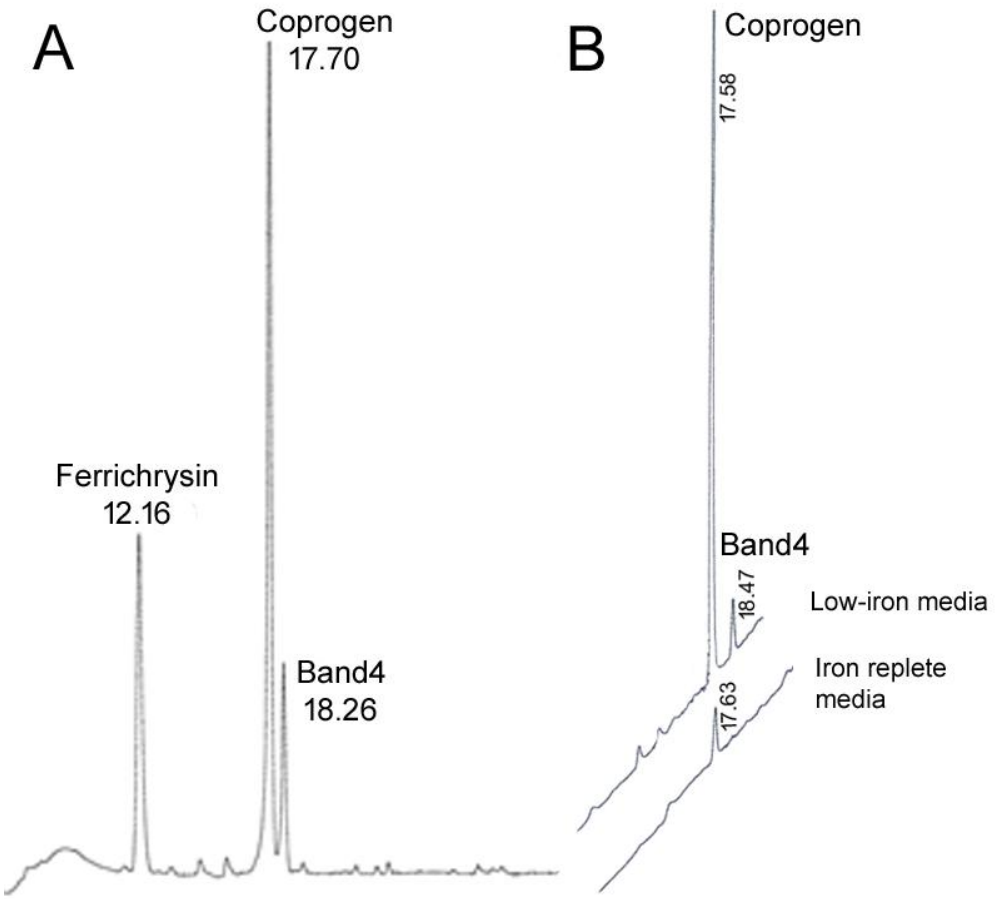

Figure 4.2. HPLC trace of culture supernatants extracted from wildtype *A. terreus* grown in low iron and iron replete media.

A. HPLC analysis of siderophores extracted from *A. terreus* include ferrichrysin (12.16 minutes), coprogen (17.70 minutes) and Band4 (18.26 minutes). **B**. HPLC excerpt of coprogen (17.58 minutes) and Band 4 (18.47 minutes) secretion in low-iron (top trace) and iron-replete media (bottom trace). The identity of ferrichrysin and coprogen was confirmed by MS analysis (see supplementary data).

Band 4 was purified from iron-limited culture supernatants of *A. terreus* by extracting siderophores using ion-exchange resins followed by gel filtration to separate out the three siderophores MS analysis showed that ferrated Band 4 had a main mass peak of 902.26 ($m/z + H^+$). Peaks for ferrated Band 4 sodium and potassium adducts were also observed (Band 4 + Na^+ = 924.24 and Band 4 + K^+ = 940.21). These data imply that ferrated Band 4 has a molecular weight of 901.26 (Figure 4.3).

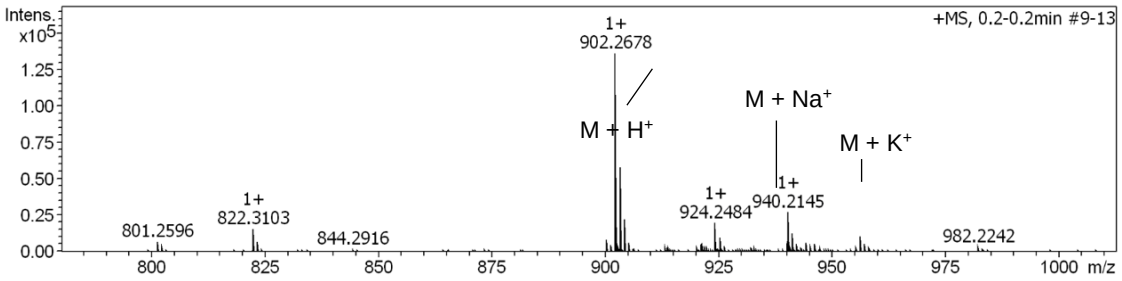

Figure 4.3. MS analysis of purified, ferrated Band 4 from *A. terreus*.
Band 4 was purified from iron limited cultures of *A. terreus* and MS analysis shows that the molecular weight of Band 4 is 901.26.

4.4.2 Band 4 is structurally distinct from TAFC

The *A. fumigatus ΔsidA* mutant does not grow in iron-limited media and requires supplementation with $FeCl_3$ or TAFC to restore growth[38]. To determine if Band 4 is structurally related to TAFC, we grew *A. fumigatus ΔsidA* in iron-restricted media with supplementation of $FeCl_3$ or various siderophores. Figure 4.4 shows that *A. fumigatus ΔsidA* can take up and use the hydroxamate siderophores, TAFC, ferrichrysin and to a lesser extent, coprogen; Band 4, however, is not used as a significant iron source and does not restore growth to the siderophore deficient *A. fumigatus ΔsidA* mutant. Importantly, these data imply that Band 4 is structurally distinct from TAFC and ferrichrysin.

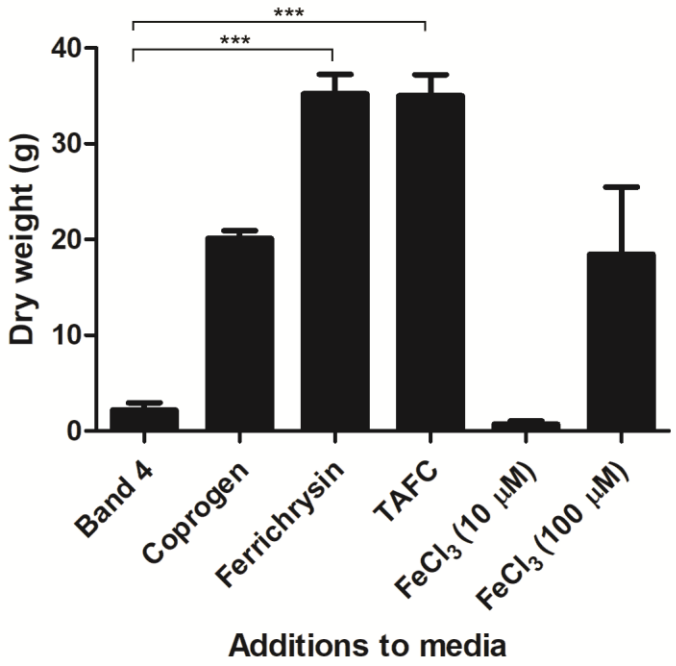

Figure 4.4. TAFC but not Band 4 can restore the growth of the *A. fumigatus ΔsidA* strain.

A. fumigatus ΔsidA was grown in liquid GA medium for 7 days at 37°C with or without amendments. Siderophores and Band 4 were dissolved in water added in 10 µM concentrations. A one-way AVONA and Dunnett's post test confirmed that growth was significantly reduced with Band 4 supplementation compared to growth with ferrichrysin and TAFC supplementation ($P<0.001$). Experiments were performed in triplicate and data represent the mean ± SD.

4.4.3 *Neurospora crassa ΔsidA* strain uses Band 4 as a siderophore

Neurospora crassa produces the hydroxamate siderophores, coprogen and ferricrocin[61]. The *ΔsidA* strain of *N. crassa* does not produce these siderophores and therefore needs iron supplementation to grow. We tested if Band 4 could restore growth to the *N. crassa ΔsidA* strain by growing it in liquid GA media with 10 µM of various siderophores. As seen in Figure 4.5, the *N. crassa ΔsidA* strain used Band 4 as a siderophore with growth levels equivalent to those seen with the wildtype siderophores, coprogen and ferrichrysin. Band 4 supported growth significantly better than $FeCl_3$ alone or no supplementation at all.

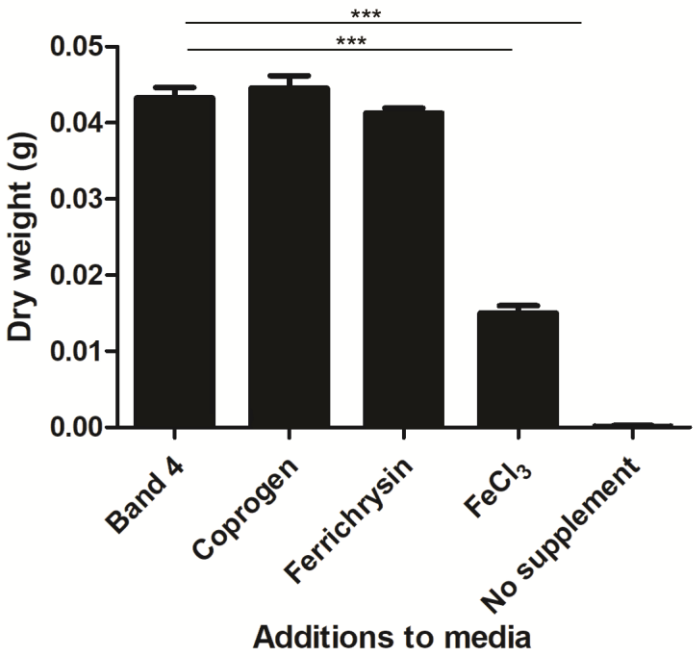

Figure 4.5. Band 4 restores growth of *N. crassa ΔsidA* mutant in iron-limited medium.

N. crassa (strain FGSC 20170) was grown in liquid GA medium with or without supplementation for 48 hours at 30°C temperature. A one-way AVONA and Dunnett's post test confirmed that growth with Band 4 supplementation was significantly different from growth with $FeCl_3$ or no supplementation ($P<0.001$). Siderophores were added as described in the legend to Figure 4.4. Experiments were performed at least in triplicate and data represent the mean ± SD.

Based on these data, and the growth assays with *A. fumigatus ΔsidA*, we predict that Band 4 is structurally more similar, although not identical to members of the coprogen family of siderophores, compared to TAFC.

4.4.4 Band 4 production is increased in an *A. terreus ΔsidA* mutant.

When *sidA* was deleted in *A. terreus*, production of ferrichrysin and coprogen was negligible as expected. In contrast, Band 4 increased in the knockout strain (Figure 4.6). Thus, biosynthesis of Band 4 is not dependent on *sidA* and therefore Band 4 is synthesized via a pathway that is distinct from the NRPS pathway used to produce the hydroxamate siderophores, coprogen and ferrichrysin.

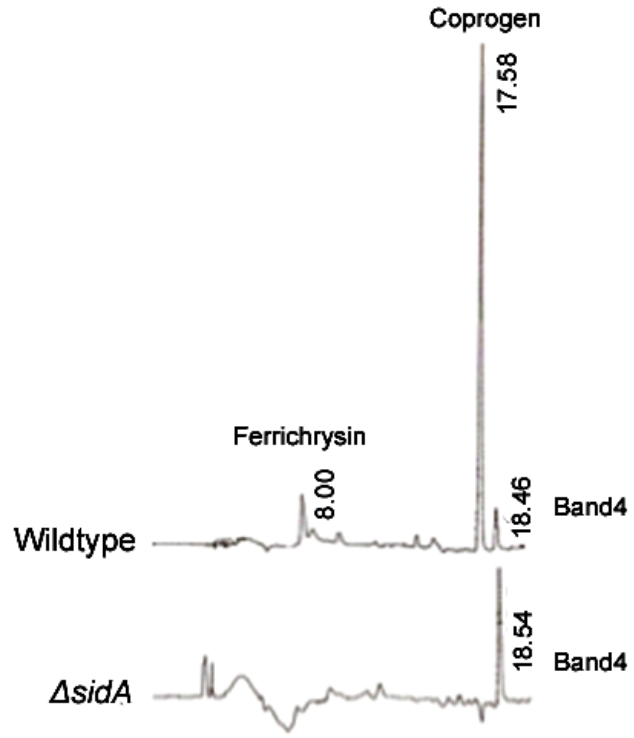

Figure 4.6. Band 4 production is increased in an *A. terreus ΔsidA* mutant.
Wildtype culture supernatants show the presence of ferrichrysin (8.00 minutes), coprogen (17.58 minutes) and Band 4 (18.46 minutes). In contrast, the *A. terreus ΔsidA* mutant produced no detectable coprogen or ferrichrysin; however, the amount of Band 4 increased.

4.4.5 Base hydrolysis of Band 4 yields dimerum acid

The chemical structure of coprogen consists of dimerum acid and N-acetyl fusarinine. To determine if Band 4 was related to coprogen, we base hydrolyzed purified Band 4 and examined the products by MS (Figure 4.7). A peak for dimerum acid was present (*m/z*: 538.2), however, a peak for N-acetyl fusarinine is not (*m/z*: 316.5). These data indicate that Band 4 may be related to coprogen but that coprogen is not the parent compound.

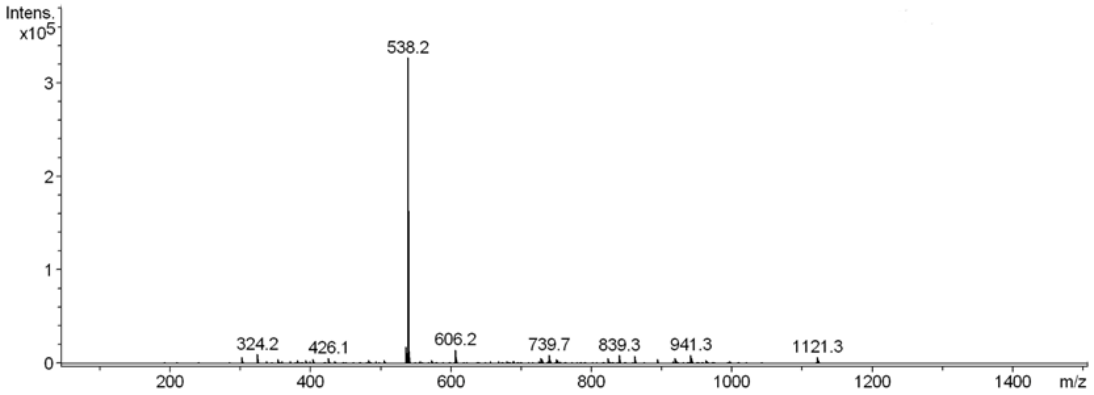

Figure 4.7. Mass spectrometry of base hydrolyzed Band 4.
The major product formed is dimerum acid (*m/z*: 538.2). N-acetyl fusarinine (*m/z*: 316.5) is not found indicating that the parent compound for Band 4 is not coprogen (*m/z*: 822.3).

4.4.6 Identification of an *A. terreus* NIS enzyme and bioinformatic analyses

The other major siderophore biosynthetic pathway used by fungi is the NRPS-independent pathway catalyzed by NRPS-independent siderophore (NIS) synthetases. To date, these enzymes have been described in Bacteria and Fungi in the order Mucorales. A Blastp search of the *A. terreus* genome (A1156) using the fungal NIS enzyme, Rfs[57], revealed the presence of a hypothetical protein (gi: 115437856; AtNIS) with 30% identity and 78% coverage to Rfs. Regions of conservation appear dispersed throughout Rfs and AtNIS; there are no absolutely conserved regions between the proteins (Figure 4.8).

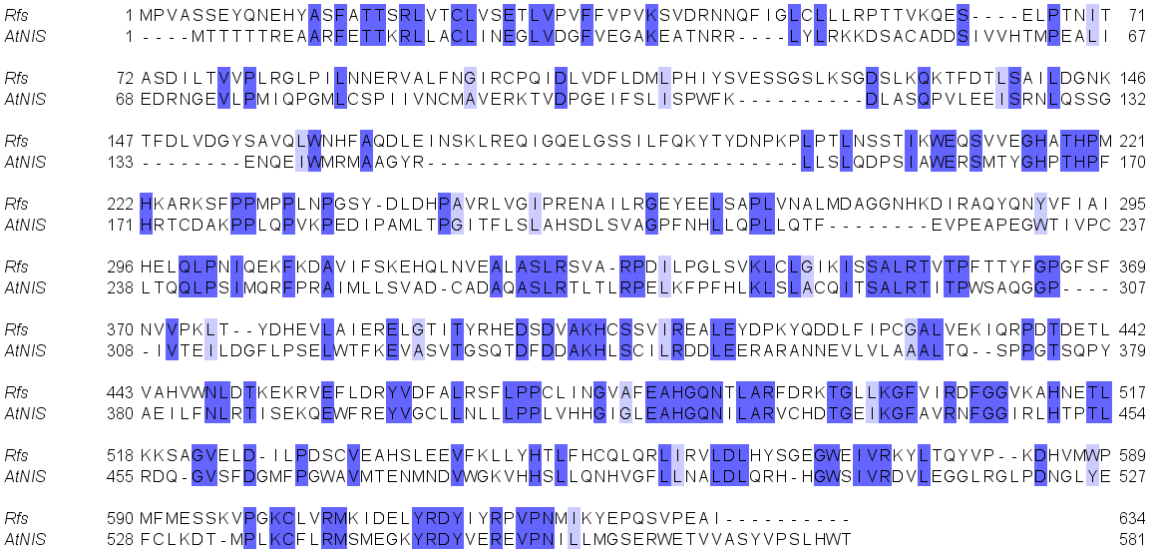

Figure 4.8. MUSCLE alignment of Rfs and AtNIS highlighting residues conserved between the two proteins.

Amino acids shaded in dark purple represent 100% conservation and residues shaded in light purple indicate 75% conservation between Rfs and AtNIS.

Blastp also predicted AtNIS to be a member of the IucA/IucC superfamily of proteins, a hallmark of NIS proteins, and have an RhbC domain, a siderophore synthetase component domain. Alignment of the putative AtNIS protein was done using Phyre[53]. AtNIS aligned with AlcC, an NIS enzyme from *Bordetella bronchiseptica*, with 15% identity and 100% confidence. Using another program, I-TASSER[54], AtNIS showed 18% identity and 94% coverage with AsbB, an NIS enzyme from the bacterium, *Bacillus anthracis* that is involved in the synthesis of the mixed carboxylate/catecholate siderophore, petrobactin[62–65]. The relatively low sequence similarity between NIS enzymes is not uncommon. For example, IucA, an NIS that catalyzes aerobactin synthesis in bacteria has ~20% sequence identity with the closely related NIS enzymes AcsD, AlcC and AsbB but structural alignments had RMSD values of 3.1 Å or lower[66]. Similarly, structural alignment of the AtNIS model with AlcC, a predicted Type C NIS that is involved in alcaligin biosynthesis[67–71], had an RMSD of 0.5 Å. In addition, several catalytic residues were conserved between the two proteins, including Arg312 and His449 from AlcC with Arg269 and His394 in AtNIS, respectively (data not shown).

The overall alignment between AsbB and AtNIS had an RMSD of 5.6 Å and alignment of catalytic residues was not as clear as with AlcC. Nevertheless, structural alignment showed that Lys311 in AsbB, an important catalytic amino acid[62] aligned with Lys314

(Figure 4.9). Glu459 from AsbB has also been implicated in specificity and regioselectivity for the nucleophilic substrate[62]; however, in AtNIS there does not appear to be an equivalent residue. This may highlight differences in the substrate usage profile between the two enzymes.

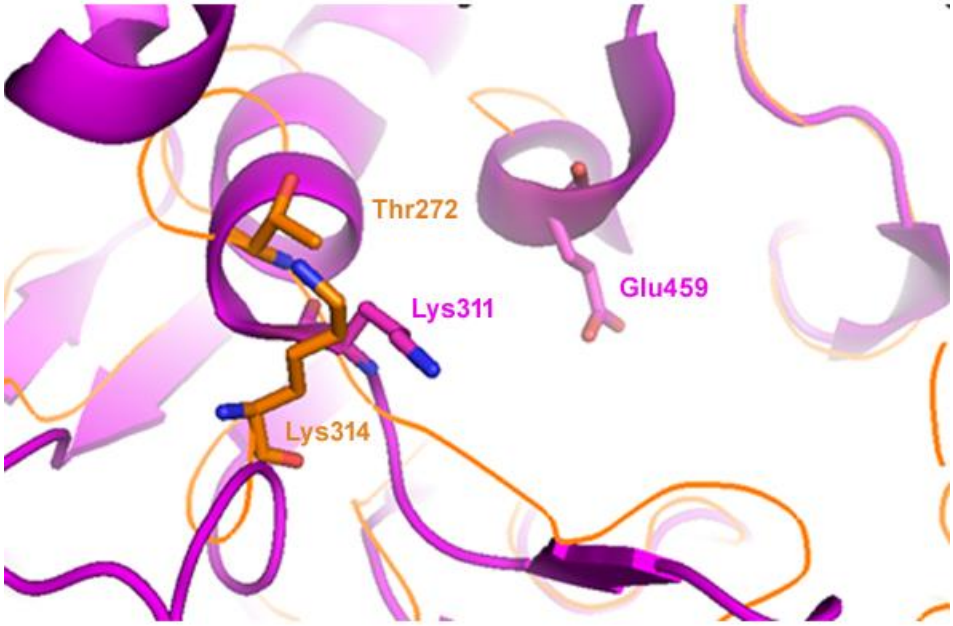

Figure 4.9. Alignment of AsbB and the AtNIS model showing residues important for catalytic functioning. Structural modelling showing conserved residues in AsbB (magenta) and closely related residues is AtNIS (orange).

4.4.7 Identification of the AtNIS reading frame and confirmation of iron-regulated expression

The *A. terreus ΔsidA* mutant strain was grown in iron-limited and iron-replete media, RNA was harvested, cDNA synthesized and PCR amplification of approximately 500 bp of *AtNIS* was performed. Amplification of *AtNIS* was seen in RNA extracted from hyphae grown in iron-limited media, while no amplification was seen in iron-replete conditions (Figure 4.10).

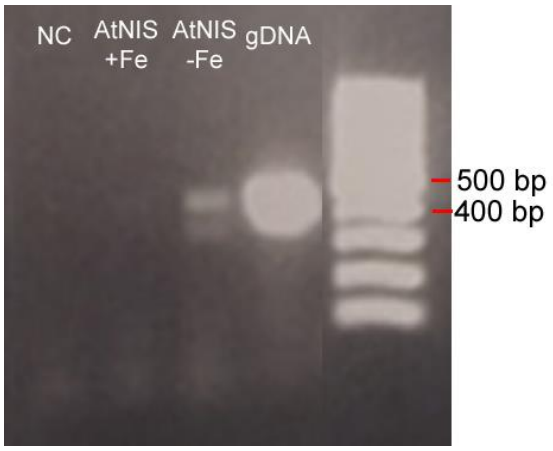

Figure 4.10. RT-PCR amplification of *A. terreus ΔsidA* cDNA in iron-limited and iron-replete conditions.

RT-PCR was performed to amplify AtNIS in iron-limited (-Fe) conditions and not from iron-replete (+Fe) conditions. NC: no-template control; gDNA: genomic DNA. The expected size of the AtNIS fragment is 500 bp. Photoshop was used to remove intervening lanes in the gel. Sizes were not changed in the figure.

RT-PCR amplification from wildtype *A. terreus* cDNA grown in iron-limited conditions, yielded two bands of approximately the correct size for AtNIS (Figure 4.11); one band was seen at 1.7 kb (AtNIS-4), the other band was seen at 1.9 kb (AtNIS-6). Both bands were gel purified, cloned into pJET and sequenced. The initial annotation of AtNIS predicted 5 introns; however, sequencing of AtNIS-4 revealed only 4 introns and the presence of an additional 27 amino acids encoded by the cDNA (Figure S4.18). AtNIS6 did not contain any introns indicating it was most likely amplified from contaminating genomic DNA. To confirm this, both AtNIS-4 and AtNIS-6 were cloned into pEHISTEV and induced for protein expression. pEHISTEV-AtNIS6 did not produce protein (data not shown) and it was therefore omitted from future experiments.

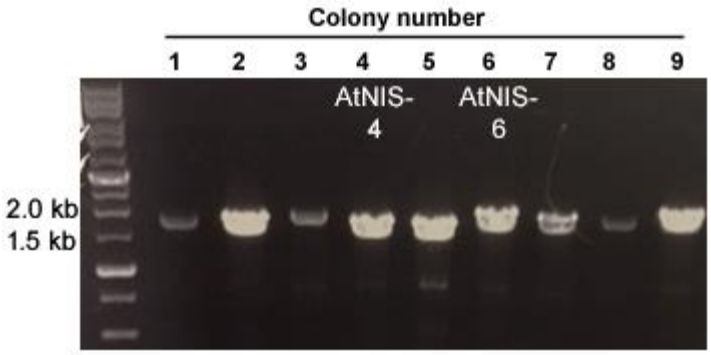

Figure 4.11. RT-PCR amplification of full length AtNIS from *A. terreus* cDNA produced under iron-limited conditions.
RT-PCR showed two different sized bands corresponding to AtNIS spliced mRNA (AtNIS-4) and genomic DNA (AtNIS-6).

pEHISTEV-AtNIS4 produced a protein at the expected molecular weight of 68 kDa. Unfortunately, the wildtype protein was not soluble when induced with 0.5 mM IPTG at various temperatures (Figure 4.12A). To increase solubility, purification of AtNIS was performed in the presence of citrate, a predicted substrate, using a lower IPTG concentration (0.25 mM); however, this was unsuccessful as the protein was still found in the cell pellet or inclusion bodies (Figure 4.12B).

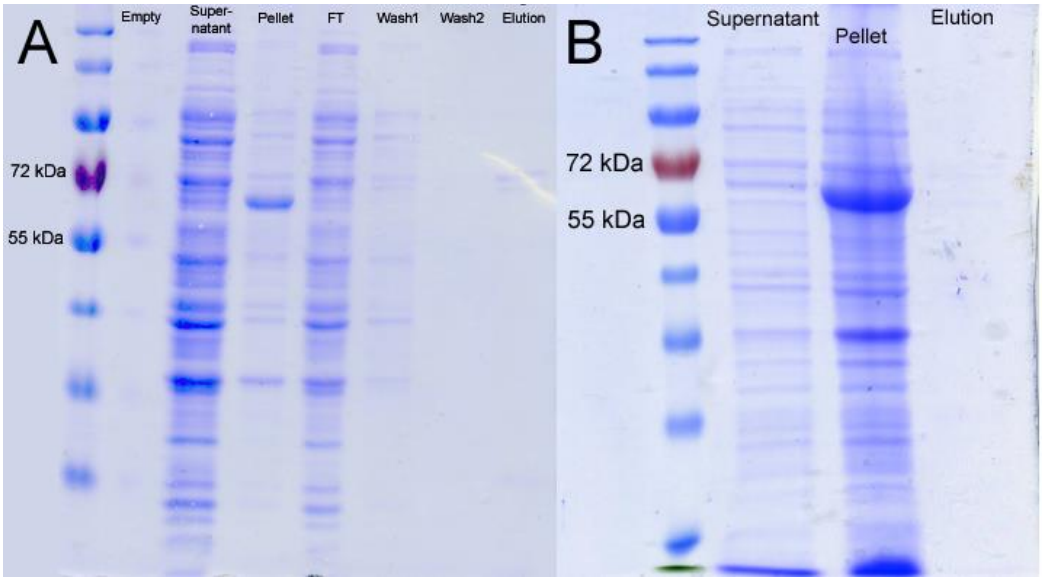

Figure 4.12. Induction of full length AtNIS under native conditions.
(**A**) Induced *E. coli* Tuner cells were lysed, spun down, and samples of the supernatant and pellet were taken. The supernatant was incubated with Ni^{2+} beads, and beads were collected in a column and the flow-through (FT) was discarded. The beads were washed two times in Wash Buffer and eluted in Elution Buffer with 250 mM imidazole. (**B**) Induced Tuner cells were lysed in the presence of citrate and glycerol and purification was performed as stated above and samples of the supernatant, pellet and elution from Ni^{2+} beads were run on the gel.

The N-terminal domain in NIS enzymes is predicted to be involved in oligomerization of the enzymes[72]. Therefore, to reduce oligomeric structures, we made two truncation mutants of AtNIS: one mutant had a deletion of the first 91 amino acids at the N-terminus (ΔAtNIS91) and the second mutant had a deletion of 138 amino acids at the N-terminus (ΔAtNIS138). These constructs were expressed in *E. coli* Tuner cells and proteins were induced in the presence and absence of citrate and glycerol supplementation in the buffers. Nevertheless, the N-terminal truncated versions of AtNIS were still found in the cell pellet (Figure 4.13).

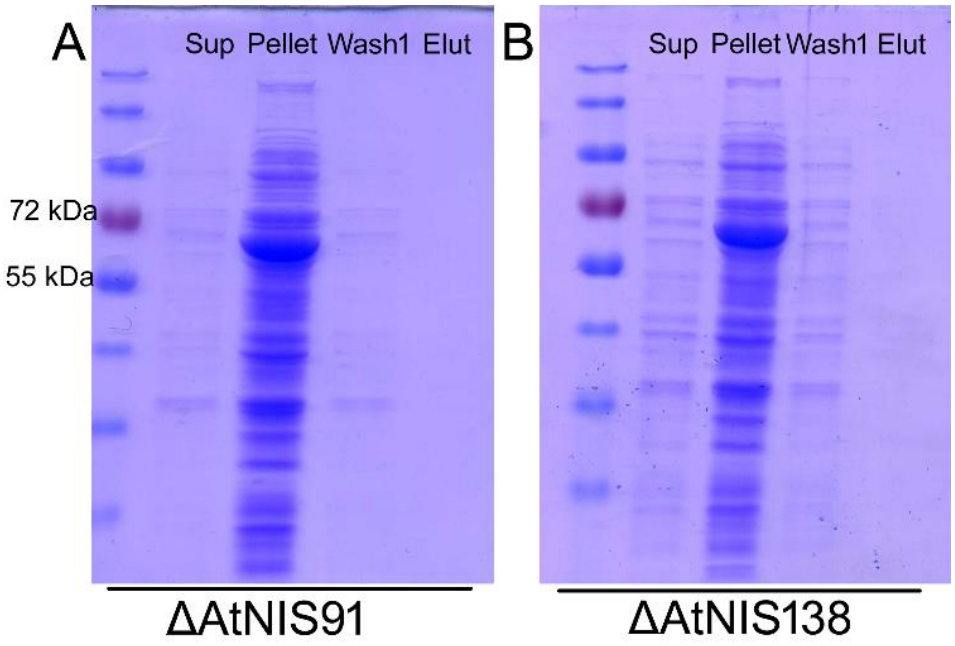

Figure 4.13. N-terminal truncated AtNIS proteins were expressed in *E. coli* and purified in the presence of citrate and glycerol.
Both ΔAtNIS91 (**A**) and ΔAtNIS138 (**B**) remained in the cell pellet. Sup: supernatant; Elut: elution.

AtNIS also remained in the cell pellet in experiments without citrate and glycerol supplementation in the buffer (data not shown). Experiments are underway to extract sufficient concentrations of AtNIS from inclusion bodies for activity assays or to purify AtNIS under denaturing conditions with urea[73].

4.4.8 Localization of NIS enzymes by indirect immunofluorescence microscopy

Rhizoferrin synthetase (Rfs) is an NIS enzyme from the Mucorales fungus, *Rhizopus delemar* that is predicted to be a cytosolic enzyme[57]. Using WoLF PSORT, the putative

AtNIS was also predicted to be cytosolic, with possible associations with the mitochondrial matrix. However, Phyre predicted two transmembrane helices to be present in AtNIS (amino acids 372-388 and 455-470). We localized Rfs in fixed *R. delemar* sporangiospores and hyphae using indirect immunofluorescence microscopy. Figure 4.14 shows that in iron-limited growth, Rfs was not distributed throughout the cytosol as expected but rather, it formed punctate structures close to the *R. delemar* plasma membrane (Figure 4.14). Under iron-replete growth conditions, less fluorescent signal was detected, as expected.

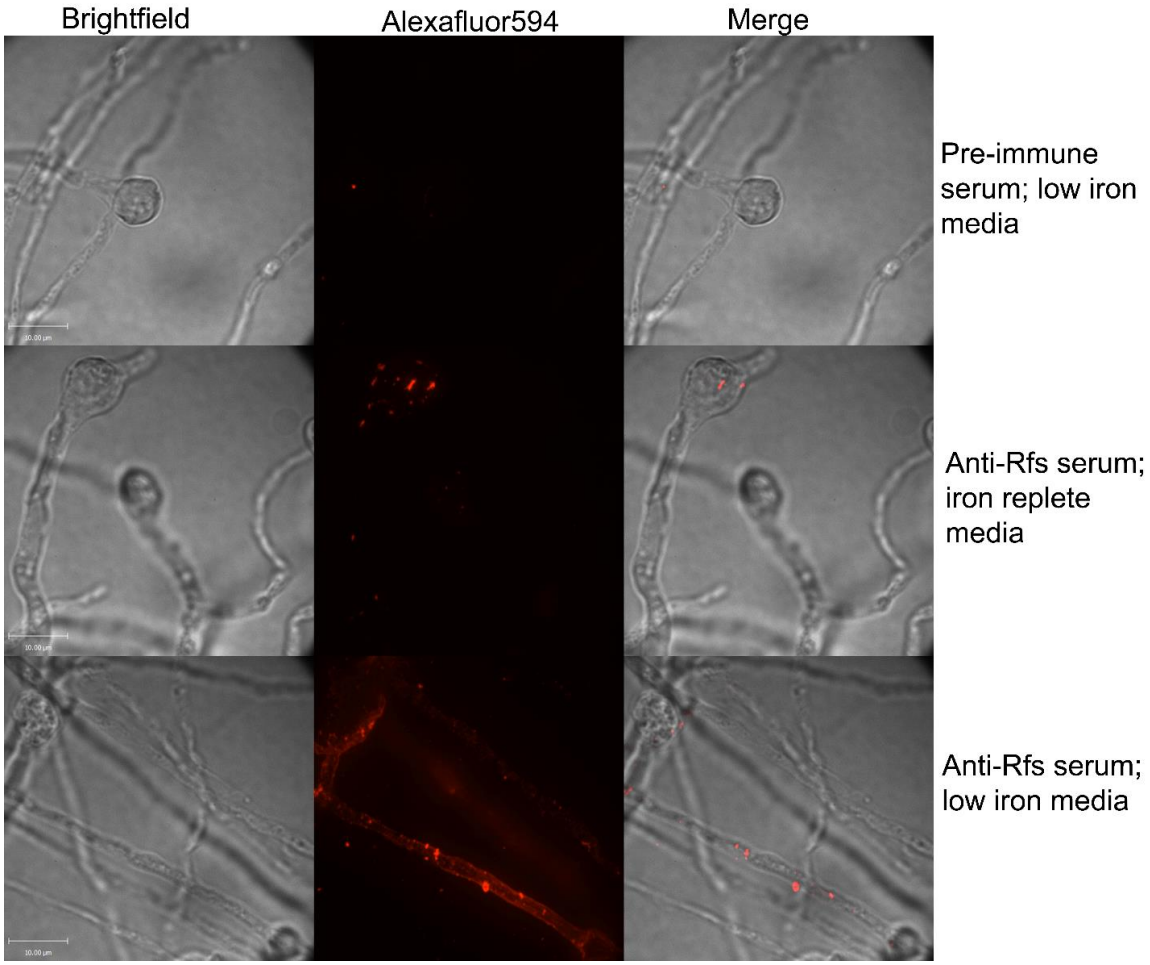

Figure 4.14. Localization of Rfs in *R. delemar* by indirect immunofluorescence microscopy.

R. delemar was grown in iron-limited or iron-replete medium, fixed and permeabilized. Anti-Rfs antiserum was added and the secondary antibody conjugated to Alexafluor594 was added. Pre-immune serum was used as a control. All fluorescence images were captured at the same exposure time and laser intensity, and 2 µm z-stacks were taken and compressed. Scale bars represent 10 µm.

We performed a similar experiment to localize the putative AtNIS in *A. terreus* using the polyclonal affinity purified anti-Rfs antibody and discovered that the fluorescence had a similar pattern as found with Rfs in *R. delemar* (Figure 4.15). Staining was not as intense, most likely due to lower cross-reactivity between Rfs and AtNIS (AtNIS has 30 % identity to Rfs at the amino acid level). As found with Rfs, AtNIS was localized in punctate structures around the edge of hyphae and spores and addition of iron reduced the intensity of fluorescence (Figure 4.15). This gives support to the Phyre prediction that AtNIS may be cell membrane associated or directly linked to the plasma membrane via transmembrane helices.

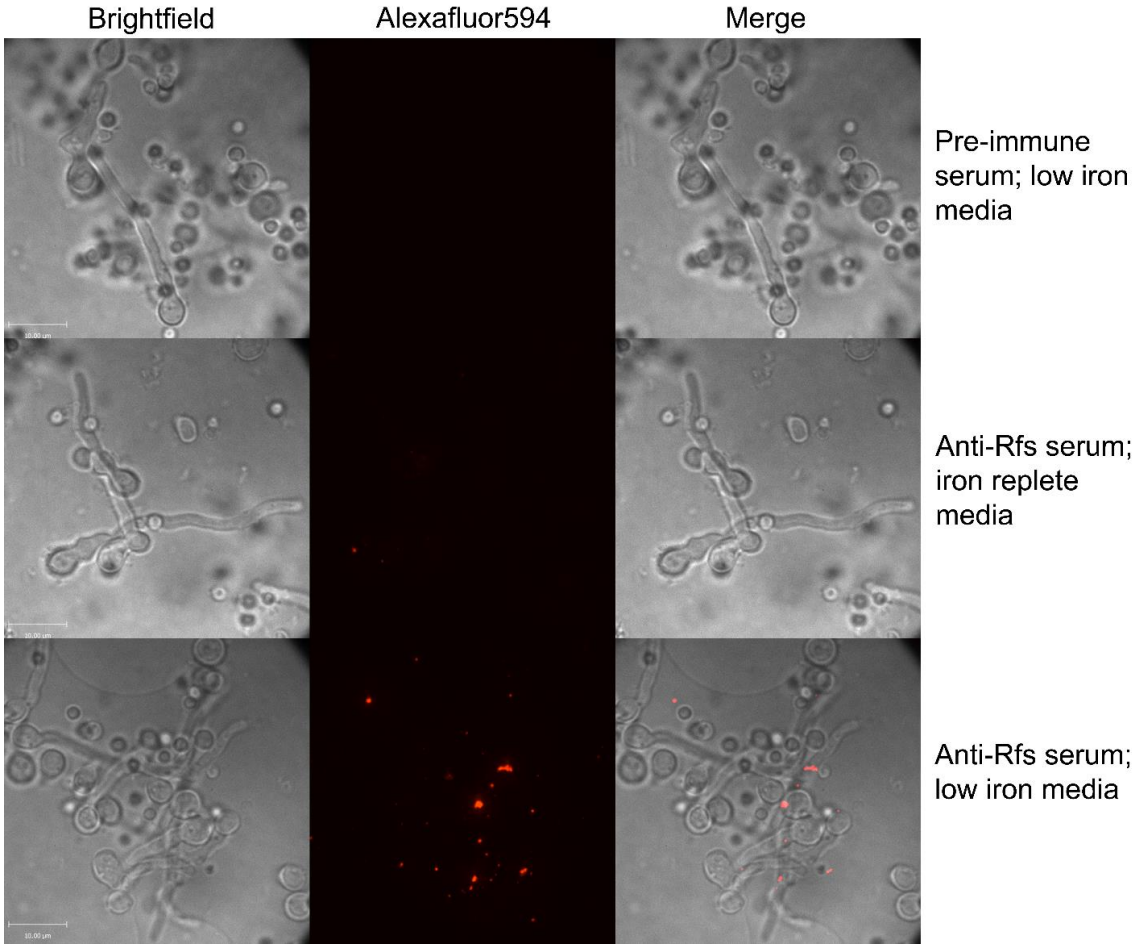

Figure 4.15. Immunolocalization of the putative AtNIS in *A. terreus* using polyclonal anti-Rfs antiserum.

Fungi were grown in low iron or iron replete media and immuno-staining was done using anti-Rfs antiserum (1:50) or pre-immune serum (1:50) as a control. All fluorescence images were captured at the same exposure time and laser intensity, and 2 µm z-stacks were taken and compressed. Scale bars represent 10 µm.

In *Aspergillus fumigatus* and *N. crassa,* some of the enzymes that catalyze hydroxamate siderophore biosynthesis have been localized to peroxisomes (see Figure 4.1)[40]. To determine whether Rfs in *R. delemar* was localized in peroxisomes, we examined Rfs co-localization with an anti-SKL antibody that targets the Type I peroxisomal localization signal[74]. Anti-SKL-reactive signal appeared as punctate structures throughout the cytoplasm, as expected. However, co-localization between peroxisomes and Rfs was not evident in *R. delemar;* these formed two distinct structures without overlap (Figure 4.16).

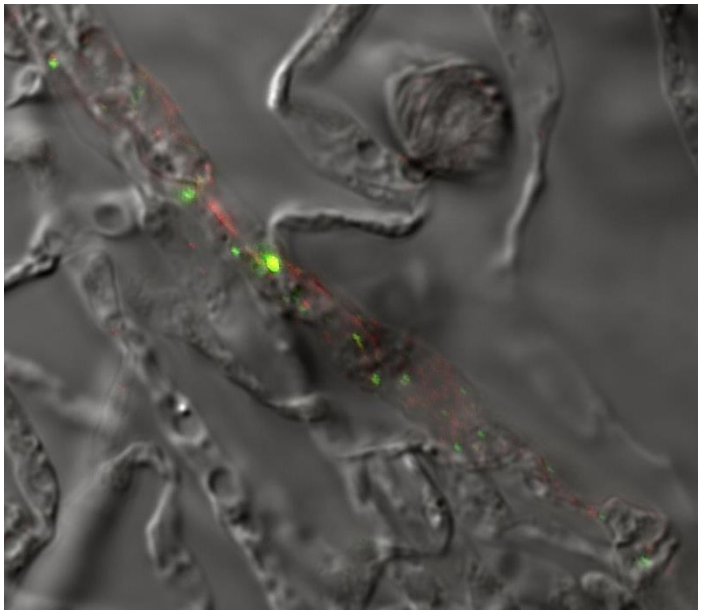

Figure 4.16. Rfs is not localized to peroxisomes in *R. delemar*.
Peroxisomes were labelled using an anti-SKL antibody and detected using CF405S-conjugated secondary antibodies (here, false coloured red). Rfs was detected with anti-Rfs polyclonal antisera and detected using secondary antibodies conjugated to Alexafluor594 (here, false coloured green). The images were acquired using the FV3000RS high resolution confocal laser scanning microscope (Olympus) and merged in ImageJ Fiji[75]. Co-localized proteins would yield yellow fluorescence but no overlap between signals is evident.

4.5 Discussion

In this study, we have confirmed that *A. terreus* produces coprogen and ferrichrysin and we describe the presence of a novel iron-regulated siderophore that is not produced by canonical *sidA* pathway used to initiate hydroxamate siderophore biosynthesis, including the synthesis of the hydroxamates coprogen and ferrichrysin in *A. terreus*. We have shown that Band 4 can restore growth to a *Neurospora crassa ΔsidA* mutant deficient in siderophore biosynthesis, however Band 4 does not promote growth of an *Aspergillus fumigatus ΔsidA* mutant. These data indicate that the structure of Band 4 is distinct

enough from the main siderophore secreted by *A. fumigatus*, TAFC[42], such that it is not transported by the *A. fumigatus* siderophore transporter, MirB[76]. Radio-labeled transport assays have shown that MirB transports TAFC, coprogen and ferricrocin but not ferrichrysin[76]. *N. crassa* secretes coprogen and ferricrocin[61] and appears to have two receptors for siderophore uptake[77], however, studies have not been performed to elucidate specific proteins responsible for siderophore uptake. Radio-labeled uptake assays in *N. crassa*, have shown that it transports coprogen, and its derivatives neocoprogen I and neocoprogen II, as well as ferrichrysin, asperchrome D1, asperchrome B1 and ferrirubin[78]. As Band 4 was efficiently used by *N. crassa ΔsidA* and not by *A. fumigatus ΔsidA,* we speculate that the chemical structure of Band 4 is more closely related to the coprogen family of siderophores, than to TAFC. In support of this, when Band 4 was base hydrolyzed, MS analysis showed dimerum acid, a component of coprogen, to be the major product. As Band 4 was still produced in an *A. terreus ΔsidA* mutant, we hypothesized that biosynthesis of Band 4 must occur via a NRPS-independent pathway using NIS enzymes. NIS enzymes typically catalyze the biosynthesis of polycarboxylate or mixed-type siderophores although NIS enzymes have also been implicated in biosynthesis of hydroxamate and catecholate siderophores such as alcaligin and petrobactin, respectively[62,64,68,69,79,80]. To date, NIS enzymes have been characterized in Bacteria and in one fungus, the Mucorales pathogen, *Rhizopus delemar*. In this report, we describe a putative NIS enzyme from *Aspergillus terreus*, a member of the Ascomycota phylum. Because only one NIS protein is predicted to be present in the *A. terreus* genome, we speculate that AtNIS may be responsible for a single step in a NRPS-dominated siderophore biosynthetic pathway. For example, the biosynthesis of petrobactin, a catecholate siderophore, is catalyzed in part by two NIS enzymes, AsbA and AsbB, to create a citryl spermidine backbone to which the NRPS enzymes, AsbC, AsbD and AsbE, add 3,4 dihydroxybenzoic acid to form the catecholate functional groups[64,80,81]. Structural predictions suggest that AtNIS shares homology to AsbB, which condenses spermidine on to a citryl-spermidine or dihydroxbenzoyl spermidinyl citrate intermediate. AtNIS shares significant structural homology to AlcC, an NIS enzyme that is predicted to catalyze the biosynthesis of the hydroxamate siderophore, alcaligin[68,69]. Biochemical characterization of AlcC has not been performed, however, it is predicted to function in dimerization and macro-cyclization of two succinyl-dihydroxy-putrescine intermediates[82,83]. Thus, we propose that AtNIS may function in the dimerization of and/or possible macrocyclization of a hydroxamate or mixed-type

siderophore similar to TAFC found in *Aspergillus fumigatus*[42] and *Aspergillus nidulans*[44,45].

Some enzymes of the hydroxamate siderophore biosynthetic pathway in *A. fumigatus* and *N. crassa* have been localized in peroxisomes[40]; however, Rfs did not co-localize with the peroxisomal marker. Interestingly, the enzyme was not diffusely distributed within the cytoplasm but formed punctate structures that were associated with the plasma membrane. Gasser and coworkers (2015) showed that in *Pseudomonas aeruginosa,* NRPS-mediated biosynthesis of its major siderophores, pyoverdine I and pyochelin, occurs in 'siderosomes' which are siderophore-specific, multi-enzyme assembly sites, linked to the inner membrane[84]. Fluorescent microscopy of GFP and mCherry fused-siderophore biosynthetic enzymes showed intense fluorescence localized to cell poles during log phase growth and then more dispersed fluorescence during late log and stationary phase; however, some cells were observed with no fluorescence. The dispersed localization pattern during late log and stationary phase for *P. aeruginosa* was not seen in *A. terreus* or *R. delemar*, possibly because bacteria cells are 'programmed' to divide at certain cellular size limits while fungi continue polarized growth and therefore require important cellular nutrients throughout cell growth. The presence of 'siderosomes' interacting directly or indirectly with the plasma membrane and/or other proteins would also account for the low-solubility or inclusion body-formation of AtNIS under native protein purification conditions. Unlike our experience with Rfs and despite the prediction by WoLF PSORT that AtNIS would be active as a soluble protein[53], AtNIS was highly insoluble under native purification conditions. This gives support to the Phyre prediction that AtNIS is localized to the cell membrane. If AtNIS is aggregated in inclusion bodies, numerous strategies are employed to extract proteins from inclusion bodies including the use of detergents and chaotropic agents, such as urea[73]. Alternatively, it may be necessary to purify AtNIS using membrane protein purification protocols or express AtNIS in another cell type such as yeast to obtain active protein.

This study has confirmed the presence of an iron-regulated enzyme in *A. terreus* whose structure and subcellular localization suggest that it may be a novel member of the NIS family of adenylating enzymes. Further research is required to obtain active soluble enzyme and ultimately and confirm its activity as an NIS enzyme. Although circumstantial evidence suggests that it may be involved in the biosynthesis of Band 4,

only structural identification of this molecule along with a full understanding of the substrate specificity of this enzyme will be able to link AtNIS to the synthesis of Band 4.

4.6 Supplementary data

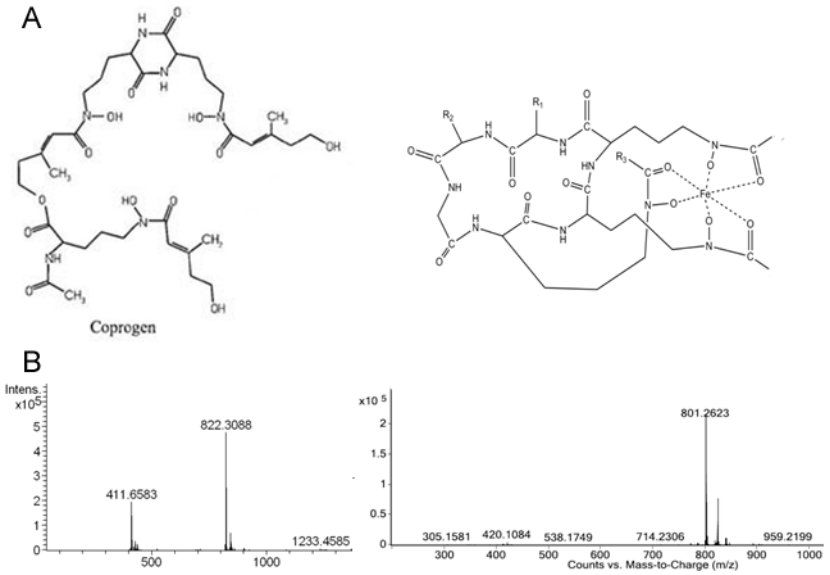

Figure S4.17. Structures of coprogen and ferrichrysin.
A. Coprogen and ferrichrysin were found to be secreted by *A. terreus*. They were purified, and MS was used to identify their structures. **B**. MS analysis of coprogen and ferrichrysin purified from *A. terreus*.

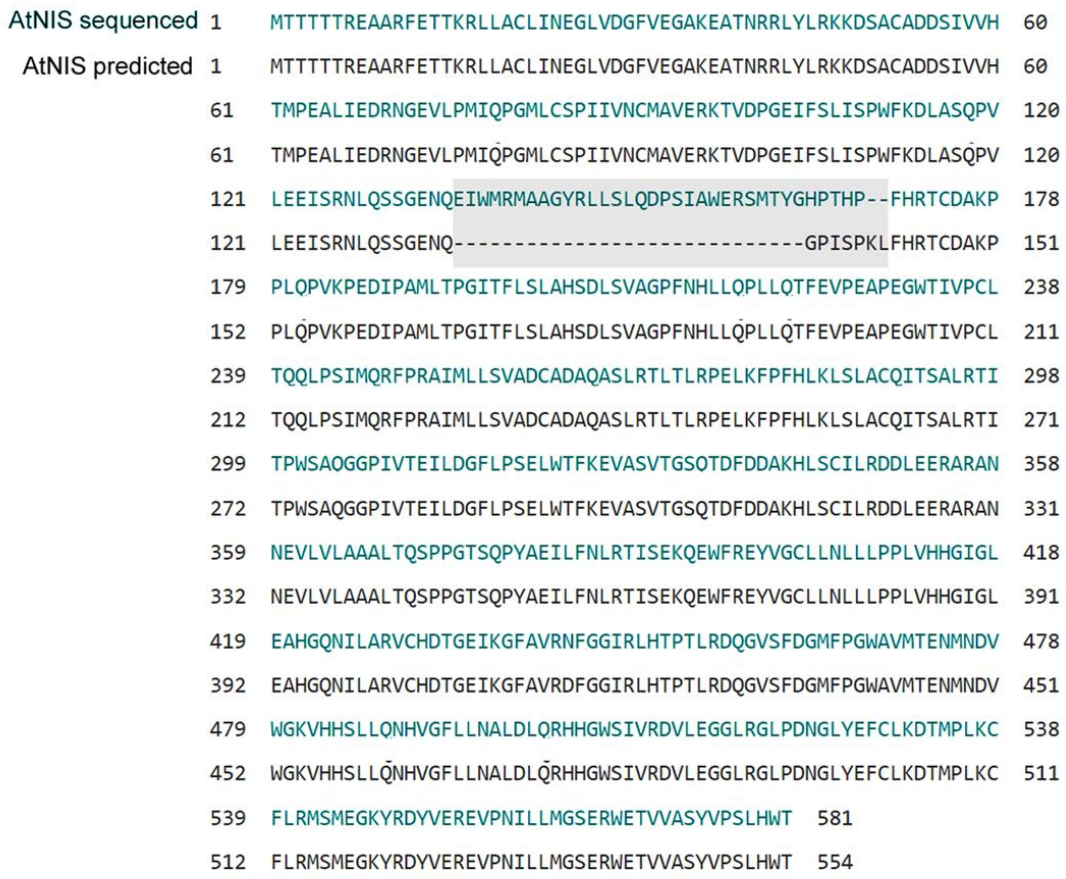

Figure S4.18. Alignment of the actual AtNIS sequence based on sequencing PCR amplicons from cDNA (teal) and the predicted AtNIS protein sequence (black).

The shaded box indicates the additional amino acids not present in the predicted sequence.

4.7 References

1. Deak, E., Wilson, S. D., White, E., Carr, J. H. & Arunmozhi Balajee, S. *Aspergillus terreus* accessory conidia are unique in surface architecture, cell wall composition and germination kinetics. *Cell Wall Compos. Germination Kinet. PLoS ONE* **4,** (2009).

2. Deak, E. *et al. Aspergillus terreus* accessory conidia are multinucleated, hyperpolarizing structures that display differential dectin staining and can induce heightened inflammatory responses in a pulmonary model of aspergillosis. *Virulence* **2,** 200–207 (2011).

3. Mukhtar, H. Upstream and downstream processing of lovastatin by *Aspergillus terreus*. *Cell Biochem Biophys* **70,** 309–320 (2014).

4. Huang, X., Lu, X., Li, Y., Li, X. & Li, J.-J. Improving itaconic acid production through genetic engineering of an industrial *Aspergillus terreus* strain. *Microb. Cell*

Fact. **13,** 119 (2014).

5. Yasuoka, A., Tachikawa, N., Shimada, K., Kimura, S. & Oka, S. (1->3) beta-D-glucan as a quantitative serological marker for *Pneumocystis carinii* pneumonia. *Clin. Vaccine Immunol.* **3,** 3–6 (1996).

6. Zhao, C., Lei Guo, B., Liping Wang, B., Guoliang Zhu, B. & Weiming Zhu, B. Improving the yield of (+)-terrein from the salt-tolerant *Aspergillus terreus* PT06-2. *World J. Microbiol. Biotechnol.* **32,** (2029).

7. Rehman, S., Aslam, H., Ahmad, A., Ahmed Khan, S. & Sohail, M. Production of plant cell wall degrading enzymes by monoculture and co-culture of *Aspergillus niger* and *Aspergillus terreus* under SSF of banana peels. *Brazilian J. Microbiol.* **45,** 1485–1492 (2014).

8. Liu, Z., Yao, L. & Fan, C. Optimization of fermentation conditions of pectin production from *Aspergillus terreus* and its partial characterization. *Carbohydr. Polym.* **134,** 627–634 (2015).

9. Narra, M., Dixit, G., Divecha, J., Madamwar, D. & Shah, A. R. Production of cellulases by solid state fermentation with *Aspergillus terreus* and enzymatic hydrolysis of mild alkali-treated rice straw. *Bioresour. Technol.* **121,** 355–361 (2012).

10. Louis, B. *et al.* Invasion of *Solanum tuberosum* L. by *Aspergillus terreus*: a microscopic and proteomics insight on pathogenicity. *BMC Res. Notes* **7,** (2014).

11. Zaehle, C. *et al.* Terrein biosynthesis in *Aspergillus terreus* and its impact on phytotoxicity. *Chem. Biol.* **21,** 719–731 (2014).

12. Kelly, S., Shaw, S. & Clark, W. Long-term survival of four dogs with disseminated *Aspergillus terreus* infection treated with itraconazole. *Aust. Vet. J.* **72,** 311–313 (1995).

13. Pal, M. Disseminated *Aspergillus terreus* infection in a caged pigeon. *Mycopathologia* **119,** 137–9 (1992).

14. Lewis, R. E. *et al.* Epidemiology and sites of involvement of invasive fungal infections in patients with haematological malignancies: a 20-year autopsy study. *Mycoses* **56,** 638–45 (2013).

15. Steinbach, W. J. *et al.* Clinical epidemiology of 960 patients with invasive aspergillosis from the PATH Alliance registry. *J. Infect.* **65,** 453–464 (2012).

16. Hachem, R. *et al.* Invasive aspergillosis caused by *Aspergillus terreus*: an emerging opportunistic infection with poor outcome independent of azole therapy. *J. Antimicrob. Chemother.* **69,** 3148–3155 (2014).

17. Laham, M. N. & Carpenter, J. L. *Aspergillus terreus*, a pathogen capable of causing infective endocarditis, pulmonary mycetoma, and allergic bronchopulmonary aspergillosis. *Am. Rev. Respir. Dis.* **125,** 769–72 (1982).

18. Khan, Z. U. *et al.* Bilateral pulmonary aspergilloma caused by an atypical isolate of *Aspergillus terreus*. *J. Clin. Microbiol.* **38,** 2010–4 (2000).

19. José Castó, J. *et al.* Risk factors for pulmonary *Aspergillus terreus* infection in patients With positive culture for filamentous fungi. *Chest* **131,** 230–236 (2007).

20. Patterson, T. F. *et al.* Practice guidelines for the diagnosis and management of aspergillosis: 2016 update by the Infectious Diseases Society of America. *Clin. Infect. Dis.* **63,** 1–60 (2016).

21. Mortensen, K. L. *et al.* A prospective survey of *Aspergillus spp*. in respiratory tract samples: prevalence, clinical impact and antifungal susceptibility. *Eur. J. Clin. Microbiol. Infect. Dis.* **30,** 1355–1363 (2011).

22. Steinbach, W. J. *et al.* Infections due to *Aspergillus terreus*: A multicenter retrospective analysis of 83 cases. *Clin Infect Dis* **39,** 192–198 (2004).

23. Sutton, P., Waring, P. & Müllbacher, A. Exacerbation of invasive aspergillosis by the immunosuppressive fungal metabolite, gliotoxin. *Immunol. Cell Biol.* **74,** 318–22 (1996).

24. Bok, J. W. *et al.* GliZ, a transcriptional regulator of gliotoxin biosynthesis, contributes to *Aspergillus fumigatus* virulence. *Infect. Immun.* **74,** 6761–8 (2006).

25. Sugui, J. a *et al.* Gliotoxin is a virulence factor of *Aspergillus fumigatus: gliP* deletion attenuates virulence in mice immunosuppressed with hydrocortisone. *Eukaryot. Cell* **6,** 1562–9 (2007).

26. Spikes, S. *et al.* Gliotoxin production in *Aspergillus fumigatus* contributes to host-specific differences in virulence. *J. Infect. Dis.* **197,** 479–86 (2008).

27. Monod, M., Jaton-Ogay, K., Fatih, A., Paris, S. & Latgé, J.-P. The secreted proteases of pathogenic species of *Aspergillus* and their possible role in virulence. *Botany* **73,** 1081–1086 (1995).

28. Thau, N. *et al.* rodletless mutants of *Aspergillus fumigatus*. *Infect. Immun.* **62,** 4380–8 (1994).

29. Wasylnka, J. A, Simmer, M. I. & Moore, M. M. Differences in sialic acid density in pathogenic and non-pathogenic *Aspergillus* species. *Microbiology* **147,** 869–77 (2001).

30. Nesbitt, J. R. *et al.* The *Aspergillus fumigatus* sialidase (Kdnase) contributes to cell wall integrity and virulence in amphotericin B-treated mice. *Front. Microbiol.* **8,** 1–17 (2018).

31. Maurer, E. *et al. Galleria mellonella* as a host model to study *Aspergillus terreus* virulence and amphotericin B resistance. *Virulence* **6,** 591–598 (2015).

32. Loo, A. S., Muhsin, S. A. & Walsh, T. J. Toxicokinetic and mechanistic basis for the safety and tolerability of liposomal amphotericin B. *Expert Opin. Drug Saf.* **12,**

881–895 (2013).

33. Miethke, M. Molecular strategies of microbial iron assimilation: from high-affinity complexes to cofactor assembly systems. *Metallomics* **5,** 15–28 (2013).

34. Drechsel, H. *et al.* Rhizoferrin—a novel siderophore from the fungus *Rhizopus microsporus var. rhizopodiformis*. *BioMetals* **4,** 238–243 (1991).

35. Marahiel, M. A. & Essen, L. O. *Chapter 13 Nonribosomal Peptide Synthetases. Mechanistic and Structural Aspects of Essential Domains*. *Methods in Enzymology* **458,** (Elsevier Inc., 2009).

36. Oves-Costales, D., Kadi, N. & Challis, G. L. The long-overlooked enzymology of a nonribosomal peptide synthetase-independent pathway for virulence-conferring siderophore biosynthesis. *Chem. Commun. (Camb).* 6530–41 (2009).

37. Hissen, A. H. T., Chow, J. M. T., Pinto, L. J. & Moore, M. M. Survival of *Aspergillus fumigatus* in serum involves removal of iron from transferrin: The role of siderophores. *Infect. Immun.* **72,** 1402–1408 (2004).

38. Hissen, A. H. T., Wan, A. N. C., Warwas, M. L., Pinto, L. J. & Moore, M. M. The *Aspergillus fumigatus* siderophore biosynthetic gene *sidA*, encoding L-ornithine N^5 -oxygenase, is required for virulence. *Infect. Immun.* **73,** 5493–5503 (2005).

39. Schrettl, M. *et al.* Siderophore biosynthesis but not reductive iron assimilation is essential for *Aspergillus fumigatus* virulence. *J. Exp. Med.* **200,** 1213–9 (2004).

40. Gründlinger, M. *et al.* Fungal siderophore biosynthesis is partially localized in peroxisomes. *Mol. Microbiol.* **88,** 862–875 (2013).

41. Gressler, M. *et al.* Phytotoxin production in *Aspergillus terreus* is regulated by independent environmental signals. *Elife* **4,** (2015).

42. Nilius, A. M. & Farmer, S. G. Identification of extracellular siderophores of pathogenic strains of *Aspergillus fumigatus*. *J. Med. Vet. Mycol.* **28,** 395–403 (1990).

43. Tadenuma, M. & Sato, S. Agricultural and biological chemistry studies on the colorants in saké: Presence of ferrichrysin as iron containing colorant in sake. *Agric. Biol. Chem.* **3112,** 1482–1489 (1967).

44. Charlang, G. *et al.* Extracellular siderophores of rapidly growing *Aspergillus nidulans* and *Penicillium chrysogenum*. *J. Bacteriol.* **150,** 785–787 (1982).

45. Charlang, G., Ng, B., Horowitz, N. H. & Horowitz, R. M. Cellular and extracellular siderophores of *Aspergillus nidulans* and *Penicillium chrysogenum*. *Mol. Cell. Biol.* **1,** 94–100 (1981).

46. Franken, A. C. W. *et al.* Genome mining and functional genomics for siderophore production in *Aspergillus niger*. *Brief. Funct. Genomics* **13,** 482–492 (2014).

47. Jalal, M. A. F. *et al.* Extracellular siderophores from *Aspergillus ochraceous*. *J. Bacteriol.* **158,** 683–688 (1984).

48. Antelo, L. *et al.* Siderophores produced by *Magnaporthe grisea* in the presence and absence of iron. *Z. Naturforsch. C.* **61,** 461–4

49. Howard, D. H., Rafie, R., Tiwari, A. & Faull, K. F. Hydroxamate siderophores of *Histoplasma capsulatum*. *Infect. Immun.* **68,** 2338–43 (2000).

50. Anke, H., Kinn, J., Bergquist, K.-E. & Sterner, O. Production of siderophores by strains of the genus *Trichoderma*. *Biol. Met.* **4,** 176–180 (1991).

51. Michielse, C. B., Hooykaas, P. J. J., van den Hondel, C. A M. J. J. & Ram, A. F. J. *Agrobacterium*-mediated transformation of the filamentous fungus *Aspergillus awamori*. *Nat. Protoc.* **3,** 1671–8 (2008).

52. Geer, L. Y., Domrachev, M., Lipman, D. J. & Bryant, S. H. CDART: Protein Homology by Domain Architecture. *Genome Res.* **12,** 1619–1623 (2002).

53. Kelley, L. A., Mezulis, S., Yates, C. M., Wass, M. N. & Sternberg, M. J. E. The Phyre2 web portal for protein modeling, prediction and analysis. *Nat. Protoc.* **10,** 845–858 (2015).

54. A. Roy, A. Kucukural, Y. Z. I-TASSER: a unified platform for automated protein structure and function prediction. *Nat. Protoc.* **5,** 725–738 (2011).

55. Vogel, H. A convenient growth medium for *Neurospora crassa*. *Microb. Genet.* **13,** 42–47 (1956).

56. Payne, S. M. Detection, isolation, and characterization of siderophores. *Methods Enzymol.* **235,** 329–44 (1994).

57. Carroll, C. S. *et al.* The rhizoferrin biosynthetic gene in the fungal pathogen *Rhizopus delemar* is a novel member of the NIS gene family. *Int. J. Biochem. Cell Biol.* **89,** (2017).

58. Sambrook, J. & Russell, D. W. The Inoue method for preparation and transformation of competent *E. Coli*: 'Ultra-Competent' cells. *Cold Spring Harb. Protoc.* **2006,** pdb.prot3944-prot3944 (2006).

59. Chatterton, S., Jayaraman, J. & Punja, Z. Colonization of cucumber plants by the biocontrol fungus *Clonostachys rosea f. catenulata*. *Biol. Control* **46,** 267–278 (2008).

60. Liu, H. & Naismith, J. H. A simple and efficient expression and purification system using two newly constructed vectors. *Protein Expr. Purif.* **63,** 102–111 (2009).

61. Hider, R. C. & Kong, X. Chemistry and biology of siderophores. *Nat. Prod. Rep.* **27,** 637 (2010).

62. Nusca, T. D. *et al.* Functional and structural analysis of the siderophore

synthetase AsbB through reconstitution of the petrobactin biosynthetic pathway from *Bacillus anthracis*. *J. Biol. Chem.* **287,** 16058–16072 (2012).

63. Lee, J. Y. *et al.* Biosynthetic analysis of the petrobactin siderophore pathway from *Bacillus anthracis*. *J. Bacteriol.* **189,** 1698–1710 (2007).

64. Oves-Costales, D. *et al.* Petrobactin biosynthesis: AsbB catalyzes condensation of spermidine with N^8-citryl-spermidine and its N^1-(3,4-dihydroxybenzoyl) derivative. *Chem Commun* **0,** 4034–4036 (2008).

65. Wilson, M. K., Abergel, R. J., Raymond, K. N., Arceneaux, J. E. L. & Byers, B. R. Siderophores of *Bacillus anthracis, Bacillus cereus,* and *Bacillus thuringiensis. Biochem. Biophys. Res. Commun.* **348,** 320–325 (2006).

66. Bailey, D. C., Drake, E. J., Grant, T. D. & Gulick, A. M. Structural and functional characterization of aerobactin synthetase IucA from a hypervirulent pathotype of *Klebsiella pneumoniae*. *Biochemistry* **55,** 3559–3570 (2016).

67. Brickman, T. J., Hansel, J. G., Miller, M. J. & Armstrong, S. K. Purification, spectroscopic analysis and biological activity of the macrocyclic dihydroxamate siderophore alcaligin produced by *Bordetella pertussis* and *Bordetella bronchiseptica*. *Biometals* **9,** 191–203 (1996).

68. Young Kang, H., Brickman, T. J., Beaumont, F. C. & Armstrong, S. K. Identification and characterization of iron-regulated *Bordetella pertussis* alcaligin siderophore biosynthesis genes. *J. Bacteriol.* **178,** 4877–4884 (1996).

69. Giardina, P. C., Foster, L.-A., Toth, S. I., Roe, B. A. & Dyer, D. W. Analysis of the *alcABC* operon encoding alcaligin biosynthesis enzymes in *Bordetella bronchiseptica*. *Gene* **194,** 19–24 (1997).

70. Moore, C. H., Foster, L. a., Gerbig, D. G., Dyer, D. W. & Gibson, B. W. Identification of alcaligin as the siderophore produced by *Bordetella pertussis* and *B. bronchiseptica*. *J. Bacteriol.* **177,** 1116–1118 (1995).

71. Nishio, T. *et al.* Isolation and structure of the novel dihydroxamate siderophore alcaligin. *J. Am. Chem. Soc.* **110,** 8733–8734 (1988).

72. Schmelz, S. *et al.* AcsD catalyzes enantioselective citrate desymmetrization in siderophore biosynthesis. *Nat. Chem. Biol.* **5,** 174–82 (2009).

73. Spriestersbach, A., Kubicek, J., Schäfer, F., Block, H. & Maertens, B. *Purification of His-Tagged Proteins*. *Methods in Enzymology* **559,** (2015).

74. Usuda, N., Johkura, K., Hachiya, T. & Nakazawa, A. Immunoelectron microscopy of peroxisomes employing the antibody for the SKL sequence PTS1 C-terminus common to peroxisomal enzymes. *J. Histochem. Cytochem.* **47,** 1119–1126 (1999).

75. Schindelin, J. *et al.* Fiji: an open-source platform for biological-image analysis. *Nat. Methods* **9,** 676–682 (2012).

76. Raymond-Bouchard, I. *et al.* Structural requirements for the activity of the MirB ferrisiderophore transporter of *Aspergillus fumigatus. Eukaryot. Cell* **11,** (2012).

77. Huschka, H., Naegeli, H. U., Leuenberger-Ryf, H., Keller-Schierlein, W. & Winkelmannl, A. G. Evidence for a common siderophore transport system but different siderophore receptors in Neurospora crassa. *J. Bacteriol.* **162,** 715–721 (1985).

78. Huschka, H.-G., Jalal, M. A. F., Van Der Helm, D. & Winkelmann1, G. Molecular recognition of siderophores in Fungi: Role of iron-surrounding N-acyl residues and the peptide backbone during membrane transport in *Neurospora crassa*. *J. Bacteriol.* **167,** 1020–1024 (1986).

79. Pfleger, B. F. *et al.* Characterization and analysis of early enzymes for petrobactin biosynthesis in *Bacillus anthracis*. *Biochemistry* **46,** 4147–4157 (2007).

80. Oves-Costales, D. *et al.* Enzymatic logic of anthrax stealth siderophore biosynthesis: AsbA catalyzes ATP-dependent condensation of citric acid and spermidine. *J. Am. Chem. Soc.* **129,** 8416–8417 (2007).

81. Oves-Costales, D., Song, L. & Challis, G. L. Enantioselective desymmetrisation of citric acid catalysed by the substrate-tolerant petrobactin biosynthetic enzyme AsbA. *Chem Commun* **11,** 1389–1391 (2009).

82. Pradel, E., Guiso, N. & Locht, C. Identification of AlcR, an AraC-type regulator of alcaligin siderophore synthesis in *Bordetella bronchiseptica* and *Bordetella pertussis*. *J. Bacteriol.* **180,** 871–880 (1998).

83. Brickman, T. J. *et al. Bordetella* iron transport and virulence. *Biometals* **20,** 303–322 (2007).

84. Gasser, V., Guillon, L., Cunrath, O. & Schalk, I. J. Cellular organization of siderophore biosynthesis in *Pseudomonas aeruginosa*: Evidence for siderosomes. *J. Inorg. Biochem.* **148,** 27–34 (2015).

Chapter 5.

Detection of a serum siderophore as a potential biomarker of invasive aspergillosis

This chapter has been published in PLOS ONE, by the Public Library of Science, 2016, with permission, under the authorship of Carroll CS, Amankwa LN, Pinto LJ, Fuller JD and Moore MM. Detection of a Serum Siderophore by LC-MS/MS as a Potential Biomarker of Invasive Aspergillosis. PLoS ONE 11(3): e0151260.

Author contributions: This project was designed by Prof. Margo Moore, Cassandra Carroll and Linda Pinto. Linda Pinto purified TAFC from *Aspergillus fumigatus* and assisted in development of an extraction procedure for TAFC from serum. Lawrence Amankwa performed all UPLC-MS/MS experiments. Jeffrey Fuller supplied all human patient serum and performed galactomannan (GM) testing. Cassandra Carroll analyzed patient data for GM values and interpreted and analyzed UPLC-MS/MS data for TAFC detection.

5.1 Abstract

Invasive aspergillosis (IA) is a life-threatening systemic mycosis caused primarily by *Aspergillus fumigatus.* Early diagnosis of IA is based, in part, on an immunoassay for circulating fungal cell wall carbohydrate, galactomannan (GM). However, a wide range of sensitivity and specificity rates have been reported for the GM test across various patient populations. To obtain iron *in vivo*, *A. fumigatus* secretes the siderophore, *N,N′,N″*-triacetylfusarinine C (TAFC) and we hypothesize that TAFC may represent a possible biomarker for early detection of IA. We developed an ultra performance liquid chromatography tandem mass spectrometry (UPLC-MS/MS) method for TAFC analysis from serum, and measured TAFC in serum samples collected from patients at risk for IA. The method showed lower and upper limits of quantitation (LOQ) of 5 ng/ml and 750 ng/ml, respectively, and complete TAFC recovery from spiked serum. As proof of concept, we evaluated 76 serum samples from 58 patients with suspected IA that were investigated for the presence of GM. Fourteen serum samples obtained from 11 patients diagnosed with probable or proven IA were also analyzed for the presence of TAFC.

Control sera (n=16) were analyzed to establish a TAFC cut-off value (≥6 ng/ml). Of the 36 GM-positive samples (≥0.5 GM index) from suspected IA patients, TAFC was considered positive in 25 (69%). TAFC was also found in 28 additional GM-negative samples. TAFC was detected in 4 of the 14 samples (28%) from patients with proven/probable aspergillosis. Log-transformed TAFC and GM values from patients with proven/probable IA, healthy individuals and SLE patients showed a significant correlation with a Pearson r value of 0.77. In summary, we have developed a method for the detection of TAFC in serum that revealed this fungal product in the sera of patients at risk for invasive aspergillosis. A prospective study is warranted to determine whether this method provides improved early detection of IA.

5.2 Introduction

Invasive aspergillosis (IA) is a life-threatening infection that affects immunosuppressed individuals including those with neutropenia, chronic granulomatous disease, acquired immune deficiency syndrome, those undergoing hematopoietic stem cell transplantation (HSCT) or solid organ transplantation, especially those with graft-versus-host disease[1–3]. The causative agent of IA is most commonly *Aspergillus fumigatus*, although other *Aspergillus* species such as *A. flavus*, *A. nidulans* and *A. terreus* can cause invasive infections [4–6]. Invasive infections occur when fungal conidia are inhaled, germinate and penetrate the epithelia lining of the sinuses or lungs. In some cases, the fungus may disseminate hematogenously to other organs. Despite appropriate antifungal therapy, the outcome is fatal for many patients[7–9].

A major challenge for the management of IA is the lack of early diagnosis[10,11]. Antifungal therapy is often administered only after a prolonged febrile illness unresponsive to antibiotic therapy and confirmation of IA in many cases is made at autopsy[6]. Delays in diagnosis contribute to the morbidity and mortality rates from these infections; therefore, it is critical to identify mechanisms for the early detection of fungal growth *in vivo*.

Several methods are used to diagnose invasive aspergillosis including CT scanning[12], microscopic or histopathologic identification of fungal hyphae in tissue specimens, or culturing the organism from the infected area. However, direct microscopic examination of the fungus in clinical samples may be difficult to achieve in seriously-ill patients in whom biopsy is inadvisable, and in processed tissue samples, harsh sample preparation

procedures may fragment hyphae, making them difficult to identify[13]. Non-culture based approaches for detection of *Aspergillus* include the immunodetection of cell-wall derived galactomannan (GM) or (1→3)-β-D-glucan (BG)[14,15] or by amplifying *Aspergillus*-specific DNA[16]. The reported sensitivity and specificity for serum GM testing ranges from 48-77% and 81-100%, respectively[17–20] while sensitivity and specificity for the BG test ranges from 85-100% and 36-70%, respectively[17,21,22]. A report from Brasier et al. (2015) found that combining GM with a suite of host proteins improved detection of invasive aspergillosis in patients undergoing treatment for leukemia[23]. The wide range of sensitivity and specificity in these studies may be due in part to the heterogeneity in the patient populations analyzed. Immunoassays using lateral flow devices (LFD) have been developed to detect *Aspergillus*-specific compounds in serum, urine or BAL of suspected IA patients[24–26].

DNA extraction for use in PCR is often done from formalin-fixed tissue samples; however, formalin fixation may damage DNA, and prevent amplification[27]. Quantitative PCR (qPCR) can also be used to diagnose IA, especially from whole blood, serum or BAL samples. This technique relies on amplification of the inter-transcribed (ITS) ribosomal region, or the 28S or 18S rRNA genes[18,19,28]. However, due to inefficient DNA extraction procedures, the requirement for large samples volumes[29], and non-standardized approaches, it has been suggested that qPCR and PCR be used as a confirmatory test rather than an initial diagnostic test[30,31] or in combination with other approved diagnostic tests[18,19]. Due to the problems associated with all of the current approaches and the need to treat invasive fungal infections in a timely manner, new diagnostic methods for IA are needed to improve clinical outcomes.

Iron is essential for growth, and in low iron environments, such as in serum, many microorganisms secrete Fe(III)-chelating molecules called siderophores. In *A. fumigatus,* the hydroxamate siderophore, *N,N′,N″*-triacetylfusarinine C (TAFC) is secreted soon after conidiospore germination in iron-limited media[32]. The biosynthesis of TAFC is required for fungal germination and has been shown to be essential for virulence of *A. fumigatus* in a mouse model of invasive aspergillosis[33,34]. We hypothesized that TAFC would be present in the serum of patients with IA and that it could represent an early diagnostic marker of invasive aspergillosis. The purpose of our study was to establish the detection limits of TAFC in human serum using ultra high performance liquid chromatography coupled with tandem mass spectrometry (LC-MS/MS). We applied this

method in a proof of concept study using serum samples from patients for which we had GM test results.

5.3 Materials and methods

5.3.1 Serum samples and LC-MS/MS reagents

Serum samples were obtained from healthy individuals (n = 3) and from patients diagnosed with systemic lupus erythematosis (SLE) (n=13) from volunteers who had signed a Simon Fraser University Informed Consent Form. The Simon Fraser University Research Ethics Board specifically approved this study (samples were a kind gift from Dr. Jamie Scott, Department of Molecular Biology and Biochemistry, SFU). Samples were de-identified before analysis to maintain anonymity. A sampling of archived serum specimens from hematology patients suspected of having invasive aspergillosis were analyzed for TAFC and GM. Other than the suspected IA diagnosis and GM value, no other clinical data were available for these patients. A total of 76 serum samples were analyzed from 58 patients. Samples were collected between January 2008 and July 2011 and were stored at -80°C until analysis. An additional set of 14 GM positive serum samples (≥0.5 GM index) were analyzed from 11 patients identified as having proven or probable aspergillosis. For these samples, the requirement for informed consent was waived by the SFU Research Ethics Board who approved the study. Samples from these patients met at least one of the criteria for proven or probable aspergillosis based in the EORTC guidelines for diagnosis[31]. The serum samples were collected between June 2014 and February 2015 and stored at -80^0 C until analysis. LC-MS/MS analysis of clinical specimens was carried out in a blinded fashion. Control serum for analytical optimization (male, AB positive) was purchased from Sigma-Aldrich (Ontario, Canada). Methanol and acetonitrile (LCMS grade) were purchased from EMD Science (Massachusetts, USA). Formic acid (HPLC grade) was obtained from Acros Organics (New Jersey, USA).

5.3.2 Galactomannan testing

Testing for galactomannan was performed using the Platelia *Aspergillus* enzyme immunoassay (Bio-Rad Laboratories, Quebec, Canada) according to the manufacturer's recommendations and density galactomannan index (GMI) reading of ≥ 0.5 was

considered positive. The serum from SLE patients (n=13) was analyzed in three separate pooled samples as there was insufficient volume to run GM tests on the samples individually.

5.3.3 Preparation of stock solutions, calibration standards and quality control samples

TAFC was isolated from low iron cultures of *A. fumigatus* as previously described[35]. All stock solutions of TAFC were prepared in 0.1% formic acid in acetonitrile and subsequently diluted into serum samples. Calibration standards of TAFC spiked into serum were prepared by defrosting serum from -20°C, vortexing briefly and adding an appropriate volume into a 2 mL glass vial. Standard solutions of TAFC were spiked into serum and the vials were vortexed briefly. TAFC spiked serum samples were prepared over the range 0.5 ng/mL to 5000 ng/mL and were used to assess linearity of the method. Quality control standards were prepared by spiking TAFC standard solutions into serum over a range of 5 ng/mL to 750 ng/mL.

5.3.4 Extraction of TAFC from serum for LC-MS/MS analysis

Three volumes of 0.1 % formic acid in acetonitrile were added to 200 µL of serum sample in an ISOLUTE PPT+ 1 mL filter well (Biotagé, North Carolina, USA). This was incubated at room temperature for five minutes and vacuum filtered into a 96 well collection plate. The collection plate was sealed with tape and briefly agitated at low speed for one minute. Samples were concentrated by evaporating the solvent using Turbo-Vap/ N2 gas purge at 45°C. The residue was reconstituted in 200 µL of 0.1 % formic acid in acetonitrile/water (50/50 v/v%) and agitated again for 1 – 2 minutes. This resulted in the samples being concentrated 4-fold. Five microliters of reconstituted solution was injected for LC-MS/MS analysis. Control extractions of TAFC from spiked serum samples were similarly extracted but without concentrating the extracts and used to generate a calibration curve for quantitation of TAFC in the test serum samples.

5.3.5 LC-MS/MS instrument parameters and conditions

UPLC-MS/MS analysis was performed using Waters Acquity™ UPLC with tandem Waters Acquity™ PDA and TQD detectors (Waters Limited, Ontario, Canada).

Separation of TAFC was done using the Waters Acquity BEH reverse phase C18 column (1.7 µm, 2.1 mm x 50 mm). Mobile phase A consisted of 0.1 % formic acid in water while mobile phase B was 0.1 % formic acid in acetonitrile. A gradient separation, using 10 % - 90 % mobile phase B was performed at a flow rate of 0.3 mL/min. The injection volume was 5 µL and the column temperature was set at 30°C. The eluted TAFC was injected directly into the tandem quadrupole mass spectrometer operated in the positive electrospray ionization (ESI+) mode with a capillary voltage of 0.50 kV with nitrogen gas at a temperature of 400°C. Data was acquired in the multiple reaction monitoring (MRM) mode and Waters Empower™ chromatography software was used for control of the equipment and data acquisition (Waters Limited, Ontario, Canada). TAFC product ions were extracted with a span of 0.1Da.

5.3.6 Statistical analyses

Each serum sample was analyzed only once because of the small volume of serum available. Quality control and calibration samples were prepared in triplicate and duplicate, respectively and analyzed individually by LC-MS/MS. Statistical analysis of the serum TAFC data in the different patient groups was performed using the Kruskal-Wallis test followed by Dunn's post test. Logarithmically transformed TAFC and GM values were used to determine the correlation. We used the log transformation of the variables to normalize the data[36,37]. All statistical analyses were performed using GraphPad Prism software.

5.4 Results

5.4.1 LC-MS/MS method validation

The analytical method for determination of serum concentration of TAFC was reverse-phase UPLC with mass spectrometry detection. Serum concentrations of TAFC in test samples were measured against a TAFC standard calibration curve over the range 0.5 ng/mL- 5000 ng/mL. The method was evaluated for specificity, linearity, accuracy, recovery, precision, limit of detection, and limit of quantitation of the assay.

LC-MS/MS detection of TAFC was performed by positive electrospray ionization and with MRM data acquisition. At physiologically relevant concentrations, TAFC exhibits two

molecular ions; the [M+H] ion at 906.0 m/z, and the [M+Na] ion mass at 928.59 m/z[32], with the [M+Na] ion being the most abundant molecular ion of TAFC. Consequently, the [M+Na] ion at 928.59 m/z was chosen for the LC-MS/MS method development. Two MRM transitions were monitored for quantitation of TAFC: $[M+Na]^+$ 928.59 m/z to two main fragment ions, 134.8 m/z and 248.6 m/z. Quantification was performed by summing the MS/MS signal responses of both product ions. Figure 5.1 shows the UPLC-MS (ESI+) mass spectra of the TAFC standard (1 µg/mL) and the MS/MS fragmentation spectra.

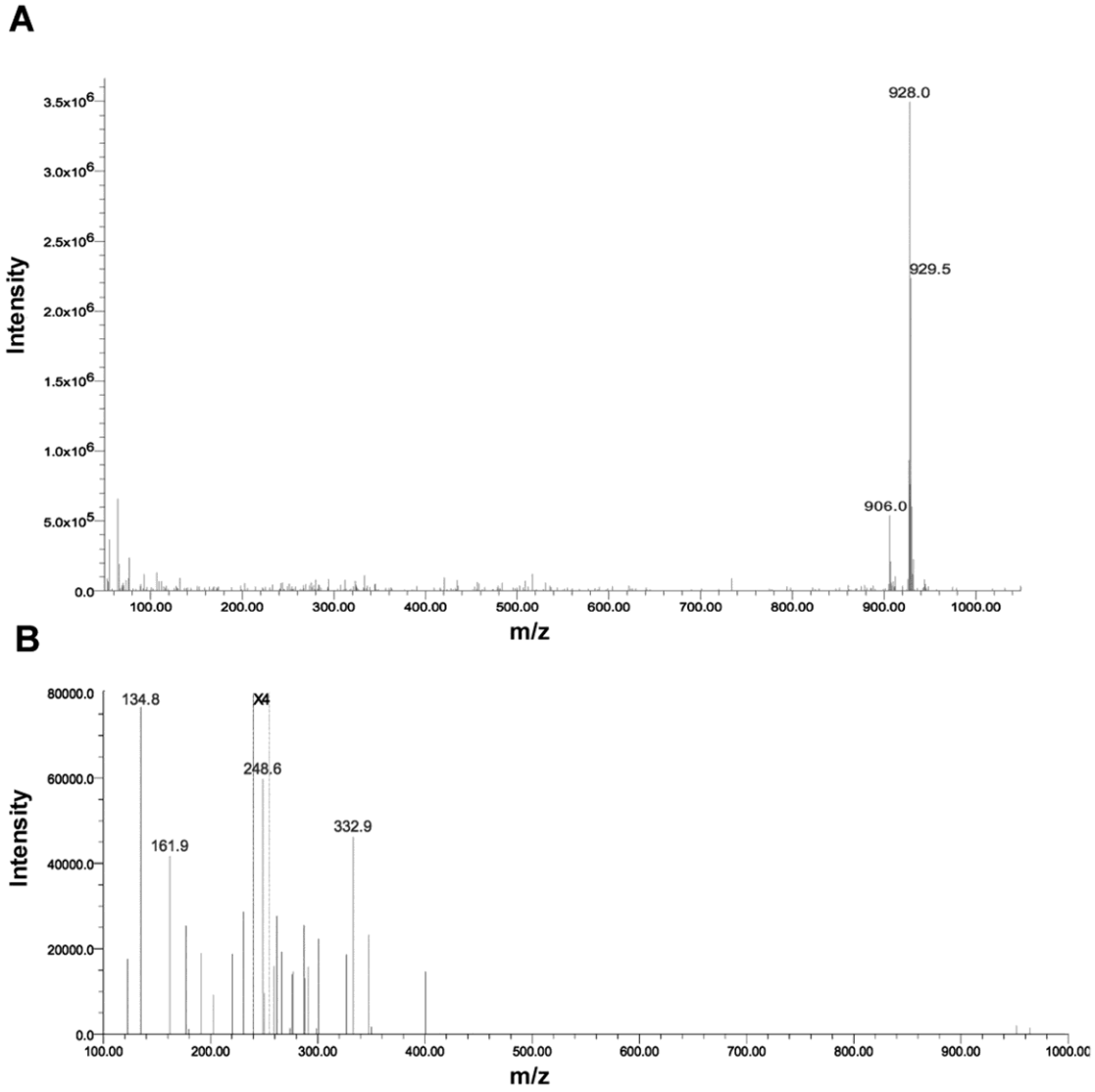

Figure 5.1 UPLC-MS/MS of a TAFC standard in acetonitrile water/0.1% formic acid.

A. UPLC-MS (ESI+) of 1 µg/mL TAFC standard in acetonitrile/0.1% formic acid. The signal at 906 m/z corresponds to the [M+H] ion mass of TAFC, and the signal at 928 m/z corresponds to the

[M+Na] ion mass. The data show that the [M+Na] ion is the most abundant molecular ion of TAFC. **B.** MS/MS (ESI+) fragmentation spectra of the [M+Na] ion of the TAFC standard showing the two product ions, 134.8 m/z and 248.6 m/z, acquired under similar MS/MS conditions as in the test method. The spectrum was acquired using a collision energy of 60 eV. The signals between m/z 200 to 255 were enhanced 4 times (X4).

Sample chromatograms of serum extracts with and without TAFC spiking are shown in Figure 5.2. The limit of detection (LOD) for the instrument was found to be ≤1 ng/mL of TAFC, while the lower limit of quantitation (LLOQ) was 5 ng/mL.

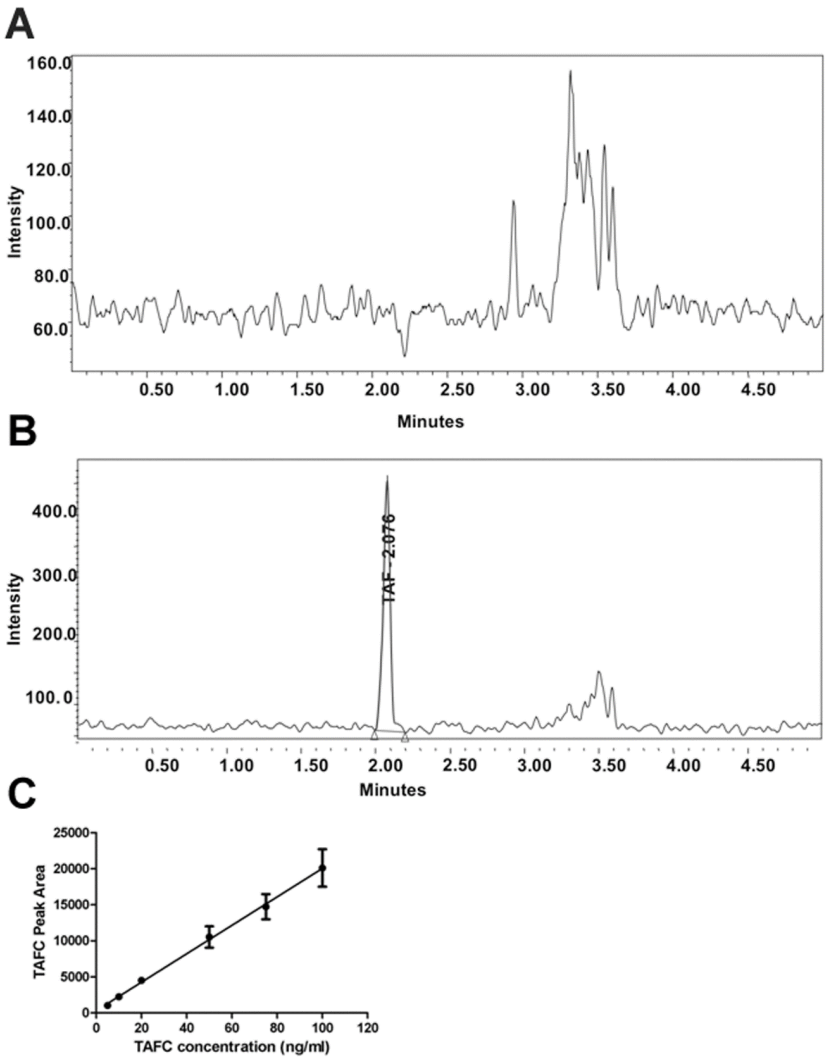

Figure 5.2 UPLC-MS/MS detection of TAFC in serum.
A. Chromatogram of healthy serum without the addition of TAFC. **B.** Pure TAFC (5 ng/mL) was spiked into healthy serum, extracted and detected via UPLC-MS/MS. Note the difference in magnitude of the Y-axis. **C**. Representative standard curve of TAFC over a range of 1 – 100 ng/mL. The values represent the mean ± SD of n=3 samples.

A standard curve for TAFC detection was constructed and found to be linear over the range of 5 ng/mL to 1000 ng/mL with a correlation coefficient (r) of 0.999. Figure 5.2C shows the curve in the 1-100 ng/mL range. Furthermore, the UPLC-MS/MS method was determined to be specific for TAFC as no interfering serum matrix component co-eluted with TAFC and there was no carry-over seen when a blank sample was analyzed immediately after analysis of an extracted serum sample (Table 5.1). The percent deviation from theoretical values of the measured amounts of TAFC in standard solutions of TAFC in serum were less than 15% over the 5 ng/mL to 750 ng/mL quality control (QC) standards evaluated. The method was found to be accurate and precise and has high recovery of TAFC from spiked serum samples. The accuracy (% deviation), precision (%RSD) and recovery (%) of the method at the LLOQ were ≤ ±15.0%, 3.4% and 117.1% respectively (Table 5.1).

Table 5.1 Evaluation of method accuracy, precision, and recovery of TAFC from spiked serum samples.

Concentration of TAFC spiked into QC standards, or spiked into serum (ng/mL)	Measured TAFC in QC standards ng/mL (%RSD)	Recovery of TAFC from serum % (%RSD)
0	Not detected	Not applicable
5	4.6 ± 0.2 (-8.7)	117.1 ± 9.7 (3.4)
100	111.1 ± 2.4 (11.1)	119.6 ± 17.5 (2.2)
750	747.2 ± 39.6 (-0.4)	120.6 ± 6.0 (5.3)

All values represent the mean of three independent samples ± SD.

5.4.2 Patient sample testing using LC-MS/MS

Human serum samples were analyzed and serum from SLE patients and healthy individuals was used to establish the background TAFC level. Representative chromatograms of patient samples are shown in Figure 5.3.

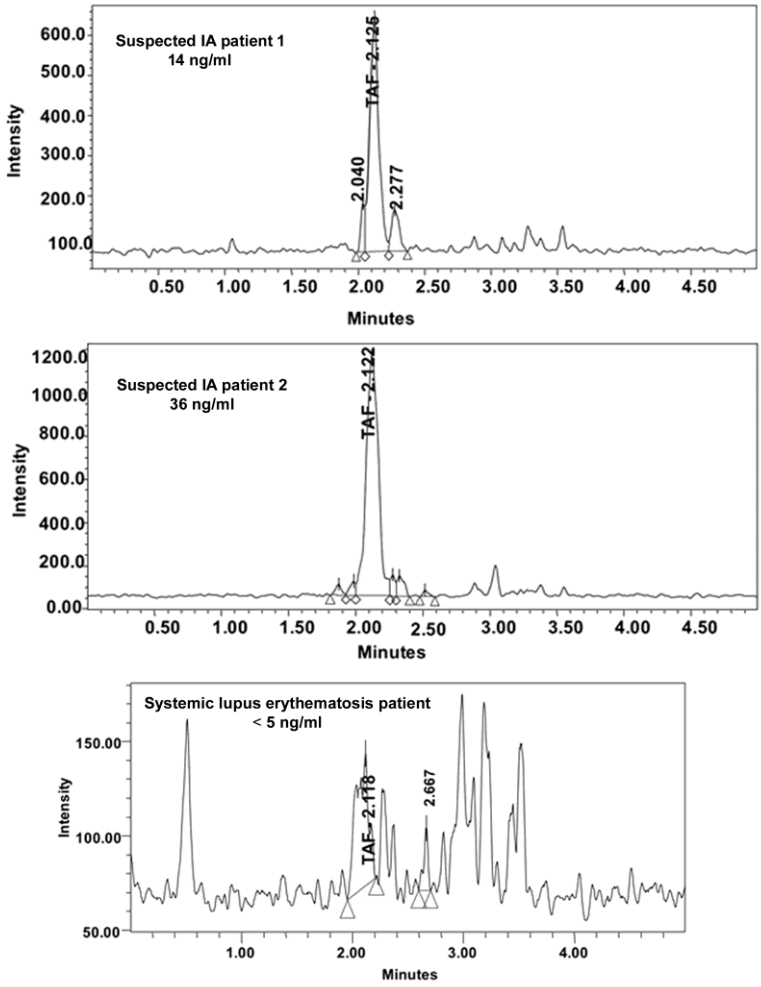

Figure 5.3 Representative TAFC chromatograms from various patient serum samples.

Note the difference in scale of the Y-axis. All samples were concentrated 4-fold prior to TAFC measurement.

Serum from 3 healthy individuals had TAFC levels of 0.8 ± 1.1 ng/mL, well below the LLOQ of 5 ng/mL. Sera from SLE patients were also analyzed. The mean of the SLE group was slightly higher (2.6 ± 1.1 ng/mL) than the healthy patients though still below the LLOQ (Figure 5.4).

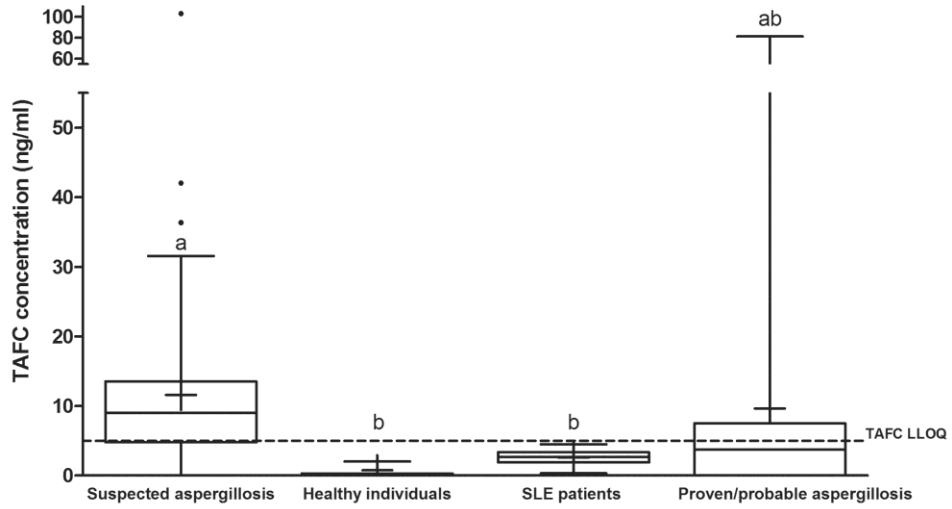

Figure 5.4 Box and whisker plots of the TAFC levels detected in healthy individuals, in patients with SLE, in patients suspected of having aspergillosis and those diagnosed with proven or probable IA.

The bars represent the lower and upper limits of the data points within the 95% confidence interval. The bar in the middle of each box represents the median; outliers are shown as dots. Data are from 4-fold concentrated extracts. The LLOQ of TAFC is shown as a dotted line (5 ng/mL). Means with the same letter are not significantly different from each other (Dunn's test, $p < 0.05$).

Using the data from the SLE group, we established a cut-off value for a positive TAFC value as 3 SD above the mean SLE value, i.e., ≥6 ng/mL. The mean and median of TAFC concentration in suspected aspergillosis serum samples were 11.6 ng/mL and 9.0, respectively. Patients with proven or probable aspergillosis had mean and median TAFC levels of 9.7 ng/mL and 3.7 ng/mL, respectively (Figure 5.4). We compared the results of the TAFC analysis with the GM analysis for each of the samples. Of the 76 samples from patients with suspected aspergillosis, TAFC was considered positive (≥ 6 ng/mL) in 53 of the samples (70%). Of 36 GM-positive suspected aspergillosis samples (GMI≥0.5) 25 were also positive for TAFC (69%; Figure 5.5). An additional 28 samples were positive for TAFC but negative for GM. Only 8 samples with a GMI greater than 1.0 (n=58) had negative TAFC values below 6 ng/mL. When serially sampled patients were excluded, TAFC was detected in 35 of 51 patients (69%); 17 of these patients were GM positive (33%).

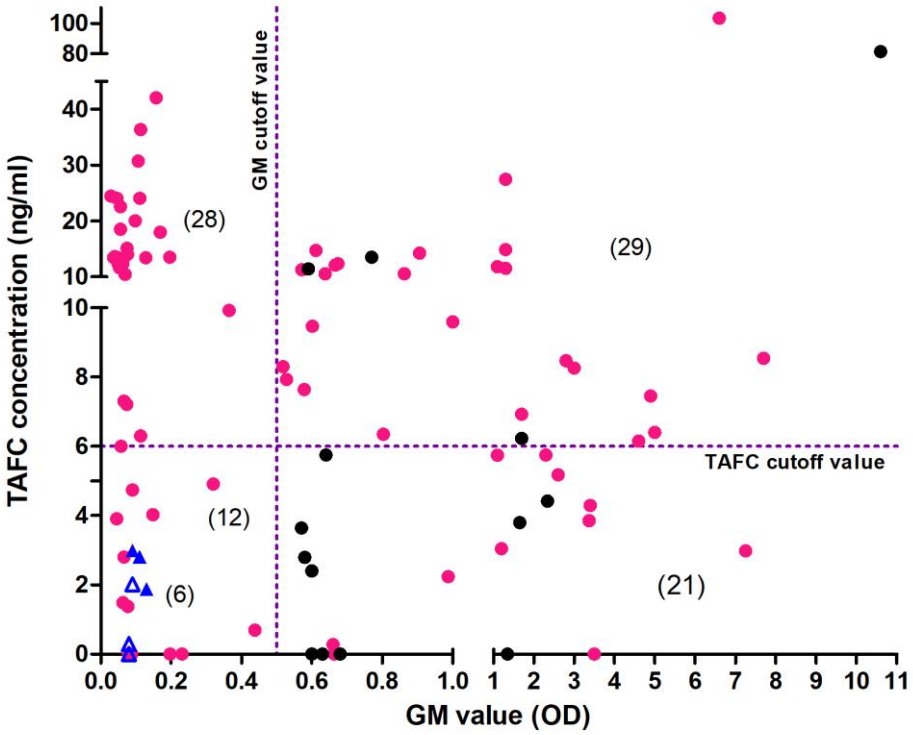

Figure 5.5 Amounts of TAFC and GM values detected in 4-fold concentrated extracts of suspected aspergillosis patient serum samples (76), 6 control patient serum samples and 14 proven or probable IA samples as analyzed by LC-MS/MS and GM testing.

Of the suspected samples (●), 25 were TAFC positive and GM positive, 28 samples were TAFC positive and GM negative, 11 samples were TAFC negative and GM positive, and 12 were both TAFC and GM negative. All control sera (n=6 representing 3 healthy sera (Δ) and 3 sets of pooled SLE sera (▲)) were TAFC and GM negative. Note that the 13 SLE patient samples were analyzed for TAFC individually; however, GM values were obtained from 3 pooled samples; therefore, the TAFC values were also averaged in these pools. Four of the proven or probable IA samples (●) were TAFC positive and GM positive. The axes are expanded in the lower ranges to show the data close to the threshold values.

Interestingly, when GM values were compared to TAFC levels in a single patient over time, the levels were inversely related (Figure 5.6). In another patient (Figure 5.6C), TAFC was positive in all 3 samples but these were negative for GM. Of the 14 proven or probable aspergillosis serum samples, TAFC was identified in 4 samples (28%).

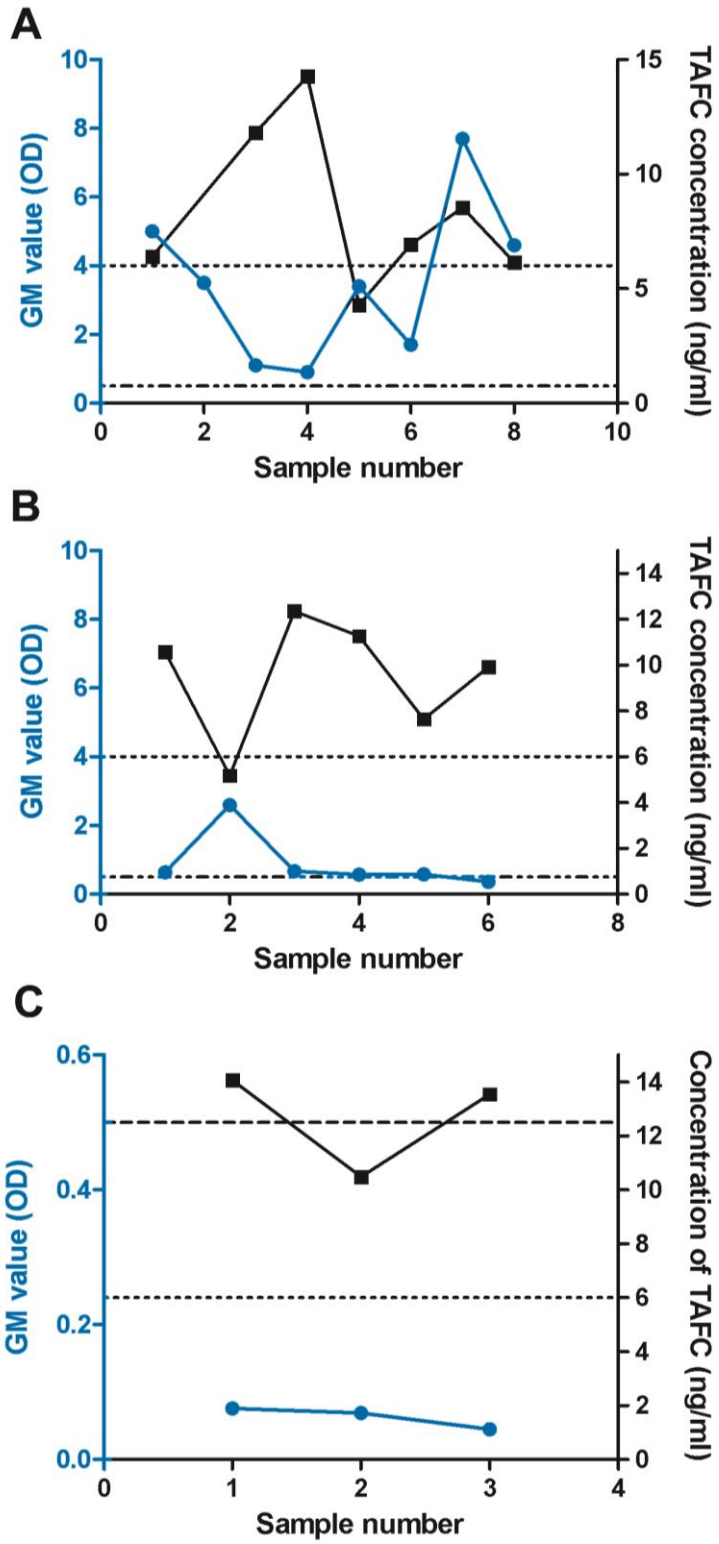

Figure 5.6 TAFC and GM values for serial samples from selected patients.
TAFC (■) and GM (●) values were determined for 3 patients (**A**), (**B**) and (**C**) over time. Detection limits are noted by the dashed line (GM) and the dotted line (TAFC). The interval between the samples for each patient averaged 13 days.

TAFC and GM values of sera from patients with known health status (those with proven/probable IA, healthy individuals and SLE patients) were further analyzed. TAFC and GM values were logarithmically transformed for normality, and a statistically significant correlation was found with a Pearson r value of 0.77 (95% confidence interval of 0.42 to 0.92) (Figure 5.7).

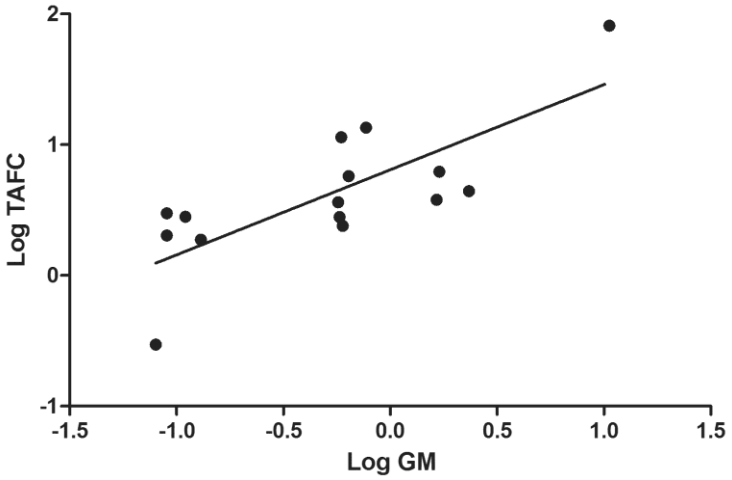

Figure 5.7 Correlation of logarithmically-transformed TAFC and GM values in sera from patients with proven/probable IA, healthy individuals and SLE patients.

The three SLE patient samples were pooled from 13 individuals. The Pearson r value was 0.77 (95% confidence interval of 0.42 to 0.92) and a P value (two-tailed) of <0.001.

5.5 Discussion

An LC-MS/MS method was developed for detecting the fungal siderophore, *N,N′,N″*-triacetylfusarinine C (TAFC) in serum from patients at risk of developing invasive aspergillosis. Evaluation of the method using control serum spiked with known amounts of TAFC revealed that the method was precise with a high recovery of TAFC and upper and lower limits of quantitation were 750 ng/mL and 5 ng/mL, respectively. The limit of detection (LOD) for TAFC was ≤1ng/mL; this is in agreement with detection of other circulating serum proteins [38]. Analysis of healthy sera (n= 3) and SLE patient sera (n= 13) indicated TAFC values less than the LLOQ. In contrast, of the 76 serum samples from patients who were suspected of having IA, 53 had levels of TAFC above the cut-off value (≥6 ng/mL). GM values were positive in 36 of these samples, and 25/36 (69%) were also TAFC positive by LC-MS/MS analysis. Of the 14 samples from patients with proven/ probable aspergillosis, 4 were found to be TAFC positive (28%). The lower

proportion of TAFC-positive samples in the proven/probable IA patients compared to the suspected IA group may reflect a higher use of antifungal drugs in the former group.

TAFC is a potential biomarker for early diagnosis of IA because it is secreted during the germination phase of fungal growth and it is chemically stable in serum. We have previously shown that micromolar levels of TAFC accumulate in vitro if *A. fumigatus* conidia (10^6/mL) are germinated in medium containing human serum[33]. The cluster of TAFC–positive samples in the suspected IA group that were GM negative may represent early stages of IA; however, this cannot be confirmed without a prospective study. Secretion of TAFC in vivo in later stages of infection may decrease as other iron sources become available to the fungus (e.g., proteolytic release of iron from host proteins[32]) at which point other markers such as GM may become more useful. In a retrospective study on hematopoietic stem cell transplant recipients, Nguyen et al. (2011) found that GM tests done using BAL fluid showed a greater test sensitivity compared to tests done on serum[39]. Hence, it would be useful to compare GM and TAFC levels in BAL fluid in patients with proven/probable invasive aspergillosis.

Diagnosis of IA requires clinical, radiographic, histologic, and microbiologic evidence. Weaknesses in all of these facets make the diagnosis difficult. Detection of the cell wall-derived compounds, GM and (1→3)-β-D-glucan (BG) are used in IA diagnosis. BG assay detects circulating levels of BG in serum samples of patients suspected to have IA. For the Fungitell assay (Assoc. of Cape Cod Inc., USA), a BG level of ≥ 80 pg/mL is considered positive for IA. However, the BG assay is not exclusively indicative of invasive aspergillosis as BG is also present in the cell wall of other pathogenic fungi and yeasts including, *Candida*, *Fusarium*, and *Pneumocystis* species[40–42]. In addition to *A. fumigatus*, TAFC is also produced by the pathogen, *Aspergillus nidulans*[43]. Detection of TAFC would be useful for diagnosis of both *A. fumigatus* and *A. nidulans* infections in hematology patients; however, a negative test would not rule out invasive mycoses by other mould pathogens such as *Scedosporium, Fusarium* or members of the Mucorales order that do not secrete TAFC.

Polymerase chain reaction (PCR) has also been proposed as a diagnostic test for IA, based on amplification and detection of *Aspergillus*-specific DNA. Typically, the 28S, 18S or inter-transcribed (ITS) ribosomal gene regions are targeted for amplification. These assays are sensitive and have been reported to detect as little as five to six

conidia per mL of spiked blood[19,44]. When using qPCR to amplify the ITS region from blood samples, the sensitivity and specificity range from 24-80% and 57-100%, respectively[19]. Using nested qPCR to detect the 28S rRNA gene, sensitivity and specificity ranged from 69-95% and 36-73%, respectively[18,19]. Results vary for qPCR results from BAL samples; Hoenigl et al., (2014) report sensitivity and specificity data of 70% and 100%, respectively, when amplifying the 18S rRNA gene, while Buess et al., (2012) obtained 0% sensitivity and 71% specificity when amplifying the same gene region[28,45]. While attempts have been made to standardize DNA extraction from whole blood and for qPCR conditions in general[29,46], qPCR results remain highly variable and optimal DNA extraction efficiency requires large volumes (≥ 3 mL), which are sometimes not possible to obtain. For these reasons, PCR is not yet used in the diagnostic criteria for invasive aspergillosis outlined by the EORTC[31,47]. For our study, we used only 200 µL of serum for the TAFC assay and assays with spiked sera showed that the precision of the method using this volume was high. It may also be possible to detect TAFC in other body fluids; for example, rapid clearance of ^{68}Ga-labelled TAFC has shown that the compound accumulates in urine[48]. Similarly, antigens containing β-(1,5) galactofuranose residues, present in the serum of guinea pigs infected with *A. fumigatus*, rapidly localized to the bladder and were detectable in urine via immunoassays[24].

The use of analytical methods, such as LC-MS/MS as diagnostic tools has many advantages over traditional molecular techniques, including high throughput capabilities, higher sensitivity, particularly for low molecular weight compounds such as siderophores, and the ease of standardization. For these reasons, the use of this technology in clinical applications has increased dramatically in recent years and LC-MS/MS is now routinely used to measure a diverse range of targets including drugs and toxins and more recently, hormones[49,50]. LC-MS/MS analysis has been used to detect other fungal-specific products in patient samples. For example, LC-MS/MS was used to detect the secreted mycotoxin, gliotoxin, in the serum of individuals suspected of having invasive aspergillosis[51]. The developed assay was sensitive, with a lower limit of quantitation (LLOQ) for gliotoxin in serum of 10 ng/mL. Upon analysis of 30 patient serum samples, the levels of gliotoxin were above the LLOQ only in two serum samples and these were both negative for GM. Furthermore, the production of gliotoxin is not essential for virulence of *A. fumigatus* in neutropenic hosts[52]. In another study, LC-MS detection of the siderophore, N^{α}-methyl coprogen B in sputum samples from cystic fibrosis patients

was shown to be indicative of infection with *Scedosporium apiospermum*; however, quantification limits have not been established for this assay[53]. Other attempts have been made to develop assays based on detection of fusarinine C in biological samples[54]; in this study, the detection limit was 3 µg/mL in guinea pig urine and serum.

We have shown that the secreted fungal siderophore TAFC can be detected in serum samples from patients at risk for developing invasive aspergillosis using LC/MS/MS with limits of quantitation of 5 ng/mL using only 200 µL of serum. These data warrant a prospective study of patients to determine whether this method provides improved detection of IA, particularly during the early stages of infection.

5.6 References

1. Morgan, J. *et al.* Incidence of invasive aspergillosis following hematopoietic stem cell and solid organ transplantation: interim results of a prospective multicenter surveillance program. *Med. Mycol.* **43,** 49–58 (2005).

2. Rogers, T. R. Treatment of zygomycosis: current and new options. *J. Antimicrob. Chemother.* **61,** i35 (2008).

3. Singh, N. & Paterson, D. L. *Aspergillus* Infections in transplant recipients. *Society* **18,** 44–69 (2005).

4. Latgé, J. P. *Aspergillus fumigatus* and aspergillosis. *Clin. micro* **12,** 310–350 (1999).

5. Neofytos, D. *et al.* Epidemiology, outcomes, and mortality predictors of invasive mold infections among transplant recipients: a 10-year, single-center experience. *Transpl. Infect. Dis.* **15,** 233–42 (2013).

6. Lewis, R. E. *et al.* Epidemiology and sites of involvement of invasive fungal infections in patients with haematological malignancies: a 20-year autopsy study. *Mycoses* **56,** 638–45 (2013).

7. Husain, S. *et al.* Opportunistic mycelial fungal infections in organ transplant recipients: emerging importance of non-*Aspergillus* mycelial fungi. *Clin. Infect. Dis.* **37,** 221–9 (2003).

8. Panda, N. K., Saravanan, K. & Chakrabarti, A. Combination antifungal therapy for invasive aspergillosis: can it replace high-risk surgery at the skull base? *Am. J. Otolaryngol.* **29,** 24–30 (2004).

9. Brakhage, A. a. Systemic fungal infections caused by *Aspergillus* species: epidemiology, infection process and virulence determinants. *Curr. Drug Targets* **6,** 875–86 (2005).

10. Lass-Flörl, C. *et al.* The value of computed tomography-guided percutaneous lung biopsy for diagnosis of invasive fungal infection in immunocompromised patients. *Clin. Infect. Dis.* **45,** e101-4 (2007).

11. Ostrosky-Zeichner, L. Invasive mycoses: diagnostic challenges. *Am. J. Med.* **125,** S14-24 (2012).

12. Greene, R. E. *et al.* Imaging findings in acute invasive pulmonary aspergillosis: clinical significance of the halo sign. *Clin. Infect. Dis.* **44,** 373–9 (2007).

13. Lass-Flörl, C. Zygomycosis: conventional laboratory diagnosis. *Clin. Microbiol. Infect.* **15 Suppl 5,** 60–5 (2009).

14. Bio-Rad. *Platelia Aspergillus EIA ™*.

15. Cod, A. of C. *Fungitell Assay (1,3) - β - D -Glucan in Pathogenic Fungi Fungitell Assay*. **510,**

16. White, P. L. *et al.* The clinical performance of *Aspergillus* PCR when testing serum and plasma: A study by the European *Aspergillus* PCR Initiative. *J. Clin. Microbiol.* **53,** 2832–2837 (2015).

17. Acosta, J. *et al.* A prospective comparison of galactomannan in bronchoalveolar lavage fluid for the diagnosis of pulmonary invasive aspergillosis in medical patients under intensive care: comparison with the diagnostic performance of galactomannan and of (1→ 3)-β-d-glucan . *Clin. Microbiol. Infect.* **17,** 1053–60 (2011).

18. White, P. L., Parr, C., Thornton, C. & Barnes, R. A. Evaluation of real-time PCR, galactomannan enzyme-linked immunosorbent assay (ELISA), and a novel lateral-flow device for diagnosis of invasive aspergillosis. *J. Clin. Microbiol.* **51,** 1510–6 (2013).

19. Rogers, T. R. *et al.* Combined real-time PCR and galactomannan surveillance improves diagnosis of invasive aspergillosis in high risk patients with haematological malignancies. *Br. J. Haematol.* **161,** 517–24 (2013).

20. Racil, Z. *et al.* Galactomannan detection in bronchoalveolar lavage fluid for the diagnosis of invasive aspergillosis in patients with hematological diseases- The role of factors affecting assay performance. *Int. J. Infect. Dis.* **15,** e874-81 (2011).

21. Sulahian, A. *et al.* Use and limits of (1-3)-β-D-Glucan Assay (Fungitell(R)), compared to galactomannan determination (Platelia™ *Aspergillus*) for diagnosis of invasive aspergillosis. *J. Clin. Microbiol.* 1–23 (2014). doi:10.1128/JCM.03567-13

22. De Vlieger, G. *et al.* Beta-D-glucan detection as a diagnostic test for invasive aspergillosis in immunocompromised critically ill patients with symptoms of respiratory infection: an autopsy-based study. *J. Clin. Microbiol.* **49,** 3783–7 (2011).

23. Brasier, A. R. *et al.* Improved detection of invasive pulmonary aspergillosis arising during leukemia treatment using a panel of host response proteins and fungal antigens. *PLoS One* **10,** e0143165 (2015).

24. Dufresne, S. F. *et al.* Detection of urinary excreted fungal galactomannan-like antigens for diagnosis of invasive aspergillosis. *PLoS One* **7,** e42736 (2012).

25. Hoenigl, M. *et al.* Bronchoalveolar lavage lateral-flow device test for invasive pulmonary aspergillosis diagnosis in haematological malignancy and solid organ transplant patients. *J. Infect.* **65,** 588–91 (2012).

26. Thornton, C. R. Development of an immunochromatographic lateral-flow device for rapid serodiagnosis of invasive aspergillosis. *Clin. Vaccine Immunol.* **15,** 1095–105 (2008).

27. Dannaoui, E. *et al.* Molecular detection and identification of zygomycetes species from paraffin-embedded tissues in a murine model of disseminated zygomycosis: a collaborative European Society of Clinical Microbiology and Infectious Diseases (ESCMID) Fungal Infection Study G. *J. Clin. Microbiol.* **48,** 2043–6 (2010).

28. Hoenigl, M. *et al.* Performance of galactomannan, beta-D-glucan, *Aspergillus* lateral-flow device, conventional culture, and PCR tests with bronchoalveolar lavage fluid for diagnosis of invasive pulmonary aspergillosis. *J. Clin. Microbiol.* **52,** 2039–45 (2014).

29. White, P. L. *et al.* Critical stages of extracting DNA from *Aspergillus fumigatus* in whole-blood specimens. *J. Clin. Microbiol.* **48,** 3753–5 (2010).

30. da Silva, T. V. M. *et al.* PCR as a screening test for invasive aspergillosis in haematological patients: a pilot study. *Mycopathologia* **177,** 111–4 (2014).

31. Pauw, B. De *et al.* Revised definitions of invasive fungal disease from the European Organization for Research and Treatment of Cancer/Invasive. *Clin. Infect. Dis* **46,** 1813–1821 (2008).

32. Hissen, A. H. T., Chow, J. M. T., Pinto, L. J. & Moore, M. M. Survival of *Aspergillus fumigatus* in serum involves removal of iron from transferrin: The role of siderophores. *Infect. Immun.* **72,** 1402–1408 (2004).

33. Hissen, A. H. T., Wan, A. N. C., Warwas, M. L., Pinto, L. J. & Moore, M. M. The *Aspergillus fumigatus* siderophore biosynthetic gene *sidA*, encoding L-ornithine N^5-oxygenase, is required for virulence. *Infect. Immun.* **73,** 5493–5503 (2005).

34. Schrettl, M. *et al.* Siderophore biosynthesis but not reductive iron assimilation is essential for *Aspergillus fumigatus* virulence. *J. Exp. Med.* **200,** 1213–9 (2004).

35. Raymond-Bouchard, I. *et al.* Structural requirements for the activity of the MirB ferrisiderophore transporter of *Aspergillus fumigatus*. *Eukaryot. Cell* **11,** 1333–44 (2012).

36. Hinckson, E. A. & Hopkins, W. G. Reliability of time to exhaustion analyzed with critical-power and log-log modeling. *Med. Sci. Sport. Exerc.* **37,** 696–701 (2005).

37. Festa, A. *et al.* Chronic subclinical inflammation as part of the insulin resistance syndrome: the Insulin Resistance Atherosclerosis Study (IRAS). *Circulation* **102,** 42–47 (2000).

38. Tucholska, M. *et al.* Human serum proteins fractionated by preparative partition chromatography prior to LC-ESI-MS/MS. *J. Proteome Res.* **8,** 1143–1155 (2009).

39. Nguyen, M. H. *et al.* Galactomannan testing in bronchoalveolar lavage fluid facilitates the diagnosis of invasive pulmonary aspergillosis in patients with hematologic malignancies and stem cell transplant recipients. *Biol. Blood Marrow Transplant.* **17,** 1043–50 (2011).

40. Khan, Z. U., Ahmad, S. & Theyyathel, A. M. Diagnostic value of DNA and (1-->3)-beta-D-glucan detection in serum and bronchoalveolar lavage of mice experimentally infected with *Fusarium oxysporum*. *J. Med. Microbiol.* **57,** 36–42 (2008).

41. Yasuoka, A., Tachikawa, N., Shimada, K., Kimura, S. & Oka, S. (1->3) beta-D-glucan as a quantitative serological marker for *Pneumocystis carinii* pneumonia. *Clin. Vaccine Immunol.* **3,** 3–6 (1996).

42. Miyazaki, T. *et al.* Plasma (1-->3)-beta-D-glucan and fungal antigenemia in patients with candidemia, aspergillosis, and cryptococcosis. *J. Clin. Microbiol.* **33,** 3115 (1995).

43. Charlang, G., Ng, B., Horowitz, N. H. & Horowitz, R. M. Cellular and extracellular siderophores of *Aspergillus nidulans* and *Penicillium chrysogenum*. *Mol. Cell. Biol.* **1,** 94–100 (1981).

44. White, P. L. *et al.* Evaluation of analytical and preliminary clinical performance of Myconostica MycAssay *Aspergillus* when testing serum specimens for diagnosis of invasive aspergillosis. *J. Clin. Microbiol.* **49,** 2169–74 (2011).

45. Buess, M. *et al. Aspergillus*-PCR in bronchoalveolar lavage for detection of invasive pulmonary aspergillosis in immunocompromised patients. *BMC Infect. Dis.* **12,** 237 (2012).

46. Bustin, S. a *et al.* The MIQE guidelines: minimum information for publication of quantitative real-time PCR experiments. *Clin. Chem.* **55,** 611–22 (2009).

47. Alothman, A. F. *et al.* Clinical practice guidelines for the management of invasive *Candida* infections in adults in the Middle East region: Expert panel recommendations. *J. Infect. Public Health* **7,** 6–19 (2014).

48. Petrik, M. *et al.* Ga-siderophores for PET imaging of invasive pulmonary aspergillosis: Proof of principle. *J. Nucl. Med.* **51,** 639–645 (2010).

49. Grebe, S. K. & Singh, R. J. LC-MS/MS in the clinical laboratory - Where to from here? *Clin. Biochem. Rev.* **32,** 5–31 (2011).

50. Ashbee, H. R. *et al.* Therapeutic drug monitoring (TDM) of antifungal agents: guidelines from the British Society for Medical Mycology. *J. Antimicrob. Chemother.* **69,** 1162–76 (2014).

51. Cerqueira, L. B., de Francisco, T. M. G., Gasparetto, J. C., Campos, F. R. & Pontarolo, R. Development and validation of an HPLC-MS/MS method for the early diagnosis of aspergillosis. *PLoS One* **9,** e92851 (2014).

52. Spikes, S. *et al.* Gliotoxin production in *Aspergillus fumigatus* contributes to host-specific differences in virulence. *J. Infect. Dis.* **197,** 479–86 (2008).

53. Bertrand, S. *et al.* N(α)-methyl coprogen B, a potential marker of the airway colonization by *Scedosporium apiospermum* in patients with cystic fibrosis. *Med. Mycol.* **48 Suppl 1,** S98-107 (2010).

54. Doyle, J., Gallagher, L., Gordon, N., Kavanagh, K. & Walshe, K. Method for detecting infections. (2012).

Chapter 6.

General conclusions

Invasive fungal infections caused by mucormycosis and invasive aspergillosis (IA) can be life-threatening, particularly for immunocompromised individuals.

Iron is essential for growth and survival. One mechanism for iron acquisition is secretion of siderophores. Siderophore biosynthesis has been shown to be a virulence factor for pathogenic microorganisms including, *Escherichia coli*[1], *Neisseria gonorrhoeae*[2], enteropathogenic *Yersinia* species[3] and the fungal pathogen, *Aspergillus fumigatus*[4,5]*.* Siderophore biosynthesis occurs either via the non-ribosomal peptide synthetase (NRPS) pathway or the NRPS-independent siderophore (NIS) synthetase pathway. NRPS enzymes function in a coordinated fashion to form peptide bonds between substrates, while NIS enzymes function independently in their pathway and typically form condensation reactions between citric acid, or a derivative, and an amino or alcohol-containing nucleophile. The substrate specificities for NIS enzymes, group them into different types. The phylogenetic analysis we presented in Chapter 2 confirms that NIS enzymes are grouped into four types, with the possibility of a Type C enzymes being split into Type C and Type C' enzymes. However, further research into the biochemistry of more Type C enzymes is needed to confirm this classification.

Crystal structures of three NIS enzymes, AscD, AsbB and IucA, were used to investigate which amino acids may involved in catalysis and desymmetrization reactions in known and predicted NIS enzymes. We also examined the involvement of NIS enzymes in the virulence of pathogenic microorganisms and suggest that future work investigate small molecule inhibitors targeted against NIS enzymes. This work may facilitate the development of antimicrobials for use in inhibiting microbial growth and treating microbial infections.

The first characterization of a fungal NIS enzyme, Rfs, is presented in Chapter 3. Rfs was shown to catalyze the biosynthesis of the polycarboxylate siderophore, rhizoferrin produced by fungi within the Mucorales order. The purified recombinant enzyme was active with citric acid and diaminobutane as well as the substrate derivatives, oxaloacetic acid, tricarballylic acid, diaminopropane, diaminopentane, hydroxylamine and ornithine.

Flexibility in the nucleophile substrate is not uncommon in NIS enzymes. AsbB, an NIS enzyme in *Bacillus anthracis*[6,7], typically uses citrate and spermidine as substrates but it is also active with citrate and dihydroxybenzoyl spermidine to compensate for loss of the upstream AsbA enzyme[8]. In contrast, flexibility in the usage of citrate derivatives is much more restricted in NIS enzymes. AcsD condenses citrate with L-serine and has near background levels of activity with α-ketoglutarate and oxaloacetic acid[9]. We probed amino acids predicted to be involved in Rfs functioning and found that H484 is crucial for Rfs activity; whereas R354 was not. A third mutant, L544R, was made to mimic the active site of AcsD, and it was found that this mutant was active with citrate and serine, a nucleophile not used by wildtype Rfs. These data highlight possible structural differences which may give rise to substrate preference in NIS enzymes.

The use of substrate derivatives and creation of full rhizoferrin derivatives, as shown by MS analyses, also provide an interesting avenue for development of a Trojan horse approach to treat mucormycosis or other infections caused by microbes which secrete rhizoferrin. The Trojan horse approach exploits the siderophore uptake system and 'tricks' the infectious organism into transporting a siderophore-drug conjugate directly into the cell[10]. Milner et al (2013)[10] created synthetic staphyloferrin A derivatives linked to fluoroquinolone antibiotics and showed that bacterial growth was supressed, although not eliminated. Optimization of this process, including use of various antibiotics and a bio-labile linker to release free antibiotic once inside the cell, has shown promise in *Pseudomonas aeruginosa* with its siderophore, pyoverdine[11]. This is particularly interesting as we have shown that Rfs can incorporate ornithine instead of diaminobutane into the structure of rhizoferrin. This would leave a carboxylic acid functional group available for conjugation, similar to staphyloferrin A. Future experiments to determine if this derivative, conjugated to various antifungals, is taken up by *R. delemar*, could lead to the development of targeted antifungal treatment options.

We also identified a putative NIS enzyme in the fungal pathogen, *Aspergillus terreus*. Members of the *Aspergillus* genus have previously only been shown to produce hydroxamate siderophores through the NRPS pathway. In this pathway *sidA*, an L-ornithine N^5-oxygenase, is the first committed step common to all siderophores biosynthesized by fungal NRPS[12]. We showed that *A. terreus* produced three siderophores: coprogen, ferrichrysin and a third putative siderophore, named Band 4. An *A. terreus ΔsidA* mutant was deficient in production of coprogen and ferrichrysin, as

expected, but maintained production of Band 4. These data suggest that Band 4 is biosynthesized via a pathway other than the NRPS pathway common to coprogen and ferrichrysin. Growth assays using *Aspergillus fumigatus* and *Neurospora crassa ΔsidA* mutants revealed that Band 4 is structurally distinct from TAFC, the main siderophore secreted by *A. fumigatus*[13]; but it may share some structural similarity to coprogen. These data are consistent with MS analysis of hydrolyzed Band 4, as the main mass peak obtained was dimerum acid, a chemical constituent of coprogen. Further structural characterization, including LC-MS/MS, is underway for Band 4. Future work involving purification of the AtNIS enzyme is also underway. Preliminary experiments have shown that purification of AtNIS is greatly improved upon the addition of 20 mM SDS to purification buffers. Experiments are underway to purify sufficient amounts of AtNIS for activity assays and confirm its involvement in biosynthesis of Band 4. This would represent the first characterization of an NIS enzyme in the Ascomycetes.

Our research has also shown that TAFC, a hydroxamate siderophore necessary for germination of *A. fumigatus* in serum[14], can be detected in serum from patients with suspected or probable invasive aspergillosis. A UPLC-MS/MS method was developed and the limit of detection (LOD) for the instrument was found to be ≤1 ng/mL of TAFC, while the lower limit of quantitation (LLOQ) was 5 ng/mL. In total, this method detected TAFC in 53/76 (69%) serum samples suspected of having IA. Of the 36 positive GM samples in this group, 25 were identified as TAFC positive. In 14 samples from patients with proven/ probable aspergillosis, 4 were found to be TAFC positive. These results show that TAFC detection in serum from patients with proven/probable aspergillosis may be diagnostic of invasive aspergillosis.

Follow-up studies comparing this method to GM and LFD testing on BAL fluid were performed by Orasch et al. (2017)[15]. The authors analyzed BAL fluid from patients with hematological malignancies and a diagnosis of probable/proven IA, or control BAL samples. TAFC concentrations were similar to what was found in our study with TAFC concentrations ranging from 1.4 – 6.2 ng/ml. These concentrations were considered true positives, while false positives ranged in concentration from 1.2 – 3.3 ng/ml of TAFC. The authors found that detection of TAFC resulted in 40% sensitivity and 79% specificity with 50% positive predictive value (PPV) and 72% negative predictive value (NPV). Interestingly, when TAFC detection was used in combination with GM detection, the

sensitivity and specificity rose to 87% and 76%, respectively. The PPV and NPV also improved to 65% and 92%, respectively.

Luptáková et al. (2017)[16] used a rat model of invasive aspergillosis and detected TAFC and an intracellular siderophore of *A. fumigatus*, ferricrocin, via HPLC-electrospray ionization (ESI)-CASI-Fourier Transform Mass Spectrometry (FTMS). In serum from infected rats, Luptáková et al. (2017) found ferricrocin in concentrations ranging from 3 – 32 ng/ml; however, TAFC was not detected in these samples. No siderophores were detected in un-infected rats. Detection limits for TAFC and ferricrocin in serum were 0.28 and 0.36 ng/ml, respectively. Siderophore levels in urine were also analyzed from infected and un-infected rats. The mean concentrations of TAFC and ferricrocin in urine were 0.37 ± 0.17 and 0.63 ± 0.12 µg/ml, respectively. Detection limits from urine were 0.02 ng/ml and 0.03 ng/ml for TAFC and ferricrocin, respectively. No siderophores were detected in un-infected control rats. It is important to note that serum and urine samples were collected 3 days post-infection. This may not be feasible in a clinical setting and further research is required to quantify siderophore levels in serum, BAL or urine samples over time.

While these data are promising for TAFC detection as a biomarker for invasive aspergillosis, ultimately, a prospective study is needed to evaluate the efficacy of TAFC detection for diagnosis of IA.

With an increased understanding of siderophores, their biosynthesis and mechanisms to inhibit their biosynthesis, along with continual efforts to optimize their detection in bodily fluids, we hope to reduce the significant morbidity and mortality caused by the fungal pathogens responsible for mucormycosis and invasive aspergillosis.

6.1 References

1. Neilands, J. B. Mechanism and regulation of synthesis of aerobactin in *Escherichia coli* K12 (pColV-K30). *Can. J. Microbiol.* **38,** 728–33 (1992).

2. Finkelstein, R. A. & Yancey, R. J. Effect of siderophores on virulence of *Neisseria gonorrhoeae*. *Infect. Immun.* **32,** 609 (1981).

3. Heesemann, J. Chromosomal-encoded siderophores are required for mouse virulence of enteropathogenic *Yersinia* species. *FEMS Microbiol. Lett.* **48,** 229–233 (1987).

4. Hissen, A. H. T., Wan, A. N. C., Warwas, M. L., Pinto, L. J. & Moore, M. M. The *Aspergillus fumigatus* siderophore biosynthetic gene *sidA*, encoding L-ornithine N^5-oxygenase, is required for virulence. *Infect. Immun.* **73,** 5493–5503 (2005).

5. Schrettl, M. *et al.* Siderophore biosynthesis but not reductive iron assimilation is essential for *Aspergillus fumigatus* virulence. *J. Exp. Med.* **200,** 1213–9 (2004).

6. Wilson, M. K., Abergel, R. J., Raymond, K. N., Arceneaux, J. E. L. & Byers, B. R. Siderophores of *Bacillus anthracis, Bacillus cereus*, and *Bacillus thuringiensis*. *Biochem. Biophys. Res. Commun.* **348,** 320–325 (2006).

7. Cendrowski, S., MacArthur, W. & Hanna, P. *Bacillus anthracis* requires siderophore biosynthesis for growth in macrophages and mouse virulence. *Mol. Microbiol.* **51,** 407–417 (2004).

8. Lee, J. Y. *et al.* Biosynthetic analysis of the petrobactin siderophore pathway from *Bacillus anthracis*. *J. Bacteriol.* **189,** 1698–1710 (2007).

9. Schmelz, S. *et al.* AcsD catalyzes enantioselective citrate desymmetrization in siderophore biosynthesis. *Nat. Chem. Biol.* **5,** 174–82 (2009).

10. Gó Rska, A., Sloderbach, A. & Marszałł, M. P. Siderophore–drug complexes: potential medicinal applications of the 'Trojan horse' strategy. *Trends Pharmacol. Sci.* **35,** 442–449 (2014).

11. Tan, G., Mislin, L. A. & Schalk, I. J. Siderophore-dependent iron uptake systems as gates for antibiotic Trojan horse strategies against *Pseudomonas aeruginosa*. *Metallomics* **6,** 408–420 (2014).

12. Gründlinger, M. *et al.* Fungal siderophore biosynthesis is partially localized in peroxisomes. *Mol. Microbiol.* **88,** 862–875 (2013).

13. Nilius, A. M. & Farmer, S. G. Identification of extracellular siderophores of pathogenic strains of *Aspergillus fumigatus*. *J. Med. Vet. Mycol.* **28,** 395–403 (1990).

14. Hissen, A. H. T., Chow, J. M. T., Pinto, L. J. & Moore, M. M. Survival of *Aspergillus fumigatus* in serum involves removal of iron from transferrin: the role of siderophores. *Infect. Immun.* **72,** 1402–1408 (2004).

15. Orasch, T. *et al.* Bronchoalveolar lavage triacetylfusarinine C (TAFC) determination for diagnosis of invasive pulmonary aspergillosis in patients with hematological malignancies. *J. Infect.* **75,** 370–373 (2017).

16. Luptáková, D. *et al.* Non-invasive and invasive diagnoses of aspergillosis in a rat model by mass spectrometry. *Sci. Rep.* **7,** 1–10 (2017).

Appendix A.

Attempts to knock out the *rfs* gene in Mucorales fungi

The purpose of this project was to knock down or eliminate *rfs* expression in Mucorales fungi and determine if this would lead to defects in growth in low iron media and/or a decrease in virulence in a mouse model of mucormycosis. Two approaches were attempted to evaluate the importance of rhizoferrin secretion in Mucorales fungi: 1) RNAi was to be used to knock down expression of *rfs* in a uracil auxotroph strain of *R. delemar* (M16), and 2) *Agrobacterium*-mediated transformation (AMT) was to be used to knock-out *rfs* expression in *Mucor circinelloides*. *R. delemar* is multi-nucleated, therefore, selection of a homokaryotic knock-out mutant is not feasible. For this reason, RNAi was attempted to knock down expression of the *rfs* gene in *R. delemar* according to Ibrahim et al. (2013)[1]. To eliminate *rfs* expression, gene knock-out studies were also attempted using the mono-nucleated species, *Mucor circinelloides*.

Agrobacterium-mediated transformation of *Mucor circinelloides*

M. circinelloides produced rhizoferrin under iron-limited conditions (see Figure 3.3), and a single copy *rfs* gene is present in the *M. circinelloides* genome. I confirmed that the majority of sporangiospores of *M. circinelloides* (UAMH 8307) are mono-nucleated (Figure A1).

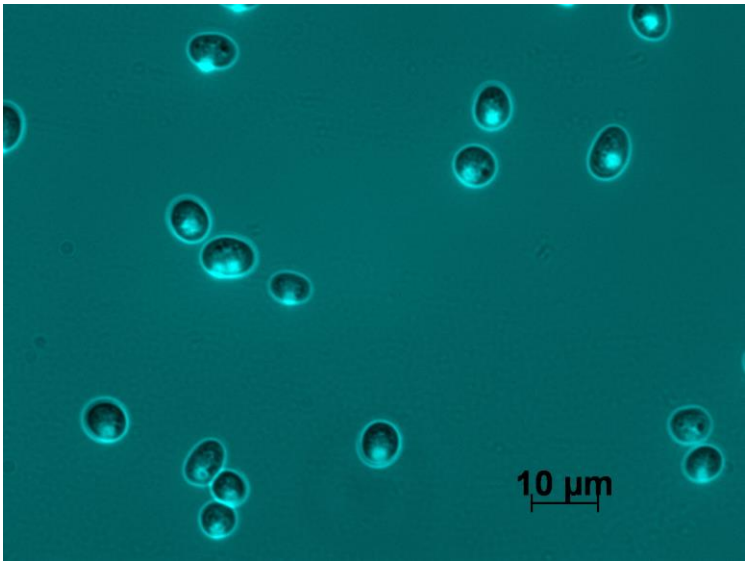

Figure A1. The majority of spores produced by *M. circinelloides* are mono-nucleated.

Using Blastp[2] an Rfs homologue in *M. circinelloides* was identified with 71% identity and 83% positives. The predicted gene, *Mc-rfs*, had the IucC/IucA domains and the FhuF domain which are characteristic of the NIS family. Protein modelling showed that the predicted Mc-Rfs protein structure aligns with the bacterial NIS enzyme, AcsD with 100% confidence. We also confirmed that *M. circinelloides* was susceptible to hygromycin at pH 7.5 on potato dextrose agar so we could use the *hph* gene as a positive selectable marker.

A hygromycin resistance cassette was created by fusing the hygromycin phosphotransferase (*hph*) gene with a *Rhizopus*-specific promoter and terminator from the pRNAi vector (a kind gift from Dr. Ashraf Ibrahim, UCLA) as shown in Figure A2.

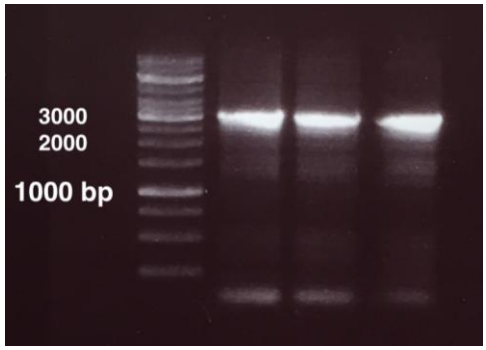

Figure A2. Successful creation of a *Rhizopus*-specific *hph* cassette using fusion PCR.

Fusion PCR successfully fused the *hph* gene (0.75 kb) to the *Rhizopus* pyruvate decarboxylate promoter (1000 bp) and terminator (1000 bp). The full construct was expected to be 2750 bp.

This cassette was then used to create an *rfs* gene deletion cassette, as described in section 4.3.3, where the *hph* cassette was fused to 1000 bp upstream and downstream of the *Mc-rfs* gene. This gene deletion cassette was cloned into pCambia0380 and transformed into *Agrobacterium tumefaciens*.

Agrobacterium-mediated transformation (AMT) was performed as described[3,4], however co-incubation of *M. circinelloides* spores and *A. tumefaciens* was only done for 24 hours to avoid fungal overgrowth. Cellophane membranes were then transferred to selective media containing up to 300 µg/ml hygromycin and various supplemental iron sources including $FeCl_3$, TAFC and coprogen.

Multiple rounds of AMT were performed and putative transformants were subjected to at least three rounds of spore selection. DNA was extracted from putative transformants and PCR was used to determine the presence or absences of the *hph* and *rfs* genes. While transformants for the *hph* gene were obtained, the *rfs* gene was not found to be absent in over 15 analyzed transformants (Figure A3).

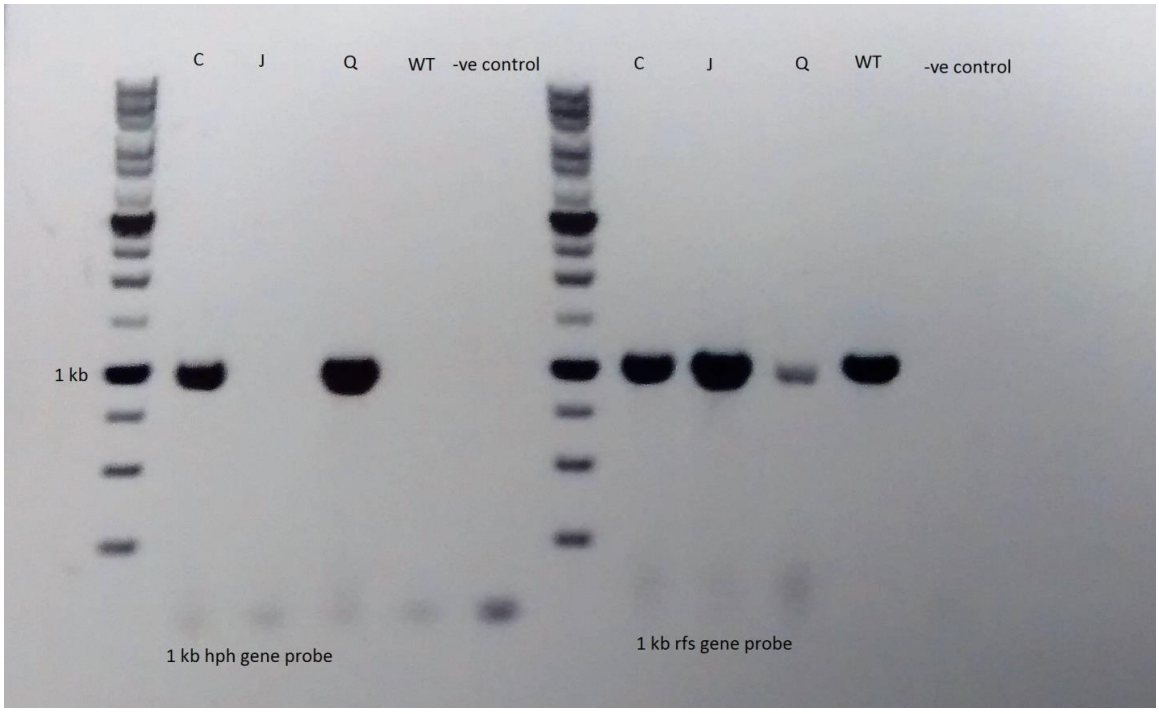

Figure A3. PCR amplification of the *hph* gene and a portion of the *rfs* gene in putative transformants obtained from AMT.
Lanes are labelled with colony identifiers. WT: wildtype *M circinelloides* DNA, -ve control: no template control.

Our inability to obtain a *M. circinelloides Δrfs* strain may be because deletion of *Mc-rfs* is lethal; however, a high affinity iron permease has been described in the related Mucorales fungus, *R. delemar*[5]. Whether this system would compensate for deletion of *rfs* though, is unclear.

The use of RNAi to reduce *rfs* expression in *Rhizopus delemar*

Attempts were made to use RNAi to reduce expression of the *rfs* gene in *Rhizopus delemar*. RNAi in this species has been described by Ibrahim et al. (2012)[5] and we received the pRNAi plasmid containing a uracil selectable marker and *R. delemar* M16, a uracil auxotrophic strain, as a kind gift from Dr. Ashraf Ibrahim (UCLA).

Growth of the *R. delemar* M16 strain was optimized on Yeast Nitrogen Base (YNB; Bioshop) and Potato Dextrose Agar (PDA; BD Difco). We confirmed that M16 will not germinate without uracil supplementation (Figure A4). Some germination is seen during growth on PDA without uracil, however this is most likely due to trace amounts of uracil present in PDA.

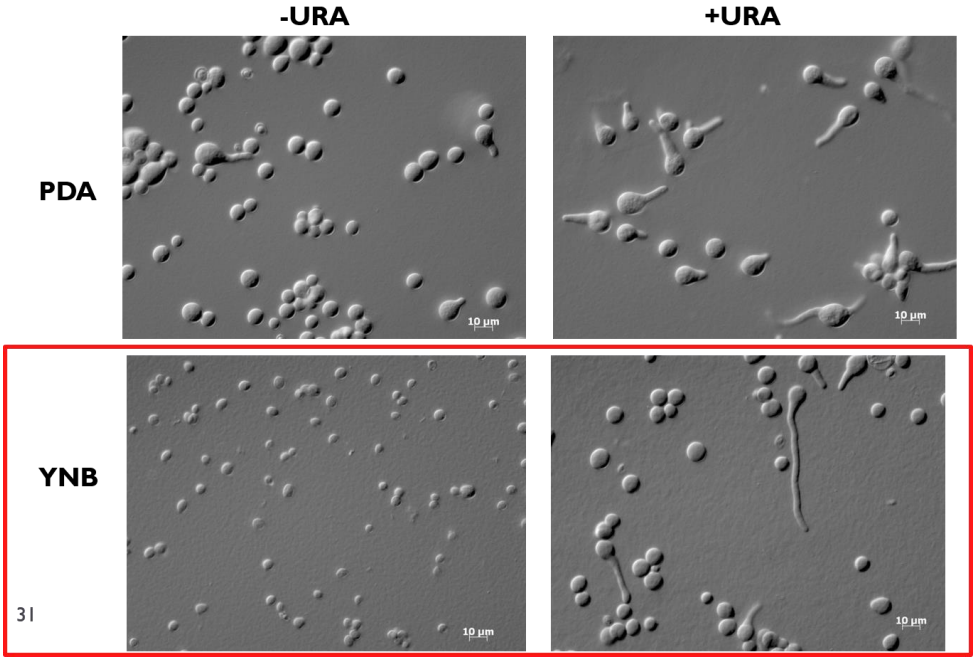

Figure A4. Growth of the M16 uracil auxotroph was optimized on YNB + uracil (URA).

-URA: media lacking uracil; +URA: media supplemented with uracil. Scale bars represent 10 µm.

We attempted to create the RNAi hairpin structure using 500 bp of sequence from the unique IucA/IucC region of *rfs* with an intervening unrelated sequence for the spacer region. Traditional cloning methods were employed and were unsuccessful in creating the RNAi construct. Other techniques were employed to try to create this construct, including fusion PCR and Gibson cloning, however none were successful at creating the desired RNAi construct.

Appendix B.

Generation of monoclonal antibodies for the recognition of siderophores in human serum

Generation of N-acetyl fusarinine and hybridoma production

N-acetyl fusarinine was prepared according to Howard et al. 2000[6]. Briefly, 20 mg of freeze-dried coprogen (a kind gift from A. Hadwin, Simon Fraser University, Canada) was dissolved in 6 M ammonium hydroxide and incubated at room temperature for 45 minutes. The reaction was snap frozen and freeze-dried overnight. The purity of the reaction was confirmed by ESI+ mass spectrometry and the sample was sent to Immunoprecise Antibodies (Victoria, British Columbia, Canada) for conjugation to carrier proteins and generation of monoclonal antibodies. Briefly, this process involved conjugating N-acetyl fusarinine to bovine serum albumin (BSA) and keyhole limpet hemocyanin (KLH). Each conjugate (25 µg) was used in the primary immunization of 2 female BALB/c mice using Complete Freud's adjuvant. Booster immunizations were administered intraperitoneally at 3 and 6 weeks post immunization using 25 µg of conjugate in Incomplete Freud's adjuvant. Test bleeds were taken and the top responding mice were chosen for hybridoma fusion.

ELISA testing of polyclonal antiserum

TAFC and coprogen were used as antigens in ELISA testing. Control reactions used the unrelated siderophores, rhizoferrin and ferrichrysin as antigens. One microgram of each antigen was bound to EIA/RIA high bind 96 well plates (Corning, Inc.) in carbonate coating buffer (pH 8.0) overnight at 4°C. Plates were washed with PBS and blocked with 3% (w/v) skim milk for one hour at room temperature. Skim milk was removed and the plates were washed once with PBS + 0.05% Tween 20 (PBST). Various serum concentrations were added to the wells and then incubated at 37°C for one hour. Serum was removed and wells were washed five times with PBST. Wells were probed separately with anti-IgG (Jackson ImmunoResearch Laboratories Inc.) or anti-IgM (ThermoFisher Scientific) HRP conjugated heavy chain specific secondary antibodies, diluted 1/10,000 in PBST. Plates were incubated for one hour at 37°C and then washed

five times with PBST. Plates were developed using TMB for two minutes. The reaction was stopped with 1 M HCl and plates were read at 450 nm.

Polyclonal antiserum from mice immunized with the BSA-N-acetyl fusarinine conjugate showed reactivity towards TAFC and coprogen; however ferrichrysin and rhizoferrin were not recognized (Figure B1), indicating that the reactivity was specific to N-acetyl fusarinine containing siderophores.

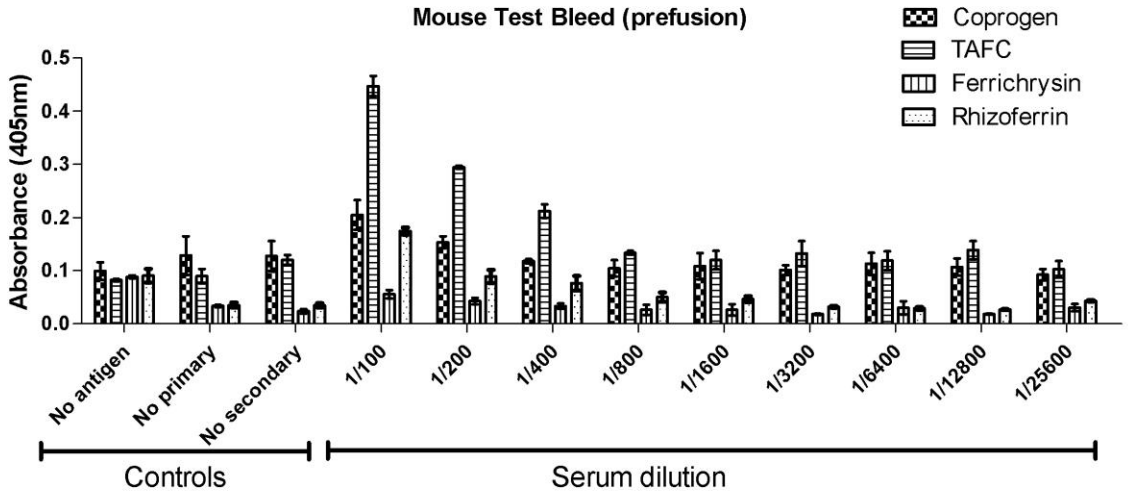

Figure B1. Activity of polyclonal antiserum from rabbits immunized with the BSA-N-acetyl fusarinine conjugate.
Data presented are the mean of 3 replicates ± standard deviation.

Rabbits immunized with the BSA conjugate were chosen for hybridoma fusion and monoclonal antibody production.

Non-competitive and competitive ELISA testing of monoclonal antibodies

Non-competitive ELISA tests were carried out as described above using the monoclonal antibodies (Figure B2). Competitive ELISA tests were performed in a similar fashion, except that anti-IgG or anti-IgM primary antibodies were competed off the bound siderophore antigen using increasing concentrations of free siderophore. Secondary antibodies were added and plates were developed as described above. Antibodies specific to TAFC or coprogen would not be competed off by free siderophore, and absorbance values would plateau for these antibodies. In contrast, antibodies with low

affinity for TAFC or coprogen would be easily competed off and absorbance values would be low for these antibodies.

Eight clones were chosen for screening based on initial non-competitive ELISA test shown in Figure B2. Four clones secreted IgG antibodies and 4 secreted IgM antibodies.

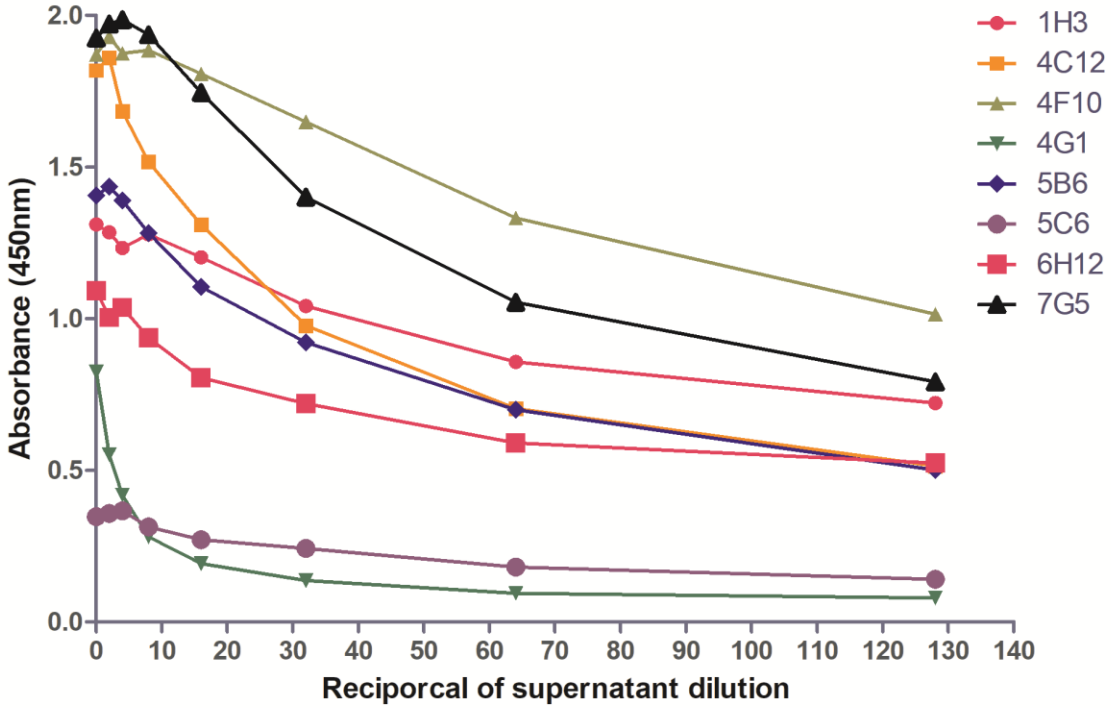

Figure B2. Non-competitive ELISA for initial monoclonal antibody screening. ELISA plates were coated in 1 µg/ml of KLH-coprogen conjugates and monoclonal supernatants were added at various concentrations, shown here as the reciprocal dilutions. All eight clones appear to have good reactivity, with the exception of 4G1 and 5C6.

As a premise for a diagnostic test, a competitive ELISA was used to evaluate the affinity of the monoclonal antibodies for the KLH-coprogen conjugates versus free TAFC. Free TAFC was used as the competitive compound as it was meant to mimic patient serum if this assay were to be used as a diagnostic test. Plates were coated with various concentrations of KLH-coprogen and antibodies from clone 5B6 were added at a 1:100 dilutions. Various concentrations of TAFC were then added to compete off any antibodies. Results were only seen when 1 µg/ml of KLH-coprogen was used and 50 µg of TAFC was required to compete off any antibodies (Figure B3).

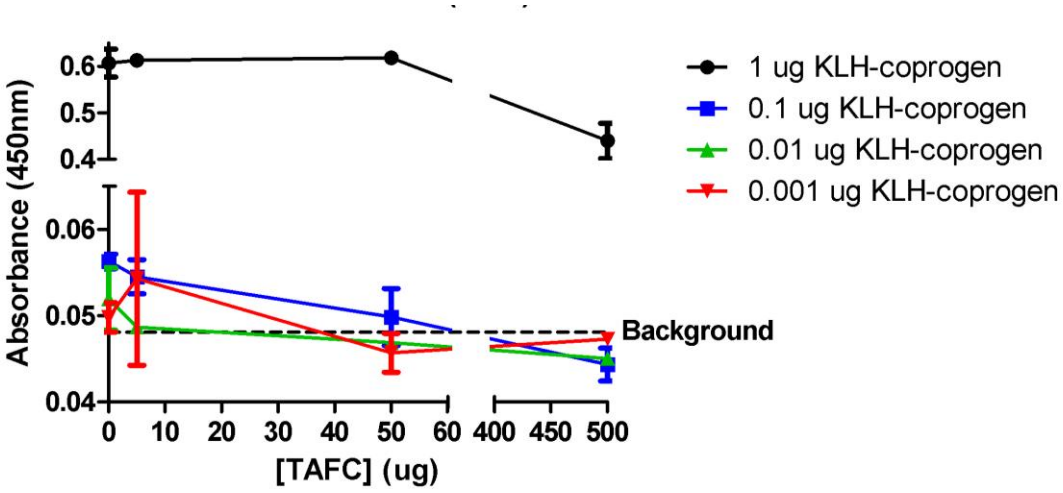

Figure B3. Competitive ELISA using antibodies from clone, 5B6, and various concentrations of KLH-coprogen.

Based on these data, patient serum would have to contain at least 50 µg of TAFC to yield a positive diagnosis. In Chapter 5, we show that nanogram amounts of TAFC are typically present in patient serum. Therefore, monoclonal antibody detection of TAFC would most likely not be a useful way to diagnose an invasive fungal infection.

Appendix References

1. Ibrahim, A. S. *et al.* The high affinity iron permease is a key virulence factor required for *Rhizopus oryzae* pathogenesis. *Mol. Microbiol.* **55,** 328–333 (2013).

2. Altschul, S. F., Gish, W., Miller, W., Myers, E. W. & Lipman, D. J. Basic local alignment search tool. *J. Mol. Biol.* **215,** 403–10 (1990).

3. Michielse, C. B., Hooykaas, P. J. J., van den Hondel, C. a M. J. J. & Ram, A. F. J. *Agrobacterium*-mediated transformation of the filamentous fungus *Aspergillus awamori*. *Nat. Protoc.* **3,** 1671–8 (2008).

4. Nyilasi, I., Acs, K., Papp, T., Nagy, E. & Vágvölgyi, C. *Agrobacterium tumefaciens*-mediated transformation of *Mucor circinelloides*. *Folia Microbiol. (Praha).* **50,** 415–420 (2005).

5. Ibrahim, A. S., Spellberg, B., Walsh, T. J. & Kontoyiannis, D. P. Pathogenesis of mucormycosis. *Clin. Infect. Dis.* **54 Suppl 1,** S16-22 (2012).

6. Howard, D. H., Rafie, R., Tiwari, a & Faull, K. F. Hydroxamate siderophores of *Histoplasma capsulatum*. *Infect. Immun.* **68,** 2338–43 (2000).